Identification of the Cell Receptors for Fibulin-4 and Latent Transforming Growth Factor-β Binding Protein-4, and their Functional Roles in Elastogenesis

Hana Hakami

Faculty of Medicine, Department of Anatomy and Cell Biology
McGill University
Montreal, Quebec, Canada

August 2020

A thesis submitted to McGill University in partial fulfillment of the requirements of the Philosophy Degree

TABLE OF CONTENTS

ABSTRACT

Introduction: Elastic fibers are abundant extracellular matrix (ECM) components that provide tissues such as skin, blood vessels and lungs with elasticity. Elastogenesis presents a cell surface located hierarchical process that requires the recruitment of several proteins, including fibulin-4 (FBLN4) and latent transforming growth factor beta binding protein-4 (LTBP4). Mutations in FBLN4 and LTBP4 cause autosomal recessive cutis laxa type B and C, respectively. Knockout mouse models of FBLN4 and LTBP4 emphasized the roles of these two proteins in elastogenesis. However, the understanding of FBLN4 and LTBP4 function in elastogenesis is not fully explored. In particular, the cellular interactions of FBLN4 and LTBP4, and their functions in elastic fiber formation is unknown. While it is clear that FBLN4 and LTBP4 interact with cells, the required cell receptors and the respective molecular mechanisms in elastogenesis remain unknown and are subject of this study.

Results: Skin fibroblasts and vascular smooth muscle cells (SMC) bind strongly to FBLN4 and LTBP4 demonstrated by real-time and end-point cell binding assays. Both, synthetic and contractile aortic SMC interacted with FBLN4 and LTBP4. FBLN4 exclusively interacted with cells as multimers. Using FBLN4 deletion mutants, we identified two cell interaction epitopes on FBLN4 located in cbEGF2-3 and in the C-terminal domain. FBLN4 multimerization sites were mapped to cbEGF4-5 and the C-terminal domain, likely representing a contiguous region. We also mapped a new cell interaction region in LTBP4 within the N-terminal half. Both, FBLN4 and LTBP4 have high affinity for heparin (an experimental model of heparan sulfate), suggesting that heparan sulfate proteoglycans mediate these interactions. Cell binding to FBLN4 and to LTBP4 was entirely abolished in the presence of heparin and significantly reduced in the presence of heparan sulfate or after treating cells with heparinases. Glypicans are not necessary for FBLN4 or LTBP4 cell interactions. Syndecan-2 or -3 siRNA knockdown in fibroblasts abolished the interaction with FBLN4, whereas only syndecan-3 knockdown abolished the interaction with LTBP4. Direct interactions between FBLN4 and the ectodomains of either syndecan-2 or -3 were determined. Also, a direct interaction between LTBP4 and the ectodomain of syndecan-3 was identified. Syndecan-2 or -3 knockdown in fibroblasts resulted in compromised elastic fiber assembly. To further investigate the underpinning mechanism, we identified that FBLN4 and LTBP4 stimulated focal adhesion kinase phosphorylation. As well, the presence of FBLN4 and

LTBP4 significantly increased the contraction of skin fibroblast-cellularized collagen gels. Cell interactions with FBLN4 or LTBP4 led to a significant increase of Erk1/2 protein levels and $RhoA^{GTP}$. Furthermore, FBLN4 and LTBP4 both enhanced skin fibroblast migration. These data suggest that FBLN4 and LTBP4 interactions with their cell receptors promote elastic fiber assembly by enhancing focal adhesion formation leading to cell contractility through Erk1/2 and RhoA activation.

Conclusions: Altogether, the data identified the responsible cell-surface receptors interacting with FBLN4 and LTBP4, and revealed a new cell-interaction role essential for elastogenesis for these two proteins.

RÉSUMÉ

Introduction: Les fibres élastiques, composants majeurs de la matrice extracellulaire (ECM), fournissent l'élasticité aux tissus comme la peau, les vaisseaux sanguins et les poumons. L'élastogenèse présente un processus hiérarchique complexe, localisé à la surface cellulaire et impliquant, plusieurs protéines dont la fibuline-4 (FBLN4) et une protéine de liaison aux facteur de croissances (LTBP4). Les mutations FBLN4 et LTBP4 sont impliquées dans la cutix laxa, maladie autosomique récessive de type B et C, respectivement. Les souris knock-out pour FBLN4 et LTBP4 soulignent les rôles de ces deux protéines dans l'élastogenèse. Cependant, les rôles de la FBLN4 et LTBP4 n'ont pas été entièrement explorés. Plus particulièrement, leur rôle des interactions entre FBLN4 et LTBP4 dans le développement de la fibre élastique reste méconnu. L'interaction entre FBLN4 et LTBP4, avec les cellules réceptrices requises et les mécanismes moléculaires dans l'élastogenèse sont abordées à l'étude ici.

Résultats: Les tests de liaison cellulaire en temps réel et en point final ont démontré que les fibroblastes cutanées et les cellules musculaires lisses vasculaires (SMC) se lient fortement à FBLN4 et à LTBP4. Les SMC d'origine synthetique ou de l'aorte contractile interagissent avec FBLN4 et LTBP4. La FBLN4 interagit exclusivement avec les cellules sous forme multimères. En utilisant des mutants de délétion FBLN4, nous avons identifié deux épitopes d'interaction cellulaire de FBLN4 situé dans les domaines cbEGF2-3 et C-terminal. Les sites de multimérisations de FBLN4 ont été cartographiés sur cbEGF4-5 et le domaine C-terminal, représentant probablement une région contiguë. Nous avons également cartographié une nouvelle région d'interaction cellulaire de LTBP4 dans au milieu de son domaine N-terminale. De plus, FBLN4 et LTBP4 ont à la fois une forte affinité pour l'héparine (un modèle expérimental de la sulfate héparane), ce qui suggère que les protéoglycanes d'héparane sulfate interviennent dans ces interactions. La liaison cellulaire FBLN4 et LTBP4 était totalement absente en présence d'héparine et significativement réduite en présence de l'héparane sulfate ou après traitement des cellules avec l'héparinase. Les glypicanes ne sont pas nécessaires pour les interactions cellulaires FBLN4 ou LTBP4. La désactivation des syndécane -2 ou -3 par l'utilisation de siRNA dans les fibroblastes a aboli l'interaction avec le FBLN4, alors que seul l'absence de syndecane-3 a aboli l'interaction avec le LTBP4. Les interactions directes entre FBLN4 et les ectodomaines de syndécanes -2 ou -3 ont été vérifiées. La désactivation des syndécanes -2 ou -3 dans les fibroblastes a entraîné un assemblage

compromis des fibres élastiques. Pour étudier plus en profondeur le mécanisme sous-jacent, nous avons identifié que FBLN4 et LTBP4 stimulaient la phosphorylation de la kinase d'adhésion focale. De plus, la présence de FBLN4 et de LTBP4 a considérablement augmenté la contraction des gels de collagène cellulaires fibroblastes cutanés. Les interactions cellulaires avec FBLN4 ou LTBP4 ont conduit à une augmentation significative des niveaux de protéine Erk1 / 2 et RhoA-GTP. En outre, la FBLN4 et la LTBP4 ont tous deux amélioré la migration des fibroblastes cutanés. Ces données suggèrent que les interactions FBLN4 et LTBP4 avec leurs récepteurs cellulaires favorisent l'assemblage des fibres élastiques en améliorant la formation d'adhérence focale conduisant à la contractilité cellulaire par l'activation d'Erk1 / 2 et de RhoA.

Conclusions: Dans l'ensemble, les données ont identifié les récepteurs de surface cellulaire responsables interagissant avec FBLN4 et LTBP4, et ont révélé un nouveau rôle d'interaction cellulaire essentiel pour l'élastogenèse de ces deux protéines.

ACKNOWLEDGMENTS

First, I would like to acknowledge and express my deepest appreciation and sincerest gratitude to my supervisor, Dr. Dieter P. Reinhardt (Faculty of Medicine, Department of Anatomy and Cell Biology and Faculty of Dentistry, McGill University) for his continuous and unlimited support with my Ph.D, project. Dr. Reinhardt gave me the opportunity to join his lab team at a very difficult intermediate period of my Ph.D. program. Since then, he has strived to secure steady progression in my Ph.D. research with valuable discussions, meetings and travelling to conferences, among others. I am very grateful for his patience, openness, trust and of most importantly his knowledge. His guidance, in either soft or tough way, enlightened my path and helped me throughout my research trek and thesis writing. He has been my constant support during this long process of my loaded Ph.D. years with all kind of lab adventures. Dr. Reinhardt is very generous with giving his time, all possible materials to create a sustainable productive research lab, and dedicating himself for his lab members. If it was not for Dr. Reinhardt's great support, I would not have had such a great PhD experience and made it all the way to here.

I would like to convey my special thanks and greatest appreciation to my mentor, Dr. Craig Mandato (Faculty of Medicine, Department of Anatomy and Cell Biology, McGill University) for his immense support and guidance from the first day I enrolled in the PhD program. All his care, time, efforts, and wise, kindness, and all his expertise were so precious to me. I believe his help during my PhD due particularly the tough time of unpleasant abusive family experience, has kept me mentally strong throughout my Ph.D. Dr. Mandato by his sage advices changed my life for the better. He has provided me with the best mentorship experience that it will be extremely beneficial for my future academic and research career.

I would like to extend my sincere thanks to the Student Affairs & Graduate Program Coordinator, Mrs. Joelle Denomy-Hasilo (Faculty of Medicine, Department of Anatomy and Cell Biology, McGill University) for her endless help. It is impossible to count all the ways of her help during my PhD studies. She has been present every single time, and extended her hands to support me, as she does for all the graduate students in the program. She is an angle.

I am certainly grateful to the Graduate Program Director Dr. Chantal Autexier (Department of Anatomy and Cell Biology, McGill University) whose dedicates herself for payless support, advice and follow-ups to all the graduate students in our department.

My genuine thanks are to all the collaborators on this project; Dr. Sylvie Ricard-Blum (University Claude Bernard Lyon, France) on providing syndecan ectodomain recombinants and Dr. Nathalie Lamarche-Vane (Research Institute of the MUHC, McGill University) for her significant inputs in the RhoA and Erk1/2 signaling analyses.

I would like also to thank my thesis advisory committee members: Dr. Lisbet Agneta Haglund (Experimental Surgery Department, McGill University) and Dr. Mari Kaartinen (Faculty of Medicine, Department of Anatomy and Cell Biology, McGill University), for guiding me and giving me insightful comments and suggestions through these years.

I am certainly thankful to my previous PhD supervisor, Dr. John Bergeron on his support and guidance during the first two years of my PhD journey.

My sincere thanks to Dr. Marc McKee (Faculty of Dentistry, McGill University), Mrs. Aisha Musa (Dr. McKee lab, Faculty of Dentistry, McGill University) and Dr. Ossama Moujaber (Department of Physiology, McGill University) for training me and governing me a full time access to use the live-cell imaging microscope in Dr. McKee's lab.

I do not have enough words to express my gratitude to all the lab members, who have been supportive and positive. They were not only my colleagues, more like my family in the lab. During the darkest days, while I was struggling after giving birth to each of my children, they stood by me and never hesitated to introduce their assistance to go through this successfully. Our respectful relationships will last for endless with Dr. Heena Kumra, Dr. Valentin Nelea, Mr. Chae Syng (Jason) Lee, Ms. Muthu Lakshmi Muthu, Mr. Rongmo Zhang, Ms. Neha Dinesh, Dr. Ling Li, Mr. Cori Lau and Mr. Joseph DiPaolo. Also, I would like to express my appreciation to all the undergraduate students who joined the lab and helped me on lab duties. This made me enjoy my lab work and improve my teaching skills at the same time, in particular Yizhou (Aviva) Zhao, Kungjun (Tom) Lee, Yiyun (Eve) Zhang, Jiongci (Lisa) Xu, Merve Younussi, Namrata Rana, Diane Sautter and Clark Thomson.

I also would like to thank all the researchers and students in the neighbor labs in Strathcona Anatomy & Dentistry Building (McGill University, Montreal) for helping me on daily basis and making themselves available for feedback and discussions which enriched my PhD experience particularly, Dr. Elaine Davis (Department of Anatomy and Cell Biology, McGill University), Dr. Eric Boucher (Department of Anatomy and Cell Biology, McGill University) and Ms. Kyoungmi Bak (Dr. Davis lab, Department of Anatomy and Cell Biology, McGill University).

I would like to thank my dear friend Ms. Awa Tamboura (Human Resourse Coordinator, CICODI International, Burkina Faso, and Author, Novelist at Edilivre Editions) for translating this thesis abstract from English to French, and to Dr. Sebastien Blaise (Université de Reims Champagne-Ardenne, France) for editing the French translation.

My sincere gratitude to McGill Counseling Services for the mental health support they provided during the most difficult days of my PhD studies. This support allowed me to see the light inside myself and return stronger, every time I fell off a cliff, to complete my goals and achieve my dreams in the best possible way.

I would like to express my mixed feelings and unsaid thoughts to my parents, two older sisters Ebtisam and Wazirah, and my cousin Nuha Hakami, who showed a strong support during these years to complete my Ph.D. studies although there are separating lands and oceans between us.

I am so thankful to my dearest friends; Ms. Rowa Bakadlag, Dr. Munira Al-Ballaa, Dr. Lama Yamani, Dr. İçten Meraş, and Dr. Ömer Faruk Ugurlu, for their support that always surrounds me and holds me up during this journey. I cannot express how I am so grateful for gaining their friendships, they are the best people ever to have in life without wishing for better.

Here, I have to stand up to show my deepest appreciation to my M.Sc. supervisor Dr. Maha Daghestani (Faculty of Sciences, King Saud University and King Faisal Specialist Hospital and Research Centre) for her unceasing and solid support extended for years to back me up, she became not only my M.Sc. supervisor, but also my kind meaningful mother.

Here, I am humble to recognize King Saud University (Riyadh, Saudi Arabia) for the PhD fellowship during the first six years of my PhD, NSERC (Natural Sciences and Engineering Research Council of Canada) for funding this project and granting me funding for the last phase of my PhD program, and Saudi Royal Embassy (Ottawa, Canada) for bench fee funding.

Last but not least, I want to express my love and respect to my husband, Murat Dursun, who came to my life as a blessing, together with me established a small happy home in the middle of my PhD journey, and made a significant and positive change in my life. My husband's extraordinary support, tolerance and patience in the last three and half years powered my strength to go through all the hardships every single day.

One more on the recognition, of course; thank you, McGill University!

DEDICATION

I dedicate this thesis to all world children starting with my own lovely children, to my dearest son Yusuf who is three years old, and to my beautiful baby daughter Maryam who is two months old, during this time of my thesis submission.

I also dedicate this thesis to all women who got stamina and work hard every single day, seeking for quality life out of poverty, injustice, and abuse.

CONTRIBUTION TO ORIGINAL KNOWLEDGE

The work presented in this thesis includes new original discoveries contributing to the knowledge of the function and dominance of cell interactions with the elastic fiber proteins, FBLN4 and LTBP4. The study established novel and fundamental paradigms that change the understanding of the roles of FBLN4 and LTBP4 cell binding in elastogenesis. The key contributions are:

1. The consistency of FBLN4 and LTBP4 cell interactions is demonstrated with various elastogenic cells.
2. The multimerization sites are located in cbEGF4-5 and the C-terminal domain, likely representing a contiguous region.
3. The cell interaction sites in FBLN4 are located in the cbEGF2-3 and the C-terminal domains.
4. A new cell binding site in LTBP4 is mapped in the N-terminal half of the long and short isoforms.
5. Human dermal fibroblast adhesion to recombinant human FBLN4 and LTBP4 occur through cell surface heparan sulfate.
6. The cell receptors for FBLN4 are SDC2 and SDC3.
7. The cell receptor for LTBP4 is SDC3.
8. Underlying cellular mechanisms activated upon the cell interaction with FBLN4 and LTBP4 are documented including focal adhesion formation, cell contraction and migration, and cell proliferation.

Overall this important characteristic and mechanistic information about how FBLN4 and LTBP4 interact with cells provide important milestones for the overarching principle of elastogenesis

CONTRIBUTIONS

Dr. Dieter Reinhardt initially conceptualized this project proposal. Mr. Christine Fagotto-Kaufmann and Dr. Reinhardt established cloning recombinant expressing the full length fibulin-4 (FBLN4). Then, Ms. Jelena Djokic contributed through the early development of this project, but not a part of this thesis, with valuable data that have been published (JBC, 2013). Part of the generated material by Ms. Djokic was cloning a set of FBLN4 deletion mutants that used in this study, named as F4_N1, F4_2-5 and F4_6C (see Fig. 3 A). At the time Ms. Djokic disassociated from Dr. Reinhardt lab another set of FBLN4 deletion mutants were under developing but the cloning was not fully completed which included F4_N1-3 and F4_N1-5. I was handled the project and completed the cloning of these mutants.

Ms. Amélie Pagliuzza cloned the used recombinant in this study for the full length of transforming growth factor-β binding protein-4 (LTBP4). Ms. Yizhou (Aviva) Zhao had a significant contribution in establishing the cloning of LTBP4 deletion mutants as she was constructed by myself with Dr. Reinhardt supervision.

Plasmids expressing syndecan ectodomains were cloned in Dr. Sylvie Ricard-Blum (University Claude Bernard Lyon, France).

The scattering light scattering experiments and analyses were performed by Dr. Valentin Nelea (Dr. Reinhardt's lab, Faculty of Medicine, Department of Anatomy and Cell Biology and Faculty of Dentistry, McGill University).

LIST OF ABBREVIATIONS

ADCL	Autosomal dominant cutis laxa
ADAMTS	A disintegrin and metalloproteinase with thrombospondin motifs
APS	Ammonium persulfate
ARCL	Autosomal recessive cutis laxa
αSMA	Alpha smooth muscle actin
BCA	Bicinchoninic acid
BSA	Bovine serum albumin
βME	β-mercaptoethanol
BMP	Bone morphogentic protein
C	Carboxyl terminal
cbEGF	Calcium-binding epidermal growth factor
cDNA	Complementary deoxyribonucleic acid
CHO	Chinese hamster ovarian cells
CLAHE	Contrast limited adaptive histogram equalization
COL	Collagen
CRL-2481	Umbilical venous smooth muscle cells
CV	Column volume
DAPI	4′,6-diamidino-2-phenylindole
d.H_2O	Deionized distilled water
DLS	Dynamic light scattering
DMEM	Dulbecco's Modified Eagle medium
DNA	Deoxyribonucleic acid
DOX	Doxycycline
DTT	Dithiothreitol
EBNA	Epstein-barr virus nuclear antigen
EBP	Elastin-binding protein
ECM	Extracellular matrix
ECIS	Electric cell-substrate impedance sensing
EDTA	Ethylenediaminetetraacetic acid
EGF	Epidermal growth factor

EGFP	Enhanced green fluorescent protein
ELISA	Enzyme-linked immunosorbent assay
ELN	Elastin
EMILIN	Elastin microfibril interface-located protein
ERC	Elastin receptor complex
FA	Focal adhesion
FAK	Focal adhesion kinase
FBN	Fibrillins
FBLN	Fibulins
FBS	Fetal bovine serum
FCS	Fetal calf serum
FT	Flow-through
FN	Fibronectin
FPM	Frames per minute
G418	Gentamicin sulfate antibiotic
GAG	Glucoseaminoglycan
GAPDH	Glyceraldehyde-3-phosphate dehydrogenase
GPC	Glypicans
HASMC	Human aortic smooth muscle cells
HEK	Human embryonic kidney
HEPES	4-(2-hydroxyethyl)-1-1-piperazineethanesulfonic acid
Hh	Hedgehog
Hi-FBS	Heat inactivated FBS
His	Histidine
HRP	Horseradish peroxidase
HSPG	Heparan sulphate proteoglycans
IF	Immunofluorescence
ITG	Integrins
kDa	Kilodalton
LTBP	Latent transforming growth factor beta binding protein-4
lox	Lysyl oxidase

loxl	Lysyl oxidase-like
MAGP	Microfibril associated glycoproteins
MFAP	Microfibrillar associated protein
MMP	Matrix metalloproteinase
mRNA	Messenger ribonucleic acid
N	Amino terminal
NGS	Normal goat serum
Ni	Nickel
NSF	normal skin fibroblasts
PBS	Phosphate buffered saline
PCR	Polymerase chain reaction
PFA	Paraformaldehyde
pFN	Plasma fibronectin
PSI	plexin-semaphorin-integrin
PMSF	Phenylmethanesulfonylfluoride
PNGase F	Peptide: N-glycosidase F
PSG	Penicillin-streptomycin-glutamine
RGD	Arginine-Glycine-Aspartic Acid
RGE	Arginine-Glycine-Glutamic Acid
RT-qPCR	Real time quantitative polymerase chain reaction
SDC	Syndecan
SDS	Sodium dodecyl sulfate
SDS-PAGE	Sodium dodecyl sulfate-polyacrylamide gel electrophoresis
SGBS	Simpson-Golabi-Behmel syndrome
SM	Starting material
SMC	Umbilical arterial smooth muscle cells
SVAS	Supravalvular aortic stenosis
TB	TGFβ-binding protein-like
TBS	Tris-buffered saline
TBST	Tris-buffered saline containing Tween-20
TCA	Trichloroacetic acid

TE	Tropoelastin
TEMED	Tetramethylethylenediamine
WB	Western Blot
YAP	Yes-associated protein

LIST OF TABLES

LIST OF FIGURES

LIST OF MOVIES

1. LITERATURE REVIEW AND INTRODUCTION

1.1 Overview

Elastic fibers are abundant extracellular matrix (ECM) components that provide tissues such as skin, blood vessels and lungs with elastic properties. Electron microscopic analyses have shown that mature elastic fibers in normal tissues consist of two distinct aspects: an inner elastin core and an outer mantle of fibrillin-containing microfibrils[1-3]. It has been shown that early interaction of these two major components of elastic fibers occurs at the cell surface[4; 5]. Tropoelastin (TE) monomers, the precursor of mature elastin fibers, are nucleated on the cell surface by a scaffold of fibrillin-containing microfibrils and then processed into assembled elastic tissue fibers. This processing represents a highly complex mechanism requiring the recruitment of several accessory proteins, including fibulin-4 and -5 (FBLN4/5), latent transforming growth factor beta binding protein-4 (LTBP4), lysyl oxidase (LOX), LOX like-1 (LOXL1), microfibril associated protein 4 (MFAP4), and elastin microfibril interface-located protein (EMILIN)[6-10]. Mutations in nearly all elastic fiber associated genes lead to heritable connective disorders in human[11]. For example, mutations in FBLN4 cause autosomal recessive cutis laxa (ARCL1) type 1B (ARCL1B), characterized by a severe and diverse array of defects including loose and sagging skin and aortic aneurysms[12-15]. Similarly, mutations in LTBP4 were reported in patients with a related disorder 'ARCL1' type C (ARCL1C)[3; 16]. The underlying cause in both disorders is the deficiencies of the mutated proteins which severely affect elastic fiber formation. However, the understanding of FBLN4 and LTBP4 functions in elastogenesis is little explored, in particular, the cellular interactions of FBLN4 and LTBP4, and the functions of these cell interactions in elastic fiber formation. FBLN4 interacts with the propeptide of LOX and tether it on TE[17]. FBLN4 is also capable of adhering to fibroblasts and smooth muscle cells[18]. The cell-surface receptor responsible for FBLN4 binding to cells remains unknown. LTBP4 is known to be recruited to TE by FBLN4[19; 20] and FBLN5[21]. Similar to FBLN4, LTBP4-cell interacting receptor is also unknown[22]. The mechanistic function of FBLN4 or LTBP4 in cell interaction and in turn in elastic fiber formation remains largely obscure. Therefore, this dissertation addressed the roles of FBLN4 and LTBP4 cell interactions in elastogenesis.

1.2 Extracellular matrix

ECM is the tissue materials expressed by cells and deposited to the extracellular space, which does not only adheres the cells together, but also acquire biochemical properties that contributes to tissue organization and functions. ECM varies among body tissues with a wide range of structures from loose to dense, and from soft to rigid[23]. 'Matrisome' is the ECM components of any given matrix, in which about 300 proteins of human proteome have been classified to this group[24]. The core mammalian matrisome comprises fibronectin (FN), fibrillin (FBN), elastin (ELN), collagen (COL), laminin and proteoglycans, among others[25]. In addition to the core proteins, ECM retains a group of enzymatic proteins that function in regulating and remodeling the ECM, such as the family members of matrix metalloproteinases (MMPs), lysyl oxidase (LOX), and members of disintegrin and metalloproteinase with thrombospondin motifs (ADAMTS)[25; 26].

ECM proteins frequently contain multiple highly-conserved domains and include a number of very ancient proteins such as collagens and laminins[27]. Also, ECM proteins commonly have repetitive arrangements of recognizable domains, e.g. the epidermal growth factor like (EGF-like), calcium-binding EGF-like (cbEGF-like), TGFβ-binding protein-like (TB), and immunoglobulin (Ig) domains[27]. However, a few known ECM proteins consist of exceptional domain arrangements such as elastin (ELN) and fibronectin (FN) matrix proteins[24; 28].

One of the characteristics of ECM proteins in general is that they are rich in disulfide bonds within modules and between modules of different molecules, which is important for the protein conformation stability and proper function[29]. In addition, ECM proteins frequently contain glycans that contribute to protein adhesion to cells and to other proteins, as well as in the tissue stiffness[30-32]. Typically, ECM proteins are deposited into the extracellular space after passing through the secretory pathway and undergoing several post-translational modifications for the correct protein folding, including disulfide bond formation, glycosylation, carboxylation and others[33; 34]. However, the modifications of ECM proteins continue toward maturation and activation even after secretion[34]. Several ECM proteins form dynamic fibrillar structures[35]. These fibrillar structures are arranged in sophisticated networks in various tissues. They do not differ only in the diverse molecules compose them, but also in how these molecules are constructed. For example, COL, the most prevalent component of the ECM in skin and bone, presents distinct arrangements in both of them[36]. While collagen fibers in skin form basketweave organizations of randomly-like oriented bundles[37; 38], bone matrix is composed of dense collagen fiber networks stiffened via mineral

crystals of hydroxyapatite (calcium apatite) that organized in higher hierarchical levels of supramolecular collagenous structures[36]. Also, the architectures of elastic fibers vary among elastic tissues. For instance, elastic fibers presents in wavy mesh-like networks spread through the dermis layer in skin, continuous sheet-like lamellae in large blood vessels, and thin branched fibers in lungs[1].

Generally, ECM provides cells and tissues with a highly dynamic structural support. ECM confers a broad functional spectrum including elasticity, rigidity, cell-adhesion, and differentiation, among others[26; 39]. Fibrillar ECM structures provide scaffold not only for adherent cells, but also for the deposition and assembly of other ECM proteins[35]. Additionally, ECM serves as a substrate for cell proliferation and migration in embryogenic development, in physiological processes such as wound healing and in pathological conditions like metastasis[40-42]. Importantly, ECM functions as a reservoir for growth factors and cytokines required for signal transductions, tissue remodeling, and immuno-response[40; 43].

ECM pathology highlighted the indispensable function of ECM in development, survival and health. Mutations in ECM genes, as well as scant deposition or deleterious aggregates of ECM proteins have been associated with many diseases[41; 44-46]. However, there are huge gaps in our understanding of ECM protein compositions, interactions and functions during physiological and pathological processes. Importantly, our knowledge about elastic fiber formation is very limited despite the considerable advances made over recent to uncover the mechanisms that regulate elastogenesis. Many mechanistic details in all the aspects of elastic fiber formation remain undefined.

1.3 Elastic fibers

Elastic fibers are major and critical ECM components for dermal, circulatory, and respiratory tissues[6]. The amount and the organization of elastic fibers confers the elastic properties required for tissue function (Fig. i). Elastic fibers in the aorta are arranged in layers of continuous lamellae alternating with vascular smooth muscle cells, which govern mechanical resistance to the aortic walls subjected to high hydrostatic pressure[47]. Short and thin elastic fiber networks in alveoli coordinate elasticity and resilience of their constantly expanding and shrinking delicate walls[6].Cutaneous elastic fibers form mesh-like networks of two groups: thick horizontally oriented fibers in reticular dermis and thinner perpendicular fibers in the papillary dermis[1]. These

arrangements of elastic fibers impart to skin the flexibility to extend and recoil, to accommodate body movements with full protection from the mechanical impacts and pressures.

Elastic fibers are composite ECM elements that are often defined as fibrous structures with a core of amorphous elastin enveloped by a fibrillin-microfibril coat[2; 11; 48]. In fact, elastic fibers include several components other than elastin and fibrillin. But the exact composition of mature elastic fibers is still not clear and needs to be completed[48].

Elastin is the core of mature elastic fibers, which is dense and highly crosslinked form of tropoelastin (TE), the elastin monomer[49]. Elastic fiber formation, termed 'elastogenesis' is a highly complex process and it is not as simple as it was thought years ago that elastin is deposited onto fibrillin-microfibril scaffold before and during crosslinking[50]. It became obvious as research revealed that elastin cannot fully self-assemble and crosslink without assistance from multiple molecules[7; 47]. However, it is not clear if the molecules that contribute in elastogenesis continue to constitute a part of the mature elastic fibers in tissues or dissociate in some phases of elastogenesis.

Mutations in elastin and elastic fiber genes result in a variety of heritable disorders affecting life-sustaining organs and tissues including aorta, cardiac valves, lungs, and skin[2; 51; 52]. Defects in elastic fibers are associated with aortic aneurysms and dissections, cardiac valvular failure, emphysema, cutis laxa, arterial tortuosity, cornea malformation and metabolic abnormalities[7; 14; 53-59].

Elastic fibers have very long lifespan with extremely slow turnover, comparable to human lifespan[60]. However, elastic fibers lose their highly extensible ability through 'elastolysis', where elastic fiber degradation occurs via elastolytic enzymes such as elastases and MMPs released by several cell types including macrophages, neutrophils, smooth muscle cells and fibroblasts, among others[51; 61-64]. In addition, elastic fibers are characterized by insufficient repair and remodeling that contribute to aging and pathological conditions, such as inflammation, burns, wounds, sun damages, cigarette smoke and hypertension[65-68].

Overall, the step by step process of elastogenesis and proteins involved during this process remain a challenging problem which likely will require intensive research for the years to come.

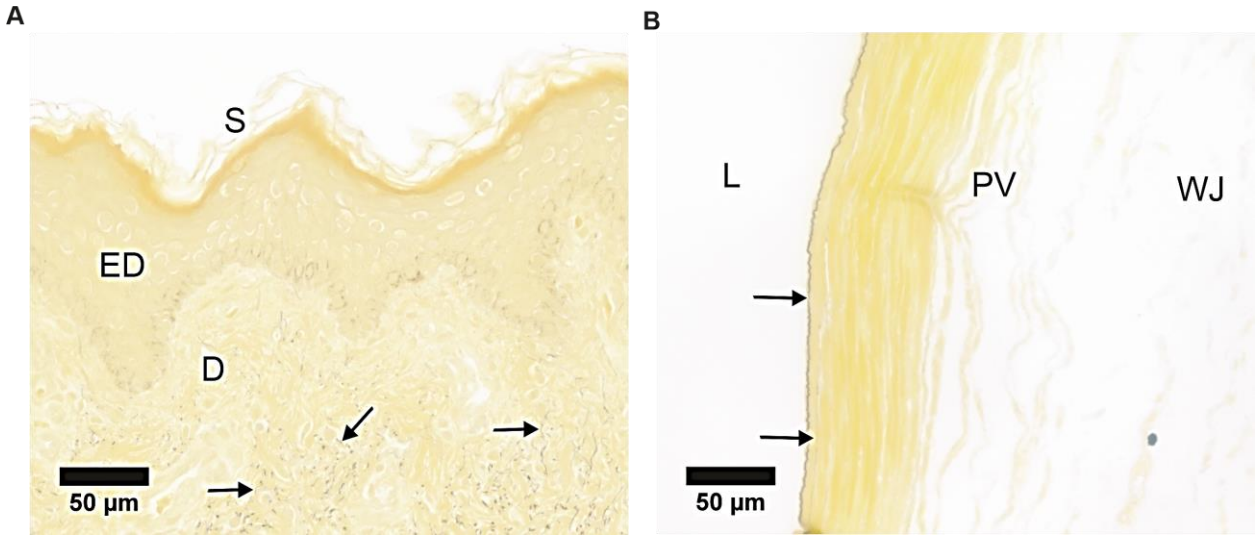

Figure i. Organization of elastic fibers in tissue

Hart's elastin staining of cross-sections in human skin (foreskin) (A) and umbilical cord vein (B). The dark brown staining shows elastic fibers. They forms networks spread over the dermis layer in skin. Elastic fibers in the umbilical vein present one continuous thick layer toward the lumen and a few thinner layers of deposited elastic fibers under it separated by layers of smooth muscle cells. S: stratum corneum, ED: epidermis, D: dermis, L: lumen, PV: perivascular region, WJ: Wharton's jelly.

1.4 Elastic fiber proteins

Numerous ECM proteins are involved in each step of elastogenesis guiding and facilitating elastic fiber formation[1; 2; 11; 47]. Several proteins have been featured as elastic fiber building blocks. The key elastic fiber proteins include TE, FBN1, FN, FBLN4, FBLN5, LTBP4, LOX, LOXL1, and EMILIN[1; 11]. It is important to highlight that elastic fiber proteins interact with others and depend on others in dynamic mechanisms that are still not fully uncovered. These complex interactions between elastic fiber proteins are essential and defect in them disturb elastogenesis and result in compromised elastic fibers[1]. Mutations in nearly all elastic fiber associated proteins lead to heritable connective disorders in human due to defective non-functional elastic fibers, which some of the underlying disease mechanisms are confirmed by gene deletion mouse models[2; 51].

FN dimers assemble in the ECM to a fibrous network in a cell-interaction dependent mechanism[69-73]. Fibronectin interactions with cells stimulate focal adhesion formation and cell contraction events which are required for the assembly of FN fibers[70; 74-78]. Elastic fiber proteins depend on an existing FN matrix for incorporation into the ECM. A double knockout of both

cellular and plasma FN affects elastogenesis and survival of the mice, which showed the importance of FN in elastic fiber formation[79]. The assembly of FBN1, which forms a scaffold for elastin deposition[1; 80-82], is dependent on FN[83; 84]. Although FBLN4 has affinity to both FN and FBN1 *in vitro*[85], it has been shown that FBLN4 assembly directly depends on FN, not mediated via FBN1[20]. No information has been reported about FBLN5 dependency on FN. In addition, N-terminal region of LTBP4 binds to FN(Fig. ii), which is indispensable for LTBP4 matrix assembly[22]. EMILIN1 incorporation into the ECM also requires the presence of FN[86].

FBN1 does not only provide the scaffold for elastin deposition, but also FBN1- containing microfibrils constitute one of the two major components of the mature elastic fibers[1; 11]. FBN1 forms beads-on-string ECM structures[1; 87-89]. The assembly of FBN-microfibrils is a multi-step process that starts by the secretion of FBN1 proprotein which is cleaved at the N- and C-termini by proprotein convertase, furin[90-92]. Then, FBN1 multimerization via the C-terminus leads to bead like globules[93]. This facilitates N- to C-terminal interactions forming FBN1-microfibrils in a head-to-tail arrangement, which are further stabilized in bundles by lateral homotypic interactions between various regions of FBN1[94-98]. The stabilization of FBN-microfibril bundles is achieved by disulfide bond crosslinks and by transglutaminase-derived crosslinks to result in functional networks[99-101]. During TE deposition, intermolecular transglutaminase cross-links are also formed to tightly bind FBN1 to TE[102].

Mutations in FBN1 gene results in a failure in elastic fiber formation in elastic tissues, combined with other phenotypes in non-elastic tissues[81; 82; 103]. Marfan syndrome is the most common inherited fibrillinopathy, and one of its multi-tissue phenotype is an abnormal aorta due to defective elastic lamellae[104; 105]. The necessity of FBN1 in elastogenesis and development has been emphasized by several mouse models that either lack the expression of the FBN1 protein, or express either reduced FBN1 or mutated FBN1[105-108]. The *Fbn1*$^{-/-}$ mouse model is characterized by early postnatal mortality within the first two weeks after birth due to ruptured aortic aneurysms and compromised lung function[108]. Among a wide range of phenotypes, the hypomorphic mouse model *Fbn1*$^{mgR/mgR}$ develops aortic aneurysms that eventually undergo aortic rupture results in mortality around 3-4 months[107].

ELN is the core elastic fiber protein which is highly homo- and heterogeneously crosslinked[109-111]. TE does not fully acquire the ability to self-assemble and crosslink; but needs other molecules to facilitate its deposition on FBN-microfibrils and to stabilize it through an

intensive crosslinking mechanism[11; 112]. Initially, ELN is secreted into the ECM as soluble TE monomers that are deposited on FBN-microfibrils by the assistance of FBLN5, FBLN4 and LTBP4[7; 113]. FBLN4 and FBLN5 interact with TE[114; 115] and with FBN1[116] acting as adaptor molecules between FBN1 and TE. Also, both FBLN4 and FBLN5 interacts with LTBP4[19; 21]. Gene deletion of *Fbln4*, and *Fbln5* as well as *Ltbp4* in mice have provided substantial evidence for their roles in elastic fiber formation and function. *Fbln4* total knockout is prenatally lethal due to a severe elastic fibers failure in aorta and lung[115]. Deletion of *Fbln5* gene in mice resulted in disorganized elastic fibers recapitulating cutis laxa phenotype in human which presents loose skin and tortuous aortae, but the mice have a normal lifespan[117]. Similar to the *Fbln4* knockout, elastic fibers formation is largely defect in a total *Ltbp4* knockout mouse model, resulting in neonatal mortality within two weeks postnatal due to a combined effect of respiratory failure with a malformed aorta and a cardiac phenotype[19].

During and after TE deposition onto FBN-microfibrils, TE is crosslinked by LOX and other LOX family members[118; 119], which is supported by FBLN4 and FBLN5[17; 120]. Inactivation of the mouse *Lox* gene causes perinatal death with drastically defective elastic and collagen fibers, leading to aortic aneurysms, cardiovascular dysfunction, and diaphragmatic rupture[121; 122]. Although LOXL1 and other members of the LOX family appear to compensate in catalyzing cross-linking of collagen and elastin[118], they do not fully compensate the total absence of LOX. For example, *Loxl1* null mice are viable but have an abnormal deposition of elastic fibers in the uterine tract and develop pelvic organ prolapse, enlarged air sacs in lungs, loose skin with a degree of vascular abnormalities[120; 123].

EMILIN1 is another elastic fiber components that locates at the ELN-FBN-microfibril interface, where elastin and microfibrils are in a close proximity[124; 125]. EMILIN1 has binding affinity to FBLN4, FBLN5 and TE[10; 126]. This suggests EMILIN1 may function to stabilize the interactions between elastic fiber components. However, FBN1 is required for EMILIN1 deposition within the extracellular space[86]. Although *Emilin1* deficient mice did not fully recapitulate the same level of life-threatening phenotypes of the FBLN4, FBLN5 or LTBP4 knockout mice[19; 115; 117], murine *Emilin1* deficiency leads to defects in elastic fibers combined with irregular elastin deposits between the elastic laminae in the aortic wall[10].

Apart from the above mentioned key elastogenic molecules, there are other proteins associated with elastic fibers such as MFAP4, microfibril associated glycoproteins (MAGP1 and

MAGP2, respectively)[1; 127]. MAGP1 and 2 (encoded by MFAP2 and MFAP5, respectively) were first isolated from elastic fiber-associated microfibrils and thought to be involved in elastogenesis[128-130]. However, knockout mouse models of *Magp1* and *Magp2* presented intact elastic fibers[131-133]. Similarly, MFAP4 was found to colocalize only to FBN-microfibrils associated with elastic fibers[134; 135]. Nevertheless, *Mfap4*$^{-/-}$ mouse model did not present with any major defects in elastic tissues and elastic fibers developed normally[135; 136].

Although neither is required for elastic fiber assembly, MAGP1, MAGP2 and MFAP4 may promote elastin deposition onto microfibrils. In other words, there is still little known about these three proteins, whether they are essential microfibrillar components and how they might influence FBN-microfibril associated with different elastic laminae. It has been shown that the addition of MAGP1 to the N-terminal half of FBN1 accelerated the maturation of elastic-like peptides and may act as a linker protein between TE and FBN1[102; 137; 138]. Also, overexpression of MAGP2 increased elastic fiber assembly mediated by FBN1 matrix assembly[139]. While MFAP4 specifically binds to ELN/TE, desmosine, and FBN1[8; 140], MFAP4 also interacts with LOX which does not increase the effect of MFAP4 on TE coacervation[8]. Interestingly, down regulation of MFAP4 expression has been reported in Marfan syndrome related pathology[141].

Of particular interest of this study, the following sections will further described in details the three key elastic fiber proteins, ELN, FBLN4 and LTBP4.

1.5 Elastin

Initially, the soluble form of ELN, TE, is secreted to ECM after passing through the secretory pathway[142]. TE is 60-70 kDa protein encoded by a single gene. However, there is a large variety of tropoelastin isoforms as a result of extensive alternative splicing[143; 144]. Secreted TE possesses 32-34 domains (encoded by 36 exons) in which two major types of domains alternatively arranged along the protein structure[145-147](Fig. ii). TE mainly composed of hydrophobic domains rich in non-polar amino acids, and hydrophilic domains, that involve in crosslinking, rich in lysine and either alanine, or proline[146](Fig. ii). TE is the most extensible protein with a highly hydrophobic nature that forms an asymmetric coil with a protruding foot at the C-terminal tail. It is assumed that TE present a head-to-tail assembly by stacked TE monomers to create a spring-like structure[147; 148]. However, the heterogeneity of TE isoforms contributes to the structural disorder as a constitutive feature of TE that is required for the elasticity function in which the

formation of extended secondary structures is restricted[149-151]. TE tends to partially self-coacervate, as shown in test tube where a phase separation was observed when the temperature of an aqueous phase of TE increased from 25 to 37ºC[152]. This is due to the intermolecular interactions of solvent exposed lysines between TE domains number 17-27, especially domain 26[153-155].

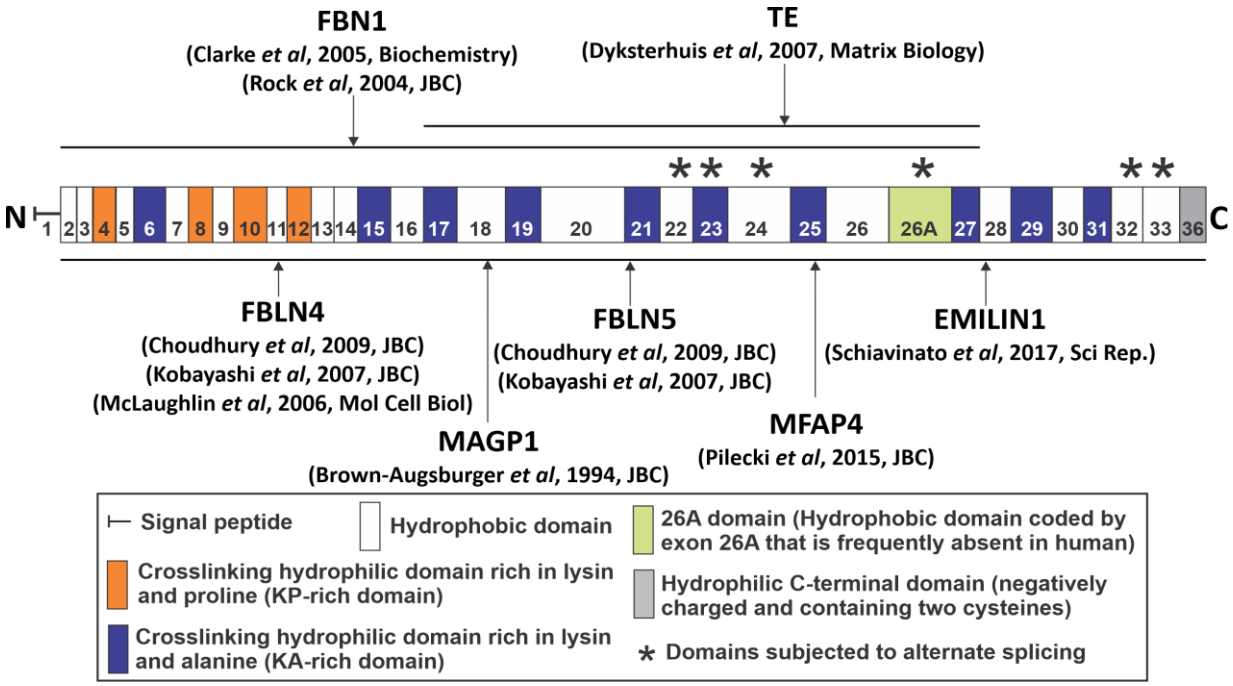

Figure ii. TE domain structure and interactions with elastogenic proteins

Schematic presentation of TE shows molecular interaction sites identified *in vitro* with elastic fiber proteins. The line encompassing all the domains indicates interactions identified with the full length TE.

Mutations in the ELN gene are associated with a variety of disorders depending on the affected functional region of the gene that a large part of these mutations is synonymous[156; 157]. The mutational spectrum in the ELN gene has been associated with supravalvular aortic stenosis (SVAS) including translocation, deletion and point mutations[158]. The main feature of SVAS is a narrowed lumina of large blood vessels caused by thickening of the media and intima in the arterial wall, including the ascending aorta, pulmonary and coronary arteries[156]. Major deletions of the ELN gene with other genes on chromosome 7 is linked to Williams-Beuren syndrome[159] defined as a congenital multisystem disorder characterized by vascular stenosis, mental retardation, and abnormal facial features[160; 161].

Mutations in the ELN gene are also associated with autosomal dominant cutis laxa (ADCL) that affected individuals have severe and early onset lung disease, including bronchiectasis and emphysema, loose skin with sagging facial skin, hooked nose, and everted nostrils, as well as abnormalities of the aorta, hernias and genital prolapse[162-164]. Also, reported point mutations in the 5' region of the ELN gene cause a mild form of autosomal recessive cutis laxa (ARCL) phenotype that is characterized by deficient dermal elastic fibers[165], which is also supported by cell culture studies[166; 167].

The absence of elastin expression in a mouse model led to similar phenotypes compared to human elastinopathy. *Eln* null mice die shortly after birth at P0-P3.5 due to aortic stenosis, and alveogenesis failure[168; 169]. Although $Eln^{+/-}$ mice had a normal life-span, ELN insufficiency in this heterogenous mouse model was associated with small aortic diameter together with other cardiovascular changes and hypertension. The phenotype was reversed by introducing a bacterial artificial chromosome expressing human elastin[170].

1.6 Fibulin-4

The fibulin family consists of eight members associated with elastic fibers, and other ECM structures[171; 172]. FBLN4 is a 53-kDa short fibulin consisting of six tandem calcium-binding EGF-like (cbEGF) domains followed by the fibulin-type C-terminus, and two N-linked glycosylation sites[173](Fig. iii). FBLN4 monomers are arranged in donut-shaped dimers while the multimers display a spheroidal shape[18]. However, the significance of this multimerization for the protein function has been poorly analyzed. It is shown that FBLN4 multimers, but not monomers or dimers, interact with heparin[18], FN and LTBP4[20].

In addition to self-interactions[18; 20], FBLN4 interacts with many ECM proteins (Fig. iii). FBLN4 has binding activity with FN, which is the master organizer in ECM scaffolding[20] suggesting a function of FBLN4 as a mediator of several elastic fiber protein deposition to FN. FBLN4 facilitates elastogenesis and collagen stability by interacting directly with pro-LOX, an essential enzyme for elastin and collagen cross-linking[17; 174]. Additionally, FBLN4 binds to the microfibril component FBN1[20; 116; 174] and to TE[115; 174]. FBLN4 interacts strongly with LTBP1forming a stable ternary complex with FBN1, speculating that FBLN4 acts as a linker in the association of LTBP1 with microfibrils[175]. FBLN4 also binds to LTBP4 which promotes

elastogenesis[19; 20]. FBLN4 has affinity to FBLN5[174] and EMILIN1[126]. The multimeric form of FBLN4 binds to heparin in calcium dependent manner[18].

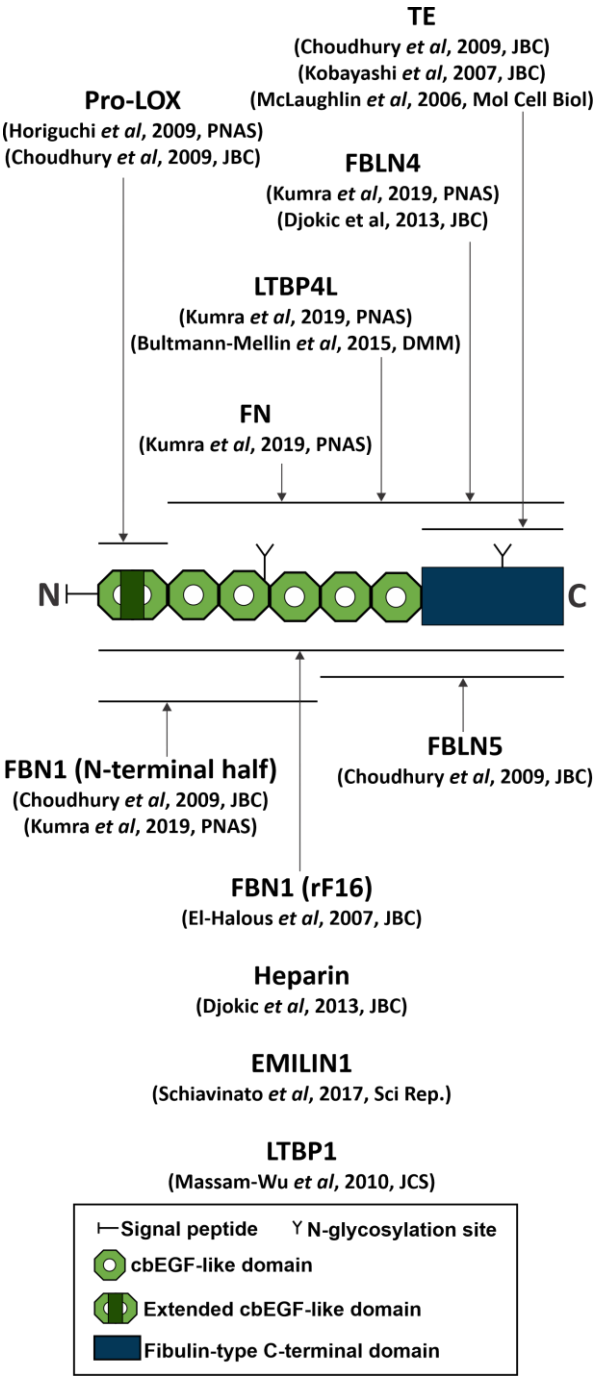

Figure iii. FBLN4 domain structure and interactions with ECM proteins

Schematic presentation of FBLN4 shows the known interacting ECM proteins involved in elastic fiber assembly. The lines indicate interacting domains of FBLN4 determined by solid-phase interacting assays, BIAcore, or CO-IP as reported in the literature. The line encompassing all the domains indicates interactions identified with the full length FBLN4.

FBLN4 can adhere to skin fibroblasts, lung fibroblasts, as well as artery and vein smooth muscle cells while it does not contain a conserved arginine-glycine-aspartic acid (RGD)-integrin

binding sequence[18]. Consequently, FBLN4 binds to cells not through RGD-dependent integrins but requires other unknown cell surface receptors.

Mutations in the FBLN4 gene (*EFEMP2* as EGF containing fibulin extracellular matrix protein-2) cause a severe form of ARCL type-1 B (ARCL1B) in human, characterized by a diverse array of defects, including aortic aneurysms, arterial tortuosity, cutis laxa, skeletal and craniofacial anomalies, as well as respiratory problems[12-15].

FBLN4-hypomorphic mice (*Fbln4*$^{R/R}$) are characterized by aneurysms and arterial tortuosity[176]. Markedly, elastic fiber assembly largely fails in FBLN4 global knockout mice and mice die prenatal or immediately after birth[115]. Interestingly, *Fbln4*$^{-/-}$ mice did not develop elastic fibers. Analysis of elastic laminae in *Fbln4*$^{-/-}$ mouse aortas by electron microscopy showed unusual elastic fiber aggregation with random distributions and rod-like filaments[115]. Lung development was also incomplete in these mice as a result of the failure in the formation of elastic laminae[115].

1.7 Latent transforming growth factor-β binding protein-4

LTBP4 is another ECM protein with important functions in elastogenesis. It is one of four members in the LTBP family[177-179]. LTBP4 is a 165-187 kDa protein composed of multiple domains and harbors five N-glycosylation sites[177-179](Fig. iv). The domains consist of two 4-cysteine domains unique to LTBP4, three TB domains, one hybrid domain and twenty EGF domains, seventeen of them are cbEGF domains[177; 178]. LTBP4 occurs as two alternatively spliced isoforms; the long isoform (LTBP4L) and the short isoform (LTBP4S) that contains only one of the two unique 4-cysteine domains[177; 178]

In addition to its role in mediating TGF-β activity[180], LTBP4 promotes elastic fiber assembly by interacting with a number of ECM proteins such as FN[22], FBN1[181], FBLN4[19] and FBLN5[21](Fig. iv). Similar to FBLN4, LTBP4 also lacks an RGD-integrin binding motif, but has cell interaction activities[18; 22] while its sequence. However, there has been no information about the cell surface receptor that interacts with LTBP4.

Mutations in LTBP4 were reported in patients with ARCL1 type C (ARCL1C) that leads to severe to lethal emphysema, pulmonary arterial stenosis, redundant skin and gastrointestinal malformations[3; 16; 182; 183]. *Ltbp4S*$^{-/-}$ mice exhibit thinner elastic fibers in the lungs but do not replicate the entire phenotype of human ARCL1C[184]. Electron microscopy of *Ltbp4S*$^{-/-}$ lungs demonstrated large globular elastic fibers that are not completely integrated with microfibrils[184].

The more severe phenotype of the *Ltbp4* global knockout mice, lacking both LTBP4 isoforms (*Ltbp4*$^{-/-}$), as compared to *Ltbp4S*$^{-/-}$ highlighted the crucial role of LTBP4L in elastogenesis and postnatal survival[19]. *In vitro*, LTBP4 knockdown in human dermal fibroblasts did not change mRNA expression levels of elastic fibers proteins including FBN1, LOX, LOXL1, FBLN5 and FBLN4, whereas elastin mRNA expression levels were increased[21]. The presence of exogenously added LTBP4S protein enhanced the deposition and assembly of the accumulated elastin[21]. This confirm the prominence of LTBP4S isoform along with LTBP4L, that both isoforms play overlapping but non-redundant roles in elastic fiber formation.

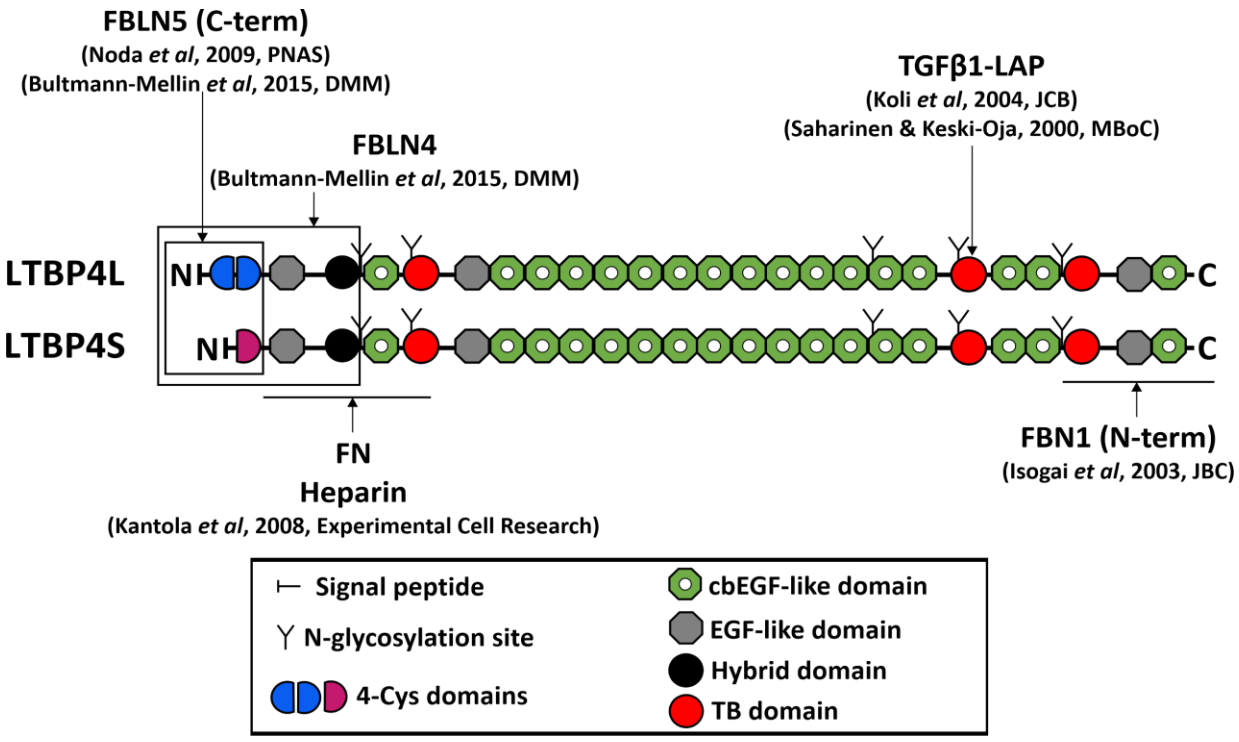

Figure iv. LTBP4 domain interactions with ECM proteins

Schematic presentation of LTBP4 showing the known interacting ECM proteins involved in elastic fiber assembly. The boxes and lines indicate interacting domains of LTBP4 determined by protein-protein interaction analyses as reported in the literature. The boxes indicate interaction sites mapped using both LTBP4 long and short forms including the variant sequences between them. Lines represent the identified interaction sites on regions with identical sequences between the two isoforms.

Interestingly, a double mutant mouse model, *Ltbp4S*$^{-/-}$*;Fbln4*$^{R/R}$, presents with a severer phenotype, compared to *Ltbp4S*$^{-/-}$ or *Fbln4*$^{R/R}$ mice, characterized by high perinatal/neonatal

mortality and severe defects in elastic fibers[19; 115; 185]. This emphasizes that the presence of both, FBLN4 and LTBP4, is critical for elastogenesis and survival[185].

1.8 Elastogenesis

Elastogenesis predominantly takes place *in utero* and in early childhood producing durable elastic networks that last until old age[146; 147]. ELN is assembled by a hierarchical mechanism includes diverse elastic protein interactions, depositions, conformational switches and crosslinking. Elastogenesis starts as early as TE and other elastogenic proteins are synthesized and secreted into the extracellular space[186]. Numerous TE monomers accumulate on a microfibrillar skeleton that is laid onto a FN matrix. Then, elastin fibrillogenesis continues close to the cell membrane until it later results in an amorphous elastin central core tightly enveloped by FBN-containing microfibrils in tissues[1; 2; 49; 51](Fig. v).

Timer reporters and lentiviral transfection techniques were recruited to follow elastic fiber synthesis at early elastogenesis in cell culture where labelled-TE was shown to assemble into micro and macro assemblies deposited on the cell surface[4; 5; 187]. Nevertheless, how other elastic fiber proteins are recruited on the molecular level during elastogenesis remains largely unknown. There are three mechanisms that have been partially elucidated for this multi-step process of elastic fiber formation regarding the functional involvement of FBLN4 and LTBP4 with other elastogenic molecules (Fig v B).

FBLN4 binds to both TE and FBN1 acting as a mediator to deposit TE onto FBN-microfibrils[85; 116; 174]. It has been shown that FBLN4 also interacts with the inactive pre-LOX, and this interaction activates LOX which consequently enhances TE polymerization[17; 115]. This suggests the dual role of FBLN4 in deposition of TE on FBN-microfibrils and in activation of LOX responsible for crosslinking (Fig. v B, left panel).

The N-terminal region of LTBP4 interacts with both FBLN4 and FBLN5 (Fig. iv)[19; 21]. Actually, evidences show a specific functional link between FBLN4 and LTBP4L, and between FBLN5 and LTBP4S[19; 21; 184; 185]. LTBP4L depends on FBLN4 for its expression as shown *in vivo* using the *Ltbp4S*$^{-/-}$;*Fbln4*$^{R/R}$ mouse model that resulted in impaired elastogenesis[185]. Yet, the exact mechanism remains to be determined. In contrast, FBLN4 depends on LTBP4L while FBLN5 depends on LTBP4S for their assembly/deposition as shown using *Ltbp4S*$^{-/-}$ and *Ltbp4*$^{-/-}$ mouse models and cell culture studies[19]. These data together distinguish the involvement of LTBP4 in

elastogenesis in two distinct scenarios; in the first, FBLN4 acts with LTBP4L while FBLN5 acts with LTBP4S in the second (Fig. v B, middle and right panel).

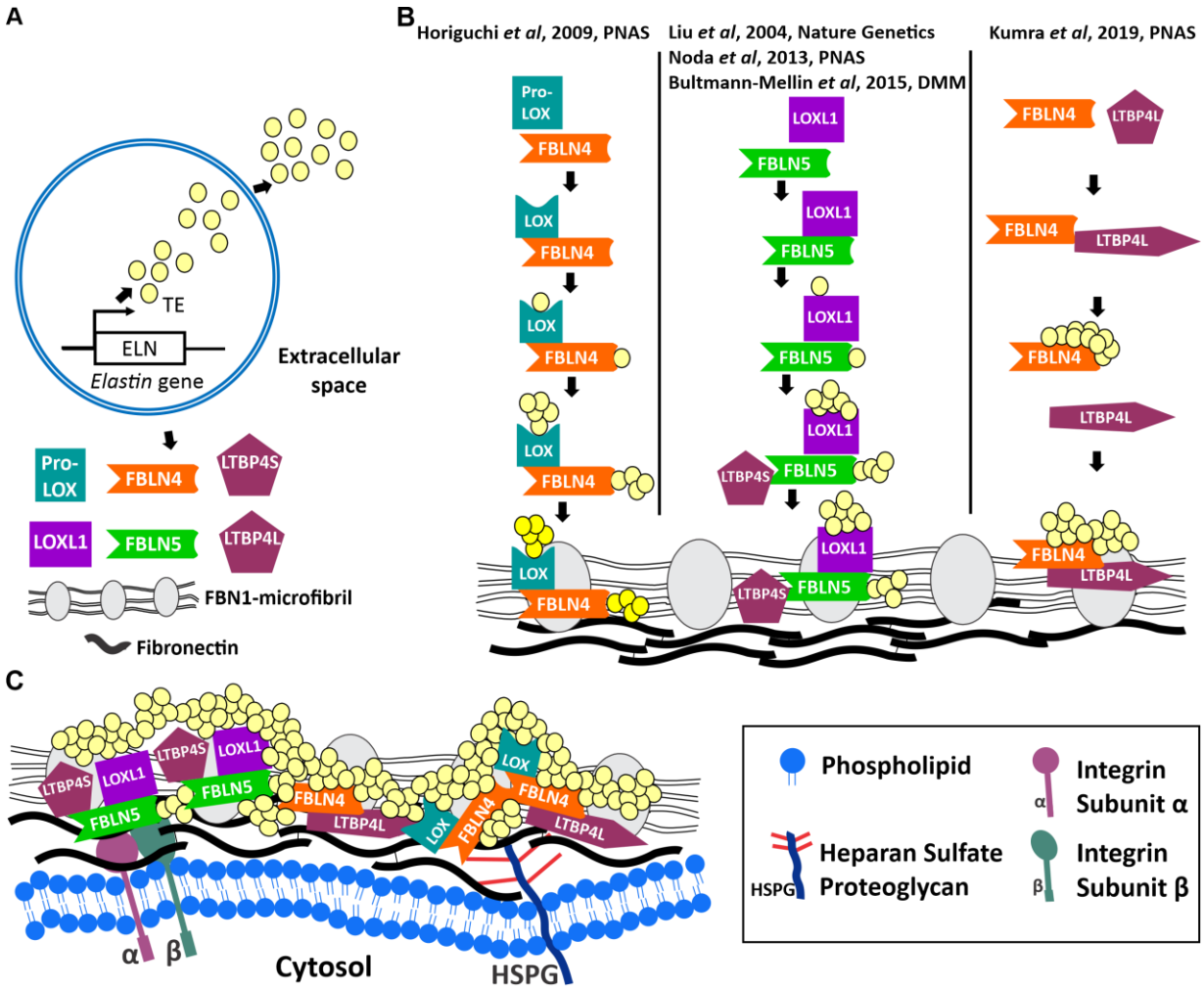

Figure v. FBLN4 and LTBP4 in early elastogenesis

Diagrammatic representation of elastic fiber assembly elucidates the involvement of FBLN4 and LTBP4 along with other elastic fiber-associated proteins. (A) Secretion of TE and elastic fiber proteins. (B) Through guidance of FBLN4 and LTBP4, TE microaggregates are deposited on the assembled FBN-microfibrils that previously deposited onto a FN matrix, and are also crosslinked by LOX enzymes. (C) The deposition of elastic fiber proteins takes place close to the cell surface in early elastogenesis before the fully mature elastic fibers separate from the cell surface to incorporate in tissue in late elastogenesis.

FBLN5 is known also to interact with LOXL1[120] and with TE[85; 174] while LTBP4 has no affinity to TE but to FBN1[181] and to FBLN5[19; 21]. This suggested the possible mechanism in which

LTBP4S guides FBLN5/LOXL1/TE complex to be deposited on FBN1-microfibrils (Fig. v B, middle panel). Recently, it was shown that a transient binding of FBLN4 to LTBP4L causes a conformational change in the LTBP4 protein from a compact to an extended shape[20]. This leads to an increased TE deposition in which FBLN4 tethers TE to LTBP4L and, in turn, the extended LTBP4L assists FBLN4/TE complex deposition onto FBN-microfibrils (Fig. v B, right panel).

While FBLN4 and LTBP4 are involved in interaction with and deposition of elastogenic proteins, they also interacts with cells[18; 22], on the plasma membrane where early elastogenesis takes place (Fig. v C). By now, it is known that FBLN4 and LTBP4 play diverse vital roles in elastin fibrillogenesis with a possible involvement of FBLN4 or LTBP4 cell interactions in a mechanistic function in elastogenesis. However, how elastic fiber formation is initiated near the cell membrane to produce mature fibers in tissue remains elusive.

1.9 Cell interactions with extracellular matrix proteins

Cells in connective tissues are surrounded by ECM. Therefore, it is not surprising that cells and ECM molecules, including elastogenic proteins, establish defined connections, communications and transduce signals through cell surface receptors. In fact, there has been significant efforts to identify the cell surface receptors that interact with the ECM molecules, and to define how cells and ECM interpret the transduced information between them[39]. Receptors on the cell membrane respond to specific extracellular recognition that further affects several cellular events. The downstream of ECM cell interactions includes focal adhesion formation, cytoskeleton organization, cell migration, cell growth and proliferation, as well as apoptosis[188-190]. ECM constitutes the cell microenvironment in which cell adhesions and spreading on ECM influence tissue development, angiogenesis and tumor metastasis[190; 191].

For many years, tissue engineering and cell biology research have progressed with considering the advantages of understanding the ECM-cell interfaces. For example, cell adhesions to FN and collagen have been used as tools in cell culture optimization[192-194]. Cell responses to interactions with MMPs have been used in applications to construct engineered tissues[189; 195]. Precoated beds with FN have been utilized to promote tissue repair and wound healing based on its cell interactions[196].

ECM proteins interact with cells directly or indirectly through diverse cell receptors. FN interacts strongly with cells through several integrins and heparan-sulfate proteoglycans, such as

$\alpha_5\beta_1$, $\alpha_v\beta_3$, and syndecan-4 (SDC4)[28; 197; 198]. FN cell interactions trigger RhoA activity and promote focal adhesion formation and cell contractions, which in turn provide mechanical forces required for FN fibrillogenesis[197; 198]. Similar to FN, FBN1 interacts with several cell receptors including $\alpha_5\beta_1$, $\alpha_v\beta_3$ and $\alpha_v\beta_6$, as well with heparan sulfate proteoglycans[199-203]. Cell adhesion to FBN1 regulates focal adhesion formation and actin cytoskeletal assembly[204]. Inhibiting FBN1 adhesion to heparan sulfate negatively affected the assembly of FBN1 into a microfibrillar network suggesting the function of FBN1 cell interactions in microfibrillar assembly[203].

TE interacts directly with several types of cell surface receptors; TE binds to $\alpha_v\beta_3$, $\alpha_v\beta_5$, glycosaminoglycans (GAGs), and elastin receptor complex (ERC) that contains elastin binding protein and neuraminidase-1[205-209]. The functional contribution of TE cell interactions with integrins and GAGs have not been investigated. However, it has been shown that ERC has preponderant role in elastic fiber formation involving in the secretion and deposition of TE[209; 210]. Disturbing ERC results in impaired elastic fibers which is associated with metabolic and cardiovascular pathology[211]. In addition, TE indirectly interacts with cells via other elastic fiber proteins such as FBLN4, FBLN5, and LTBP4[18; 22; 117; 206].

FBLN5 cell interactions are mediated by integrins $\alpha_v\beta_3$, $\alpha_v\beta_5$ and $\alpha_9\beta_1$ through its N-terminal domain[117]. FBLN5 cell adhesion play roles in cell migration and invasion[212]. Although the significance of integrin binding has been shown in FN fibrillogenesis, disturbed FBLN5-integrin binding did not affected elastic fiber assembly in the *Fbln5*$^{RGE/RGE}$ mouse model[213]. The cell interactions of FBLN4 and LTBP4 have been previously addressed[18; 22], but the responsible cell surface receptors have not been discovered. Additionally, the role of FBLN4 or LTBP4 in cell interaction and in turn in elastic fiber formation remains largely unknown.

Heparan sulfate proteoglycans and integrins have been frequently reported in cell interactions with ECM proteins particularly with elastic fiber proteins. In the following section, existing literature about these two groups of cell receptors are described.

1.10 Heparan sulfate proteoglycans

Heparan sulfate proteoglycans (HSPGs) form a large group of glycoproteins. They serve as cell surface receptors, co-receptors and adaptors. All HSPG share a common characteristic of carrying one or more covalently attached heparan sulfate chain[214]. Along with heparan sulfate

oligosaccharides, HSPGs also can carry other types of GAG chains such as chondroitin sulfate[214; 215].

Heparan sulfate is a type of GAGs that is composed of a complex unbranched carbohydrate chain identical to heparin in the chemical backbone, yet it is undersulfated[216]. Heparan sulfate and heparin (unconjugated-to-cell/free GAG) are synthesized in the secretory pathway passing through significant modifications, including deacetylation and sulfation, requiring the recruitment of several enzymes in a tightly regulated process[217-219]. The modification process conducted on heparan sulfate polysaccharides continue extracellularly by specific enzymes (e.g. sulfatases and heparanases) to remodel the contents of their chains, and consequently the function[220-222]. Also, the extracellular domains of HSGPs are exposed to protease-mediated process, shedding them off the cell surface into the ECM[223; 224]. Proteolytic shedding of HSPG extracellular domains may cause loss of Heparan sulfate function as receptors, or may change their function to role as antagonists instead[225; 226].

Heparan sulfate produced roughly by all body cell types and encoded by several genes. However, only one core protein (encoded by a single gene) carry heparin is produced by very certain cell type, mast cells[227; 228]. Heparin functions differently from heparan sulfate, as it is a crucial anticoagulant that binds to and activates antithrombin, leading to accelerated inhibition of the coagulation cascade[229]. Heparan sulfate on proteoglycans binds to a plethora of ligands including ECM proteins, growth factors, cytokines and other cell-surface receptors on the same cell membrane or in cell-to-cell communication[214]. Heparan sulfates vary in their length, location and distribution patterns on the protein core, which all contribute in their affinity to the binding epitopes. As well, the widely spaced sulfated regions over the polysaccharide chains display conformational versatility[216; 230; 231]. This diversity in the sulphation patterns and the length of heparan sulfate chains are necessary for the specific function in protein interactions[216; 232]. Heparan sulfates adopt very fine structures that accommodates a large number of specific interactions with protein ligands as theoretically analyzed using fitting models[233]. Some HSPGs present at the cell surface such as SDCs and glypicans (GPCs)[191; 234; 235], and others are secreted to the ECM as adaptors link between ECM proteins and/or between ECM proteins and cell-surface receptors such as perlecan, agrin, and collagen XVIII[236].

1.10.1 Syndecans

The SDC family consists of four distinct members, SDC1-4 that share similar structural domain arrangements. Each SDC has an extracellular domain (ectodomain) at the amino-terminal end, followed by a transmembrane domain and tail-like intracellular domain (cytoplasmic domain) at the carboxyl-terminal end[237]. The SDC domain structure is highly conserved cross all syndecans with an ancient history as evolved from one coding gene in *C. elegans* to 4 copies present in *Homo sapiens*[238; 239]. Each SDC protein is embedded in the cell membrane to serve as cell surface receptor in homo- or hetero-dimers with other SDC members[240]. SDCs also display hierarchal clustering that homotypic and heterotypic interactions form larger oligomers of SDC2[240]. SDC dimerization/oligomerization occurs via non-covalent links between their transmembrane domains[241]. In addition, SDCs form receptor complexes with other cell membrane proteins such as integrins[242].

The ectodomains of SDC have the most variable sequences between the four members, which carry heparan sulfate, and some of the SDC ectodomains possess also chondroitin sulfates[243]. The distribution of covalently attached heparan and chondroitin sulfates on SDC ectodomains divides SDC into two groups. One group consists of SDC1 and 3 that carry heparan sulfate chains located at the distal ends of the ectodomain and chondroitin sulfate chains at the proximal end near the cell membrane. The other group of SDCs includes SDC2 and 4 that each contains only heparan sulfate chains at the distal end toward their N-termini[223; 228]. The ectodomain of all mammalian syndecans shed from the cell surface as an intact proteoglycan into the ECM cleaved by proteases after a specific duration of cell-surface associated life-span[223; 239]. As the SDC ectodomains provide the ability to interact extracellularly with many proteins, the cytoplasmic domains endow them with the capacity to response intracellularly initiating signaling processes[244]. SDC cytoplasmic domain has three regions: conserved domain-1, variable domain, and conserved domain-2. The variable domain differentiates a unique cell signaling to each SDC. The SDC transmembrane domains are the anchoring units span the plasma membrane and the most conserved domains cross SDCs[245].

So far, it is not clear if mutations in any SDC in human can lead to a disease. The absence of reports about disease conditions associated with SDC genes is possibly due to compensatory mechanisms between SDCs which makes disease phenotypes subtle or undetectable. However, variants in the expression patterns of SDC proteins have been associated with cardiac fibrosis,

fibrodysplasia ossificans progressive (a disabling disorder of progressive heterotopic bone formation), muscular dystrophy, and lung cancer, among others[246-250].

Knockout animal models have been described for *Sdc1, 3* and *4*, but not for *Sdc2*. *Sdc1* deficiency in mice has been utilized to analyze the role of its ectodomain in tumorigenesis and in the inflammatory response as a cell membrane protein and as a soluble ectodomain (CD138) in the blood stream[251-253]. *Sdc1* null mice develop normally[251; 252]. However, *Sdc1*deficiency in mice was associated with dysregulation of inflammatory markers and aggravation of leukocytes in the ocular vasculature and kidney after treatments to enhance inflammation[252; 253]. In addition, a study included Wnt-1 signaling to induce mammary gland tumorigenesis showed that SDC1 is a critical modulator in breast carcinogenesis[251]. *Sdc1* null mice subjected to corneal and skin wound healing, showed defects in cell proliferation and variations in integrin expression and localization at the wounded tissues combined with prolonged hypoplasia[252]. In addition to inhibited angiogenesis, delays in wound healing were observed in *Sdc1*$^{-/-}$ mice as well as in *Sdc4*$^{-/-}$ mice[254]. A remarkable decrease in ADAMTS-5 activity in *Sdc4*$^{-/-}$ mice have been linked to the regulatory role of SDC4 in inducing collagen type X-producing chondrocytes, and in inhibiting the breakdown of cartilage matrix during osteoarthritis via a direct interaction with ADAMTS-5[255]. The *Sdc3*$^{-/-}$ mouse model was exclusively analyzed for brain development and shown to have impaired neural migration[256]. *Sdc* knockdown in both *C.elegans* and *Drosophila* caused disrupted neuronal migration and defected axon guidance[257; 258].

The long evolutionary history of SDCs is indicative of important functions. However, these functions have not been profoundly investigated elastogenesis.

1.10.2 Glypicans

GPCs constitute with SDC the two major families of cell surface HSPGs[259]. GPCs contain six GPC members, GPC1-6, that share a similar protein core domain structure with moderately conserved amino acid sequences[260; 261]. GPCs evolutionarily old. Human has six members while there are two GPCs in *Drosophila* (referred as division abnormally delayed, Dally, and Dally-like), and one in *C. elegans*[260; 262-265]. The GPC protein structure consists of two domains, cysteine-rich N-terminal domain and hydrophobic C-terminal domain[266]. All GPC core proteins have fourteen conserved cysteine residues that engage in forming disulfide bonds resulting in a highly compact globular protein core of the N-terminal domain (globular domain)[260]. GPCs are peripheral

membrane proteins situated on the extracellular side of the plasma membrane. GPCs are covalently linked to the cell membrane at their hydrophobic C-termini via a glycosylphosphatidylinositol (GPI) lipid anchor[260]. Unlike SDCs, heparan sulfate chains on GPC are located at the C-terminal domain close to the cell membrane, rather than the distal location on SDC ectodomains[266]. However, GPCs also undergo shedding into the extracellular space through cleavage of the protein core at a furin cleavage site or by removal of the GPI lipid anchor[267; 268].

Distinct GPC proteins present cell surface receptors that mediate significant functions by active interactions with other molecules at the cell membrane extracellularly and intracellularly[269; 270]. By that, GPCs modulate the signaling of multiple pathways influenced by interactions with ECM proteins and growth factors, such as bone morphogenetic protein (BMP), yes associated protein (Yap) and hedgehog (Hh) signaling[270-273].

In human, mutations in *GPC* genes have been only reported in *GPC3, GPC4* and *GPC6*[274; 275]. Deletion and duplication mutations in *SDC3* and *SDC4* genes are associated with Simpson-Golabi-Behmel syndrome (SGBS) that manifests withprenatal and postnatal overgrowth and morphological phenotypes including craniofacial and skeletal abnormalities[276-278]. SGBS causes in some individuals additional phenotypes affecting several body tissues such as congenital heart defects, dysplastic kidneys, hernias, vertebral and rib abnormalities[277]. Deletion mutations in *GPC3* found in many SGBS families have been associated with Wilms' tumor, the most common kidney carcinoma in children, particularly males[279]. Mutations in *GPC6* cause recessive omodysplasia characterized by skeletal dysplasia with severe limb shortening and facial dysmorphism[275].

Gene deletion mouse models have been generated for all *Gpc* genes, except *Gpc5*. Some of them were found to be viable and fertile, except *Gpc3*$^{-/-}$ mice that died before weaning, and *Gpc6*$^{-/-}$ mice that display embryonic lethality[280-282 283-285]. Mice lacking *Gpc1* showed a highly significant reduction in the brain size which was associated with a transient decrease in fibroblast growth factor signaling during embryonic brain development[280]. A null mutation in murine *Gpc2* was found with no abnormalities[281]. Consistent with the phenotype observed in human, *Gpc3*$^{-/-}$ mice were affected by overgrowth, limb defects, and renal cystic dysplasia[283]. These phenotypes are due to impaired Wnt and BMP signaling pathways[286-288]. Mutations in the *C. elegans Gpc* (*lon-2*), closely related to human GPC3, also produced increased body size phenotype with a significantly greater body length due to irregular BMP-like signaling[265]. *Gpc4* knockout mice

exhibited juvenile hyperactivity and adult social interaction deficits caused by a damage in the synaptic transmission system[282; 289; 290]. Podocyte-specific or systemic *Gpc5* knockdown mice showed resistance to podocyte injury in the nephrosis model[291; 292]. *Gpc6*- null mice died before or at birth, and the embryos showed reduced body size and bone abnormalities[285]. Chondrocyte-specific *Gpc6* null mice survived to adulthood but displayed shorted long bones, confirming the reported phenotype in human due to the mutated GPP6 gene that causes autosomal-recessive omodysplasia[285].

1.11 Integrins

Integrins constitute a large family of cell adhesion receptors which in total are encoded by 26 distinct genes in mammalians[293]. Integrin genes code for 18 alpha (α) subunits and 8 beta (β) subunits that all fully span the plasma membrane[294]. Integrins form non-covalently associated heterodimers of α and β subunits, that in total form 24 different integrins[293].

Integrins are larger comparing to SDC and GPC core proteins. Both α and β integrins consists of three major domains: the N-terminal ectodomain, the single-pass transmembrane domain, and the cytoplasmic tail that contains the C-terminus[295]. The total protein sequence of each integrin varies between 750-1000 amino acid residues but typically α integrin subunits are larger than β subunits[296]. All α subunits have four to five ectodomains starting at the N-terminus with a seven-bladed β-propeller domain, a thigh domain, two calf domains. Nine α integrins have an α-I domain inserted in seven bladed β-propeller[297]. The extracellular region of β integrins contains eight ectodomains, a plexin-semaphorin-integrin (PSI) domain toward the N-terminus, a hybrid domain inserted in the PSI, β-I domain which is inserted in the hybrid domain, all are followed by four EGF domains and one β-tail domain[297].

The divalent cations such as Ca^{2+}, Mg^{2+} and Mn^{2+} affect integrin function, i.e., ligand binding affinity to integrins is strikingly regulated in divalent cations-dependent manner[298; 299]. Divalent cations are essential for stabilizing integrin heterodimers, and modulating integrin-ligand binding by either activating or suppressing[299; 300].

Integrin-ligand bindings have been intensively investigated, including integrin-ECM proteins, -growth factors, and -cells[295]. These interactions of integrins mediate cell attachment, focal adhesion formation, cytoskeletal remodeling, and transmit various downstream/upstream

signals[294]. Importantly, integrins have a predominant role in cell sensing and responding to ECM microenvironment shown in cell contraction, migration, differentiation and survival[301].

A number of ECM proteins contain an RGD motif, which mediates cell-matrix interactions by binding toRGD-dependent integrins[302]. However, other integrin-binding motifs have been identified such as LDV or GFOGER sequences[302; 303]. ECM protein binding to integrins causes conformational changes in the cytoplasmic domains that results in recruiting different cytosolic proteins[303]. A significant mechanism is that talin links the cytoplasmic domain of integrins to the cytoskeleton upon ECM interaction with integrin ectodomains[304]. Important components of this signaling complex are Src-family kinases, focal adhesion kinase (FAK), vinculin and paxillin[295; 305].

Human mutations have not been reported in α_v, β_1, and β_5 integrins. However, alteration in the expression of some of these integrin genes have been reported in other gene mutations and disease conditions like in Marfan syndrome, autosomal dominant osteoporosis and cancers[306-309]. Mutations have been reported in other integrin genes like α_3, α_6, α_{2b}, β_2, and β_3. Reported mutations in α_3 integrin confer pulmonary fibrosis, epidermolysis bullosa (fragile blistering skin disease) and major renal developmental faluire[310; 311]. Missense mutations in α_6 integrin also cause a sever form of epidermolysis bullosa[312]. Mutations in the β_2 subunit caused an absent or reduced expression are associated with leukocyte adhesion deficiency syndrome. This syndrome is characterized by a massive leukocytosis with defective T cell activation, absent neutrophils extravasation into infected tissues and impaired wound healing[313]. Mutations in the α_{2b} and β_3 subunits result in Glanzmann's thrombasthenia, an inherited bleeding disorder due to defective platelet function[314].

It became obvious that each of the 26 integrin subunits plays specific, non-redundant important roles as evidenced by the phenotypes of the respective knockout mice. Ablation of murine integrin genes resulted in various phenotypes *in vivo,* which some of them are lethal, including the deletion of α_3, α_4, α_5, α_6, α_9, α_v, β_1, β_4 and β_8[315]. Knocking out integrins in mice displayed a wide spectrum of malformations from variations in collagen synthesis, and cardiovascular development to defects in lungs, skin, kidneys, brain, inflammatory response and circulatory systems[316; 317]. Although mice could survive the gene deletion of several integrin genes, they showed multiple severe to moderate phenotypes except the deletion of β_5. These mice were normal and fertile with no apparent phenotype[318]. However, loss of β_5 in estrogen-deficient mice accelerated osteoclastogenesis indicative of its inhibitory role in osteoclast formation[319].

1.12 Rationale

The complex mechanisms that synthesize highly crosslinked elastin associated with fibrillin-containing microfibrils initially takes place close to the cell membrane of elastogenic cells[4; 5; 187; 320]. This suggests that cellular interactions with elastin and elastic fiber associated proteins are critical for this process. Despite the fact that mutations in human FBLN4 and LTBP4 cause genetic disorders, including ARCL1B and ARCL1C characterized by deficiencies in elastogenesis, the molecular roles of these elastic fiber associated proteins are not entirely understood. Especially, the molecular consequences of their cell interactions on elastogenesis remains completely unknown. Based on the importance of FBLN4 and LTBP4 in elastogenesis and the paucity of mechanistic insights, the focus of this project is on the roles of these two important proteins in elastogenesis. The study seeks to decipher the biochemical and functional properties of FBLN4 and LTBP4 in relationship to cells and elastogenesis. The hypothesis is that FBLN4 and LTBP4 cellular interactions play critical roles in elastogenesis.

1.13 Objectives

The project has two main goals which are to address the identity of the FBLN4 and LTBP4 cell receptors, and to explore their roles in elastogenesis.

To fulfill the main goals, the project splits in five specific aims:

1) To produce and characterize FBLN4 and LTBP4 recombinant proteins.
2) To analyze cell interactions of FBLN4 and LTBP4.
3) To map cell interaction sites on FBLN4 and LTBP4.
4) To identify cell receptors for FBLN4 and LTBP4.
5) To determine the functional consequence of the FBLN4 and LTBP4 cell receptor interaction related to elastogenesis.

2. MATERIALS AND METHODS

2.1 Cell culture

We employed various human primary elastogenic cells including normal skin fibroblasts (NSF), aortic smooth muscle cells (HASMC), umbilical arterial and venous smooth muscle cells(SMC and CRL-2481, respectively). The used NSF and SMC were collected from different donors. The ethical approval number for NSF is PED-06-054 while SMC were gifted by the donor. Fetal-HASMC were purchased from ScienCell (CAT# 6110, LOT#21330) obtained from a 21-week-fetal age, no information about sex or race are available. While adult HASMC were purchased from ThermoFisher Scientific (CAT# C0075C, LOT# 1807979) obtained from a 28-year-old American-Asian male donor. CRL-2481 cells were obtained from American Type Culture Collection (ATCC®, CAT# CRL-2481™).

NSF and CRL-2481 were maintained in Dulbecco's Modified Eagle's medium (DMEM) containing 10% fetal bovine serum (FBS), and penicillin/streptomycin (antibiotic/antimycotic) supplemented with L-Glutamine (PSG) at final concentrations of 100 IU, 100 µg/ml and 2 mM; respectively. Both HASMCs were cultured in 231 medium (Gibco, CAT# M231500) supplemented with 10% FBS, PSG and Smooth Muscle Growth Supplement (SMGS, Gibco, CAT# S-007-25) which provides 5% more serum. While SMC were maintained in DMEM:F12 1:1 ration containing heat-inactivated 10% FBS (HI-FBS) and PSG. HI-FBS were prepared by incubating FBS in water bath at 56°C for 30 minutes with gently shaking every 10 minutes.

To differentiate HASMCs from synthetic to contractile phenotype, cells were cultured to reach 70-80% confluency in media containing 15% serum. Then, cell monolayers were washed with PBS and maintained in 231 medium supplemented with 1% FBS and 1% PSG for 7 days before performing a differentiation related experiment. HASMC differentiation from synthetic to contractile phenotype was confirmed by positive immunofluorescence (IF) staining for alpha smooth muscle actin (αSMA).

In addition, two Chinese hamster ovarian cell lines: CHO-WT and CHO-677 were used in this study. CHO-WT refers to the wild type cells whereas CHO-677 is mutant lacking the expression of two enzyme activities (N-acetylglucosaminyltransferase and glucuronyltransferase) that are required for synthesis of heparan sulfate[321]. Both CHO cell lines were obtained from ATCC (CAT# CHO-K1 CCL-61™ and pgsD-677 CRL-2244™, respectively), and were cultured in DMEM:F12 1:1 ration supplemented with 10% FBS and PSG.

Human embryonic kidney (HEK) cell lines 293 (DSMZ-German Collection of Microorganisms and Cell Cultures GmbH, CAT# ACC 305) and 293-EBNA (ATCC, CAT# 293 c18 CRL-10852™) were used for transfection and producing recombinant proteins including FBLN4, LTBP4 and syndecan ectodomains. HEK cell lines were maintained in DMEM containing 10% FBS and PSG. The culture medium contained 250 µg/ml G418 as a selecting marker for 293-EBNA since they express recombinant EBNA1 by a plasmid containing G418 resistance element.

All used cells were maintained in the respective media contents (outlined above) at 37ºC in humidified incubator supplied with 5% CO_2. Cell cultures were regularly examined using an inverted microscope.

Upon reaching confluency, cells were subcultured using trypsinization. Cells were briefly washed with phosphate buffered saline (PBS) after discarding from the culture media. Then, cell monolayers were treated with 0.05%Trypsin containing 0.53 mM EDTA for 1-3 minutes at 37°C incubator to allow cell detachment. Trypsin was neutralized by addition of serum containing medium followed by a proper homogenization of the suspended cells. The cells were centrifuged to obtain the cell pellets, which were re-suspended into fresh medium and distributed in new culture flasks. In addition, cells were counted for experimental setting after trypsinization using a hemocytometer.

2.2 cDNA cloning of FBLN4 and LTBP4 full length and deletion mutants

To analyze the cell interactions of FBLN4 and LTBP4 with their cell receptors, we produced human recombinant proteins. In previous work, FBLN4 full length (F4_FL) and subfragments F4_N1, F4_2-5 and F4_6C, as well as full lengths of both LTBP4 isoforms long and short (L4L and L4S, respectively) were designed and recombinantly produced successfully[18; 20] (Fig. 3 A & Fig. 5 A).

2.2.1 Cloning strategy

The protein yield for **F4_N1** was high (~1.2 mg/L), whereas **F4_2-5** and **F4_6C** yielded very little protein (~0.1 mg/L) which was difficult to purify. We reasoned that the addition of the first N-terminal domain might help in protein synthesis/secretion. Therefore, several new deletion fragments were designed with most of them containing the N-terminal domain, but without several other domains: **F4_N1-3**, **F4_N1-5**, **F4_N1,C**, **F4_N1,6C**, **F4_N1,4-6C** and **F4_4-6**(Fig. 3 A). Similarly, a set of LTBP4 recombinant constructs were designed (Fig. 5 A) to produce the LTBP4

N-terminal half for both isoforms (**L4L-N** and **L4S-N**, respectively) and the C-terminal half (**L4-C**).

To ensure proper translation into the endoplasmic reticulum, protein folding and secretion, all FBLN4 and LTBP4 constructs were designed to contain signal peptide sequence at the 5' end. FBLN4 constructs were designed with a heterologous signal peptide (from BM40). LTBP4 deletion mutants L4L-N and L4S-N were constructed with the endogenous signal peptide, however, the L4-C construct was designed with a BM40 signal peptide.

All FBLN4 and LTBP4 constructs were engineered to contain eight consecutive histidine residues on their carboxyl terminus to facilitate protein purification using nickel-chelating chromatography. For some constructs for which existing antibodies were not sufficiently reactive were designed with an additional V5 epitope at the carboxyl terminus preceding the His-tag, to facilitate specific detection.

We used two vectors for cloning FBLN4 and LTBP4 fragments: pCEP4 and pcDNA3.1(+), respectively. Both vectors contain an ampicillin (Amp) resistance element sequence for bacterial selection. However, the transfected mammalian cells with pCEP4 plasmid are selectable using hygromycin B (Wisent Inc, CAT# 450-141-XL) whereas pcDNA3.1(+) plasmid are selectable using G418 (Wisent Inc, CAT# 450-130-QL). Stable 293-EBNA clones were generated for all FBLN4 constructs cloned in the episomal pCEP4 plasmid, while stable recombinant 293 clones were generated for LTBP4 constructs cloned in pcDNA3.1(+) plasmid. For each FBLN4 and LTBP4 fragment, the transfected HEK cells were tested for recombinant protein expression using Western blotting and SDS-PAGE.

2.2.2 Insert to vector ligation

The vectors pCEP4 and pcDNA3.1(+) were used to clone FBLN4 and LTBP4 recombinant proteins, respectively. Designed gBlocks contained the sequence of the recombinant cDNA of each FBLN4 fragment. Unique restriction enzymes were used to linearize the vectors for inserting each gBlock appropriately. For LTBP4, the same restriction enzymes were used to digest gBlocks and to linearize pcDNA3.1(+) plasmid. The linearized plasmids were ligated to each insert using Gibson assembly strategy for FBLN4 gBlocks to pCEP4, while T4 DNA ligase was used to ligate LTBP4 gBlocks to pcDNA3.1(+).

For Gibson assembly, NEBuilder HiFi DNA Assembly Cloning Kit (New England BioLabs, CAT# E5520S) was used. The kit allows different sizes of DNA fragments with overlap

sequences of 15–80 bp to ligate in the presence of DNA ligase, 3’ exonuclease and DNA polymerase in the same reaction buffer. This strategy worked efficiently with FBLN4 gBlocks ligation to pCEP4 vector. However, the sequences of LTBP4 gBlocks were GC-rich and long which makes Gibson assembly less efficient. In order to overcome this limitation, T4 DNA kit containing 10 mM ATP in the reaction buffer (New England BioLabs, CAT# M0202S) was used for LTBP4 gBlock ligation into the pcDNA3.1(+) vector. The vector:insert ratio used in the ligation was 1:3 for FBLN4 constructs and 1:10 for LTBP4 constructs. The ligation reaction was performed according to the manufacturer’s instructions using 50 ng vector for each reaction. Ligation products were freshly used for subsequent transformation of competent bacteria.

2.2.3 Competent bacteria transformation

The competent cells for transformation were chemically competent E.coli strain NEB 5-alpha, High Efficiency (New England BioLabs, CAT# C2987H). For each ligation product, 2 µl of the chilled assembled plasmids, containing about 25-50 ng DNA were transferred to one vial of 50 µl competent cells thawed on ice, mixed gently by flicking the tube 4-5 times avoiding vortexing. The mixture of each was placed on ice for 30 minutes, followed by heat shock at 42°C for 30 seconds and promptly placed back to ice for 2-5 min. Then, 250 µl of room-temperature SOC outgrowth media (New England BioLabs, CAT#B9020S) were added to each vial. A suspension of transformed bacteria with SOC media was transferred to a 13 ml bacterial vial and incubated at 37°C for 60 minutes tilted and shaken vigorously at 250 rpm. From each transformed bacteria vial, a volume of 20-200 µl was spread on selecting agar plates (10% Tryptone, 5% Yeast Extract, 10% NaCl, pH 7, 20% agar, 100 µg/ml ampicillin). The plates were warmed to room temperature prior plating. The bacteria suspension growths were evenly spread to allow growth of well-spaced colonies. Bacterial clones grown on the agar dishes were counted in a relation to the clone number of bacteria grown on the background agar plates which were transfected with ligation products of vector only (without inserts). A number of 4-10 individual clones were picked and each transferred to one 13ml bacterial tube containing 2 ml selecting Amp-Lysogeny Broth (LB: 10% Tryptone, 5% Yeast Extract, 10% NaCl, pH 7, with 100 µg/ml ampicillin), and incubated at 37°C to grow for 8-10 hours with shaking vigorously at 250 rpm. Then, 1 ml of the bacterial growth for each clone was used for mini DNA preparations using NucleoSpin Plasmid Kit (MACHEREY-NAGEL, CAT# 740588.250) according to the manufacturer’s instructions. The DNA minipreps for each clone were analyzed by restriction analysis with appropriate enzymes. Digested plasmid

products were analyzed using agarose gels to determine the positive clones. Then, 2-3 positive clones per construct were Sanger sequenced at the McGill University and Genome Quebec Innovation Centre (Montréal, Québec, Canada). For each FBLN4 and LTBP4 recombinant construct, at least one clone was confirmed with the correct DNA insert and the absence of any mutations. High quality plasmid DNA was prepared using NucleoBond Xtra Maxi Kit (MACHEREY-NAGEL, CAT# 740414.10) according to the manufacturer's instructions. The DNA from these purifications were used for subsequent transfection of HEK cells.

2.2.4 HEK cell transfection

For recombinant protein production in the mammalian system, HEK cells were transfected with 50 µg plasmid DNA of the FBLN4 or LTBP4 constructs when reached about 25% confluency in T175 flasks. The circular pCEP4 plasmids of FBLN4 constructs were transfected to 293-EBNA cells because pCEP4 contains the EBNA element. Whereas pcDNA3.1(+) plasmids of LTBP4 fragments were linearized first, and transfected to 293 cells. The pcDNA3.1(+) plasmid of LTBP4 constructs were linearized using a unique restriction enzyme that can cut the plasmid DNA only in one site where is not located in the insert sequence, the promoter region, or G418 sequence. PvuI restriction sequence was found only in one site in all LTBP4 plasmids in the Amp resistance sequence. For that, PvuI-HF (New England BioLabs, CAT# R3150S) was used to linearize the pcDNA3.1(+) plasmids containing LTBP4 constructs overnight at 37°C. Fully linearized plasmids were confirmed on analytical agarose gels prior to the enzyme heat inactivation at 62°C for 20 min. The linearized pcDNA3.1(+) plasmids of LTBP4 constructs were ethanol precipitated in two steps. First, the linearized plasmids were incubated with a mixture of 1:10 3M sodium acetate, pH 5.2 and 3 volumes of absolute ethanol at -80°C for 30 minutes, followed by spinning at 12,000 x g for 15 minutes at 4°C. Second, after discarding the supernatant, the DNA pellets were washed twice with 70% ethanol followed by centrifugation at 12,000 x g for 15 minutes at 4°C at each wash. The DNA pellets were air dried and resuspend in sterile d.H_2O.

The circular pCEP4 plasmids for FBLN4 constructs as well as linearized pcDNA3.1(+) plasmids for LTBP4 constructs were used to transfect into HEK cells using Lipofectamine 2000 (Invitrogen, cat#11668-019). HEK cells were first cultured in T175 flasks to reach about 50% confluency for transfection. For each plasmid, 75 µl Lipofectamine 2000 was diluted with 1250 µl Opti-MEM medium (Gibco, CAT#31985-062). Similarly, the 50 ng of each plasmid DNA was diluted in 1250 µl Opti-MEM medium. The diluted DNA and Lipofectamine 2000 were mixed

gently in a 1:1 ratio and incubated for 20 minutes at room temperature. HEK cells from one T175 flask were detached using trypsinization and suspended in 12.5 ml fresh culture media for each plasmid transfection. The pre-incubated plasmids/Lipofectamine 2000 mixture was then added to the cell suspension, followed by cell seeding to a new T175 flask. The transfected cells were incubated for 48-72 hours and monitored every day. The transfection media was replaced by fresh selection media containing the selection marker appropriate for each HEK cell line and according to the transfecting plasmid. The selection markers are G418 and hygromycine for the transfected cells with the plasmids of FBLN4 constructs, and only G418 for the transfected cells with the plasmids of LTBP4 constructs (media information detailed in section *2.1 Cell culture*). The selection was performed on subconfluent cells which were subcultured to new flasks upon reaching to 70-90% confluency. After 7 days of selection, the transfected cells were tested for the recombinant protein expression (see section *2.2.5 Test for recombinant protein expression*). Transfected cells confirmed for the expression of the recombinant proteins, were further expanded in cultures for protein purification.

2.2.5 Test for recombinant protein expression

For each transfection with a plasmid of FBLN4 or LTBP4 constructs, a spare T75 flasks was used for protein expression screening. When cells reach 90% confluency, the selecting medium was discarded and cells were washed with HEPES buffer (20 mM HEPES, 150 mM NaCl, 2.5 mM $CaCl_2$, pH 7.4, autoclaved) and then 12 ml of serum free conditioned media were added for 2-3 days. The conditioned medium was then collected and analyzed for the recombinant protein secretion. The total protein in the collected conditioned media was precipitated using trichloroacetic acid (TCA). To every 1 ml of conditioned media, a 391 µl amount of freshly prepared TCA/Triton X-100 mixture (139 µl of 1% Triton X-100 in H2O + 252 µl of 55% TCA) was added, followed by vortexing for 30 seconds and incubated for 10 minutes on ice. The tubes were then centrifuged at the maximum speed (12,000 x g) for 10 min at RT. Supernatants were discarded and the precipitated protein pellets were washed two times with 100% acetone, each followed by centrifugation at the maximum speed for 10min at room temperature. Protein pellets were air dried and resuspended in 1x SDS-loading buffer (5x SDS-loading buffer: 250 mM Tris pH 6.8, 30% glycerol, 10% SDS, 0.1% bromophenol-blue) either under non-reducing or reducing conditions by the addition of 100 mM dithiothreitol (DTT). TCA-precipitants were separated on

sodium dodecyl sulfate poly-acrylamide gel electrophoresis (SDS-PAGE) and analyzed using Coomassie Brilliant Blue staining and Western blotting.

2.3 Recombinant FBLN4 and LTBP4 protein preparations and purification

All recombinantly engineered FBLN4 and LTBP4 constructs are histidine tagged on their carboxyl terminus (C-terminus). Inclusion of a His-tag facilitates protein purification by immobilized metal affinity chromatography (IMAC) using His Trap columns that contains pre-charged Ni^{2+} Sepharose medium (GE Healthcare). Recombinant FBLN4 and LTBP4 proteins were purified from the collected conditioned media from the transfected HEK cells grown on triple layer flasks. This allowed the recombinant FBLN4 and LTBP4 proteins to have the signal peptide cleaved, and to undergo proper folding and post translational modifications.

The transfected HEK cells expressing the recombinant proteins were expanded to eight T175 triple layer flasks, each contains 60 ml selection complete medium. When the transfected cells reach 100% confluency, the cells were first washed with HEPES buffer (20 mM HEPES, 150 mM NaCl, 2.5 mM CaCl2, pH 7.4, autoclaved), followed by the addition of 60 ml serum free medium supplemented with PSG per flask. The conditioned medium was collected every 2-3 days and replaced with fresh medium until the cell monolayers detached after ~12-15 media collections. The collected conditioned medium was centrifuged at 6000 rpm at 4°C. Cell pellets were discarded and the medium was treated with 100 µM phenylmethylsulfonyl fluoride (PMSF) under stirring for 15 min at room temperature, to be stored in -80°C until the subsequent recombinant protein purification.

2.3.1 Crossflow filtration

Since purifying our recombinant FBLN4 and LTBP4 proteins requires collection of large volumes of conditioned media, there was a need to dialyze and concentrate. Thus, recombinant proteins in the conditioned media were concentrated using crossflow filtration (tangential flow filtration)[322] prior to chromatographic purification. This allows to concentrate about 2-3 L of conditioned medium to 40-50 ml for the next step of nickel-chelating chromatography.

2-3L of collected conditioned medium containing the secreted recombinant protein were thawed and filtered through 5.0 µm nitrocellulose filter membrane (Millipore, CAT# SMWP09025). Then, KrosFlo Automatic Backpressure Valve System (Spectrum Laboratories Inc, RESEARCH II TFF Model) was used for crossflow filtration. The crossflow system was

connected with a fiber filter and a suitable size of Masterflex® L/S® pump tubing (Cole-Parmer, CAT# ZN-96242). An appropriate dialysis fiber filter was selected to have pore size two times smaller than the molecular weight of the targeted recombinant protein. After connecting the crossflow system, the fiber filter was washed with 500 ml d.H_2O, followed by a wash with 500 ml HEPES-NaCl buffer (20 mM HEPES, 500 mM NaCl, pH 7.2). Then, the conditioned medium was passed through the fiber filter, followed by 2 L of HEPES-NaCl buffer. The concentrated recombinant protein in the filter fiber was flushed back with 30 ml HEPES-NaCl buffer to the reservoir bottle to collect the concentrated start material (SM). The SM was centrifuge at 5000 x g for 15 min at 4°C. Then, the SM supernatant was filtered using 0.45 µm SFCA filter (Corning Inc, CAT#431220) and transferred to a new tube, ready for recombinant protein purification that is detailed next (see *2.3.2 Nickel-chelating chromatography*).

2.3.2 Nickel-chelating chromatography

Recombinant proteins were purified from SM through Ni-chelating chromatography. An ÄKTA Avant liquid chromatography system (GE Healthcare Life Sciences, Model# 25) with the UNICORN software (GE Healthcare Life Sciences, Version# 7.0, Workstation for ÄKTA avant) was used for chromatographic purification using a His Trap HP (1 ml) column (GE Healthcare Life Sciences, CAT#17524701).

All required buffers were freshly prepared and filtered through 0.22 µm nitrocellulose membrane filter (Millipore, CAT# GSWP04700). His Trap HP 1 ml columns were stored in 20% ethanol. Therefore, at the start of the purification process, the His Trap column was washed in three steps with d.H_2O, the elution buffer, and the binding buffer at a flow rate of 1 column volume (CV)/min for 5 CV, and a maximum column delta pressure of 0.3 MPa. Next, the purification method program was performed automatically including three phases: binding, washing, and elution. First, the SM passed over the His-trap column at a slow flow rate (0.2 CV/min) to maximize the binding of the recombinant His-tagged protein to the column matrix. Then, the column was washed before elution with a flow rate of 0.5 CV/min. Both phases of binding and washing were performed in HEPES-NaCl buffer. The elution of His-tagged proteins was achieved by competition with imidazole. To maximize the purity of the recombinant His-tagged protein, the elution phase was strategized to be performed 0-500 mM imidazole gradient in HEPES-NaCl buffer at a slow flow rate of 0.2 CV/min. This allowed the weakly binding His-containing proteins to elute in the early fractions while the strongly binding recombinantly His-tagged protein was

eluted in later fractions. Each fraction contained 1 ml eluent. Upon the completion of the purification, the His Trap column was washed with d.H_2O and with 20% ethanol, each with a flow rate of 1 CV/min for 5 CV. Then, the column was stored in 4°C. Each column was used five times for protein purification. The flow through and the fractions were analyzed comparing to the SM on SDS-PAGE followed by Coomassie Brilliant Blue staining. The fractions containing the recombinant protein in high purity (>80%) were pooled. The purified protein present in the pooled fractions was dialyzed against TBS, Ca^{2+} buffer (50 mM Tris Base, 150 mM NaCl, 2 mM $CaCl_2$, pH7.4) using a dialysis tubing made of a cellulose membrane with a pore size at least two times smaller than the protein molecular weight (Spectrum Laboratories Inc, CAT#25225). Dialysis of the purified protein was performed twice at 4°C under stirring, for 8 hours and for 16 hours to ensure a complete dialysis of the elution buffer.

2.3.3 Storing purified recombinant protein

The concentrations of the purified recombinant proteins were using Pierce BCA Protein Assay Kit (ThermoFisher Scientific, CAT# 23225) according to the manufacturer's instructions. The purified proteins were either used immediately for experimental analyses, or stored in -80°C until usage.

2.4 Syndecan ectodomains

The constructs for the ectodomains of syndecan 2, 3 and 4 (SDC2-ED, SDC3-ED, and SDC4-ED respectively) were obtained from Dr. Sylvie Ricard-Blum lab (ICBMS UMR5246 - Université Lyon 1, France). The syndecan ectodomains were inserted into a modified episomal expression vector pCEP-Pu^{323}. Each SDC-ED construct contained the sequence of the BM40 signal peptide at the 5' of the construct followed by an N-terminal 6-His tag sequence. FLAG tag sequence was located at the 3' end of each SDC-ED construct prior to the stop codon.

Stable recombinant 293-EBNA clones were generated for each SDC-ED plasmid with culture media containing 2-6 µg/ml puromycin as a selecting antibiotic for pCEP-Pu plasmids, and tested for the expression of recombinant SDC-EDs using Western blotting and SDS-PAGE.

2.5 Protein characterizations of fibulin4, ltbp4 and syndecan ectodomains

As detailed in the next parts, the purified proteins were characterized using SDS-PAGE, followed by Coomassie Brilliant Blue staining and Western blotting with specific antibodies. Structural characterization was performed by dynamic light scattering to analyze protein multimerization.

2.5.1 SDS-PAGE

Protein lysates were resolved by SDS-PAGE. A protein sample was prepared in 1x SDS-loading buffer either under non-reducing or reducing conditions by the addition of 100 mM DTT or 5% of 14.3 M pure liquid β-mercaptoethanol (βME) (Millipore Sigma, CAT# M3148). All samples prepared in loading buffer were incubated at 99°C for 10 minutes which is necessary for denaturing the polypeptides and addition of a negative charge from the anionic detergent, SDS. SDS-PAGE was performed using 4% staking, and 6-12% resolving minigels either in a gradient or a single concentration. Minigels were prepared in designed glass cassettes first by pouring the resolving gel layer at the bottom topped with 300 µl isopropanol until fully polymerized. The isopropanol was then discarded, and a layer of stacking gel was poured followed by inserting a gel comb to create wells for protein loading. Resolving gels were made of 25% 1.5 M Tris solution pH 8.8, 0.2% SDS, 0.15% TEMED and 0.1% ammonium persulfate (APS) mixed with volumes of d.H_2O and polyacrylamide solution (Bio-Rad, CAT# 1610148) according to the required concentration to be prepared. Stacking gels were made of 12% 1 M Tris solution pH 6.8, 0.1% SDS, 0.2% TEMED, 0.05% APS and 4% polyacrylamide solution. The SDS gel cassettes were placed in 1x Tris-glycine running buffer (10x Running Buffer was prepared by dissolving 30 g Tris, 144 g glycine and 10 g SDS in 1L d.H_2O, pH 8.3). Protein samples and markers were loaded into the gel wells and electrophoresed for 2-3 hours at 80 Volt in Bio-Rad Mini-PROTEAN vertical electrophoresis cell connected to a power supply (Bio-Rad, CAT# 1658005 and 1645050). The resolved proteins on the gels were subsequently analyzed by Coomassie Brilliant Blue staining or Western blotting.

2.5.2 Coomassie Brilliant Blue staining

After running the protein samples with a selection of globular marker proteins on a minigel using SDS-PAGE, gels were gently transferred out from the cassettes to a small container to be

stained for 10 min by Coomassie Brilliant Blue dye (10% Acetic Acid, 45% Methanol, 2.5% Brilliant Blue G250). Then, the dye was removed and the minigels were subsequently washed for 30 minutes with a sufficient amount of destaining solution (40% methanol, 10% acetic acid) for 3-4 times until the stained protein bands visualized with a clear background. Protein bands were imaged using an ultraviolet transilluminators (KODAK, Model# Gel Logic 200 Imaging System).

2.5.3 Western blotting

Protein samples resolved by SDS-PAGE were blotted onto a 0.2 µm nitrocellulose membrane (GE Healthcare Life Science, CAT# 45004024) in a wet transfer system using Mini Trans-Blot Electrophoretic Transfer Cell (Bio-Rad, CAT# 1703930). First, the protein transfer buffer (borate buffer: 10 mM sodium tetraborate decahydrate, pH not adjusted) was prepared and cooled at 4°C for 2 hours before the assembly of the transfer cassette. The nitrocellulose membrane, 2 filter papers and 2 fiber pads were soaked in the transfer buffer. The transfer sandwich was comprised of a foam pad (Bio-Rad, CAT# 1703933), a filter paper, the minigel, the nitrocellulose membrane, another filter paper and a fiber pad, as arranged from the negative charge side to positive charge side. Then, the transfer cassette was secured and placed in the protein transfer cell containing a frozen icepack to run at 0.4 Ampere with stirring for 75 minutes at room temperature.

The blot membrane was then washed briefly with TBS buffer containing 0.05% Tween-20 (TBST), followed by a protein staining using Pierce™ Reversible Protein Stain Kit (ThermoFisher, CAT# 24580) according to the manufacturer's instructions to enable protein detection on nitrocellulose membranes after transfer. Blot membranes were incubated in blocking buffer (5% non-fat dry milk in TBST) for 45 minutes at room temperature, and then exposed to the desired primary antibody in 2% non-fat dry milk-TBST at 4°C overnight (refer to table 1 for the information of all the used antibodies in this study). The blotting membranes were washed in TBST vigorously for 15 min on a shaker for three times. Post washing, the blots were treated with the proper HRP-conjugated secondary antibody against the primary antibody in 2% non-fat dry milk-TBST at room temperature for 2 hours. The membranes were washed in TBST for 15 min on shaker for three times and immunoreactive bands were visualized using a colorimetric signal developing method or an enhanced chemiluminescence detection. In the colorimetric method, the immunostained protein bands were developed using a freshly prepared solution of 17.5 mg 4-chloro-1-napthol in 6 ml absolute methanol with 23 µl H_2O_2 in 29 ml 1x TBS until the bands show

a grey black color. Then, the developing solution was removed, the membrane was washed with TBST briefly and imaged in white light using a gel imaging system (Bio-Rad, Model# ChemiDoc MP Imaging System). In the enhanced chemiluminescence method, the signal of HRP-conjugate on a specific protein was developed by incubating the blot membrane for 30-60 second in the working developing solution prepared freshly using SuperSignal® West Pico Chemiluminescent Substrate Kit (ThermoFisher, CAT# 34079). The blots were imaged under ultraviolet light using the ChemiDoc™ Imaging System (Bio-Rad, Model#12003153).

2.5.4 Dynamic light scattering

To determine the distribution of sizes and molecular conformation of particles/populations constituting the protein in solution, dynamic light scattering (DLS) experiments were performed with freshly purified recombinant proteins in TBS, Ca^{2+} buffer using DynaPro® Molecular-Sizing Instrument (Wyatt Technology, Model# DynaPro 99-E-50 Protein Solutions) equipped with the Dynamics software (Version 6) of the manufacturer. The light source in the DLS instrument is a semiconductor diode laser emitting at circa 830 nm wavelength. The light scattered by the protein sample is collected and guided via fiber optics to an actively quenched solid-state single photon counting module. Photons were converted to electrical pulses and correlated. The measurements are conducted at 90-degree scattering angle with respect to the incident beam.

The protein concentrations used in DLS experiments ranged from 100-350 µg/ml. A volume of 15 µl of each protein sample was loaded into a clean and dry cuvette made of high transparency quartz. The cuvette was then placed in the instrument in the sample holder and DLS analysis was performed at room temperature. Cuvette cleaning was performed with d.H_2O followed by a wash with 100% ethanol and then again with d.H_2O. After that, the cuvette was left to dry in air at ambient condition.

Forty acquisitions of 10-second-long readings were recorded for each measurement and averaged. Each protein sample from different batches were measured in triplicates and the scattering parameters determined were the mean of the values recorded from the 40 acquisitions. Time scales of the scattered light intensity fluctuations were analyzed using the autocorrelation function; i.e. the convolution of the intensity with itself as a function of time. Translational diffusion coefficients (D) of the molecules were determined in real time from the decay of the intensity autocorrelation function. The hydrodynamic radius (R_h) of the scattering molecules was

then derived from *D* using the Einstein–Stokes equation using a hard (rigid) non-deformable sphere model.

$$R_h = k_B T / 6 \pi \eta D$$

k_B is the Boltzmann constant, T is the temperature, π value is approximately 3.14, η is the solvent viscosity, D is the molecule translational diffusion coefficients.

Molecular mass estimations were made from the measured hydrodynamic radii by applying globular (compact) and linear (extended) models for protein shape using calibration curves, provided by the manufacturer and developed from standards of known molecular weight and size. The results from mass distribution data were averaged.

2.6 Gel filtration chromatography

Freshly purified F4_FL recombinant was separated for different populations (multimers, dimers & monomers) using gel filtration chromatography with an ÄKTA Avant liquid chromatography system. First, Superose 12 10/300 GL column (GE Healthcare Life Sciences, CAT#17517301) was packed according the manufacturer's instructions and washed in two steps with d.H_2O and TBS, Ca^{2+} buffer, respectively at a flow rate of 0.1 ml/min, and a maximum column delta pressure of 0.7 MPa. Then, pooled fractions of purified recombinant F4_FL from Ni^{2+}-chelating chromatography were immediately loaded manually using a syringe onto the Superose 12 10/300 GL column within a volume of 0.5-2 ml containing 0.25-0.5 mg protein. After loading the protein sample, the column was operated at a flow rate of 0.1 ml/min with TBS, Ca^{2+} buffer. Fractions of 0.5 ml volume containing the separated high, intermediate and low molecular mass protein assemblies were collected. The fractions were analyzed using SDS-PAGE followed by Coomassie Brilliant Blue staining under non-reducing conditions. This allowed determination of the enrichment protein population in each fraction for further analysis. The Superose 12 10/300 GL column was washed with d.H_2O and stored at room temperature in 20% ethanol after each use.

2.7 Lectin affinity chromatography

For functional analysis of FBLN4 glycosylation in cell binding, purified recombinant deletion mutant proteins were passed through a lectin affinity column to separate the glycosylated

populations from the non-glycosylated proteins. The separation was conducted using HiTrap Con A 4B 1 ml column (GE Healthcare Life Sciences, CAT# 28952085) on an ÄKTA Avant liquid chromatography system according to the manufacturer's instructions. Buffer used for lectin chromatography were filtered through 0.22 µm nitrocellulose membrane. A protein sample was from freshly pooled fractions of purified recombinant protein from Ni^{+2} chromatography. The sample was treated to contain 1 mM $MnCl_2$ and 1 mM $CaCl_2$ before loading to the HiTrap ConA 4B column as a preparation for optimal binding conditions to the column medium (Concanavalin A). Prior to lectin affinity chromatography, a HiTrap Con A 4B 1 ml column was washed with d.H_2O, and equilibrated with the binding buffer (20 mM Tris-HCl, 0.5 M NaCl, 1 mM $MnCl_2$, 1 mM $CaCl_2$, pH 7.4) at a flow rate of 1 ml/min, maximum column delta pressure of 0.3 MPa for 10 CV. Then, 0.5-1 mg protein was loaded using superloop into the column at a low flow rate of 0.15 ml/min. The collected flow through contained the unglycosylated protein. To elute the bound glycosylated protein, the column was first washed with the binding buffer for 10 CV at a flow rate of 1 ml/min. Then, the glycosylated protein protein was eluted from the column in 0.5 ml fraction volumes at 0.5 ml/min flow rate with 20 CV of the elution buffer (0.1-0.5 M methyl-α-D-glucoside, 20 mM Tris-HCl, 0.5 M NaCl, pH 7.4). Eluted fractions were subsequently analyzed using SDS-PAGE followed by Coomassie Brilliant Blue staining to determine the fractions containing the glycosylated and non-glycosylated protein. The column was washed the end with d.H_2O and stored in 20% ethanol.

2.8 N-Deglycosylation assay

Purified recombinant F4_FL and deletion mutant proteins were deglycosylated at their N-glycosylation sites by peptide-N-glycosidase (PNGase F, New England BioLabs, CAT# P0704S). A 20 µl solution containing 10 µg protein was prepared with 1 µl (300 unit) of PNGase F and 1x glycoprotein denaturing buffer provided in the PNGase kit. The solution was incubated for 1 hour at 37ºC in 1x SDS-loading buffer. The samples were then denaturated at 95ºC for 5 min and separated on SDS-PAGE, followed by Coomassie Brilliant Blue staining.

2.9 Crystal violet cell attachment assay

Cell adhesion to FBLN4 and LTBP4 recombinant proteins was tested by either with an end-point cell binding assay using crystal violet staining or a real-time cell binding assay (detailed

in the next section below, *2.10 Electrical Cell-Substract Impedance Sensing*). For the crystal violet cell attachment assay, 96-well Nunc plates (ThermoFisher Scientific, CAT# 439454) were used. Wells were coated with FBLN4 and LTBP4 recombinant proteins in triplicates at 4ºC overnight. Plasma FN (pFN) and bovine serum albumin (BSA) coats were used a positive and a negative cell binding control, respectively. In addition, wells coated with TBS, Ca^{2+} buffer served as a background for cell binding since protein coating was performed in TBS, Ca^{2+} buffer. The coated wells were blocked for 45 min at 37ºC incubator with 100 µl 2.5 mg/ml heat- denatured (80ºC for 11 min) BSA in TBS buffer. Cells upon reaching 70-80% confluency were washed with PBS and trypsinized briefly allowing only sufficient detachment of cells and preventing cleavage of cell receptors by trypsin. Fresh complete medium was added to the cell suspension to inhibit trypsin activity, followed by centrifugation. Cell pellets were then re-suspended in fresh serum free medium. The process was repeated twice to ensure complete removal of serum and trypsin residues. Cell counting was performed using a homocytometer. Blocking buffer was removed from the wells, 15000 cells/well were seeded in 200 µl/well serum free medium, and cells were incubated for 1 hour of cell adhesion at 37ºC to allow cell adhesion. All subsequent steps were performed at room temperature. Non-attached cells were gently washed with TBS buffer and the attached cells were fixed with 100µl/well freshly prepared 5% glutaraldehyde solution in TBS for 10 min. Fixed cells were stained with 80 µl/well crystal violet solution (0.1% crystal violet in 200 mM 2-(4-morpholino)-ethane sulfonic acid, pH6) for 45 min. excess crystal violet solution was removed and wells were washed gently for 3-4 times with 200 µl/well TBS buffer. Attached cells were examined under the microscope using 20x objectives. The dye was solubilized from the attached cells with 100 µl/well 10% glacial acetic acid in TBS, incubated for 10 min on shaker at 500 rpm. The absorbance was measured at 570 nm in a spectrophotometer microplate reader (Beckman Coulter, Model# DTX 880). Reads from wells coated with TBS, Ca^{2+} buffer were averaged and considered background crystal violet staining readings, which were subtracted from experimental cell percentage readings.

2.10 Electric cell-substrate impedance sensing

Electric cell-substrate impedance sensing (ECIS) is a real-time technology implemented for biophysical analyses to measure cellular impedance/resistance of an electric current. It is

designed for analyzing the changes *in-vitro* of the electric impedance due to adhering and spreading cells on special cell culture wells with circular gold electrodes. ECIS cell culture plates are available with different shapes and sizes of electrodes to be used for analyzing a wide range of cell functions, including cell adhesion, spreading, migration and contractility. Here, ECIS was employed for two different assays: 1) to analyze the cell interactions with FBLN4 and LTBP4, and 2) to examine the effect of FBLN4 and LTBP4 cell interactions on cell migration. An ECIS Zθ instrument (Applied Biophysics, Model# ZTheta 16 or 96 Well Array Station) equipped with the manufacturer ECIS software (Version 1.2.186 PC, 2015) was used for the indicated assays.

2.10.1 ECIS for Cell Binding

ECIS culture wells type 96w20idf (Applied Biophysics, CAT#96W20idf PET, 96 Well Array) were used for real-time cell binding assays. These culture plates are designed to hold 96 wells where each well has two interdigitated microelectrodes, one generator and one collector. The electrode configuration is designed to record impedance readings throughout the cell adhesion surface, and it is optimal to study ECM protein-cell interactions and cell proliferation.

Wells were coated overnight at 4ºC with a volume of 100 µl containing 10 µg/ml FBLN4, LTBP4, pFN and BSA in TBS, Ca^{2+} buffer. Wells were coated with TBS which served as a background control. Next day, all coated wells were blocked for 45 min at 37ºC with 100 µl 2.5 mg/ml heat- denatured BSA in TBS buffer. Similar to the crystal violet cell binding assay, 70-80% confluent cells were trypsinized briefly, the cell suspension was centrifuged and cells were resuspended in serum free medium trice. BSA blocking buffer was gently aspirated from the wells and 100 µl serum free medium was added to each well. The ECIS plate was then connected to the ECIS station on the 96-well array stage located inside 37ºC CO_2 cell culture incubator. Prior to cell seeding, a base line was established for the wells for 10 minutes. Then, reading the impedance was paused for about 2 minutes, during which 15000 cells/well were seeded in a total volume of 200 µl/well serum free medium. Post cell seeding, changes in impedance were recorded for 4-6 hours to analyze cell adhesion and spreading. All ECIS cell binding assays were measured for electric impedance (ohm; Ω) reads at 32000 Hz frequency.

2.10.2 ECIS for Cell Migration

ECIS culture plates type 8W10E (Applied Biophysics, CAT# 8W10E, 8 Well PC) were used for studying cell migration. This is an 8-well chamber slide, where each well contains one large counter electrode that has 10 small active electrodes. Each active electrode creates an electrical fence pulsing constantly with 1 mA electric current at 40,000 Hz frequency, which prevents cell adhesion and spreading on the areas of these active electrodes. When a cell monolayer is formed on the large electrode surface, the small active electrodes created gaps for cell migration to be measured after deactivating the electric fence.

To determine cell migration through ECIS, wells were coated in duplicates with a volume of 100 µl containing 25 µg/ml protein or only TBS, Ca^{2+} buffer overnight at 4ºC. The proteins included FBLN4, LTBP4, pFN, BSA. Cells upon reaching 70-80% confluency were serum starved for 18 hours prior to seeding into the ECIS plates. Serum starvation is imperative to stop/minimize cell proliferation. This ensures that the cells covering the electrodes exclusively due to cell migration. Coated wells were then blocked for 45 min at 37ºC with 100 µl 2.5 mg/ml heat-denatured BSA in TBS buffer. At the time of blocking, cells were trypsinized briefly and washed for two times with serum free medium, each wash followed by centrifugation. Then, cells were resuspended in serum free medium and counted using a hemocytometer prior to cell seeding. The blocking buffer was removed and 200 µl serum free medium was added to each well. The plate was connected to ECIS station on the 16-well array stage located inside a 37ºC CO_2 incubator. A base line was established for the wells before cell seeding for 10 minutes with the electrical fence feature active. Then, recording the impedance was paused for about 2 minutes during which 75000 cells/well were seeded in a total volume of 400 µl serum free medium per well. Then, the base lines were recorded for 10 hours allowing cells to form a monolayer binding to the coated protein and spreading on the culture surface. Within the time of cell monolayer formation, the small active electrodes were in electric fence mode, which created gaps in the cell monolayer for subsequent cell migration. After 10 hours of cell monolayer formation, the electric fence was deactivated and cell migration to the gaps on the small electrodes was measured for 30 hours. All ECIS cell migration assays were measured for electric impedance reads at 64,000 Hz frequency.

2.11 Live-cell imaging

Live cell imaging was recruited for studying cell adhesion and spreading, as well as cell migration on culture plates coated with FBLN4 and LTBP4 using differential interference contrast (DIC) microscopy. For this purpose, cells were live-imaged in culture vessels under an inverted microscope (Leica, Model# DMI6000B) provided with a digital camera (Leica, Model# DFC365 FX Cooled B&W). The imaged cell cultures were placed on the microscope stage inside a humidified incubation chamber connected to an incubation system (TOKAI, Model# HIT INU-F1 Incubator System) set at 37ºC and 5% CO_2.

2.11.1 Imaging Cell Adhesion and Spreading

Wells in 24-well plates (Corning, CAT# C3524) were coated at 4ºC overnight with a volume of 300 µl/well containing 25 µg/ml FBLN4, LTBP4, pFN or only TBS, Ca^{2+} buffer. Then, wells were blocked with 2.5 mg/ml heat-denatured BSA for 45 minutes at 37ºC incubator. At the same time, 70-80% confluent cells were trypsinized briefly and washed for twice with serum free medium, each wash followed by centrifugation. The blocking buffer removal was followed by the addition of 250 µl serum free medium. Then, the culture plate was placed in the incubation chamber for live cell imaging. Cells were seeded at a density of 50,000 cells/well, in a total volume of 500 µl/well. Live cell imaging was established at 40 x objective in time interval was 30 seconds between successive images for a duration of 6 hours.

2.11.2 In-vitro scratch assay

In-vitro scratch assay is a commonly used method for cell migration studies in which a scratch is created in a cell monolayer, then the scratch closure is analyzed over time. Six-well plates (Corning, CAT# C3516) were coated at 4ºC overnight with a volume of 1 ml/well containing 50 µg/ml FBLN4, LTBP4, pFN or only TBS, Ca^{2+} buffer. Also, serum starvation was applied on 70-80% confluent cell cultures for 18 hours before trypsinizing the cells for seeding on the coated wells. The following day, the wells were blocked with 1 ml 2.5 mg/ml heat-denatured BSA for 45 min at 37ºC. Meanwhile, the starved cells were briefly trypsinized and washed twice with serum free medium, each wash was followed by centrifugation. Then, BSA was removed from the well and 5 x 10^5 cells/well were seeded in a total volume of 3 ml/well of serum free medium. The cells were incubated for 10 hours to form a cell monolayer. Using 10 µl-size sterile tips, a scratch was created in the middle of each well after removing the medium. The scratches were gently washed with fresh serum free medium for removing the debris and smoothening the edge of the scratch.

Then, the medium was replaced with 3 ml fresh serum free medium. The culture plate was then gently placed in the incubation chamber for a 48-hour live cell imaging with 5 minute time intervals between successive images at 5 x objective.

2.12 Immunofluorescence

Immunofluorescence microscopy was employed in this study to analyze the effect of FBLN4 and LTBP4 cell interactions on elastic fiber formation and the underpinning intercellular mechanism. All IF experiments were performed in a dark container at room temperature, if not indicated otherwise. First, the prepared adherent cell cultures were washed gently with TBS buffer. Then, cells were fixed for 10 minutes with cold 4% paraformaldehyde (PFA) freshly prepared in TBS buffer for immunostaining extracellular matrix proteins and cell surface receptors. To immunostain intercellular proteins, cells were fixed using a clod solution of 70% methanol:30% acetone. Fixed cells were then washed with TBS buffer, followed by blocking for 1 hour using normal goat serum (NGS). The used NGS in all IF steps preparations was diluted with TBS in 1:10 ratio. The blocking buffer was then discarded, and primary antibodies were added in NGS for overnight incubation at 4ºC. For information about all the used antibodies in this study, refer to table 1. Primary antibodies were removed and the cells were washed for 5 minutes with TBS buffer for three times. Cells were incubated for 1 hour with secondary antibodies and 4′,6-diamidino-2-phenylindole (DAPI, 1:3,000 dilution) prepared in the NGS. The secondary antibodies conjugated with specific fluorophores distinguishable under non-overlapping fluorescence filter sets. A final step of washing was applied for 5 minutes with TBS buffer for three times. The slides were mounted with Vectashield anti-fade medium (Vector Laboratories, CAT# H-1000). A coverslip was gently placed on the top of each slide and sealed at the edges with a transparent nail polish. Representative images were taken from freshly stained slides using a fluorescence microscope (Zeiss, Model# Axio Imager M2) and Zen software (Zeiss, Version 2012 blue edition) provided by the manufacturer.

2.13 Collagen gel contraction assay

To analyze FBLN4 and LTBP4 induced cell contraction, collagen gel contraction assays were employed. Commercially available rat tail collagen type I solution (Cultrex, R&D Systems, CAT# 3440-100-01) was used to prepare disk-shaped gels cellularized with skin fibroblasts. Skin

fibroblasts from late passages were cultured to reach confluency at the day of preparing collagen gels. Complete medium was freshly prepared using DMEM with 10% pFN-depleted FBS and PSG (Depletion of pFN from serum is detailed in section *2.15*). FBLN4, LTBP4, pFN or TBS, Ca^{2+} were added to the prepared medium. Cells were trypsinized and washed two times with serum free medium before suspending them in the prepared DMEM containing pFN-depleted serum. Then, 250 µl of cell suspension containing $5x10^5$ cells/ml were mixed in a microfuge tube with 250 µl collagen type I solution to obtain a final concentration of 1.5 mg/ml collagen. Non-cellularized gels were prepared with DMEM only as a background control. The pH of collagen-DMEM solution was adjusted to pH 7.2 using sterile 1M NaOH. The solution was immediately transferred to a 24-well plate and allowed to solidify for 1 hour at room temperature. When the gels were polymerized, they were gently detached from the well walls and bottoms with a microspatula, and 500 µl more medium was added to each well. The gels were maintained in 37°C, 5% CO_2 humidified incubator for 7 days and imaged every day using a gel imaging system (Bio-Rad, Model# ChemiDoc MP Imaging System).

2.14 Cell proliferation assay

The effect of FBLN4 and LTBP4 cell interactions on cell proliferation was determined at 24 hours and 48 hours of cell interactions by two strategies, 1) comparing the total cell numbers, and 2) comparing the number of proliferating cells. However, to omit the effect of pFN from serum supplemented in the culture medium on cell proliferation, pFN-depleted serum was used in all cell proliferation assay settings. Depletion of pFN from sera is detailed in the next section.

In both strategies for examining cell proliferation, 8-well chamber slides (ThermoFisher Scientific, CAT# 154534) were coated at 4ºC overnight with 100 µl TBS, Ca^{2+} buffer containing 10µg/ml FBLN4, LTBP4 or pFN. Wells coated with TBS, Ca^{2+} buffer were used as a background control. In addition, 50-60% confluent cell cultures were washed with PBS and new complete medium containing only pFN-depleted FBS was added for 18 hours before harvesting the cells for cell proliferation assays. Next day, blocking step was performed on the coated wells for 45 minutes with 100 µl 2.5 mg/ml heat-denatured BSA at 37ºC. In the meantime, cells were trypsinized briefly and resuspended also in pFN-depleted FBS containing media. After removing the blocking buffer, cells were seeded at a density of 10,000 cells per well in 500 µl volume. The cells were incubated

thereafter in a humidified incubator at 37ºC and 5% CO_2. At the end of each time point, the cells were washed with TBS buffer and fixed with 4% PFA for 10 minutes.

For counting the total cell number using crystal violet method, cells were stained with 100 µl/well crystal violet solution for 45 minutes. Excess of crystal violet solution was washed with TBS buffer. Slides were mounted using permount medium (Fisher, CAT# SP15-100) and gently coverslipped. Slides were examined under the microscope using 10 x objective and cell numbers were counted.

For counting the proliferating cells, the cells were IF stained for Ki67 protein, as a cell proliferation marker. Representative images were captured using an Axio Imager M2 microscope. DAPI staining was utilized for counting total cell numbers and positively stained cells for Ki67 were counted as proliferative cells. The ratio of proliferative cell numbers to total cell numbers were plotted.

2.15 Depletion of Plasma Fibronectin from Sera

pFN was depleted from FBS using Gelatin Sepharose 4B affinity chromatography as gelatin binds to fibronectin with high specificity[324; 325]. Gelatin Sepharose 4B resin (GE Healthcare Life Sciences, CAT# 17095601) was packed into a column according to the manufacturer's instructions. The column was operated with an ÄKTA Avant liquid chromatography system and washed first with d.H_2O, followed by equilibration in binding buffer (TBS buffer containing 1mM PMSF), at a flow rate of 2 ml/min and maximum delta column pressure of 0.5 MPa. Then, 50 ml FBS was loaded onto the column using a superloop at a flow rate of 0.5 ml/min. The flow through was collected containing the pFN-depleted serum. pFN bound to the column was eluted using the elution buffer (50 mM sodium acetate, 1M sodium bromide, pH 5.0). The elution step was conducted at 2 ml/min flow rate. Finally, the column was washed with d.H_2O and stored in 20% ethanol at 4ºC. pFN depletion was confirmed by an analytical Western blotting with a specific antibody against FN.

2.16 Focal adhesion formation study

Focal adhesion (FA) formation upon cell interactions with FBLN4 and LTBP4 was determined using IF staining for FA in fixed cell cultures and using Western blotting for cell lysates. First, cells were freshly passaged to new cell culture flasks to reach about 50% confluency.

Then, cells were serum starved for 18 hours. At the same time, wells in 8-well chamber slides and in 6-well plates were coated at 4ºC overnight in duplicates with FBLN4, LTBP4, pFN or only TBS, Ca^{2+} buffer. The 8-well chamber slides were coated with 100 µl/well volume containing 10 µg/ml protein while the 6-well plates were coated with 1 ml/well volume containing 50 µg/ml protein. Micropatterns in a large Y-shape (CYTOO, CAT# 10-012-00-18) were also used to unify the cell shape, which facilitates the quantification of FA maturation and distribution. Micropattern chips were arranged in 6-well plates in the format of one chip/well. Then, a protein coat was applied at 4ºC overnight in a 2ml/well-volume containing 25 µg/ml protein. Next, the coated wells (but not the micropatterns) were blocked with 2.5 mg/ml heat-denatured BSA for 45 min at 37ºC. The cells were trypsinized and washed for two times with serum free medium, followed by centrifugation. Then, the blocking buffer was removed from the micropattern wells. The cell suspension was seeded in serum free medium at 250 µl/well in 8-well slides, and 2 ml/well in 6-well plates that include wells containing the micropatterns. Cells were seeded at a density of 10,000 cell/well for 8-well chamber slides for IF staining, and 150,000 cells/well for 6-well plates for Western blot analysis, or 15,000 cells/well for micropatterns followed by IF analysis. The seeded cells were incubated for 24 hours at 37ºC in humidified incubator supplemented with 5% CO_2. The conditioned medium was removed from wells and cells were washed with TBS buffer. The cells in 8-well slides and micropattern wells were fixed for IF staining. While cell lysates were collected from 6-well plates to be processed for Western blotting, by scrubbing in 250 µl/well cell lysing buffer for (50 mM Tris pH8.0, 1 mM EDTA, 150 mM NaCl, 10% Glycerol, 1% NP-40, 0.5% Sodium deoxycholate, 10 mM NaF, 0.1% SDS) containing cOmplete™ protease inhibitors (Roche, CAT# 11836153001) as recommended by the manufacturer. The cell lysates were collected in microfuge tubes and incubated on ice for 1 hour with a brief vertexing every 10 minutes. That was followed by 15-minute centrifugation at 12,000 x g at 4ºC. Then, the protein supernatants were transferred into new tubes and their concentrations were measured. For each lysate, 25 µg protein was resolved on SDS-PAGE for Western blotting.

2.17 Image analysis

All original IF images were exported to 8-bit .tiff format using Zen software, and imported into the ImageJ software (Wayne Rasband, National Institutes of Health, Version 1.52a). All images were processed in ImageJ in two steps: 1) reducing the background in each individual

channel, and 2) enhancing the signal using contrast limited adaptive histogram equalization (CLAHE). To apply the Image processing steps in ImageJ, the following procedures were executed:

- From Process menu, subtract background was clicked. In the configuration pop-up menu, the rolling ball radius value was set at 50 pixel and on only sliding paraboloid was checked.
- From Plugins menu, CLAHE was reached through Filters>Enhanced Local Contrast. CLAHE parameters were set to 19 for the block size and 256 for the histogram bin and 6 for the maximum slope.

The images were then quantified for the mean pixel intensity across an entire image using ImageJ, from Analyze menu>Measure. The relative mean pixel intensity was then calculated for each image in different experimental conditions/groups.

FA quantification was performed following the published method by the Reinhardt laboratory[326; 327]. After subtracting the background and enhancing the signal steps, FA images were further processed in three steps: 1) optimizing the image quality for a single object quantification using mathematical exponential feature (EXP), 2) enhancing the brightness/contrast and 3) setting up averaged threshold values that distinguish background from specific signal and fit to all the quantified objects (FA) in the presentative images. To apply these three steps for FA quantification in ImageJ, the following commands were executed:

- From Process>Math menu, EXP was performed.
- From Image>Adjust menu, Brightness/Contrast configurations were adjusted for average minimum and maximum values fixed among all the processed imaged from one experiment repeat to show the specific FA objects/particles as it appears in the original representative images.
- Similarly, from Image>Adjust menu, the Threshold values were averaged to fixed values applicable to all the quantified images for FA.

Finally, the FA number (count), total area, and average size per cell were obtained by selecting the area of one cell and executing particle analysis from the Analyze menu. Analyzing particles was performed considering the quantified particles (FA objects) having circularity values ranging from 0.00-0.99, which reduced the noise from false positive signal measurement for artifacts.

2.18 Cell-surface heparan sulfate degradation

Cell-surface heparan sulfate chains were subjected to degradation in cell binding experiments to determine the contribution of heparan sulfate in FBLN4 and LTBP4 cell interactions. For this purpose, harvested cells were treated with heparinases II (Sigma, CAT# H6512) and III (Seikagaku-amsbio, CAT# EC4.2.2.8) combined. First, 70-80% confluent cells were trypsinized and washed for two times with serum free medium. Then, the harvested cells were suspended in PBS containing 1g/L Glucose and 0.1 mM $CaCl_2$ and 0.1 mM $MgCl_2$ in the presence or absence of 1.25 unit/ml heparinases II and 0.0125 unit/ml heparinases III. The cell suspensions were incubated in Falcon tubes for 20 minutes at 37ºC, 5% CO_2 humidified incubator with a gentle shaking every 5 minutes to avoid cell aggregation and allow the enzymes function effectively. The treated cells with were seeded at a cell density of 10,000 cells/well to coated wells with 10µg/ml FBLN4, LTBP4, pFN and BSA in 96-well Nunc plates. Cell binding was performed for 1 hour as described previously using the crystal violet cell attachment assay (see the method in section *2.9*).

2.19 Small Interfering RNA (siRNA) Knockdown

siRNA knockdown was used to silence the expression of syndecans and glypicans in NSF and SMC cultures. Then, the siRNA transfected cells were analyzed for their interactions with FBLN4 and LTBP4, and for elastic fiber formations upon inhibiting the expression of the indicated cell receptors. The used strategy for siRNA knockdown was to target the inhibition of the mRNA expression of each indicated gene with a set of four siRNAs that each binds to a different motif on the respective mRNA sequence. The siRNA used here were available to ordered from Qiagen (refer to table 2 for information about all the used siRNA in this study). A cocktail containing a scramble of functional, non-human targeting siRNAs was used as negative control for cell transfection with siRNA (AllStars siRNA).

The cell transfection with siRNA was performed using Lipofectamine 2000. First, Lipofectamine was 10 x diluted in Opti-MEM medium and incubated for 5 minutes. A solution with 2 µM siRNA with Opti-MEM medium was prepared and mixed gently with Lipofectamin solution, then incubated for 20 minutes. Cell cultures at 70% confluency were trypsinized and washed two times with complete medium without PSG. The siRNA transfection was performed in a ratio of 30% siRNA in Lipofectamine to 70% cell suspension containing 1.5 x 10^5 cells/ml. The

transfected cells were seeded into cell culture vessels and incubated at 37ºC, 5% CO_2 humidified incubator, and then harvested at different time points for cell binding assays and IF analyses.

2.20 Real-Time Quantitative Polymerase Chain Reaction (RT-qPCR)

Expression of various target genes was analyzed throughout the study using RT-qPCR. This involved four steps: 1) mRNA isolation, 2) mRNA to cDNA reverse transcription, 3) RT-qPCR and 4) data analyses.

For mRNA extraction, cells were seeded in triplicates in 12-well plates (Corning, CAT# C3513). At the experimental endpoints, cells were washed shortly with PBS. Cold TRIzol reagent (Invitrogen, CAT# 15596018) was added in a volume of 200 µl/well, in a pipetting motion. The cell lysates were collected to microfuge tubes and allowed to stand for 5 minutes to permit a complete lysing. Then, 40 µl chloroform was added to the tubes and securely capped to be incubated for 3 min. The cell lysates were centrifuged at 12,000 x g at 4ºC for 15 minutes. This resulted in lysate separation into a lower phenol red-chloroform organic phase, a thin interphase, and a colorless upper aqueous phase. The aqueous upper phase containing the RNA was gently transferred for each to a new tube by angling the tube at 45° and pipetting the solution out very carefully. The aqueous upper phase in the new tube was treated with 100 µl isopropanol and incubated for 10 minutes. The new tubes were centrifuged at 12,000 x g at 4ºC for 10 minutes. The total RNA precipitated forming a white gel-like pellet at the bottom of each tube. The supernatants were gently discarded with a micropipette and 200 µl 75% ethanol was added to each tube. The tubes containing the RNA pellets were centrifuged at 7500xg xg at 4ºC for 5 minutes. The supernatants were again discarded gently with a micropipette and pellets were airdried for 5-10 minutes. The RNA pellets were solubilized in 20-50 ul RNase-free d.H_2O and the RNA concentrations were measured using a nanodrop spectrophotometer. The isolated RNA samples were either used immediately for the subsequent steps or stored at -80ºC.

The extracted mRNA was subjected to cDNA reverse transcription in which the reaction was performed using ProtoScript II First Strand cDNA Synthesis Kit (New England BioLabs, CAT# E6560S) following the manufacturer standard protocol. Only freshly synthesized cDNA was used for RT-qPCR after diluting in RNase-free d.H_2O to reach 1:10 dilution.

RT-qPCR were conducted using SYBR Green dye to detect the PCR product as SYBR Green binds in a high specificity to double strand DNA emitting a fluorescence signal in which

accumulates when the PCR cycles progress. For this RT-qPCR, a 10 µl/well mixture was made of 5 µl SYBR™ Select Master Mix (ThermoFisher Scientific, CAT# 4472918), 4 µl diluted cDNA, 1 µl of 400 nM forward primer and 1 µl of 400 nM reverse primer.

RT-qPCR mixture was prepared in triplicates using 384-well plates (ThermoFisher Scientific, CAT# 4483285). For each cDNA sample, a set of forward and reverse primers was designed specifically to analyze the targeted genes for their mRNA expression. All the used sets of primers in RT-qPCR were designed to generate product sizes range from 80-180 bp and to work efficiently at the same annealing temperature of 58-60ºC (refer to table 3 for the information about all the used primers in this study).

The RT-qPCR mixtures were added to wells in triplicates in 384-well plate. The plate was sealed with a thermal adhesive film and analyzed in a QuantStudio Real-Time PCR and Digital System (Applied Biosystems, Model# 5). Prior to the RT-qPCR cycles start, an initial activation was performed in two steps of heating, each for 2 minutes; the first step was at 50ºC and the second step was at 95ºC. Then, a 3-step RT-qPCR was conducted for 40 cycles. Each RT-qPCR cycle included denaturation step at 95ºC for 15 seconds, annealing step at 58-60ºC for 15 seconds and extension at 72ºC for 1 min.

2.21 Solid Phase Assay

Interactions of FBLN4 and LTBP4 with SDC2-, 3-, and 4-ED in conditioned media were determined by solid phase binding assays. Wells in 96-well Nunc plates were coated overnight at 4ºC with 100 µl of 10 µg/ml FBLN4, LTBP4L, LTBP4S, TE, pFN or BSA. Next, a blocking step was applied using 2.5 mg/ml heat-denatured BSA for 1 hour at room temperature. All the steps hereafter were performed under continuous shaking at 500 rpm. The blocking buffer was removed and the wells were washed for 5 minutes with TBS, Ca^{2+} buffer for 3 times. Then, serial dilutions from a soluble ligand were added at a volume of 100 µl/well, in triplicates. The added soluble ligands consisted of 20x concentrated conditioned media containing either recombinantly-FLAG-tagged SDC2-, 3-, or 4-ED, in which were titrated in the serial dilutions. The soluble ligands were incubated in the coated wells for 1 hour at room temperature. Later, wells were washed for 5 minutes with TBS, Ca^{2+} buffer for 3 times. Detection of bound ligands to the coated proteins was detected using a primary antibody against FLAG-tag. The wells were incubated at 4ºC overnight with 100 µl/well primary antibody solution prepared in 2.5 mg/ml heat-denatured BSA. The wells

were then washed for 5 minutes with TBST buffer for 3 times, followed by the addition of 100 µl/well HRP-conjugated secondary antibody prepared in 2.5 mg/ml heat-denatured BSA. The wells were then incubated with the secondary antibody for 2 hours at room temperature. The wells were washed again for 5 minutes with TBST buffer for 3 times. The immunoreaction in the solid phase assay was developed based on a color reaction method by adding 100 µl/well of freshly prepared developing solution of 1 mg/ml 5-aminosalicylic acid in 20 mM phosphate buffer (NaH_2PO_4) at pH 6.8 containing 0.045% H_2O_2. The reaction was stopped by addition of 100 µl/well of 2M NaOH. The absorbance was measured at 492 nm in a spectrophotometer microplate reader. The signals were corrected for antibody cross-reactivity with the coated ligand and for non-specific protein interaction of the soluble ligand with wells coated with TBS, Ca^{2+} buffer only.

2.22 Statistics

All statistical analyses of the quantified data and the generated graphs in this study were performed using Origin software (Origin Lab Corporation, Version 9.6.0.172 2019). Student T-test and ANOVA (analysis of variance) were used to calculate the *p*-values for each quantified experiment as applicable. The selection of the appropriate statistical test was made for individual sets of experiments according to the data distribution, the independency of variables, as well as the number of variables and samples groups in a comparison. *P*-values ≤ 0.005 were considered statistically significant.

2.23 Supplemental Tables

Table 1. The used antibodies in this study

Antigen	Antibody	Host	Source/Provider	Applications
FN	Anti-fibronectin	Rabbit polyclonal	Sigma, CAT# F3648	IF 1:500
FBLN4	Anti-FBLN4	Rabbit polyclonal	McGill CMARC antibody production services	IF 1:500
LTBP4	Anti-hLTBP4 (30-F)	Rabbit polyclonal		IF 1:1000
TE/Elatin	Anti-tropoelastin	Rabbit polyclonal		IF 1:500
V5-Tag	V5 Tag Antibody	Mouse Monoclonal	Invitrogen, CAT# R96025	WB 1:1000
His-Tag	6x-His Tag (C-term) Antibody	Mouse Monoclonal	Invitrogen, CAT# R93025	WB 1:500
Heparan sulfate	Anti-heparan sulfate	Mouse monoclonal	Seikagaku-amsbio, CAT# 370255-S	IF 1:1000
FLAG-Tag	Anti-Flag	Rabbit polyclonal	Sigma, CAT# F7425	WB 1:500, Solid phase assay 1:1000
pFAK	Anti-FAK (phospho Y397)	Rabbit monoclonal	Abcam, CAT# Ab812980	IF 1:400
Erk1/2	p44/42 MAPK (Erk1/2) (137F5) Antibody	Rabbit monoclonal	Cell signaling, CAT# 4695S	IF 1:500, WB 1:1000
pErk1/2	Phospho-p44/42 MAPK (Erk1/2) (Thr202/Tyr204) (197G2) Antibody	Rabbit monoclonal	Cell signaling, CAT# 4377S	IF 1:500, WB 1:1000
Rac1	Anti-Rac1	Mouse monoclonal	BD Biosciences, CAT# 610650	IF 1:500, WB 1:1000

Active RhoA (RhoAGTP)	Active RhoA -GTP Antibody	Mouse Monoclonal	Neweast Biosciences, CAT# 26904	IF 1:500, WB 1:1000
Actin	β-Actin (13E5) Antibody	Rabbit monoclonal	Cell Signaling, Cat# 4970	IF 1:1000
αSMA	Actin (Smooth Muscle) (Clone 1A4) Antibody	Mouse monoclonal	Dako, CAT# M0851	IF 1:1000
GAPDH	GAPDH (14C10) Antibody	Rabbit monoclonal	Cell Signaling, Cat# 2118	WB 1:1000
HRP-Anti Rabbit sera	Peroxidase AffiniPure Goat Anti-Rabbit IgG (H+L)	Goat	Jackson ImmunoResearch Laboratories, CAT#111035003	WB 1:1000, Solid phase assay 1:800
HRP-Anti Mouse sera	Peroxidase AffiniPure Goat Anti-Mouse IgG (H+L)	Goat	Jackson ImmunoResearch Laboratories, CAT#115035146	WB 1:1000
anti-Rabbit, Alexa Fluor 488	Goat anti-Rabbit IgG (H+L) Highly Cross-Adsorbed Secondary Antibody	Goat	Invitrogen, CAT# A32731	IF 1:1000
anti-Mouse, Alexa Fluor 488	Goat anti-Mouse IgG (H+L) Highly Cross-Adsorbed Secondary Antibody	Goat	Invitrogen, CAT# A32723	IF 1:1000
anti-Rabbit, Cy3	Goat anti-Rabbit IgG (H+L) Cross-Adsorbed Secondary Antibody	Goat	Invitrogen, CAT# A10520	IF 1:1000

anti-Mouse, Cy3	Goat anti-Mouse IgG (H+L) Cross-Adsorbed Secondary Antibody	Goat	Invitrogen, CAT# A10521	IF 1:1000

Table 2. The used siRNA in this study (purchased from QIAGEN)

Gene	siRNA	Product Number	Catalogue Number
Syndecan2	FlexiTube GeneSolution GS6383 for SDC2 4 siRNAs for Entrez gene 6383 (1 nmol each): SI03034045 (FlexiTube siRNA) SI03028249 (FlexiTube siRNA) SI00046809 (FlexiTube siRNA) SI00046802 (FlexiTube siRNA)	1027416	GS6383
Syndecan3	FlexiTube GeneSolution GS9672 for SDC3 4 siRNAs for Entrez gene 9672 (1 nmol each): SI04777612 (FlexiTube siRNA) SI04145043 (FlexiTube siRNA) SI00712894 (FlexiTube siRNA) SI00712887 (FlexiTube siRNA)	1027416	GS9672
Syndecan4	FlexiTube GeneSolution GS6385 for SDC4 4 siRNAs for Entrez gene 6385 (1 nmol each): SI03076339 (FlexiTube siRNA) SI03068016 (FlexiTube siRNA) SI00046823 (FlexiTube siRNA) SI00046816 (FlexiTube siRNA)	1027416	GS6385
Glypican2	FlexiTube GeneSolution GS221914 for GPC2 4 siRNAs for Entrez gene 221914: SI03091746 (FlexiTube siRNA) SI03078516 (FlexiTube siRNA) SI03059693 (FlexiTube siRNA) SI00155414 (FlexiTube siRNA)	1027416	GS221914
Glypican3	FlexiTube GeneSolution GS2719 for GPC3 4 siRNAs for Entrez gene 2719: SI03098291 (FlexiTube siRNA) SI03031525 (FlexiTube siRNA)	1027416	GS2719

	SI00064309 (FlexiTube siRNA) SI00064302 (FlexiTube siRNA)		
Glypican4	FlexiTube GeneSolution GS2239 for GPC4 4 siRNAs for Entrez gene 2239: SI03100825 (FlexiTube siRNA) SI03096737 (FlexiTube siRNA) SI02626323 (FlexiTube siRNA) SI00026089 (FlexiTube siRNA)	1027416	GS2239
Glypican5	FlexiTube GeneSolution GS2262 for GPC5 4 siRNAs for Entrez gene 2262: SI04223555 (FlexiTube siRNA) SI04221700 (FlexiTube siRNA) SI03132038 (FlexiTube siRNA) SI00429877 (FlexiTube siRNA)	1027416	GS2262
Glypican6	FlexiTube GeneSolution GS10082 for GPC6 4 siRNAs for Entrez gene 10082 (1 nmol each): SI03090339 (FlexiTube siRNA) SI03041423 (FlexiTube siRNA) SI03029873 (FlexiTube siRNA) SI02635787 (FlexiTube siRNA)	1027416	GS10082

Table 3. The sequences of the used primers for RT-qPCR analyses

Gene	Primer Sequence 5' – 3'	Primer Length	GC %
Syndecan 1	GATGGCTCTGGGGATGACTCTGA	23	56.5
	GTGGGAATAGCCGTCAGGAGC	21	61.9
Syndecan 2	TGTTGACTAGTGCTGCTCCAAAAGTG	26	46.2
	CTCTTCGGCTGGGTCCATTTTCC	23	56.5
Syndecan 3	GCGGAAGGAGGTGCTCGTAG	20	65
	CGTGTAGCTGCCCTCATCCTT	21	57.1
Syndecan 4	GACGATGAGGATGTAGTGGGGCC	23	60.9
	GACAACTTCAGGGCCGATCATGG	23	56.5
Glypican 1	GCAGATCATGCAGCTGAAGATCATGACC	28	50
	CTTCCTGCTGACCTTCCGGCT	21	61.9
Glypican 2	GTTCGTGGCTGTCTCAGCAGCAG	23	60.9
	GTCAGCTCAAAGGAAAAGGGGCC	23	56.5
Glypican 3	GCATTGGAGGCTCTGGTGATGGAATG	26	53.8
	GTTTCCAGGCGCATCATCCAC	21	57.1
Glypican 4	GGGAGATGTCGTGAGCAAGGTC	22	59.1
	GAGCAGTAGTTGTAACATGGCTTCACAGTC	30	46.7
Glypican 5	GGGGGATCAGGAAGTGGAGAAGTC	24	58.3
	GCTCCTGTTGTGTCTAAAGTACTGCCAG	28	50
Glypican 6	AACTACTGTCTCAACGTCATGAAGGGC	27	48.1
	ACCGACTCAATGTTGAATGGCCCC	24	54.2
Integrin Subunit Alpha 1	TCAAAATTCTCCAGACGCTCAGTGG	25	48
	TGCTCCTCCTTCTCTGTTCCCA	22	54.5
Integrin Subunit Alpha 2	TAGCCCTGCCCTTGAAGCC	19	63.2
	CAGCTGGTATTTGTCGGACATCTAGGA	27	48.1
Integrin Subunit Alpha 2b	CACCTTCTATGCAGGCCCCAAT	22	54.5
	TCCAGGGGCACAGGAACAC	19	63.2
	CTTCCACGGCTTCTTCTCCATGC	23	56.5

Integrin Subunit Alpha 3	GGAGATGATGATGGGGCGGAGTT	23	56.5
Integrin Subunit Alpha 4	ATCAGAGAGGAAGGAAGAGTGTTTGTGT	28	42.9
	ATGTCGCCAAGATTAACTATAGATTCCCCA	30	40
Integrin Subunit Alpha 5	ACTTTGTTGCTGGTGTGCCC	20	55
	GAGGCCATCTGTTCCCCTGAGAA	23	56.5
Integrin Subunit Alpha 6	TATGATGTGGCGGTGGTGGAC	21	57.1
	CACTGCACCTCCAACTTCTCCATCTC	26	53.8
Integrin Subunit Alpha 7	GTGGTTGGGAGTCAGTGTTCGG	22	59.1
	ACCAATCATATCCCGCGTCTCC	22	54.5
Integrin Subunit Alpha 8	CGCAACAACAAGGGATTTCGACC	23	52.2
	CGTGGAACTGCAAATCGGAGGC	22	59.1
Integrin Subunit Alpha 9	CCGACCACATCCTACCCCATG	21	61.9
	GTGAAGAAGCCCGCTATCCCAG	22	59.1
Integrin Subunit Alpha V	TGCCGCGCCTTCAACCTAGA	21	57.1
	GGGTGGTGTTTGCTTTGGGAG	21	57.1
Integrin Subunit Beta 1	TGGAGAATGTATACAAGCAGGGCCA	25	48
	CTCTGGGATTTTCTATGTCATCTGGAGGG	29	48.3
Integrin Subunit Beta 2	CAGAAGCAGCTGTCCCCACAA	21	57.1
	TCAGATAGTACAGGTCGATGGGGTAGC	27	51.9
Integrin Subunit Beta 3	GCCTGTGTCACCATACATGTATATCTCCC	29	48.3
	CTCATTGAAGCGGGTCACCTGGTC	24	58.3
Integrin Subunit Beta 4	GTCTGGCCTTCAATGTCGTCTCC	23	56.5
	CCAGCACTTTCTTCATGGGCCC	22	59.1
Integrin Subunit Beta 5	GTGCGACAACTTCTCCTGTGCC	22	59.1
	CGAGCAGTTACAGTTGTCCCCGA	23	56.5
Integrin Subunit Beta 6	GTTCAGATTGCGCCTCAAAGCTTG	24	50
	GTGTTGAGGTCGTCATCCATGGAG	24	54.2
Integrin Subunit Beta 7	GTCACCCATTCTGTGCGCATTG	22	54.5
	GGTGAAAGCTGAATGGTGACTGGC	24	54.2

Integrin Subunit Beta 8	AGAAGGAGGTTTTGACGCCATGC	23	52.2
	CACCACTATGCCTGCCAATTTGC	23	52.2
Fibulin-4	CAGATGGCTATGAGTGGGACCC	22	59.1
	AGGGGTTGGGGTGTTGAGC	19	63.2
Latent Transforming Growth Factor Beta Binding Protein-4	TGTGGGTGAGGGCTGGG	17	70.6
	CGCCACTCTTGCACACCT	18	61.1
Fibronectin-1	CCAACATTGATCGCCCTAAAG	21	47.6
	GATTCCATCCTCAGGGCTC	19	57.9
Fibrillin-1	ATTTACCCAACACCATACGTCCTGC	25	48
	TTACCCTCACACTCGTCCAC	20	55
Elastin[328]	GGTATCCCATCAAGGCCCC	19	63
	TTTCCCTGTGGTGTAGGGCA	20	55
GAPDH	GGTCTCCTCTGACTTCAACA	20	50
	AGCCAAATTCGTTGTCATAC	20	40
RPL13A	TCTTAGTCACTGCCTCCCGA	20	55
	TCACAAGATAGGGCCCTCCA	20	55

3. RESULTS

Previous reports showed heparin binding of FBLN4 and LTBP4, and for both proteins binding to cells via cell surface heparan sulfate moieties was suggested[18; 22]. The overall scope of this study was to characterize how cells interact with FBLN4 and LTBP4, to define the cell surface receptors, and to explore the downstream functional consequences of these cell interactions.

3.1 FBLN4 multimerization is essential in cell interactions and LTBP4 isoforms interact similarly with cells

The Reinhardt laboratory has previously shown that full length FBLN4 interacts with different human cells[18]. In In addition, it has been reported that mouse lung fibroblasts interact with a recombinant human LTBP4 isoform missing the first two 4-cys domains unique to LTBP4[22; 329]. The sequence of this LTBP4 isoform has been reported only in a cDNA library, but not in any proteomic analysis[178]. However, the cell interactions with the two isoforms for LTBP4 confirmed to occur in human (long and short) have not been investigated. Here, we aimed to further elucidate cell interactions with FBLN4 and LTBP4.

The Reinhardt laboratory has previously uncovered that FBLN4 self-oligomerizes under physiological conditions into multimers[18]. However, the functional implication of FBLN4 multimerization in cell interactions has not been analyzed. To assess the cell interaction properties of FBLN4 multimers and of both LTBP4 isoforms, we used two *in vitro* cell binding assays, end-point crystal violet staining and ECIS analysis that allows monitoring cell attachment in real-time (Fig. 1A and B). Skin fibroblasts bound strongly to gelfiltrated FBLN4 multimers, similar to the non-gelfiltrated FBLN4 preparation that consisted of multimers, dimers and monomers. FBLN4 dimers showed weak interactions in the crystal violet assay, but no interaction in the ECIS approach, whereas FBLN4 monomers were completely inactive. For LTBP4, both the long and short isoforms interacted strongly and similarly with skin fibroblasts in both assays.

Cell attachment and spreading on FBLN4 and LTBP4 was further visualized and analyzed by live-cell imaging (Fig. 1C and Movie 1-4). All supplemental movie legends are enclosed at the end of this chapter in section *3.17.* pFN served as a positive control and TBS, Ca^{+2} as a buffer control. Cells attached very quickly to both FBLN4 and LTBP4 as can be appreciated in the "0-minute images" that were recorded immediately 2-3 min after cell seeding (Fig. 1C). At this early time point, cells already adhered to the coated surfaces (FBLN4, LTBP4 and pFN) with the

cytoplasm slightly spread around the nuclei, whereas cells did not adhere well on the control surface (TBS, Ca^{+2}).

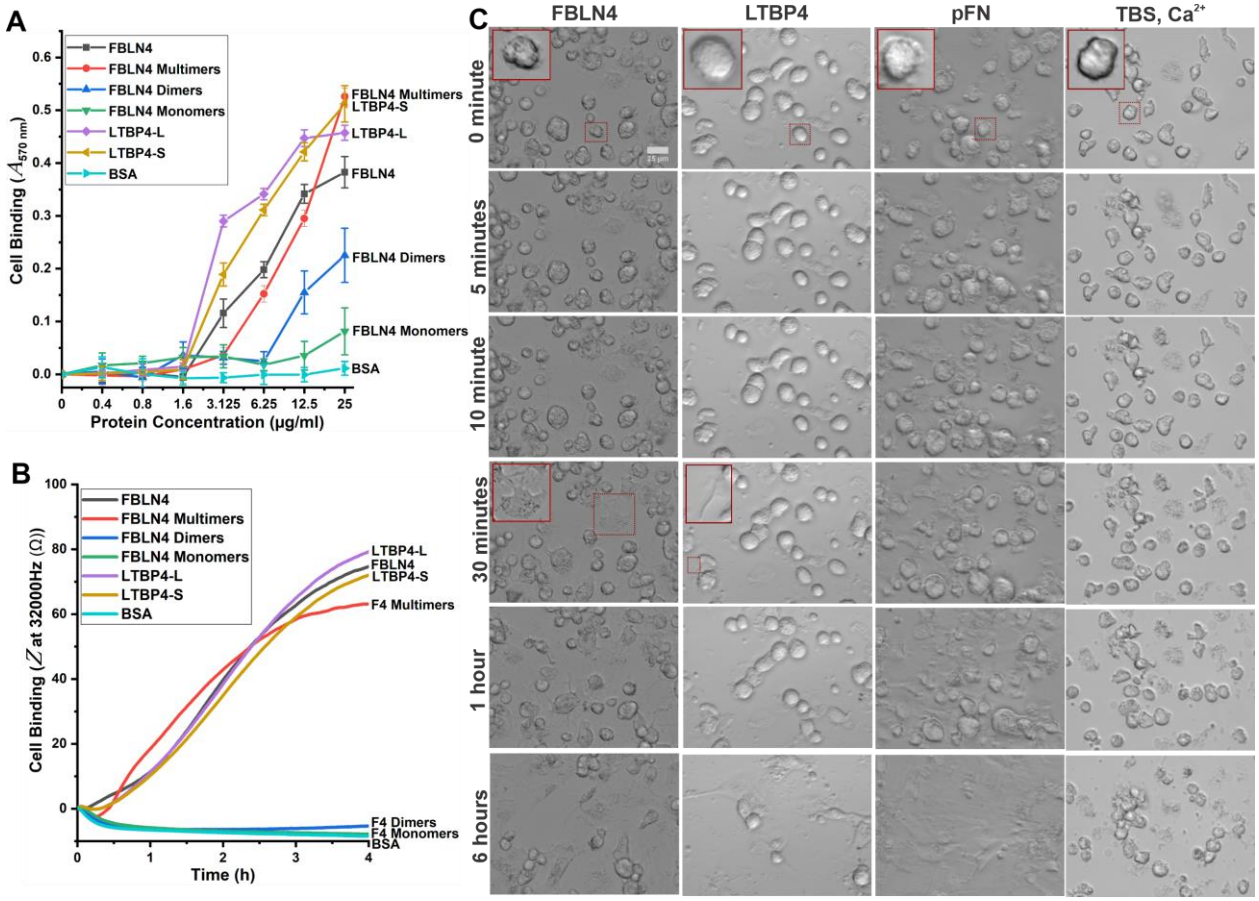

Figure 1. Cell interactions with FBLN4 and LTBP4
Shown graphs present skin fibroblast interactions with immobilized recombinant FBLN4 and LTBP4 using two cell binding assays: a crystal violet end-point assay in (A) and an ECIS real-time assay in (B). In A, proteins were coated at the indicated concentrations, in B, the protein concentration was 10 µg/ml. The cell binding data in (A, Absorbance at 570 nm) and (B, impedance in ohm at an electrical current frequency of 32000 Hz) are averaged technical quadruplicates of a representative experiment. The experiment was repeated 5-6 times using skin fibroblasts from different donors. BSA was used as a negative control. TBS, Ca^{+2} treated wells were used as a background control since all proteins were immobilized in TBS, Ca^{+2}. Background cell binding on TBS, Ca^{+2} coated wells were subtracted from all other values. Error bars indicate standard deviations of mean (SD±mean) of four technical replicates of one representative experiments out of 6 repeats. Statistical analyses were performed using one-way ANOVA. (C) DIC microscopy images were obtained from *in vitro* live cell imaging of skin fibroblast adhesion and spreading on FBLN4, LTBP4, pFN and TBS, Ca^{+2} coated wells (n=3-5 per protein). The scale bar represents 25 µm. Inset images show magnified areas indicated by the small dashed-frame boxes. The inset images in the 0-minute time point show the adhesive cytoplasmic areas around the nuclei within 2-3 min after cell seeding. In the 30-minute time point, the inset image presents a shared pool of cytoplasm between the cells spread on FBLN4, whereas the LTBP4 inset image indicates an example of a thin long protruded cytoplasmic extension (see Movie 1 and 2).

The cell adhesion and spreading patterns varied between the different ECM protein coats. On FBLN4, skin fibroblasts started extending cytoplasmic projections after about 10 min of cell

interactions. These cytoplasmic projections formed shared cytoplasmic pools (thin connections) as the cells touched each other. Dynamic networks between the cells continued to develop until the cells fully spread between 6-24 h (Movie 1 and Fig. 1C, FBLN4 inset at 30-minute image). During the observation time, a considerable number of intracellular vesicles formed around the nuclei, and some of them migrated along the shared cytoplasmic projections between the cells (Movie 1). When skin fibroblasts were seeded on LTBP4, they first clustered in short threads with relatively small cytoplasmic projections (Movie 2). Within a short time (5-10 min), the LTBP4-interacting skin fibroblasts projected remarkable thin and long cell protrusions which sometimes showed a flagellum-like movement (Movie 2 and Fig. 1C, LTBP4 inset at 30 min image). These cell protrusions became denser as the cells spread further up to 6 h. Unlike FBLN4 and LTBP4, skin fibroblasts quickly spread and flattened after initial adhesion on pFN coated surfaces (Movie 3 and Fig. 1C). As expected, throughout the experimental time frame, the fibroblasts seeded in control wells coated with buffer (TBS, Ca^{+2}) adhered and spread very little (Movie 4 and Fig. 1C).

3.2 Elastogenic cells bind consistently and strongly to FBLN4 and LTBP4

It has been already demonstrated previously by the Reinhardt lab that FBLN4 interacts with skin and lung fibroblasts, as well as with umbilical arterial and venous smooth muscle cells[18]. However, cell interaction with LTBP4 has been analyzed only with mouse lung fibroblasts[22]. Since FBLN4 and LTBP4 are pivotal elastic proteins, we set out to examine the consistency of their interactions to various elastogenic cell types other than skin fibroblasts. All elastogenic cells chosen to investigate FBLN4 and LTBP4 cell binding properties are of human origin to match the species with the recombinant human FBLN4 and LTBP4. We tested FBLN4 and LTBP4 binding to adult and fetal aortic smooth muscle cells (HASMC), and to umbilical arterial and venous smooth muscle cells (SMC and CRL-2481, respectively). All these primary cells showed strong and consistent binding to FBLN4 and LTBP4 (Fig. 2A). Since smooth muscle cells can be in a contractile or a synthetic phenotype, we addressed whether these phenotypes affect the ability to interact with FBLN4 and LTBP4. Serum starvation was used to differentiate both adult and fetal HASMCs into the contractile phenotype by maintaining them for one week in culture medium containing 1% serum, whereas the synthetic phenotype was preserved by maintaining the cells in culture medium containing 15% serum. To distinguish and confirm the phenotypes of adult and fetal HASMCs grown under these two culture conditions, we immunostained cells with αSMA, a

cell contractility marker (Fig. 2B). The differentiated cells grown in the presence of 1% serum showed a much higher level of αSMA with well-defined filamentous organization, compared to the cells grown in the presence of 15% serum where αSMA was almost absent, confirming a contractile and synthetic phenotype, respectively. Using differentiated adult HASMC in cell binding assays demonstrated a similar ability of both phenotypic cells to adhere to FBLN4 and LTBP4 (Fig. 2C). For fetal HASMC, differentiation into the contractile phenotype significantly decreased the overall binding by about 12% for FBLN4 and 30% for LTBP4, albeit with a strong remaining ability to interact (Fig. 2C).

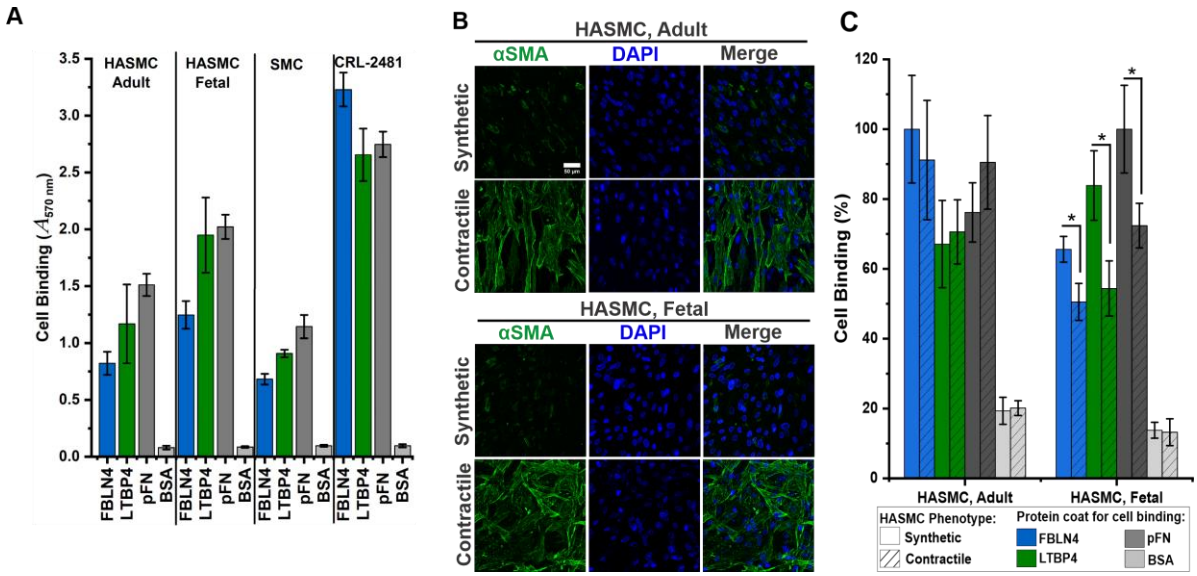

Figure 2. Synthetic and contractile smooth muscle cells both interact with FBLN4 and LTBP4
(A) Crystal violet end-point cell binding assay to analyze FBLN4 (blue) and LTBP4 (green) interactions with different smooth muscle cells as indicated. pFN (dark gray) represents a positive control, and BSA (light gray) the negative control. Error bars represent SD±mean of three technical replicates of one representative experiments out of 4 repeats. (B) IF of adult and fetal HASMC with αSMA, which is highly expressed in the contractile phenotype, and low in the synthetic phenotype. HASMCs were cultured for 7 d under synthetic or contractile conditions using culture media containing either 15% or 1% serum, respectively. Cell nuclei were counterstained with DAPI (blue). The scale bar represents 50 µm for all images. (C) Cell binding assay of synthetic (open) and contractile (hatched) adult and fetal HASMC plated on FBLN4, LTBP4, pFN (positive control) and BSA (negative control) using crystal violet staining (color coding as in A). Error bars represent SD±mean of four technical replicates of one representative experiments out of 3 repeats. Statistical analyses were performed using two-way ANOVA.

3.3 Mapping of multimerization and cell binding domains in FBLN4

To identify the domain(s) responsible for multimerization and cell adhesion in FBLN4, several expression plasmids for truncation and deletion mutants were designed (Fig. 3A). All constructs include a signal peptide for secretion and posttranslational modification in the secretory

pathway and a C-terminal histidine-tag. After transfection of the plasmids into HEK-EBNA cells, and purification of the recombinant proteins from the conditioned medium by Ni^{2+}-chelating chromatography, they were resolved by SDS-PAGE under non-reducing and reducing conditions and stained with Coomassie Brilliant Blue (Fig. 3B). The purified full length FBLN4 and non-overlapping F4_N1, F4_2-5 and F4_6C have been previously described[18; 20]. All recombinant FBLN4 mutant proteins migrated at the expected molecular mass under reducing conditions (arrows in Fig. 3B). Most FBLN4 mutants, except F4_N1-3, showed various levels of multimerization under non-reducing conditions. Double bands at the monomeric position of some fragments likely represent differential glycosylation as determined previously[18] (see also chapter *3.4*). F4_N1-3, F4_N1-5, and F4_N1,C showed purities of >90%, F4_N1,6C was about 70% pure, and F4_N1,4-6C and F4_4-6 could only be obtained at an estimated 25-40% purity. Additional purification steps did not improve the purity of the latter two fragments, because of the relatively low amount of recombinant protein in the conditioned medium (despite using 2 L conditioned medium as start material). To still be able to use those partially purified FBLN4 fragments in cell binding assays, we generated the following control. Conditioned medium was prepared from non-transfected HEK-EBNA cell cultures and treated in an identical manner to the FBLN4 deletion mutant protein purifications. This preparation contained all background bands present in F4_N1,4-6C and F4_4-6, and can thus serve as a background control.

Since several FBLN4 mutant proteins showed higher molecular bands under non-reducing conditions (Fig. 3B), we analyzed the purified proteins by DLS in physiological buffer and under non-reducing conditions, which provided information on the hydrodynamic radius of the molecules and thus on the molecular masses of monomers and potentially multimers present in solution (Fig. 3C). We have previously shown that F4_N1 produced a single monodisperse population of particles with a hydrodynamic of 2.5 nm, representing monomers[20]. F4_N1-3 which contains two additional downstream cbEGF domains, also shows primarily a single monodisperse population of particles with a hydrodynamic radius of 3 nm, correlating with the SDS-PAGE analysis under non-reducing conditions. This demonstrates that the N-terminal FBLN4 domain and the two downstream cbEGF domains are not able to multimerize. All other FBLN4 deletion mutants analyzed here show a major peak between 7-18 nm and a minor peak between 69-95 nm. This demonstrates that these deletion mutants form higher molecular mass particles, because the monomeric populations of these fragments have predicted hydrodynamic radii of ≤3 nm. Again,

the data correlate well with the SDS-PAGE analysis of the fragments under non-reducing conditions (Fig. 3B), and demonstrate that the multimerization domains in FBLN4 map to cbEGF5-6 and to the C-terminus, potentially a contiguous site in this region.

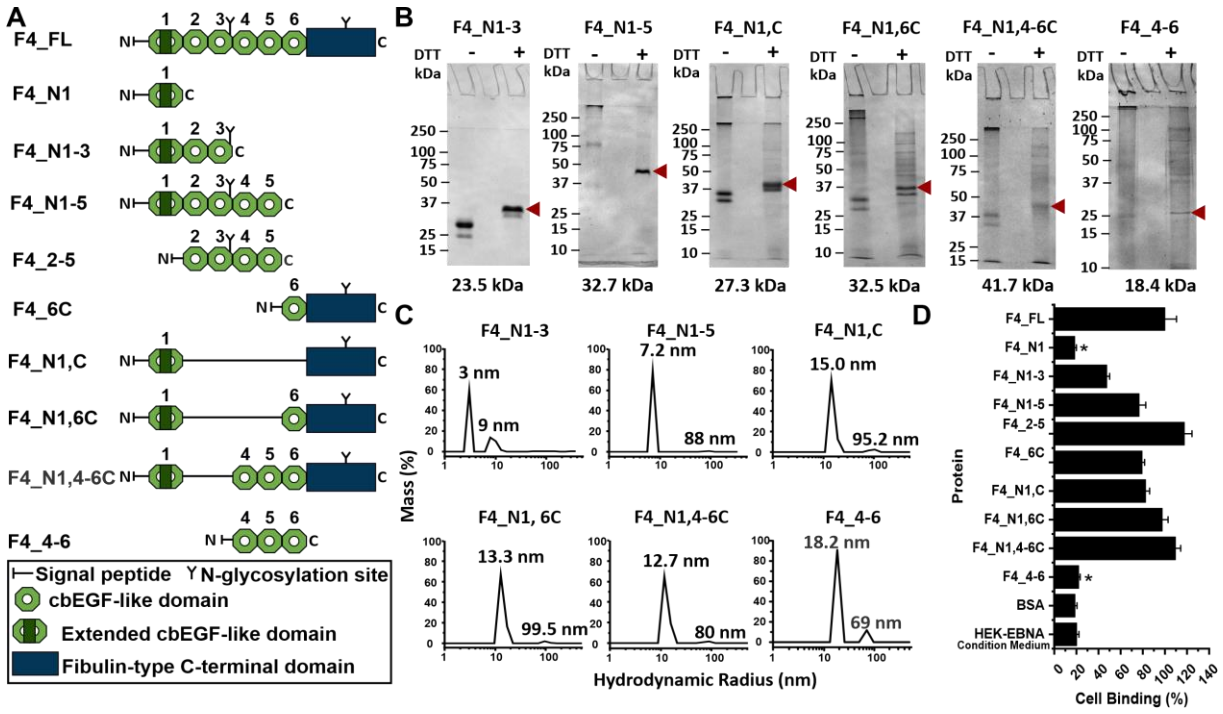

Figure 3. Mapping of multimerization and cell interaction sites on FBLN4
(A) Schematic presentation of the domain arrangement of human full length FBLN4 (F4_FL) and all FBLN4 deletion mutants recombinantly produced and used in this study. They were constructed with a BM40 signal peptide at the N-termini and with a His-tag at the C-terminal ends. (B) Coomassie Brilliant Blue staining of the purified recombinant FBLN4 deletion mutants resolved on gels using SDS-PAGE. The indicated molecular mass under each deletion mutant gel was calculated theoretically based on the amino acid composition. Red arrow heads indicate the purified FBLN4 recombinants. (C) DLS analysis of recombinant FBLN4 mutants to determine monodispersity and multimerization. The analyses shows the hydrodynamic radius (Rh, nm) on a logarithmic scale on the X-axis versus the mass size (%) on the Y-axis for each FBLN recombinant construct analyzed. (D) Crystal violet end point cell binding assay to analyze skin fibroblast interactions with FBLN4 FL and deletion mutants. Coated wells with BSA were used as a negative control, respectively. Due to the low purity of some purified FBLN4 deletion mutants, conditioned media from non-transfected HEK-EBNA cell culture were collected, processed identically to the schemes used for FBLN4 deletion mutant purification, and used as a background/negative control in the cell binding assay. Error bars represent SD±mean of three technical replicates of one representative experiments out of 5 repeats. Full length FBLN4 was set to100% binding. Statistical analyses were performed using two-way ANOVA.

To determine which FBLN4 domain is required for cell adhesion, we analyzed all generated deletion mutants along with the full length FBLN4 in crystal violet cell binding assays using skin fibroblasts (Fig. 3D). Most deletion mutants interacted with skin fibroblasts between 30-100% compared to the full length FBLN4, except F4_N1 and F4_4-6, which did not interact at

all (Fig. 3D). This data identified two cell interaction epitopes on FBLN4, one located in cbEGF2-3 and a second one in the C-terminal domain (Fig. 3A and D). cbEGF3 and the C-terminal domain are sufficiently positively charged under physiological conditions to possibly interact with negatively charged heparan sulfate cell surface receptors, as predicted previously[18].

3.4 FBLN4 N-linked glycans can modulate cell binding

Interestingly, each one of the two mapped cell interacting domains in FBLN4 contains one of the two N-linked glycosylation sites (Fig. 3A), leading to the hypothesis that cell interactions with FBLN4 occur through these N-linked glycans. To test this hypothesis, we first utilized two small FBLN4 deletion mutants, F4_N1-3 and F4_6C, that both contain only one glycosylation site to determine whether both sites are occupied. These FBLN4 mutants were treated with PNGase F to enzymatically remove the N-linked glycans (Fig. 4A). The Reinhardt lab has shown previously that full-length FBLN4 under reducing conditions consists of two species with differential N-linked glycosylation patterns, with either one or two sites occupied[18]. We used F4_N1-3 to represent the first N-linked glycosylation site on FBLN4, since it could be purified with sufficient yield and purity. Also, we used F4_6C in the PNGase F analysis, but not other mutants containing the C-terminal glycosylation site, because of the molecular mass of this mutant protein that can be better resolved relative to the PNGase F band. Treatment of F4_N1-3 and F4_6C with PNGase F confirmed that both glycosylation sites on FBLN4 are occupied, based on the resulting mobility shifts in SDS-PAGE (Fig. 4A). Both fragments are characterized by two bands under reducing conditions that shift to one band after PNGase F treatment, demonstrating that the respective N-linked glycosylation site of each fragment is only partially occupied.

We used lectin affinity chromatography to effectively separate the glycosylated from the non-glycosylated forms of the deletion mutants F4_N1-3 and F4_N1,6C instead of F4_6C (Fig. 4B). This because it was purified in larger amounts that can be subjected to a further chromatographic analysis than F4_6C that was purified in very small amounts. The purified F4_N1-3 and F4_N1,6C proteins along with the unseparated protein preparation (mixture of glycosylated and non-glycosylated forms) were then characterized for their cell adhesion properties (Fig. 4C). Skin fibroblasts interacted with both the glycosylated and non-glycosylated forms of F4_N1-3, but the interaction was significantly reduced with the glycosylated protein. For F4_N1,6C the fibroblasts bound to the glycosylated form and even more to the non-glycosylated

form (Fig. 4C). This data demonstrates that the cell interactions with FBLN4 do not occur directly through the N-linked glycans. However, the results suggested that the cell binding sites can be modulated by N-linked glycans.

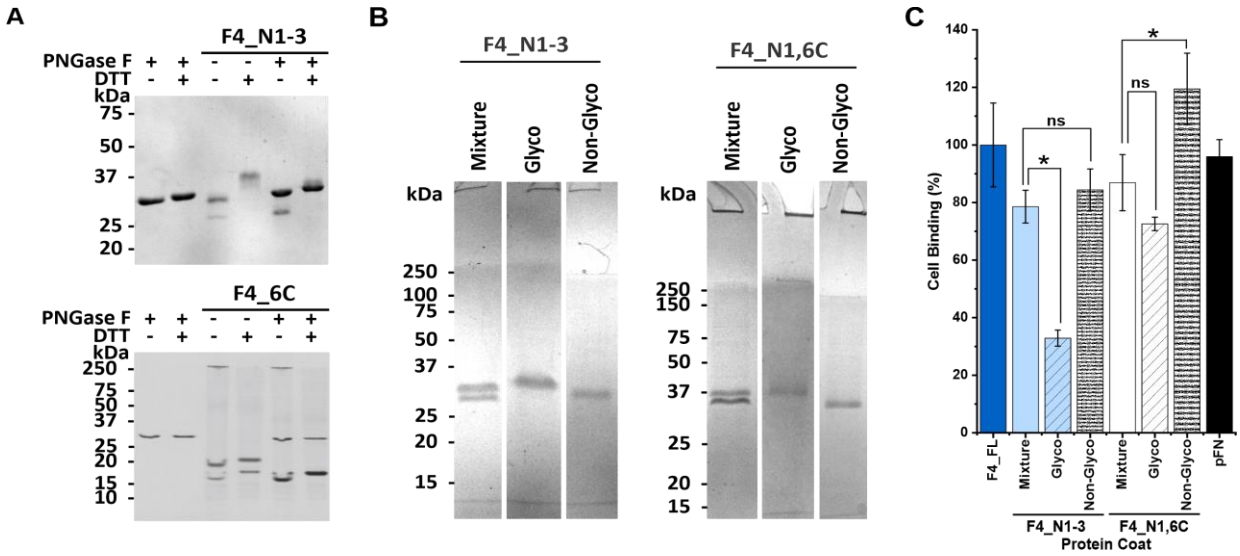

Figure 4. N-linked glycans of FBLN4 modulate cell binding
(A) and (B) show SDS-PAGE gels stained by Coomassie Brilliant Blue of FBLN4 mutant proteins (F4_N1-3 and F4_6C in A, F4_N1-3 and F4_N1,6C in B) that each harbors one of the two FBLN4 N-glycosylation sites. In (A), each mutant was analyzed either non-treated or treated with PNGase F under non-reducing (-DTT) or reducing (+DTT) conditions. In (B), the previously purified (by Ni^{2+}-chelating chromatography) F4_N1-3 and F4_N1,6C were passed through a lectin affinity column to separate the glycosylated form (Glyco) from the non-glycosylated form (Non-Glyco). The starting material contained two bands representing both forms (Mixture). All proteins were analyzed under reducing conditions. (C) Crystal violet cell binding assay using the separated glycosylated and non-glycosylated forms for each FBLN4 mutant analyzed in (B), compared to the starting material (Mixture). Full length FBLN4 (F4_FL) and pFN were used as positive controls. Error bars represent SD±mean of four technical replicates of one representative experiments out of 3 repeats. Full length FBLN4 was set to100% binding. Statistical analyses were performed using two-way ANOVA.

3.5 LTBP4 N- and C-terminal halves mediate cell binding

Kantola *et al*. previously discovered one cell binding region near the C-terminus of LTBP4, using the full length LTBP4S isoform and several smaller fragments[22] (Fig. 5A). To compare cell interaction between LTBP4S and LTBP4L, and to potentially identify additional cell interaction sites that were previously missed due to the design of the recombinant fragments, we have produced the following recombinant LTBP4 constructs: Full length LTBP4S, LTBP4L, the N-terminal halves of both LTBP4 isoforms, and the C-terminal half (Fig. 5A).

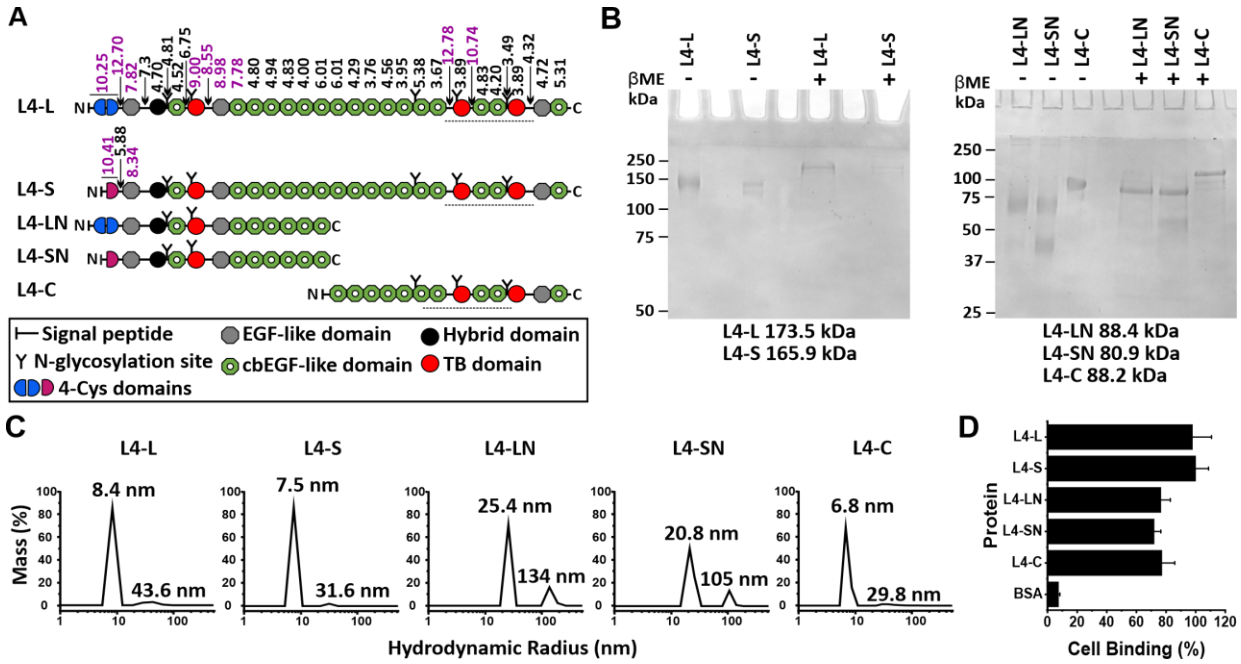

Figure 5. LTBP4 contains at least two cell interaction sites

(A) Domain structure of the full-length human LTBP4 long and short isoforms (L4-L and L4-S, respectively) and the LTBP-4 truncation mutants. All LTBP4 recombinant proteins were constructed with their endogenous signal peptide except the C-terminal half (L4-C) which was constructed with the BM40 signal peptide at the N-terminus. All recombinant proteins contained a C-terminal V5 and a histidine-tag. Isoelectric points of each domain and linker region (arrows) are indicated above L4-L (ExPASy Compute pI/Mw Tool). The isoelectric points for the domains with 100% identical amino acid sequences between the long and the short form are indicated only above the long form scheme. Basic isoelectric values are magenta colored. The dashed lines indicate the mapped cell binding region by Kantola et al[22]. (B) Purified recombinant LTBP4 full length and deletion mutants were analyzed under non-reducing (-βME) and reducing (+βME) conditions using SDS-PAGE followed by Coomassie Brilliant Blue staining. Calculated molecular masses of the recombinant proteins are indicated below the gel images. Molecular masses of marker proteins are indicated on the left. (C) DLS analyses of the purified proteins. Hydrodynamic radii (R_h, nm) were determined at a single protein concentration in TBS, Ca^{+2} buffer and plotted on a logarithmic scale on the X-axis versus the mass size (%) on the Y-axis. The peaks represent particle populations with the respective R_h values indicated on top. (D) Cell interaction assay of the recombinant LTBP4 proteins using crystal violet staining. LTBP4 full length (L4-L and L4-S) were used as positive controls whereas BSA was used as a negative control. Error bars represent SD±mean of three technical replicates of one representative experiments out of 3 repeats. Statistical analyses were performed using two-way ANOVA.

Coomassie Brilliant Blue staining of the recombinant proteins are shown in Fig. 5B, and characterization of the purified proteins by DLS is shown in Fig. 5C. As expected from other studies, the full-length LTBP4S and LTBP4L migrate at ~200 kDa under reducing conditions, which is higher than the calculated molecular masses of 165.9 kDa (LTBP4S) and 173.5 kDa (LTBP4L), likely due to the contribution of the N-glycans. DLS analysis showed primarily monodisperse population of particles with hydrodynamic radii of 7.5 nm (LTBP4S) and 8.4 nm (LTBP4L), demonstrating that the full-length proteins did not multimerize in solution. The N-terminal recombinant halves of LTBP4S (L4-SN) and LTBP4L (L4-LN) migrate at ~100 kDa, also

somewhat higher than the calculated values of 80.9 kDa (L4-SN) and 88.4 kDa (L4-LN). DLS analysis showed hydrodynamic radii of 20.8 nm (L4-SN) and 25.4 nm (L4-LN), demonstrating that both recombinant fragments are present as multimers in solution, possibly through unmasking of a multimerization site in the absence of the C-terminal half. Both N-terminal halves showed minor bands of ~60 kDa under reducing conditions, which likely represent proteolytic cleavage products. The common C-terminal half migrated at ~130 kDa in SDS-PAGE and showed monodisperse particle populations in DLS with a hydrodynamic radius of 6.8 nm, demonstrating that this fragment is monomeric in solution.

We performed crystal violet cell adhesion assays using the purified LTBP4 full length and deletion mutants to determine their ability to interact with skin fibroblasts (Fig. 5D). The cells bound strongly and similarly to full length LTBP4S and LTBP4L. The fibroblasts adhered to all three deletion constructs at about 75% compared to the full-length proteins. As the N- and the C-terminal halves did not contain overlapping domains, the data demonstrate that both, LTBP4S and LTBP4L, contain at least two independent cell interacting sites, one located in the N-terminal half and the other in the C-terminal half.

To obtain information about possible heparan sulfate interaction epitopes which are predicted to consist of positively charged regions in the proteins, isoelectric points of each domain and linker sequence between the domains were calculated (Fig. 5A). Three domain clusters with basic isoelectric points were determined: i) the N-terminal 4-Cys domains of both isoforms, ii) the region including the first TB domain and two downstream EGF domains, and iii) the linker region adjacent to the second TB domain. All represent candidate regions for interactions with cell surface heparan sulfate, and the latter likely represents the interaction site previously identified by Kantola et al[22].

3.6 FBLN4 and LTBP4 cell binding is mediated by heparan sulfate

Certain cell surface receptors, including heparan sulfate proteoglycans (HSPG) and integrins, can mediate interactions with ECM proteins. We first surveyed the primary fibroblasts and smooth muscle cells used in this study for the mRNA expression spectrum of HSPGs and integrins by real-time qPCR and summarized the data in Fig. 6. The focus was on syndecans (SDC) and glypicans (GPCs) as these HSPGs commonly interact with ECM proteins, as well as on a list

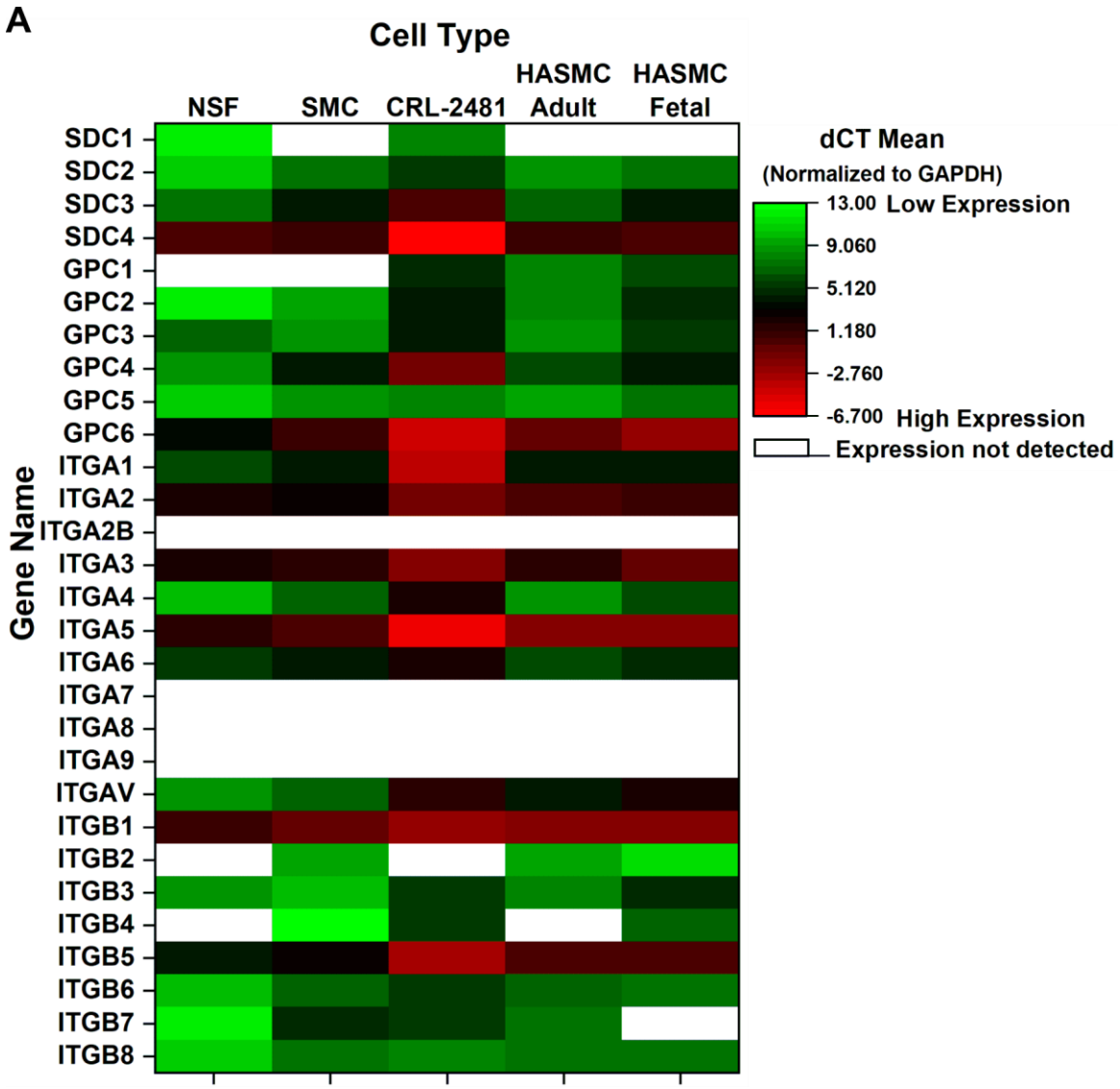

Figure 6. Profiling mRNA expression of cell surface receptors in elastogenic cells
Heatmap showing mRNA expression data of cell surface receptors commonly interacting with ECM proteins obtained from real-time qPCR analyses using elastogenic primary fibroblasts (NSF) and smooth muscle cells (SMC, CRL-2481, fetal and adult HASMC). Data in the heatmap are presented for each mRNA (rows) and each cell type (columns). Expression values are presented as ΔCT after normalization to GAPDH. Black blocks indicate that mRNA expression levels of the respective protein and GAPDH have the same value. If a mRNA level is lower than that of GAPDH, the blocks are green, if the level is higher they are depicted in red. White blocks indicate no mRNA expression was detected.

of alpha and beta integrins subunits (ITGAs and ITGBs, respectively). With this strategy, it was possible to exclude some candidate receptors. For example, the real-time qPCR data showed no detected expression levels for SDC1 and GPC1 in some of the analyzed elastogenic cells that interact with FBLN4 and LTBP4. However, most other members of the syndecan and glypican families are expressed in these cells. Some integrins were commonly not expressed in all examined

cells, including ITGA2B and ITGA7-9, whereas other integrin subunits were only expressed in some cells, such as ITGB2, ITGB4 and ITGB7 (Fig. 6).

Both, FBLN4 and LTBP4 have high affinity for heparin (an experimental model of heparan sulfate), suggesting that HSPGs mediate cell interactions with these proteins[18; 22]. However, cell adhesion activities of many ECM proteins are mediated by integrins and heparan sulfate proteoglycans, as well, such as fibronectin (FN)[74; 330] and tropoelastin (TE)[205; 207]. ECM protein interactions with integrins require divalent cations, including Ca^{2+}, Mg^{2+}, and Mn^{2+} that bind to the α and β integrin subunits[300]. Therefore, to test the possibility of integrin involvement in FBLN4 and LTBP4 cell interactions, we used the divalent cation chelator EDTA and selected metal cations in the cell binding buffer. However, FBLN4 and LTBP4 contain arrays of cbEGF domains which require calcium for their folding[331], thus the presence of calcium is crucial for FBLN4 and LTBP4 function, including protein-protein interactions. Therefore, one caveat using EDTA to test integrin involvement through chelation of divalent cations is that it may interfere with correct function of FBLN4 and LTBP4. Therefore, we used a serial titration of EDTA from 0-100 mM in the cell binding buffer to test skin fibroblast attachment to FBLN4 and LTBP4 (Fig. 7A). In this setup, EDTA was present in the binding buffer during the entire cell interaction time and thus in contact with cells and the coated proteins. Cells interacting with the positive controls, pFN and TE which both bind to integrins, lost ~70-80% of their ability to attach in the presence of 1.5 mM EDTA. Contrary, cells reduced adhesion to FBLN4 and LTBP4 only by about 10-20% up to 25 mM EDTA. At 100 mM EDTA, cell interactions to all tested proteins were completely lost. The data indicate that divalent cations are removed from integrins by relatively low EDTA concentrations, resulting in loss of pFN or TE cell interaction. However, FBLN4 and LTBP4 likely bind to other cell surface receptors and lose their ability to interact with cells upon removal of divalent cations by high EDTA concentrations from cbEGF domains. To eliminate the EDTA effect on FBLN4 and LTBP4, suspended skin fibroblasts were first treated with 15 mM EDTA in serum-free medium for 15 min, followed by washing the cells and then using them in the cell binding assay with coated FBLN4, LTBP4, pFN and TE (proteins were pre-saturated with Ca^{+2}). The cell binding buffer was supplemented with increasing concentrations (0-4 mM) of Ca^{+2}, Mg^{+2} and Mn^{+2} to further assess the divalent cation dependency of cell adhesion (Fig. 7B-D). pFN and TE showed a strong increase in cell binding with all tested divalent cations, strongly indicating that they bind to integrins. However, FBLN4, LTBP4S, and LTBP4L remained at a similar cell binding level,

irrespective of available cations. In summary, these experiments strongly suggest that FBLN4, LTBP4S, and LTBP4L do interact with fibroblasts in an integrin-independent manner.

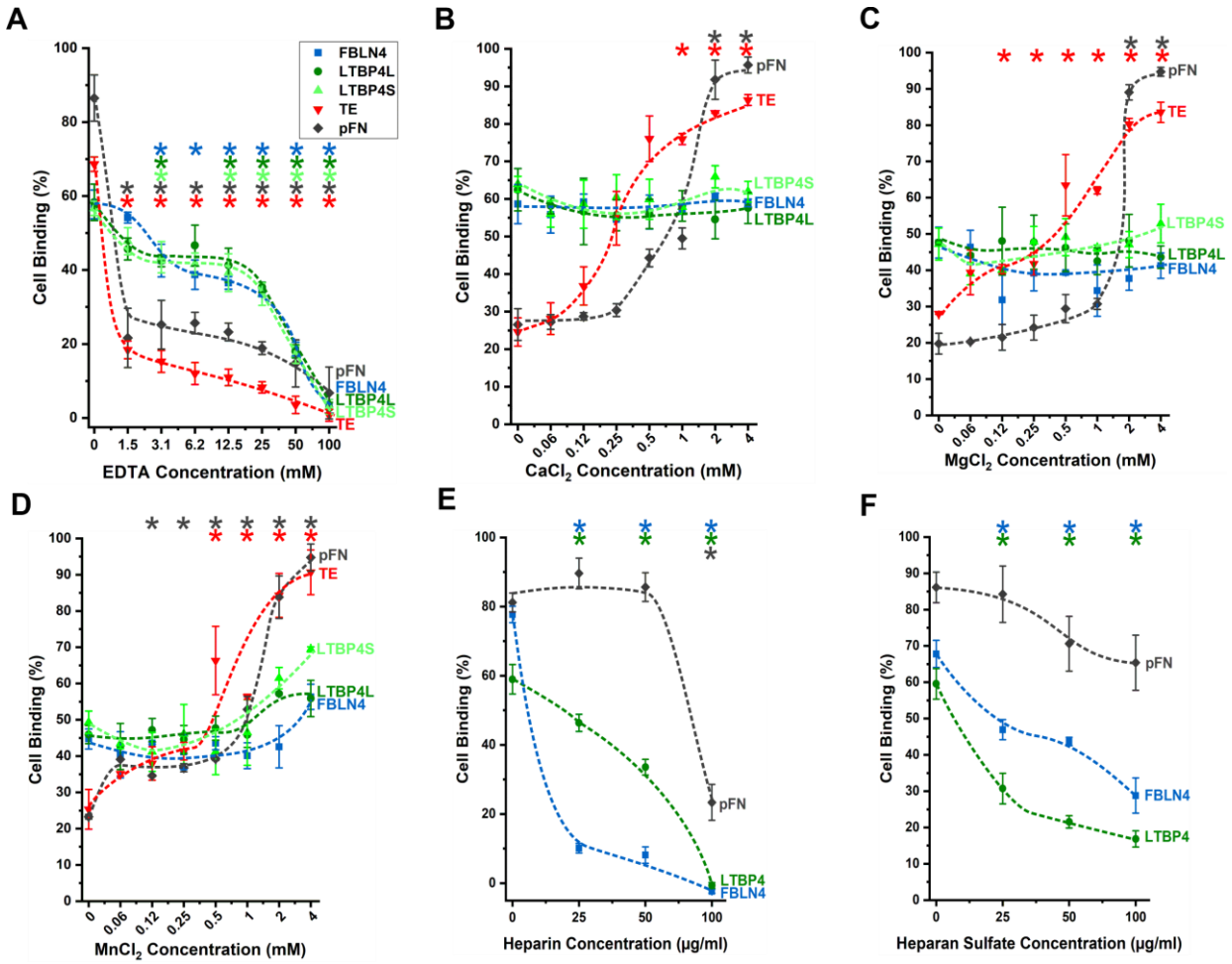

Figure 7. Characterization of the interactions of cell surface receptors with FBLN4 and LTBP4
Shown are representative crystal violet end-point cell binding assays using skin fibroblasts tested with FBLN4, LTBP4S, LTBP4L, TE and pFN. (A) The assay was performed in the presence of 0-100 mM EDTA in the binding buffer. (B-D) Skin fibroblasts were first preincubated in 5 mM EDTA for 15 min at 37°C, then washed and used in the assay in the presence of 0-4 mM divalent cations in the cell binding buffer, including calcium (B), magnesium (C) and manganese (D). (E-F) Cell interaction with FBLN4, LTBP4 and pFN as control was analyzed in the presence of 0-100 µg/ml heparin (E) and heparan sulfate (F) present in the cell binding buffer. . Error bars represent SD±mean of four technical replicates of one representative experiments out of 3 repeats. Significant differences ($p<0.05$) are indicated by color-coded asterisks matching the colored graphs. Statistical analyses were performed using two-way ANOVA.

To test if FBLN4 and LTBP4 cell interactions are heparan sulfate dependent, competitive cell binding assays were conducted in the presence of soluble heparin or heparan sulfate in the cell binding buffer (Fig. 7E-F). Cell binding to FBLN4 and to LTBP4 was significantly reduced by the presence of 25-50 µg/ml heparin and completely blocked at 100 µg/ml heparin (Fig. 7E). Similarly,

FBLN4 and LTBP4 cell adhesion was significantly reduced in the presence of 25-100 µg/ml heparan sulfate (Fig. 7F). These observations strongly suggest that FBLN4 and LTBP4 cell interactions occur via HSPG.

3.7 Cell surface-located heparan sulfate mediates FBLN4 and LTBP4 cell interactions

To explore whether the binding moiety to FBLN4 and LTBP4 on cells are heparan sulfate side chains of a proteoglycan, we first used the CHO-677 mutant cell line defective in heparan sulfate production and compared it to the wild-type CHO-WT in cell binding assays (Fig. 8A-B). CHO-WT showed a coating concentration-dependent strong cell interaction with FBLN4, whereas the mutant CHO-677 did not bind (Fig. 8A). However, both CHO-WT and -677 did not interact with LTBP4 (Fig. 8B). pFN as control showed little differences between the cell lines, as it primarily interacts with integrins.

Then, we used heparinases to degrade heparan sulfate on the cell surface to test if this treatment impedes skin fibroblast binding to FBLN4 and LTBP4 (Fig. 8C-D). We combined heparinases II and III (H'ase II & III) to ensure a maximal cleavage of heparan sulfate chains from proteoglycans on the cell surface. For that, a suspension of skin fibroblasts was treated with the heparinases for 20 min and then examined for their interactions with FBLN4 and LTBP4. In Fig. 8C, we controlled that the heparinases II/III treatment was effective in degrading cell surface located heparan sulfate using IF staining. Cells were spread on glass slides (small drops) from the cell suspensions after the heparinases II/III and buffer control treatments. Then, the cells were fixed with 4% PFA for 20 min and fixed cells were immunofluorescence stained for heparan sulfate (Fig. 8C). Treatment of skin fibroblasts with heparinases II and III significantly diminished cell binding to FBLN4 and LTBP4 (Fig. 8D). These data confirm the involvement of HSPG in FBLN4 and LTBP4 cell adhesions.

3.8 Cell interactions with FBLN4 and LTBP4 are mediated by syndecans

For identification of the FBLN4 and LTBP4 receptors, we utilized a siRNA knockdown approach of syndecans and glypicans, as candidate HSPG cell receptors. As shown above, the mRNA expression of SDC1 and GPC1 were absent in some of the examined elastogenic cells whereas these cells can interact strongly with FBLN4 and LTBP4 (Fig. 6). That excluded SDC1 and GPC1 from the candidate list as cell receptors for FBLN4 and LTBP4. To narrow down the

responsible cell receptors that bind to FBLN4 and LTBP4, we pooled multiple siRNAs and transfected cells that were subsequently used in cell interaction analyses. First, we transfected skin

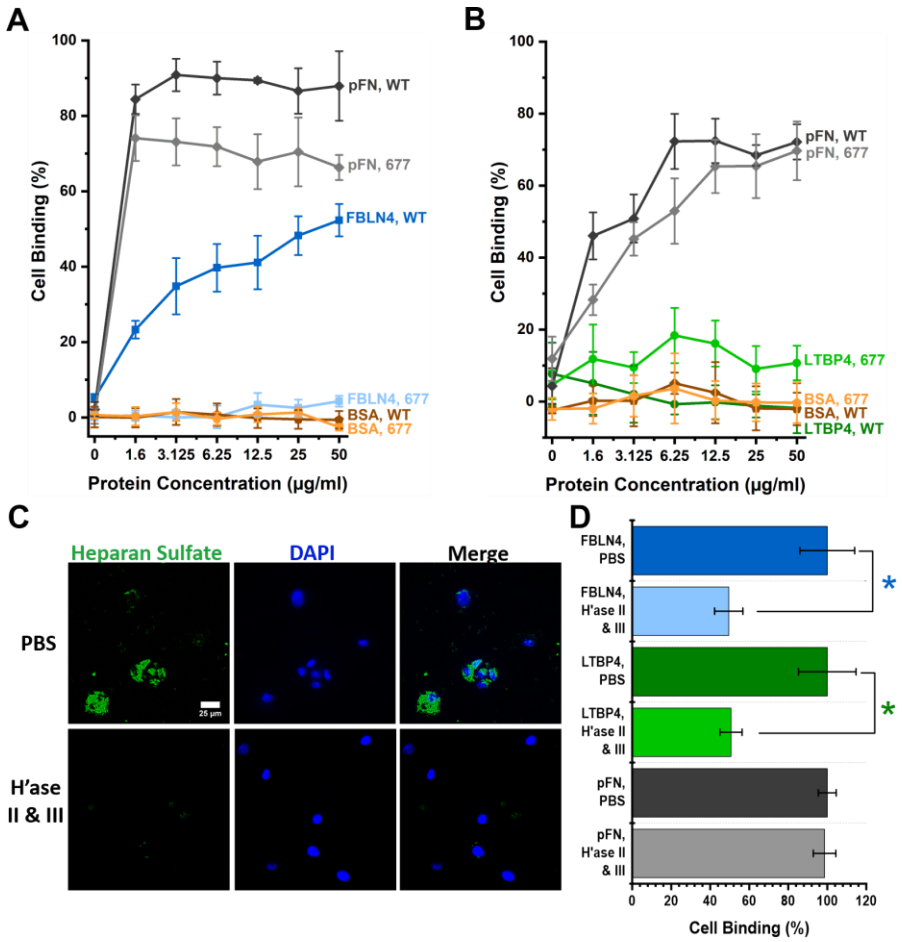

Figure 8. Cell surface-located heparan sulfate mediates FBLN4 and LTBP4 cell interactions
(A-B) Adhesion of wild-type and heparan-sulfate-deficient CHO cells to FBLN4 (A) and LTBP4 (B) as analyzed by crystal violet staining. BSA was used as a negative control while pFN was used as a positive control in cell binding. (C-D) Suspended skin fibroblasts were treated for 20 minutes at 37°C with Heparinases II and III (H'ase II & III) in PBS containing 1g/L Glucose and 0.1 mM $CaCl_2$ and 0.1 mM $MgCl_2$. Then, drops of the cell suspensions were smeared on a glass slide and fixed with 4% PFA and processed for IF staining of heparan sulfate. (C) IF images show the absence of heparan sulfate staining on the cell surface of the treated cells comparing to the buffer control. Scale bar presents 25 µm. (D) The H'ase II & III-treated cells were used for crystal violet binding assay to analyze their interactions with FBLN4 and LTBP4.pFN was used as a cell binding positive control for non-treated and treated cells. Error bars represent SD±mean of t technical replicates of one representative experiments out of 3 repeats. Statistical analyses were performed using student *t*-test.

fibroblasts with a cocktail of siRNA against SDC2-4 or GPC2-6, or with scrambled siRNA without any mammalian target sequences, which served as a negative control in all siRNA knockdown experiments. 3 d after siRNA transfection, cells were suspended for cell binding assays with FBLN4 and LTBP4, as well for qPCR analysis to confirm the knockdown efficiency. The strategy of siRNA knockdown described in the method chapter (see section *2.18* for details) was very

effective. By day 3, very little to no mRNA expression was detected for the knockdown of SDCs and GPCs relative to their scrambled control (Fig. 9A-B). Skin fibroblast adhesion to FBLN4 and LTBP4 was entirely disrupted with cells transfected with SDC2-4 specific siRNA, whereas the knockdown with the GPC2-6 siRNA pool did not affect cell binding (Fig. 9C). These data demonstrate that one or more of the SDC2-4 mediate cell interactions with FBLN4 and LTBP4.

3.9 siRNA knockdown of specific syndecans abolishes cell interactions with FBLN4 and LTBP4

To identify the exact cell receptors on elastogenic cells that interact with FBLN4 and both LTBP4 isoforms, we used individual siRNAs silencing SDCs instead of pools.

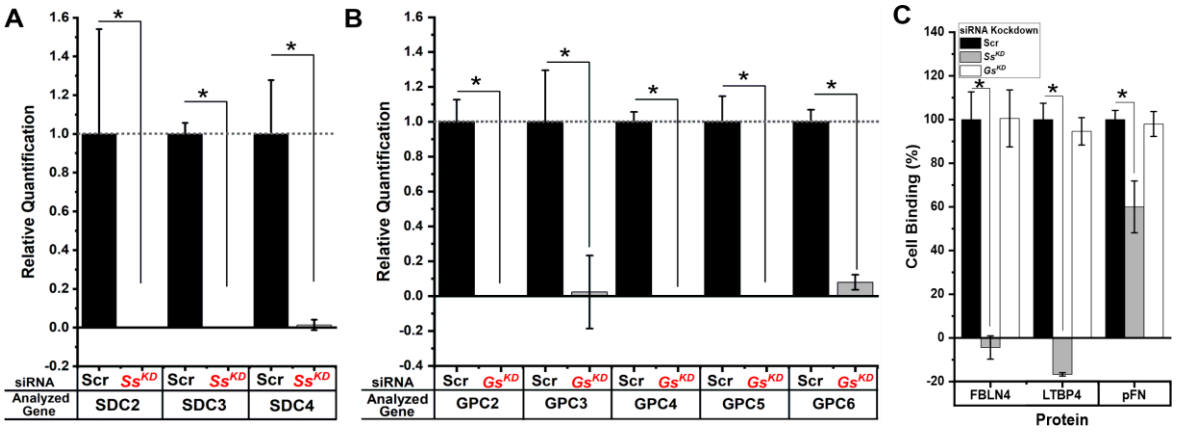

Figure 9. Knockdown of syndecans, but not glypicans, reduces cell interactions with FBLN4 and LTBP4
(A) Relative quantification of syndecan-2, -3, and -4 mRNA levels (SDC2, 3, & 4, respectively) in human skin fibroblasts that were transfected with either scrambled siRNA (Scr) as negative control, or a pool of specific siRNA designed to knockdown syndecan-2, -3, and -4 (Ss^{KD}). Cells were transfected with siRNA and cultured for 3 d. mRNA levels were quantified using real-time qPCR. (B) Similarly, the mRNA expression levels of glypican-2 to 6 (GPC2, 3, 4, 5 & 6, respectively) were relatively quantified after transfection with either scrambled siRNA (Scr) as a negative control, or a specific siRNA pool designed to knockdown glypicans-2-6 (Gs^{KD}). Data in (A) and (B) are represented as means of ΔΔCT ± SD (n=3). Two endogenous controls were used (GAPDH and RPL13A) and the mRNA level in the knockdown sample was relatively compared to its expression in the scrambled siRNA control. (C) Skin fibroblasts transfected with scrambled siRNA, or with specific siRNA pools for syndecans 2-4 or glypicans 2-6 were used to analyze their interactions with FBLN4 and LTBP4 3 d after transfection (n=3). Error bars represent SD±mean of four technical replicates of one representative experiments out of 3 repeats. Statistical analyses were performed using two-way ANOVA.

Skin fibroblasts from different donors were transfected with SDC-specific siRNA and collected on day 1 and 3 after transfection for real-time qPCR analyses to validate the siRNA knockdown efficiency and to examine the consequences of knocking down SDCs on the mRNA expression levels for elastic fiber proteins, including FBN1 and ELN, as well as FBLN4 and

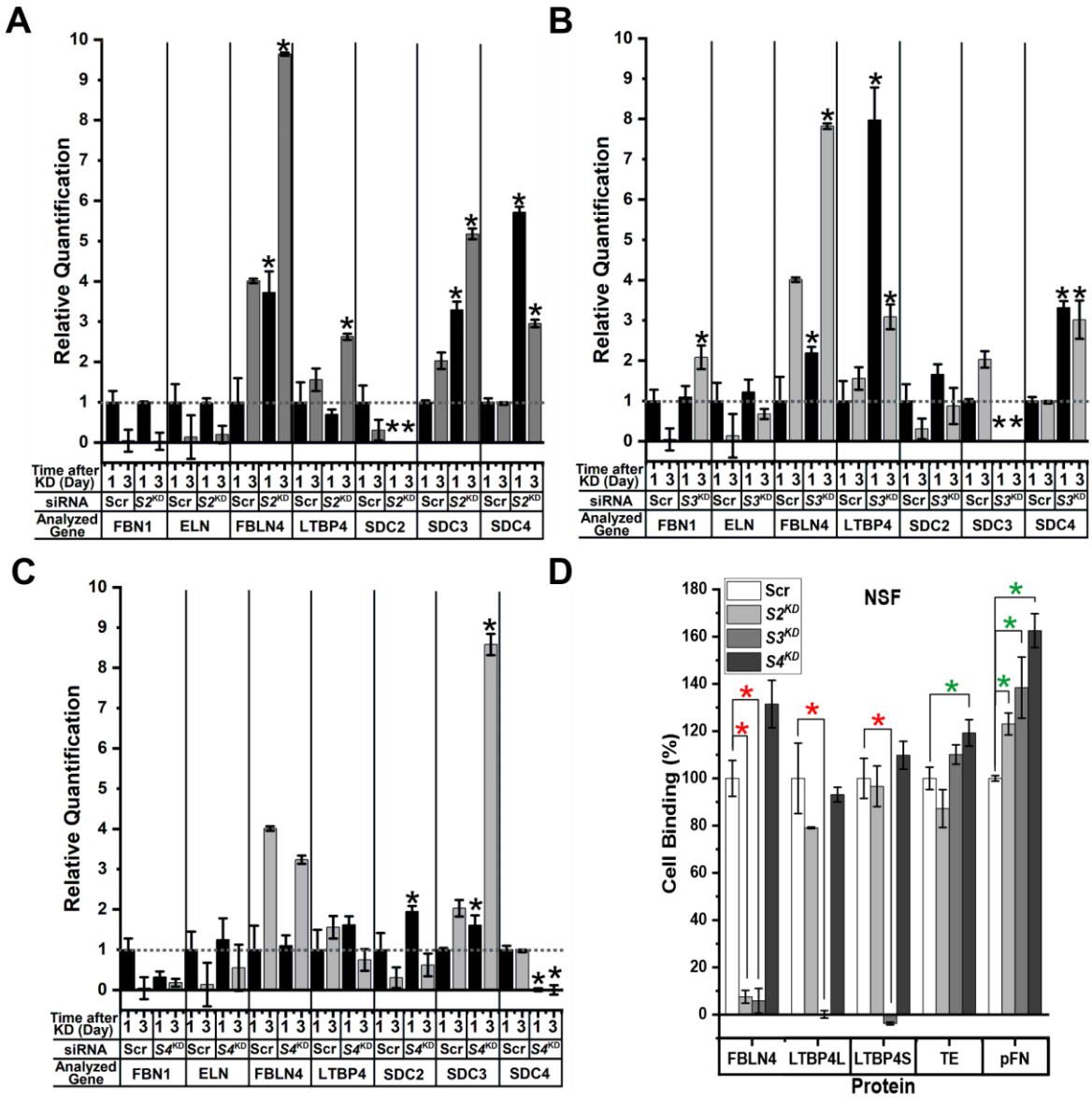

Figure 10. Silencing the expression of certain syndecans abolishes skin fibroblast interactions with FBLN4 and LTBP4

(A-C) Relative quantification of mRNA levels by real-time qPCR for fibrillin-1 (FBN1), elastin (ELN), FBLN4, LTBP4 and syndecans 2-4 (SDC2-4) in human skin fibroblasts transfected with either scrambled siRNA (Scr) or siRNA specific for (A) SDC2 ($S2^{KD}$), (B) SDC3 ($S3^{KD}$), or (C) SDC4 ($S4^{KD}$), analyzed 1 or 3 d after transfection. GAPDH and RPL13A mRNA were used as endogenous references, and each mRNA was relatively compared to its expression in the scrambled control at day 1 (set to 1). Data in (A-C) are represented as means of $\Delta\Delta CT \pm SD$ (n=3). Asterisks indicate significant changes relative to the scrambled controls. (D) Human skin fibroblast binding to FBLN4, LTBP4, TE and pFN was assayed using crystal violet staining at 3 d after siRNA transfection targeting SDC2, SDC3, and SDC4 as indicated (n=5). Red asterisks indicate significant decreases, whereas green asterisks indicate significant increases in cell adhesion, compared to the scrambled controls. Statistical analyses were performed using two-way ANOVA.

LTBP4 (Fig. 10 A-C). Consistently, the mRNA expression levels of SDC2 (Fig. 10A), SDC3 (Fig. 10B) and SDC4 (Fig. 10C) were either completely absent or drastically reduced on day 1 and 3

after siRNA transfection. Commonly, knocking down an individual SDC elevated the mRNA levels of other syndecans. When SDC2 was knocked down, SDC3 and SDC4 were significantly increased on day 1 and 3 (Fig. 10A). SDC3 knockdown resulted in upregulation of SDC4 (Fig. 10B), and SDC4 knockdown elevated SDC2 at day 1 and SDC3 at day 1 and 3 (Fig. 10C).

Interestingly, SDC2 or SDC3 specific siRNA silencing was associated with an elevation in mRNA expression of FBLN4 and LTBP4, but not SDC4 specific siRNA silencing (Fig. 10A-C). We noted also a significant increase in the expression of FBN1 mRNA on day 3 after transfecting skin fibroblasts with SDC3 siRNA (Fig. 10B). The mRNA expression of ELN in all transfected cells with siRNA specific to each SDC did not differ from the scrambled siRNA control (Fig. 10A-C). Skin fibroblasts transfected with siRNA to silence SDC2, SDC3, or SDC4 were assessed for cell adhesion to FBLN4, LTBP4L, LTBP4S, TE and pFN on day 3 after transfection (Fig. 10D). SDC2 or SDC3 siRNA knockdown in fibroblasts abolished interaction with FBLN4, whereas only SDC3 knockdown abolished the interaction with LTBP4S or LTBP4L. Interaction of the fibroblasts with TE and pFN was not reduced by knockdown of the analyzed SDCs. Contrary, knockdown of SDC4 increased interaction with TE, and knockdown of SDC2, 3, and 4 increased binding to pFN (Fig. 10D).

It has been shown that several ECM proteins interact with distinct syndecans in different cell types and species, such as FN that has affinity to SDC2[332] in some cells and SDC4 in other cell types[330], as shown using different cells. To determine the consistency of FBLN4 and LTBP4 interactions with the same individual syndecans among different cell types, we applied the same siRNA knockdown strategy to inhibit the expression of SDC2-4 in umbilical arterial smooth muscle cells (Fig. 11).

Consistent with the data obtained with skin fibroblasts, single SDC specific siRNA knockdown resulted in a higher mRNA expression of other syndecans (Fig. 11A-C). Also, the mRNA expression levels of FBLN4 and LTBP4 increased when SDC2 or SDC3 were knocked down (Fig. 11A-B). A significant increase in FBN1 mRNA expression was observed again in SMC transfected with SDC3 specific siRNA (Fig. 11B). No differential changes were monitored in the mRNA expression of FBN1, ELN, FBLN4 and LTBP4 when SDC4 was silenced in SMC (Fig. 11C). Similar effect of knocking down SDCs in skin fibroblasts, SMC adhesion to FBLN4 was significantly reduced when SDC2 or SDC3 were siRNA silenced, and only SDC3 siRNA

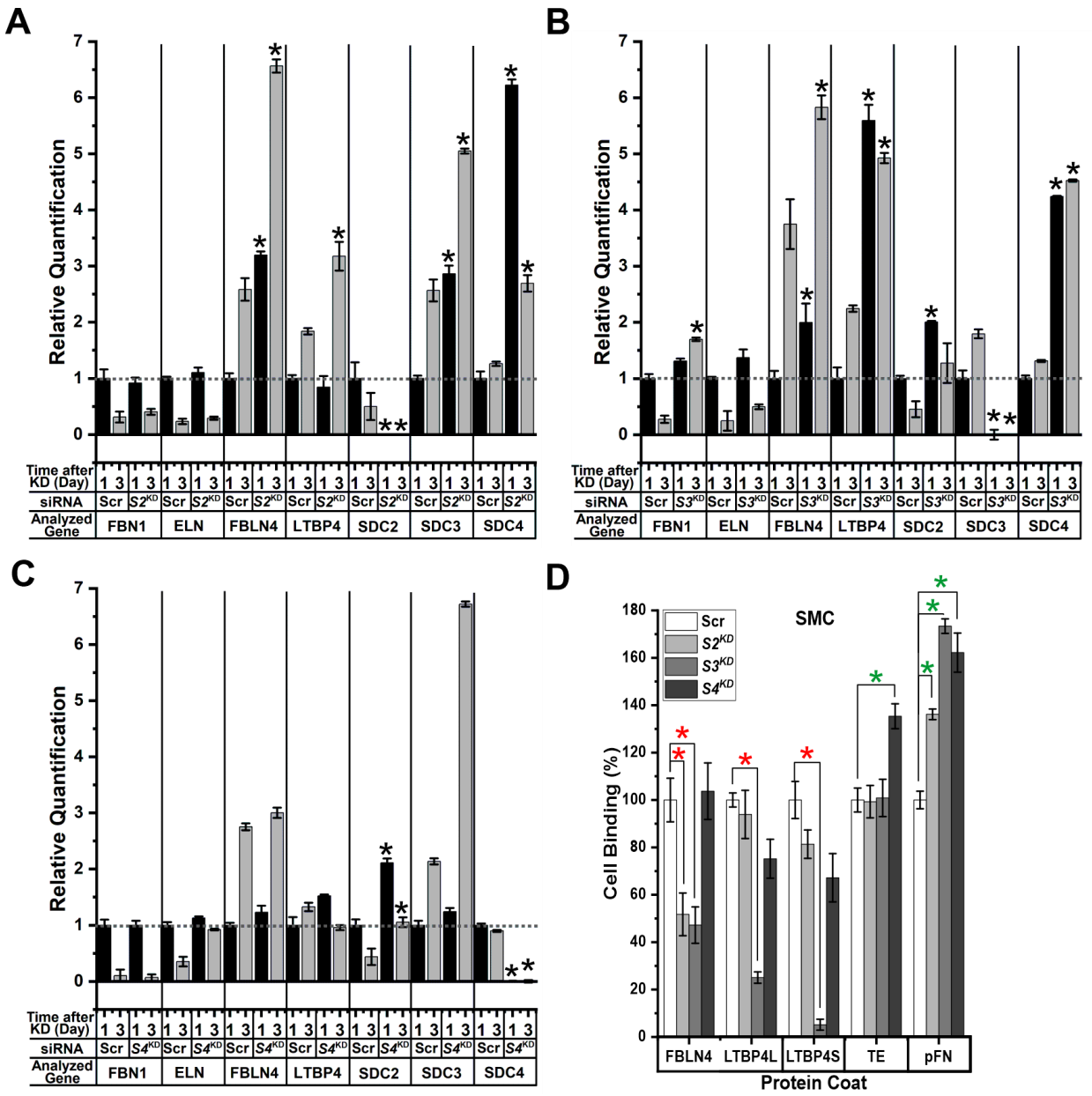

Figure 11. Knocking down Syndecan-2 and -3 in smooth muscle cells impedes interactions with FBLN4 and LTBP4

(A-C) Relative quantification by real-time qPCR of mRNA expression levels of FBN1, ELN, FBLN4, LTBP4 and SDC2, 3, and 4 in human umbilical artery smooth muscle cells (SMC) transfected with either scrambled siRNA (Scr) or siRNA specific for (A) SDC2 ($S2^{KD}$), (B) SDC3 ($S3^{KD}$), or (C) SDC4 ($S4^{KD}$), analyzed 1 or 3 d after transfection. Two endogenous references (GAPDH and RPL13A) were used, and each mRNA expression was relatively compared to its expression in the scramble control at day 1 (set to 1). Data in (A-C) are represented as means of ΔΔCT ± SD (n=3). Asterisks indicate significant changes relative to the scrambled controls. (D) Interactions of SMC with FBLN4, LTBP4, TE and pFN were assayed using crystal violet staining at 3 d after siRNA transfection targeting SDC2, SDC3, and SDC4 (n=5). Red asterisks indicate significant decreases, whereas green asterisks indicate significant increases in cell adhesion, compared to the scrambled controls. Statistical analyses were performed using two-way ANOVA.

knockdown significantly decreased SMC binding to both LTBP4 isoforms (Fig. 11D). Also correlating with skin fibroblasts, knocking down SDC4 increased SMC interactions with TE, and silencing SDC2, 3, or 4 significantly increased SMC interactions with pFN (Fig. 11D).

In summary, the results identified SDC2 and SDC3 as cell surface receptor for FBLN4, and SDC3 for LTBP4. These results are consistent for fibroblasts and smooth muscle cells.

3.10 FBLN4 interacts with the ectodomain of SDC2 and SDC3, whereas LTBP4 only interacts with SDC3 ectodomain

Each SDC has an extracellular domain on its N-terminal side, the ectodomain that carries multiple heparan sulfate chains either at the distal end (SDC2 and 4), or at both the distal and proximal ends (SDC1 and 3)[333]. The ectodomain of all SDCs is followed by conserved transmembrane and cytoplasmic domains[333; 334] (Fig. 12 A, see the domain structure of the full length SDC2-4). SDCs function as cell adhesion receptors through heparan sulfate chains on their ectodomains interacting with a range of ECM proteins[214].

After documenting the inhibitory effect of SDC-specific siRNA silencing on FBLN4 and LTBP4 cell interactions, we analyzed if FBLN4 and LTBP4 can directly interact with SDCs. Therefore, we produced recombinant ectodomains (SDC-ED) of SDC2-4 to be used in solid phase protein binding assays. It is important to produce these ectodomains by mammalian cells that facilitate proper posttranslational modifications (including heparan sulfate synthesis), since the interactions with FBLN4 and LTBP4 occur through heparan sulfate located on their ectodomains. Therefore, we transfected HEK-EBNA cells with plasmid constructs coding for FLAG- (C-terminus) and His- (N-terminus) tagged ectodomains of SDC2-4 (omitting the transmembrane and cytosolic domains). This procedure facilitated secretion of the ectodomains into the culture medium (Fig. 12 A, see SDC-ED structures). The presence of recombinant SDC-ED in the condition media was confirmed using Western blotting (Fig. 12B). The immunoblotting analysis using an anti-FLAG antibody showed faint bands staining for the SDC-ED proteins when the condition media was used in the analysis 20× concentrated. No band was detected in the negative control (conditioned medium from non-transfected cells). In summary, the data show that SDC-ED2-4 were secreted in low amounts into the cell culture medium.

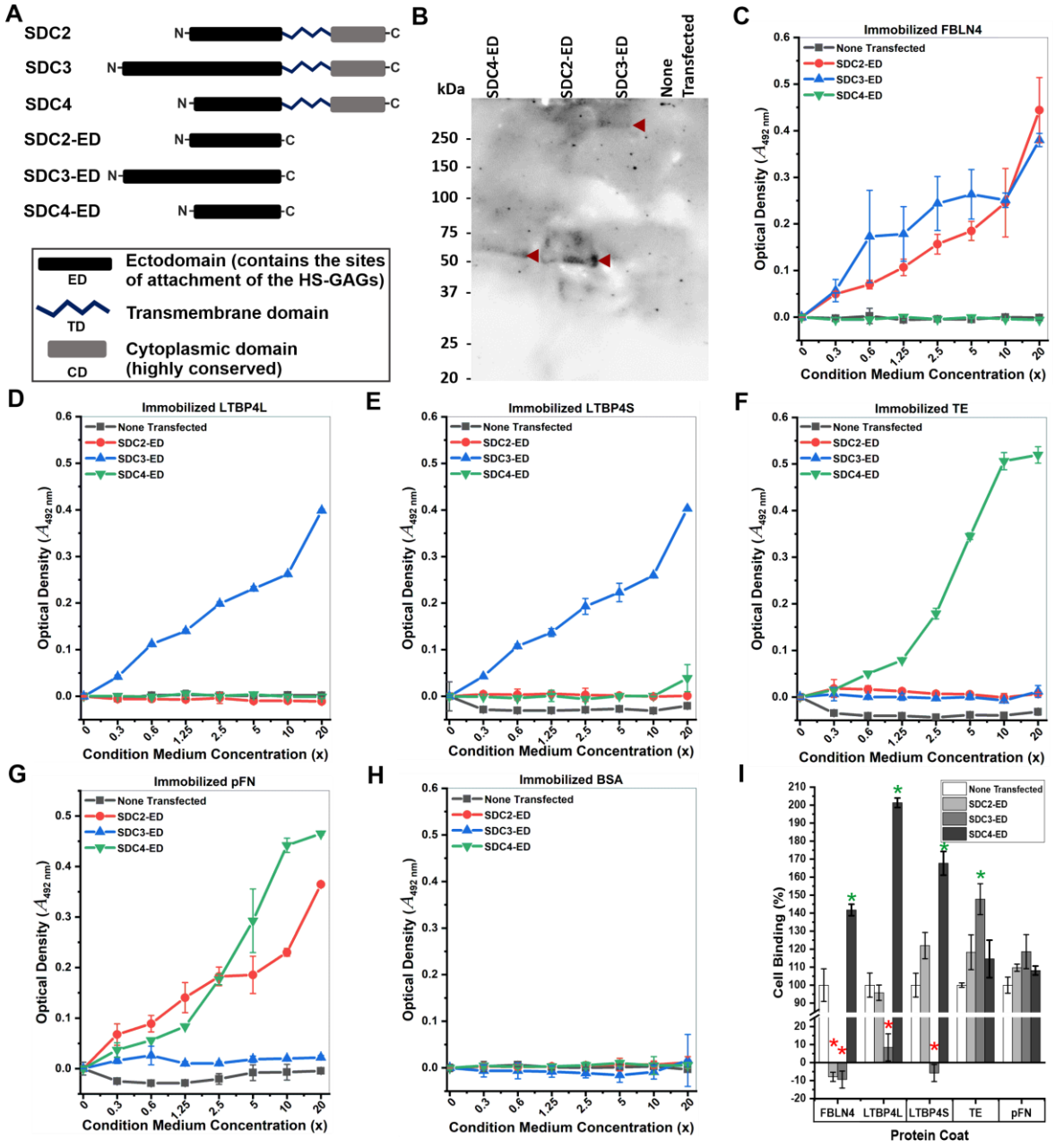

Figure 12. Syndecans interact directly with FBLN4 and LTBP4

(A) Schematic presentation of the domain arrangement of full length syndecan proteins (SDC2-4; top) and the recombinant syndecan ectodomain constructs (SDC2, 3 and 4-ED), which were FLAG-tagged at the N-terminal end following the signal peptide and contained a C-terminal His-tag. (B) Condition media were collected from non-transfected and transfected HEK-EBNA cells with SDC-ED expressing plasmids. The condition media were 20× concentrated and resolved using 7.5-15% gradient SDS-PAGE gels, followed by immunoblotting analysis using an anti-FLAG-tag antibody. The recombinant protein bands are indicated by red arrowheads. Marker proteins are shown on the left in kDa (C-H) Representative solid phase binding assays with immobilized FBLN4 (C), LTBP4L (D), LTBP4S (E), pFN (F), TE (G) and BSA (H) and serial dilutions (0-20-fold) of conditioned media collected from cell cultures of non-transfected and transfected HEK-EBNA cells with the SDC-ED expressing plasmids in the soluble phase. (I) Representative cell binding assay of fibroblast interactions with FBLN4, LTBP4L, LTBP4S, TE and pFN in the presence of 20× concentrated conditioned media collected from non-transfected and SDC-ED-transfected HEK-EBNA cells. A significant decrease in cell adhesion is marked with a red asterisk while a significant increase is indicated by a green asterisk. Statistical analyses were performed using two-way ANOVA.

The low yields of the recombinant SDC-EDs prevented effective protein purification from the collected condition media by immobilized metal ion affinity chromatography (through the His-tag). This is a typical observation for low-yield recombinant proteins, because the binding sites on the immobilized metal ion affinity column will then be occupied by weakly binding non-specific proteins present in the cell culture medium (data not shown). Therefore, to test the interactions of FBLN4 and LTBP4 with the SDC ectodomains in solid phase binding assays, we first coated the target proteins in 96-well plates and then used serially diluted conditioned media (starting from a 20× concentrate), containing the recombinant SDC-EDs, as the soluble phase. Bound SDC-EDs were specifically detected by an anti-FLAG antibody. Concentrated conditioned medium from non-transfected cells was used as negative control.

Representative solid phase binding assays between soluble SDC-EDs and immobilized FBLN4, LTBP4L, LTBP4S, TE and pFN are shown in Fig. 12C-G. BSA was used as a negative control for interactions with SDC-EDs (Fig. 12H). FBLN4 showed strong binding to both SDC2-ED and SDC3-ED (Fig. 12C), whereas both LTBP4L and LTBP4S interacted only with SDC3-ED (Fig. 12D-E). These data confirm the results obtained with the siRNA knockdown approach. Interestingly, TE interacted strongly with SDC4-ED (Fig. 12F).

As expected from previous studies, the solid phase binding data showed that pFN directly interacts with SDC2-ED and SDC4-ED, but not with SDC-ED3 (Fig. 12G)[198; 330; 332]. None of the recombinant SDC-EDs bound to BSA (Fig. 12H).

To further corroborate that FBLN4 and LTBP4 cell-interaction is mediated through the identified SDC-EDs, we implemented a cell binding inhibition strategy. 20-fold concentrated conditioned media containing recombinant SDC-EDs were added to the cell binding assay to compete for the binding of skin fibroblast to FBLN4, LTBP4L and LTBP4S. Additionally, we included TE and pFN as controls). SDC2-ED or SDC3-ED containing media inhibited cell interaction with FBLN4, whereas only SDC3-ED containing medium inhibited cell interaction with LTBP4L and LTBP4S (Fig. 12I).

3.11 siRNA knockdown of syndecans results in compromised FBLN4, LTBP4 and TE fibers

To explore the function of SDC-FBLN4, -LTBP4, and -TE interactions in elastogenesis, we assessed the consequences of SDC-specific siRNA silencing on elastic fiber assembly in skin fibroblast cultures. The siRNA transfected cells were cultured for 5 d to provide sufficient time for

these cells to produce, secret and assemble the elastic fiber proteins of interest (FBLN4, LTBP4 and TE). On the other hand, 5 d is still within the timeline of the transient siRNA effect on SDC expression. As demonstrated by immunofluorescence staining, silencing SDC2 and 3 expression in skin fibroblasts resulted in compromised elastic fiber assembly/deposition (Fig. 13A). Quantification of the signal intensities after knocking down SDC2 or -3 significantly reduced the assembly/deposition of all the three proteins, FBLN4, LTBP4 and TE in the ECM (Fig. 13B), demonstrating that SDC2 and -3 play a pivotal role in the assembly/deposition of these elastogenic proteins. This strongly suggests a mechanism in which the cell interactions with FBLN4 and LTBP4 are crucial for their subsequent roles in mediating elastic fiber assembly.

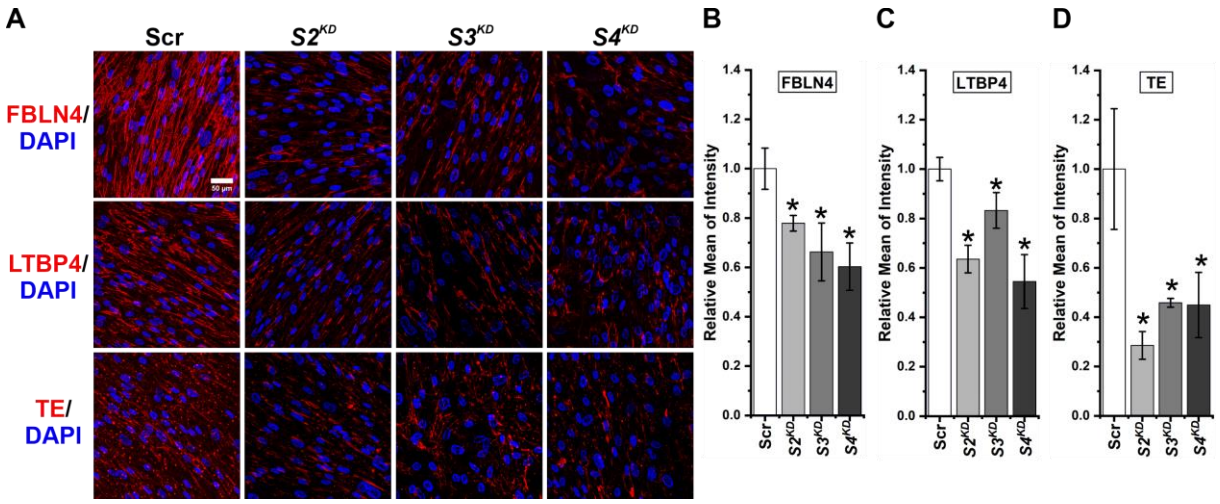

Figure 13. Knocking down syndecans results in compromised FBLN4, LTBP4 and TE fibers
(A) Representative IF images after knocking down syndecan-2 and -3 ($S2^{KD}$, $S3^{KD}$) on FBLN4, LTBP4 and TE fiber assembly in 5 d skin fibroblast cultures. Scale bar presents 50 µm. (B-D) Quantification of the IF staining in (A) including FBLN4 (B), LTBP4 (C), and TE (D) signal intensity relative to the scrambled siRNA control (Scr). Error bars represent SD±mean of four technical replicates of one representative experiments out of 3 repeats. Statistical analyses were performed using two-way ANOVA.

3.12 FBLN4 and LTBP4 stimulate focal adhesion kinase phosphorylation

It is well known that cell adhesions to ECM proteins promote FA formation which in response can reinforce matrix assembly, such as cell interactions with fibronectin[198; 335]. To investigate if FBLN4 and LTBP4 cell interactions enhance FA formation, phosphorylated focal adhesion kinase (pFAK) was evaluated as a proxy readout in skin fibroblasts cultured 24 h on immobilized FBLN4 and LTBP4. Western blotting of cell lysates revealed a significant

upregulation of pFAK when cells were cultured on FBLN4 or LTBP4, compared to the buffer control (Fig. 14 A-B).

These data were further validated by immunofluorescence analysis of fibroblasts cultured on Y-shaped protein-coated micropatterns to ensure comparability of the cells based on the available area and shape (Fig. 14C). Fibroblasts seeded on either FBLN4 or LTBP4-coated micropatterns showed significantly more as well as larger FAs visualized by pFAK staining (Fig. 14 D-E). Notably, actin staining representing stress fibers, produced more intense fluorescence signals in cells cultured on FBLN4 and LTBP4-coated wells, as compared to the buffer control (Fig. 14C). In addition, a strong actin staining localized to the nuclei when fibroblasts were seeded on immobilized LTBP4 (Fig. 14C). In summary, these results show that FBLN4 and LTBP4 promote FA formation and activation, as well as stress fiber formation.

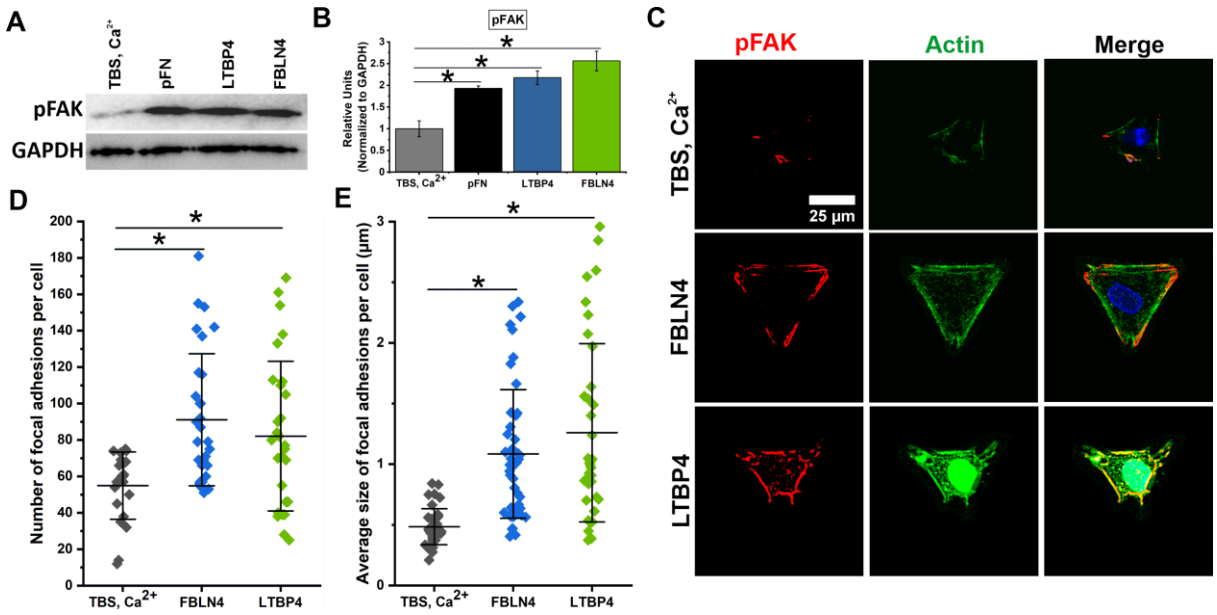

Figure 14. FBLN4 and LTBP4 cell interactions promote focal adhesion formation
(A) Skin fibroblasts were seeded in culture wells coated with FBLN4, LTBP4, pFN for 24 h. TBS, Ca^{+2} was used as a buffer/negative control. Cell lysates were prepared and used for immunoblotting with an anti-pFAK antibody. GAPDH was utilized as an internal control. (B) Quantification of pFAK levels analyzed by Western blotting (n=3). The values are presented as relative ratios to the buffer control after normalizing pFAK bands to the corresponding GAPDH band for each specific sample. (C) IF staining of pFAK (red) was performed 24 h after culturing skin fibroblasts on Y-shape micropatterns coated with either FBLN4, LTBP4 or TBS, Ca^{+2} as buffer control. Actin staining (green) was used to visualize the cell skeleton, whereas DAPI (blue) was used to stain nuclei. Scale bar represents 25 µm. (D-E) Quantification of the red pFAK signals in (C) in terms of FA number (D), and average size (E) per cell normalized to the respective control. Statistical analyses were performed using student *t*-test.

3.13 FBLN4 and LTBP4 cell interactions induce cell contraction

The stress fiber promoting effect of FBLN4 and LTBP4 suggested that these proteins can instruct cells to contract and exert tension on the surrounding matrix, including FBLN4, LTBP4 and TE which may be necessary for elastic fiber formation. To test the role of FBLN4 and LTBP4 on cell contractility, collagen gel contraction assay typical for mechanobiological studies were used. Skin fibroblasts were cultured in 3-dimensional collagen type I gels, containing either FBLN4, LTBP4, or the buffer control.

To maximize the effect size, we used skin fibroblasts in advanced passages (12-17) to ensure that the cells already maximally differentiated into contractile myofibroblasts, as shown by IF staining for the cell contractility marker αSMA (Fig. 15A). Floating disk-shaped collagen gels were prepared either without cells (background control) or populated with skin myofibroblasts. The gels were prepared with 10 µg/ml FBLN4, LTBP4, pFN or TBS, Ca^{+2} buffer as negative control (Fig. 15B). Addition of FBLN4 and LTBP4 significantly increased the contraction of the fibroblast-cellularized collagen gels starting from day 3 of incubation and continuing until the experimental end point on day 7, as measured by the reduction of the gel area (Fig. 15B-C). Altogether, these data demonstrate that FBLN4 and LTBP4 cell interactions mediate skin fibroblasts contractions.

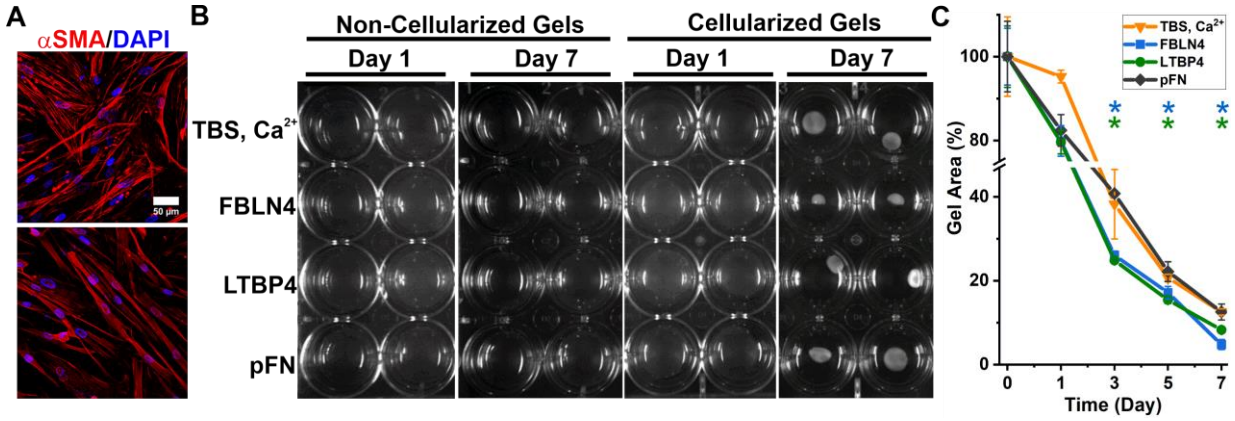

Figure 15. FBLN4 and LTBP4 cell interactions stimulate cell contraction
(A) Representative IF images of αSMA (red) in skin fibroblast cultures used in collagen gel contraction assays. Cultured cells were counterstained with DAPI (blue) showing that 100% cells were αSMA positive (red) differentiated myofibroblasts. Scale bar presents 50 µm. (B) Skin fibroblasts were subjected to a 3D-collagen type I gel contraction assay to test the effect of FBLN4 and LTBP4 on cell contractility. Images of floating non-cellularised and cellularised collagen gels were recorded at day 0, 1, 3, 5, and 7. Representative images are shown here for day 1 and 7. TBS, Ca^{+2} was used as a buffer control. (C) The collagen gel areas in (B) were quantified at the indicated time points and are presented in percentage relative to the gel areas at the start time point. The significant reduction in the gel area is indicated by color-coded asterisks on top of the graph matching the color code of the corresponding protein. Statistical analyses were performed using two-way ANOVA.

3.14 FBLN4 and LTBP4 cell interactions elevate Erk1/2 protein expression and RhoA activation

Since we determined that FBLN4 and LTBP4 cell interactions affect focal adhesion formation and trigger cell contraction, we continued to determine the signaling pathway involved in these cellular mechanisms.

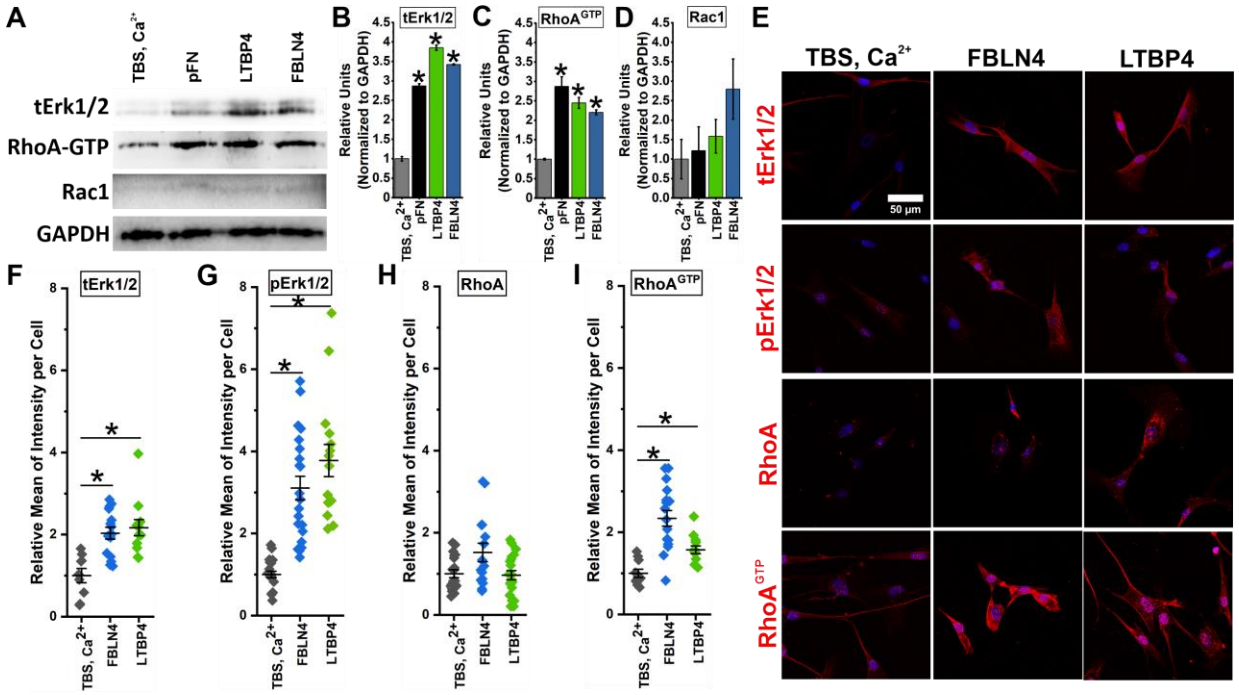

Figure 16. FBLN4 and LTBP4 cell interactions elevate Erk1/2 protein levels and RhoA activation
(A) Skin fibroblasts were seeded in culture wells coated with FBLN4, LTBP4, pFN for 24 h, then cell lysates were prepared and used for immunoblotting analysis with specific antibodies against the indicated proteins. (B-D) The levels of target signaling proteins analyzed by Western blotting in (A) were quantified by densitometry. The data are shown relative to the TBS, Ca^{+2} buffer control after normalizing each protein band with the respective GAPDH band, including tErk1/2 (B), $RhoA^{GTP}$ (C), and Rac1 (D). (E) IF analyses of tERK1/2, pErk1/2, RhoA, and RhoAGTP (all in red) in skin fibroblasts cultured for 24 h on either FBLN4 or LTBP4 coated wells. TBS, Ca^{+2} was used as a buffer/negative control. DAPI (blue) was used for nuclei counterstaining. Scale bar presents 50 µm. (F-I) The signal intensity of the IF staining presented in (E) was quantified as relative mean of intensity per cell. Statistical analyses were performed using student *t*-test.

It is well known that Rho family GTPases are regulators of actin filament remodeling leading to cell contraction[336-338]. It has been shown that Rho regulates the assembly of contractile actin filaments while Rac1 and Cdc42 regulate actin polymerization[336; 339-341]. ECM proteins and growth factors stimulate FA formation and new actin stress fibers exerting tension on the ECM via RhoA signaling[338; 342]. Also, it has been demonstrated that phosphorylation/activation of Erk1/2 induces cell contraction[343-345]. In addition, Erk promotes RhoA activation which increases actin

stress fiber formation[346]. To determine the involvement of these signaling molecules in FBLN4- and LTBP4- induced focal adhesion and actin stress fiber regulation, we examined the protein expression levels of Erk1/2, RhoA, and Rac1 in skin fibroblasts exposed to immobilized FBLN4 and LTBP4 for 24 h in serum-free media.

Cell lysates analyzed by Western blotting showed a significant increase in the levels of total Erk1/2 (tErk1/2) and active RhoA (RhoA-GTP), but not Rac1, when incubated in FBLN4, LTBP4 and pFN coated wells, as compared to the buffer control (Fig. 16A-D).

To consolidate these results and intracellularly visualize the effect of FBLN4 and LTBP4 cell interactions on the protein levels of Erk1/2 and RhoA, skin fibroblast were cultured on FBLN4 and LTBP4-coated wells and analyzed by IF imaging (Fig. 16E). After 24 h incubation, the signal intensities of tErk1/2 and phosphorylated/activated Erk1/2 (pErk1/2) were significantly increased in cells kept in FBLN4 and LTBP4 coated wells (Fig. 16E-G). While total RhoA IF staining did not differ under the examined conditions, active RhoA increased significantly in cells exposed to immobilized FBLN4 and LTBP4, as compared to the buffer control (Fig. 16E, H & I). These results suggest that cell interactions with FBLN4 and LTBP4 promote focal adhesion formation and cell contraction through Erk1/2 and RhoA activation.

3.15 FBLN4 and LTBP4 cell interactions enhance cell migration

It has been reported previously that cell migration was reduced when FBLN4 was decreased or absent, using vascular smooth muscle cells obtained from *Fbln4*$^{-/-}$ and *Fbln4*$^{R/R}$ mice. This was associated with impairment in smooth muscle actin filaments[347]. However, it is not known if these deficiencies were due to the loss of cell interactions with endogenous FBLN4 in the matrix. The role of LTBP4 in cell migration has not been addressed in the literature. Since FBLN4 and LTBP4 cell interactions resulted in increased focal adhesion formation and cell contraction, we hypothesized that the cell interactions with both proteins enhance cell migration. To test this hypothesis, skin fibroblast migration driven by FBLN4 and LTBP4 cell interactions were examined using ECIS and live cell imaging. In ECIS, we used culture wells specifically designed to analyze cell migration. These plates contain small electrodes in the center that can be activated to generate an “electric fence” preventing cell adhesion or migration onto this electrode

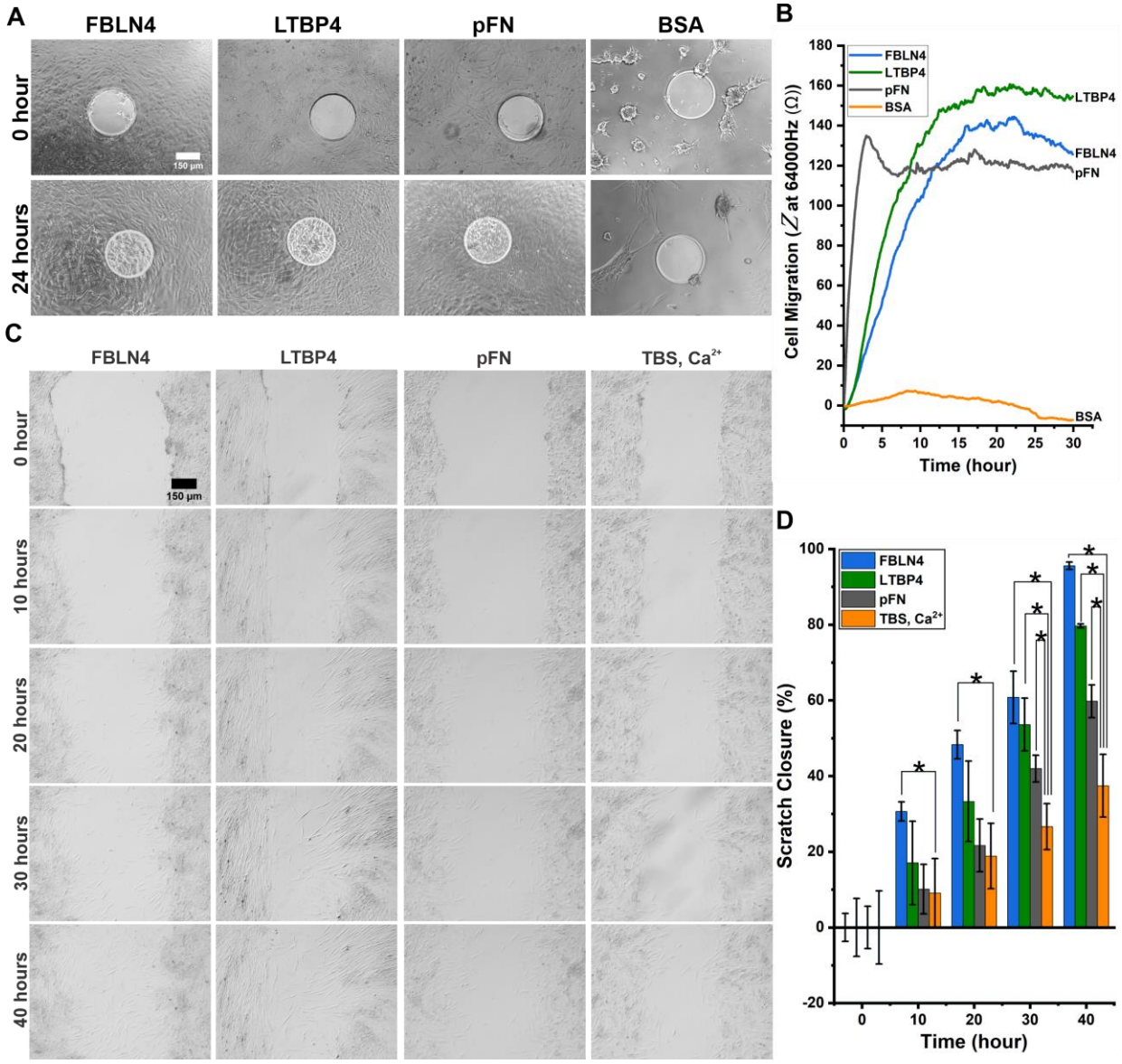

Figure 17. FBLN4 and LTBP4 cell interactions enhance cell migration

(A) ECIS based tracking cell migration on coated wells with FBLN4 and LTBP4. pFN and BSA coated wells were used for positive and negative controls, respectively. Skin fibroblasts were seeded on ECIS culture wares in serum free media to form a cell monolayer for 24 hours with electric fence activated on designed areas that will not allow any cell adhesion or migration before forming the cell monolayer. Then, electric fence was removed (0 hour) to start assessing cell migration over time. Images of the electrodes after 24 hours of cell migration show the electrode surfaces were completely covered with cells in wells coated with FBLN4, LTBP4, and pFN, but not BSA. Scale bars present 150 µm. (B) Change in cell migration was displayed in average magnitude of impedance (ohm of an electrical current frequency at 64000 Hertz) over the calibrated areas for 30 hours after removing the electric fence. Data for each curve show collected measurements averaged for duplicates. (C) Representative images of skin fibroblast migration in scratch assay at 0, 10, 20, 30 and 40 hours post scratch formation on cell monolayer in serum free media. Scale bars present 150 µm. (D) Quantitative analysis of the cell migration in the scratch area was performed for duplicates measuring the scratch closure (%). Significance was measured comparing the scratch closure values of protein coated wells to the buffer control wells (TBS, Ca^{2+}). Statistical analyses were performed using two-way ANOVA.

until a cell monolayer is formed in the outside area. At that point, the electric fence can be deactivated allowing cells to migrate onto the electrode surfaces, which can be followed by impedance measurements. Serum-starved skin fibroblasts were seeded into the ECIS culture wells coated with FBLN4, LTBP4, pFN or BSA. Cells were incubated in serum-free media for 10 h to form a cell monolayer while the electric fence was activated. Thereafter, the cells were allowed to migrate onto the electrode for up to 30 h.

Microscopic examination at 24 h of cell migration showed that the electrode surfaces have been completely covered by migrated cells in wells coated with FBLN4, LTBP4 or the positive control pFN, but not on BSA-coated wells, as compared to images at 0 h (Fig. 17A). The measured impedance showed a rapid increase in cell migration on immobilized pFN within the first 3 h, and reached a plateau characterized by minor changes in the impedance, reflecting continuous changes in cell morphology including cell contraction and motility (Fig. 17B). A relatively similar pattern was observed for the wells coated with FBLN4 and LTBP4 (Fig. 17B). However, when the plateau was reached that presents variations in the cell shape related to cell contraction and motility, the total impedance was higher in FBLN4 and LTBP4 coated wells than in pFN coated wells (Fig. 17B). This data is consistent with the results from collagen gel contraction assays in which FBLN4- and LTBP4-containing gels showed stronger contraction than pFN (Fig. 15B-C).

Complementing the cell migration data obtained by ECIS analysis, we conducted cell migration scratch assays utilizing live-cell imaging. Serum starved skin fibroblasts were seeded on wells coated with FBLN4, LTBP4, pFN or TBS, Ca^{+2} to form cell monolayers. Then, scratches were introduced to generate a gap for cell migration. The scratch closures were measured at different time points (Fig. 17C-D, Movie 5-8). Skin fibroblast migration on immobilized FBLN4 and LTBP4 was significantly accelerated compared to the buffer control (Fig. 17D). After 40 h, the scratches were closed near to 100% in FBLN4 coated wells and about 80% in LTBP4 coated wells, whereas cells in pFN coated wells showed about 60% scratch closure (Fig. 17C-D, Movie 5-8). In summary, the results prove that cell interactions of FBLN4 and LTBP4 induce cell migration.

3.16 Cell interactions of FBLN4, but not LTBP4, increase cell proliferation

It was shown in several studies that ECM-cell interactions can affect cell proliferation, with some ECM proteins exerting a promoting effect on cell proliferation[348; 349], and others decrease

it[350; 351]. As cell density determines the number and extend of elastic fiber formation, a sufficient cell proliferation might be critical for downstream elastogenesis. To assess proliferation rates of skin fibroblasts upon interaction with FBLN4 and LTBP4, we utilized two methods: IF staining specific for a cell proliferation marker, Ki67, and crystal violet staining for skin fibroblasts cultured for 24 and 48 h on FBLN4, LTBP4, pFN or TBS, Ca^{+2} coated wells (Fig. 18).

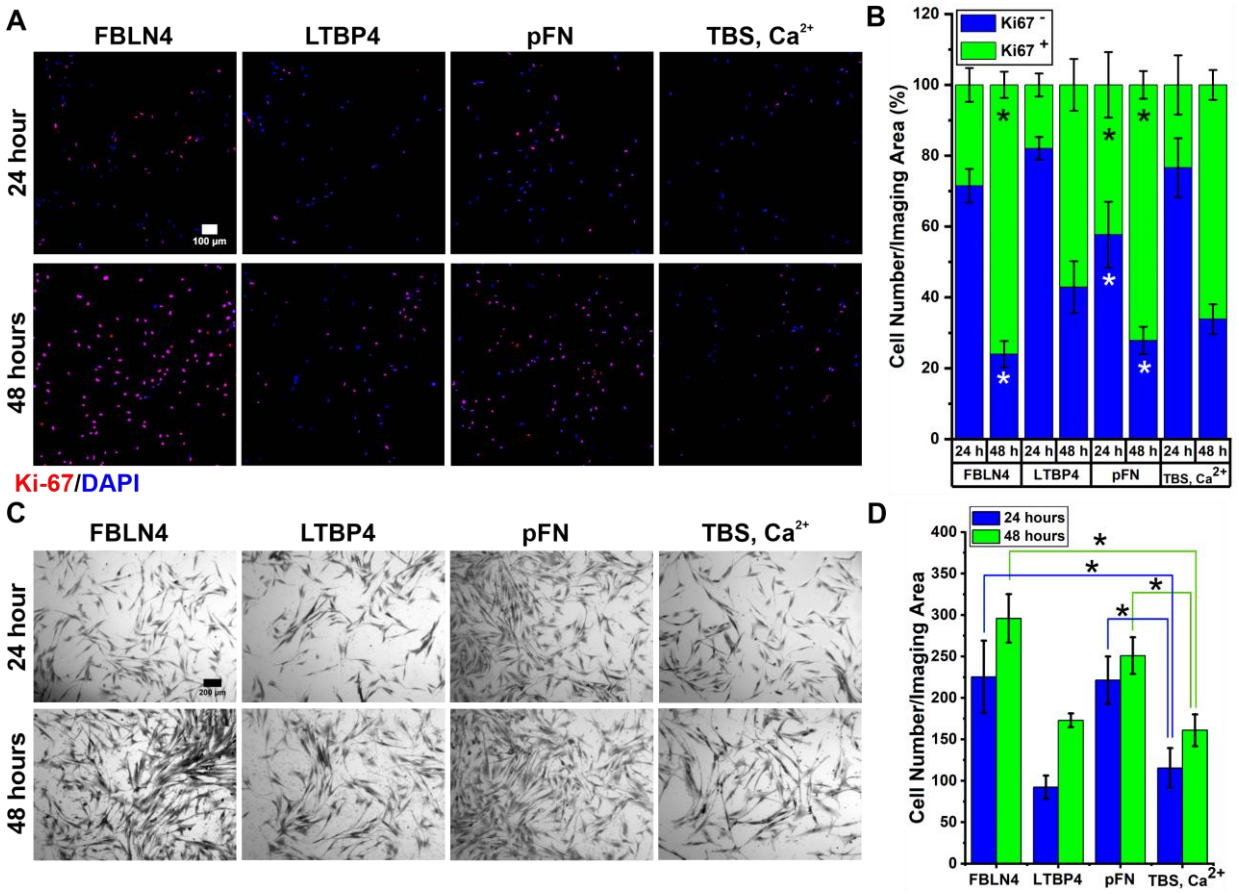

Figure 18. Cell interactions of FBLN4, but not LTBP4, increase the rate of cell proliferation
(A) IF analysis of Ki-67 (red) in skin fibroblasts cultured for 24 and 48 h on coated wells with FBLN4, LTBP4, pFN and TBS, Ca^{+2}. DAPI (blue) was used as a nuclei counterstain. Scale bar presents 100 µm. (B) Quantification of the Ki-67 positive/proliferating cells ($Ki67^{+}$) compared to non-proliferating cells (Ki-67 negative, $Ki67^{-}$). Relative to the buffer control, the significant differences in $Ki67^{+}$ cell number are indicated by black asterisks whereas the significant differences in $Ki67^{-}$ cell number are indicated by white asterisks .(C) Representative images of crystal violet stained skin fibroblasts cultured for 24 and 48 h on FBLN4, LTBP4, pFN or TBS, Ca^{+2} coated wells. Scale bar presents 200 µm. (D) Total numbers of crystal violet stained cells in (C) were counted per image (n=5). Statistical analyses were performed using two-way ANOVA.

IF staining with an anti-Ki67 antibody demonstrated that 24 h and 48 h skin fibroblast cultures displayed higher cell proliferation rates in wells coated with the positive control pFN,

whereas cells cultured on immobilized FBLN4 only after 48 h of incubation, as compared to the buffer control (Fig. 18A-B) However, skin fibroblasts incubated in wells coated with LTBP4 displayed no significant differences in cell proliferation (Fig. 18A-B). Similarly, after counting the stained cells with crystal violet after 24 and 48 h incubation on coated wells with FBLN4 and pFN revealed a significant increase in cell proliferation, but cells incubated on immobilized LTBP4 did not show altered levels of cell proliferation (Fig. 18C-D).

3.16 Summary of results

The summary and overview of the results are presented in Fig. 19. Several elastogenic cells were tested for their binding to FBLN4 and LTBP4 using real-time and end-point cell binding assays, all showed strong binding. FBLN4 contains two cell interaction regions mapped to cbEGF2-3 and the C-terminal domain (Fig. 19A). LTBP4 has at least two cell interaction sites, one is located in the N-terminal half and another in the C-terminal half (Fig. 19B). For the first time, we demonstrated that FBLN4 and LTBP4 cell interactions occurs through syndecans, but not glypicans. Specifically, SDC2 and SDC3 interact with FBLN4, whereas SDC3 interacts with LTBP4 (Fig. 19C). Interrupting cell interactions of FBLN4 and LTBP4 with SDCs resulted in impaired elastic fiber assembly. We extended our investigations on the function of FBLN4 and LTBP4 cell interactions in transmitting signals through their receptors translated into cellular events that may contribute to elastic fiber formation (Fig. 19D). Our results showed that FBLN4 and LTBP4 cell interactions significantly increased FA formation, cell contraction, and cell migration. Cell binding to FBLN4 promoted cell proliferation, but LTBP4 did not affect proliferation. FBLN4 and LTBP4 cell interactions elevated the levels of Erk1/2 and $RhoA^{GTP}$, but not Rac1.

Altogether, the data identified the responsible cell-surface receptors interacting with FBLN-4 and LTBP-4, and revealed a new cell interaction role essential for proper elastogenesis for these two proteins.

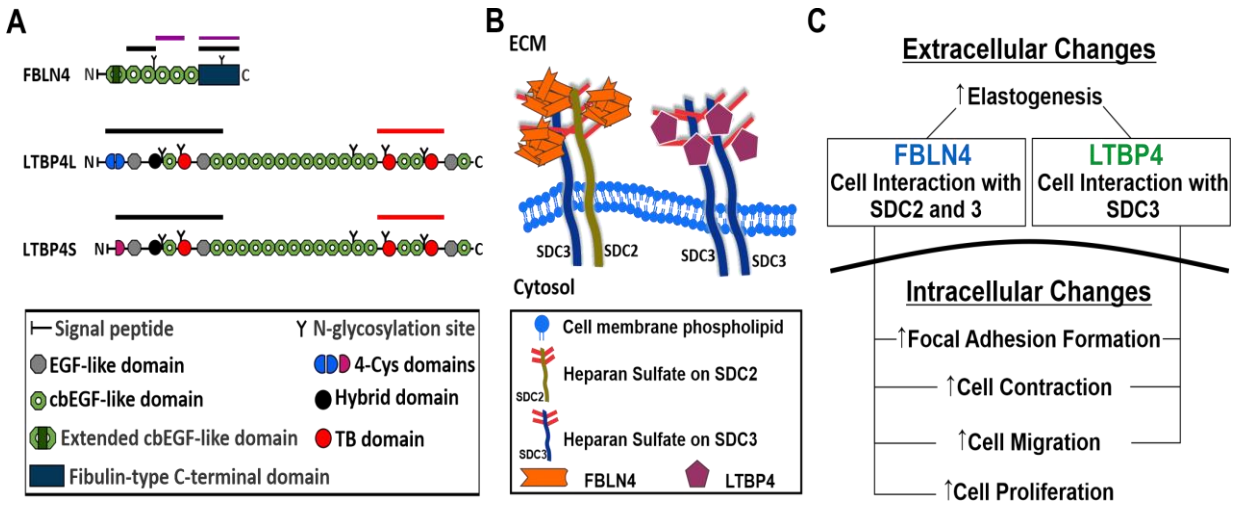

Figure 19. FBLN4 and LTBP4 cell interactions in elastogenesis
Summary of the findings in this study regarding FBLN4 and LTBP4 cell interactions and their involvement in elastogenesis as an extracellular mechanism along with intracellular changes upon cell interaction. (A) Scheme presenting the FBLN4 domain structure. Black lines indicate the identified cell interacting domains in FBLN4. Magenta lines indicate FBLN4 multimerization domains. (B) Presentation of the LTBP4 domain arrangement. Lines indicate the new cell interacting regions on the LTBP4L and LTBP4S isoforms identified in this study. The red line indicates the confirmed cell interacting region previously mapped by Kantola et al[22]. (C) Schematic presentation shows the cell surface receptors SDC2 and SDC3, interacting with FBLN4 multimers and compact LTBP4. (D) Subsequent cellular events affected upon SDC2 and SDC3 interactions with FBLN4 and LTBP4.

3.17 Supplemental Movies

Movie 1. Skin fibroblast adhesion and spreading on immobilized FBLN4

Skin fibroblast adhesion and spreading on coated wells with FBLN4 protein were monitored for 6 h after seeding using live-cell imaging. The frame interval was set at 30 s. Images at each 2.5 min were stacked at a speed of 10 frames per min (FPM). Scale bar presents 25 µm. Time stamp format is Hour:Minute (HH:MM).

Movie 2. Skin fibroblast adhesion and spreading on immobilized LTBP4

Skin fibroblast adhesion and spreading on coated wells with LTBP4 protein were monitored for 6 h after seeding using live-cell imaging. The frame interval was set at 30 seconds. Images at each 2.5 min were stacked at a speed of 10 frames per min (FPM). Scale bar presents 25 µm. Time stamp format is Hour:Minute (HH:MM).

Movie 3. Skin fibroblast adhesion and spreading on immobilized pFN

Skin fibroblast adhesion and spreading on coated wells with pFN protein were monitored for 6 h after seeding using live-cell imaging. The frame interval was set at 30 seconds. Images at each 2.5 min were stacked at a speed of 10 frames per minute (FPM). Scale bar presents 25 µm. Time stamp format is Hour:Minute (HH:MM).

Movie 4. Skin fibroblast adhesion and spreading on immobilized TBS, Ca^{+2}

Skin fibroblast adhesion and spreading on coated wells with TBS, Ca^{+2} protein were monitored for 6 h after seeding using live-cell imaging. The frame interval was set at 30 seconds. Images at each 2.5 minutes were stacked at a speed of 10 frame per min (FPM). Scale bar presents 25 µm. Time stamp format is Hour:Minute (HH:MM).

Movie 5. Skin fibroblast migration on immobilized FBLN4

Live cell imaging of skin fibroblasts migration on coated wells with FBLN4 protein monitored for 40 h after creating a scratch in a cell monolayer. Time interval was set at 5 min between successive images. Images were stacked at a speed of 25 FPM. Scale bar presents 150 µm. Time stamp format is Hour:Minute (HH:MM).

Movie 6. Skin fibroblast migration on immobilized LTBP4
Live cell imaging of skin fibroblasts migration on coated wells with LTBP4 protein monitored for 40 h after creating a scratch in a cell monolayer. Time interval was set at 5 min between successive images. Images were stacked at a speed of 25 FPM. Scale bar presents 150 µm. Time stamp format is Hour:Minute (HH:MM).

Movie 7. Skin fibroblast migration on immobilized pFN
Live cell imaging of skin fibroblasts migration on coated wells with pFN protein monitored for 40 h after creating a scratch in a cell monolayer. Time interval was set at 5 min between successive images. Images were stacked at a speed of 25 FPM. Scale bar presents 150 µm. Time stamp format is Hour:Minute (HH:MM).

Movie 8. Skin fibroblast migration on immobilized TBS, Ca^{+2}
Live cell imaging of skin fibroblasts migration on coated wells with BSA protein monitored for 40 h after creating a scratch in a cell monolayer. Time interval was set at 5 min between successive images. Images were stacked at a speed of 25 FPM. Scale bar presents 150 µm. Time stamp format is Hour:Minute (HH:MM).

4. DISCUSSION AND FUTURE DIRECTIONS

4.1 Discussion

Elastic fibers originally appeared in coincidence with the closed circulatory system[6]. The developmental success of elastic fiber formation is critical for the embryogenesis and development of vertebrates[6]. Elastogenesis occurs from the early developmental onset of skin, lungs, muscular diaphragm, cardiac valves, aorta and other blood vessels until completion of adolescence[6; 52]. The formation of such complex elastic fiber networks is required for the proper function of the ECM in elastic tissues. However, the synthesis of highly crosslinked elastin associated with FBN-containing microfibrils have been broadly investigated although there are many attempts to deeply dig in the biology and the dynamic of elastin and elastic fiber proteins either in animal models, cell culture or protein-protein interaction analyses[8; 10; 17; 20; 120]. It is clear that elastogenesis initially takes place close to the cell membrane of elastogenic cells. Some studies reported cell interactions with elastin and elastic fiber proteins[4; 5; 4; 5; 117; 206]. Also, tracking elastic fiber formation showed the early TE assembly on the cell surface[4]. However, the exact role of the cells in this fundamental process, i.e. elastogenesis, is poorly defined.

The focus of this study was to discover the nature of FBLN4 and LTBP4 cell interactions in the context of elastogenesis. The presented data revealed essential characteristics for FBLN4 and LTBP4 cell interactions, identified the necessary cell receptors for these interactions and emphasized the significance of the cell interactions with FBLN4 and LTBP4 in elastogenesis. The current study demonstrated roles of FBLN4 and LTBP4 in regard to focal adhesion formation, cell contraction and migration by which support the speculated idea that cell interactions with the elastic fiber proteins, FBLN4 and LTBP4, contribute in anchorage of elastic fibers to cells at early elastogenesis.

4.1.1 Characterizing FBLN4 and LTBP4 cell interactions

Previous studies have demonstrated that FBLN4 multimerizes, and both, FBLN4 and LTBP4 interact with cells[18; 22]. However, the mechanism of how these proteins interact with cells and what the role of multimerization is in this process has not been well characterized. This study defined FBLN4 multimerization domains, and the FBLN4 and LTBP4 cell interaction properties.

Numerous proteins function when they homogenously dimerize and oligomerize including cell receptors and ECM proteins[28; 352-354]. In fact, FBLN4 consists mostly of multimers, comparing

to other short FBLNs, including FBLN3 and 5[18]. Although it has been shown that the central and C-terminal regions of FBLN4 contain multimerization domains, excluding N-cbEGF1 domain[20], the exact domains responsible for FBLN4 multimer formation are not known. Identification of the domains and even the amino acid sequences responsible for FBLN4 multimerization will shed light on the underpinning molecular mechanism in which FBLN4 plays in elastogenesis. Previously, the FBLN4 multimerization was attributed to a region spanning cbEGF2-5 and a region encompassing cbEGF6 and the unique C-terminal domain[20]. Here, we mapped the multimerization domains more precisely to cbEGF4-5 and the C-terminal domain. Since these regions are located relatively closely to each other only separated by cbEGF6, it is possible that these two functional domains represent part of a contiguous multimerization domain spanning this region, rather than two separated functional domains. Presumably, a contiguous site at the C-terminal region of FBLN4 would only be able to mediate multimerization when the protein is completely synthesized and translocated in the endoplasmatic reticulum. However, the precise subcellular localization for FBLN4 multimerization either in the endoplasmatic reticulm, the Golgi apparatus, or on the cell surface after secretion remains to be established.

FBLN4 multimerization is required for cell interaction as determined with monomeric, dimeric and multimeric fractions of FBLN4 separated by gel filtration. While monomers and dimers of full length FBLN4 did not bind to fibroblasts, multimeric FBLN4 interacted strongly with the cells. This is not the first time where a significant function of FBLN4 multimerization has been shown. As determined by Djokic *et al.*, FBLN4 multimers showed the strongest binding to heparin[18]. This data is consistent with cells interacting with FBLN4 multimers through heparan sulfate moieties. Interaction with cell surface heparan sulfate may require a higher avidity of low affinity binding sites present in monomers, which is typically achieved by multimerization[93]. In addition, Kumra *et al.* demonstrated that only FBLN4 multimers efficiently bind to LTBP4 and to fibronectin[20]. Binding of FBLN4 and LTBP4 to cell surface heparan sulfate moieties may serve to bring these proteins in physical proximity to enable the chaperone function of FBLN4 to extend the compact LTBP4 enabling interactions with microfibrils (refer to the working model in Fig. 20)[20]. Whether or not FBLN4 and LTBP4 are sufficiently close on the cell surface of elastogenic cells could be investigated by co-staining using light and electron microscopy. In summary, FBLN4 multimerization is critically important for FBLN4 in mediating its interactions with cells and with other elastic fiber proteins.

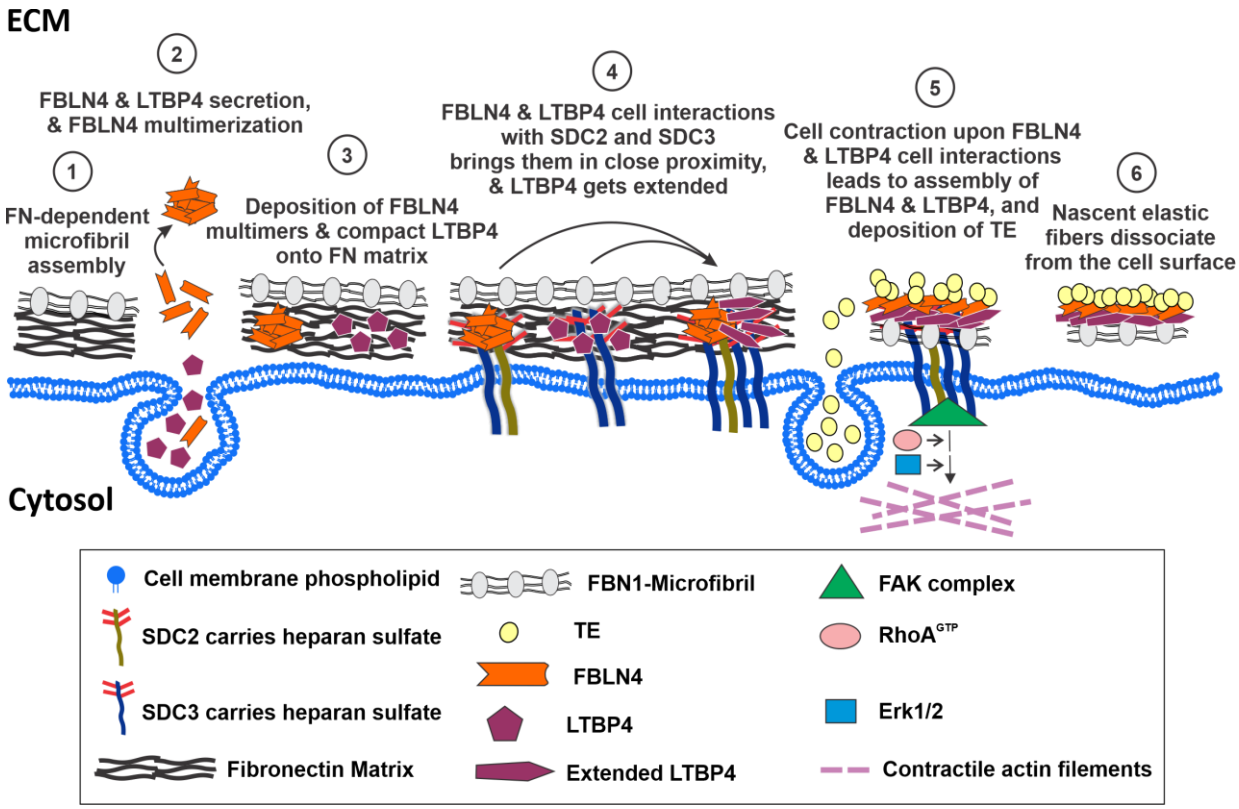

Figure 20. Schematic representation of the Hypothetical elastogenic model highlighting the role of FBLN4 and LTBP4 cell interactions.

The model is a hypothesized overview for early elastogenesis that implements experimental data of this thesis into a previous working model we have published[20]. (1) A fibronectin network is required for FBN-microfibril assembly. (2) FBLN4 and LTBP4 are secreted. FBLN4 multimerizes, whereas LTBP4 remains compact. (3) FBLN4 and LTBP4 are then deposited on an assembled FN matrix for which FBLN4 multimerization is required. (4) Through heparan sulfate, SDC2/SDC3 heterodimers interact with FBLN4 multimers whereas SDC3 homodimers interact with LTBP4. These interactions allow SDC2 and SDC3 to bring the two ligands, FBLN4 and LTBP4, in close proximity on the FN matrix. This enables FBLN4 multimers to interact with compact LTBP4, inducing its conformational change from a compact to an extended shape. (5) Subsequent intracellular signalling upon FBLN4 and LTBP4 cell interactions mediated by SDC2 and SDC3 activate cell contractility via Erk1/2 and $RhoA^{GTP}$. This cell contraction presumably supports the linear assembly of FBLN4 and LTBP4 onto microfibrils. Then, TE deposition is guided by binding to FBLN4 which interacts with extended LTBP4. (6) FBLN4 and LTBP4 dissociate from SDC2 and SDC3 leading to the dissociation of the nascent elastic fibers from the cell surface.

Gene deletion experiments in mice revealed essential roles of both LTBP4 isoforms, which overlap and differ in elastic fiber assembly[19; 185; 355]. Data from mouse models have highlighted the indispensable joint function of FBLN4 and LTBP4 during elastogenesis in several elastic tissues[185]. Elastogenesis occurs mainly during embryogenesis and in the postnatal phase[356; 357], when cells, including the differentiated elastogenic cells, are dividing and synthetic. The inclusion of various elastogenic cells such as primary skin fibroblasts and SMCs from various tissues to

characterize their interactions with FBLN4 and LTBP4 demonstrated the consistency of the observed cell interactions. These cell interactions contribute to cell proliferation, contractions and migration, as well, which are required cellular activities for tissue development, repair and remodeling. Additional information was obtained showing that SMCs maintain interactions with FBLN4 and LTBP4 even when they mature towards the contractile phenotype. These are important aspects to ultimately enhance elastogenesis and repair elastic fibers in tissues and to assess the optimal treatment regimen for medical issues from aortic dilation and emphysema to wounds and scars.

To locate the cell binding sites on FBLN4, we examined multiple deletion mutants which narrowed the cell binding properties to two regions: cbEGF2-3 and the C-terminal domain. Previously published work from the Reinhardt lab predicted cell binding sites on FBLN4 to be located in these regions[18]. The prediction was based on the assumption that FBLN4 cell interactions are heparan sulfate dependent, since clusters of basic amino acid residues in cbEGF3 and the C-terminal domain render them ideal for interacting with negatively charged heparan sulfates[18]. Interestingly, FBLN4 deletion mutants containing these domains, cbEGF2-3 and the C-terminal domain, showed self-interaction and interactions with LTBP4 and FN[20].

One cell binding site for LTBP4 has been previously mapped to a region spanning TB2-TB3 close to the C-terminus using recombinant LTBP4S and smaller fragments[22] (Fig. 19B). Here, we show that LTBP4S and LTBP4L bind similarly to elastogenic cells, which is consistent with the published data, as the previously identified cell binding site is located close to the C-terminus, a region that is identical in LTBP4S and LTBP4L. However, analyzing cell interaction in the present study with recombinant halves of LTBP4S and LTBP4L revealed at least one additional binding site in the N-terminal half of both proteins. Similar to FBLN4, LTBP4 also does not contain an RGD motif, which mediates interactions with integrins[178], but instead it has affinity to heparin[22]. Accordingly, it was suggested that LTBP4 interacts with the cells through heparan sulfate[22]. Therefore, the isoelectric points of each LTBP4 domain were calculated in this study to determine which domains contain basic amino acid sequences. Interestingly, the cell interaction region mapped on TB2-TB3 of LTBP4 contains two linker sequences adjacent to TB2 with very basic isoelectric points. This data suggests that cells interact with LTBP4 in this region. Importantly, TB2 represents the domain that covalently binds the small latent TGF-β complex[358]. Cell binding adjacent to this complex may position it on the cell surface for subsequent TGF-β

activation. Other sites with basic isoelectric points were identified in LTBP4S and LTBP4L close to the N-terminus in the region of the 4-Cys domain(s) and the downstream EGF domain, as well as in the region spanning from TB1 to cbEGF2. These are candidate regions for cell interactions with the N-terminal halves. It has been suggested that LTBP4 is held in a compact formation through N- to C-terminal self-interactions[20]. This compact conformation can be extended by interaction with FBLN4 which in turn promotes elastic fiber formation. Cell interaction with the N- and C-terminal regions of LTBP4 may play a regulatory role in this important elastogenic mechanism.

4.1.2 The role of the N-terminal domain of FBLN4 in secretion

The challenge in generating some of the FBLN4 recombinant fragments were the small amounts of protein secreted in the culture medium, and subsequently the moderate binding to a His-trap column. This indicates that the full length FBLN4 is required for efficient secretion from the cells. However, we noticed that the N-terminal F4_N1 fragment was secreted in much larger amounts into the cell culture medium, facilitating purification in much higher yields compared to several other FBLN4 mutant fragments that did not contain the N-terminal domain in FBLN4. This observation suggested that the N-terminal domain of FBLN4 promotes the synthesis and/or the secretion of FBLN4. To verify that, several FBLN4 deletion mutants were constructed including the N-terminal domain (see Fig. 3A), and subsequently tested for increased amounts of secreted recombinant proteins into the conditioned media. These FBLN4 deletion mutants were indeed secreted in higher amounts and purifiable in larger yields compared to other fragments lacking the N-terminal domain. This not only helped in producing some of the FBLN4 constructs, but it also showed that the N-terminal domain facilitates synthesis and/or secretion of FBLN4.

4.1.3 Identifying the cell receptors of FBLN4 and LTBP4

Although it has been shown cells interact with FBLN4[18] and LTBP4[22], the utilization of these cell interactions in elastogenesis has not been studied due to the required knowledge about their cell surface receptors.

The identification of FBLN4 and LTBP4 cell receptors was based on the fact that FBLN4 and LTBP4 do not contain RGD-integrin binding motifs[173; 178], but both contain clusters of basic amino acids that are candidates to interact with heparan sulfate. Importantly, both proteins have

affinity to heparin[18; 22]. However, the RGD motif is not the only integrin binding motif. Several other integrin binding sequences have been characterized[74; 359]. The results of this study using EDTA chelation experiments and divalent metal cation supplementation in cell interaction assays supported the idea that integrins do not mediate cell adhesion to FBLN4 and LTBP4. Instead, a series of evidences were obtained which prove that FBLN4 and LTBP4 cell interactions are mediated via syndecans which are heparan sulfate proteoglycans.

Competition of cell binding to FBLN4 and LTBP4 with heparin and heparan sulfate disrupted cell interactions. Heparin displayed a stronger effect than heparan sulfate, which is likely due to the chemical structure of heparin that is highly sulfated[216; 360]. Heparin completely blocked cell interactions with FBLN4 and LTBP4 at lower concentrations, compared to the porcine-sourced heparan sulfate used in this assay which is characterized by lower sulfation levels.

Other evidence came from the treatment of fibroblasts with heparinases to degrade heparan sulfate from the cell surface, which significantly reduced cell interactions with FBLN4 and LTBP4. Kantola *et al.* tested cell interactions with LTBP4 using only heparinase II for the treatment of fibroblasts, which resulted in a trend, but not in a significant reduction of cell binding to LTBP4[22]. In our experiments, enzymatically digesting heparan sulfate from the cell surface using a combination of heparinases II and III worked more efficiently and produced robust data showing that cell surface located heparan sulfate mediates interaction with FBLN4 and LTBP4.

CHO cell lines deficient in GAG synthesis have been used to study cell-ECM protein interaction analyses[207]. They are informative tools to understand whether an ECM protein interacts with cells through GAG. However, they are not an optimal model considering their origin (Chinese hamster), especially when used to examine their interactions with human protein. The homology and gene expression of different proteoglycan cell receptors in CHO cell lines should be considered. The analyzed binding of CHO cells to FBLN4 was shown to be exclusively mediated by heparan sulfate using the heparan sulfate deficient CHO-677 cell line, compare to the CHO-WT cells. However, these cells were not conclusive to study heparan sulfate dependency in regard to LTBP4 cell interactions, because both CHO-WT and CHO-677 did not adhere to LTBP4. It is possible that the LTBP4 cell receptor is not expressed in CHO cells, or the specific motif binding to human LTBP4 is not the same or missing in CHO cells.

siRNA knockdown experiments revealed specifically the key cell receptors required for FBLN4 and LTBP4 cell interactions, SDC2 and SDC3 for FBLN4, and SDC3 for LTBP4. These

findings have been further validated by solid phase binding assays that showed direct interactions of FBLN4 with SDC2 or SDC3, and a direct interaction between LTBP4 and SDC3.

Syndecans form homotypic and heterotypic dimers to function as cell receptors[240]. In this light it is possible that FBLN4 interacts with a heterodimer of SDC2 and SDC3, because knocking down one of them led to the loss of cell interactions. It is not clear if LTBP4 binds to cells through SDC3 in a monomeric or a homodimer conformation.

It has been reported that TE interacts directly with cells through several cell surface receptors including elastin-binding protein (EBP)[208], integrins αvβ3[205] and αvβ5[206], as well as with GAG[207]. However, heparan sulfate moieties that mediate TE cell interactions have been never investigated. For the first time, solid phase binding analysis uncovered a direct interaction between TE and SDC4 ectodomain. The clustering of basic amino acids at the C-terminus of TE is characteristic of heparin-binding motifs[207] and likely to be the region interacting with SDC4.

5.1.3 Revealing the significance of FBLN4 and LTBP4 cell interactions in elastogenesis

Protein knockdown by siRNA gene silencing successfully revealed critical information about the FBLN4 and LTBP4 interactions with specific syndecans and the importance of these interactions in elastogenesis.

It is known for several years that syndecans can function as co-receptors for example in a complex with integrins to serve in cell binding with cytokines, growth factors and ECM proteins[361]. However, a growing amount of data show that syndecans are not only co-receptors with a minor role in cell adhesion to ECM proteins[362; 363]. It has been shown that the heparin binding region of FN is a basic requirement to form focal adhesions and stress fibers during cell attachment and spreading[76; 364; 365]. Focal adhesion formation upon cell interaction with FN is dependent on engagement of SDC4[363]. SDC1 and 2 arrange FN fibrillogenesis in an early gastrula-stage in the *Xenopus* embryo[366]. SDC2 is implicated in the matrix assembly of FN and laminin, as was shown with cells expressing truncated SDC2 resulting in the loss of FN and laminin organization into fibrils on the cell surface[332]. Also, it was shown that the deposition of fibrillin microfibrils into the matrix secreted by retinal pigmented epithelial cells depends on SDC4[367]. Interestingly, normal elastic fibers developed in the *Fbln5*$^{RGE/RGE}$ knock-in mouse, indicating that FBLN5-integrin binding is not required for elastogenesis[368]. Although it is not known if FBLN5 establish cell adhesion through heparan sulfate proteoglycan, the results with the *Fbln5*$^{RGE/RGE}$

mice suggested that FBLN5 cell attachment through cell surface heparan sulfate proteoglycans might be necessary for elastic fiber formation[18]. In the current study, the essential roles of syndecans as indispensable cell receptors for FBLN4 and LTBP4 became evident. Hence, defining certain syndecans as key cell receptors that bind to FBLN4 and LTBP4 facilitated exploring the function of these cell interactions in elastogenesis. Elastic fiber formation was impaired in cell cultures after siRNA knockdown of SDC2 and SDC3.

The results of this study showed that FBLN4 and LTBP4 regulate cell adhesion, spreading and a subsequent function in elastogenesis mainly through SDC2 and SDC3 binding, using end-point immunofluorescence analysis. This approach could be extended by time course experiments or live cell imaging. Currently, there are only a few published studies successfully analyzing fluorescently tagged TE in live cell imaging. This is despite the knowledge that elastogenesis occurs with the involvement of different crucial elastic fiber proteins with a possible engagement of cell receptors in elastic fiber formation. Kozel *et al.* used a bovine TE-Timer construct, which was transiently expressed in rat lung fibroblasts, and documented elastogenesis first as a microassembly on the cell surface, and then as a macroassembly and deposition into the extracellular space[4]. Halm *et al.* used a long-term elastic fiber tracking system in human skin fibroblast cultures, using lentiviral transfection, which offers a stable expression to overexpress a human recombinant TE with a citrin fluorescence tag[5]. Although this lentiviral transfection system enabled tracking TE up to 14 d, TE expression was weakly detectable after cells were passaged. A key challenge in this type of experimental setting is in transiently expressing relevant fluorescently tagged recombinant proteins for the extended time needed for elastogenesis. Another challenge refers to generating multiple recombinant proteins with different fluorescence tags as several elastic fiber proteins are involved in elastogenesis, as well as cell receptors. Additionally, syndecan ectodomains can shed off from the cell surface into the extracellular space as a part of the turn-over, which results in soluble ectodomains that possess binding properties to other ligands[369]. This makes it difficult to track their spatial involvement in elastogenesis while they are located on the cell surface versus in the ECM.

5.1.4 Downstream effects of FBLN4 and LTBP4 cell interactions

FBLN4 and LTBP4 interact with syndecans, which are known to transduce signals from the ECM through their transmembrane and cytoplasmic domains[369]. This suggested a regulatory

role of SDC2 and SDC3 in elastic fiber assembly that implies intracellular mechanisms. The molecular basis of possible cellular mechanisms activated upon FBLN4 and LTBP4 cell interactions was addressed in the current study.

Focal adhesion formation is one of the significant downstream events after cell interactions with several ECM proteins including FN[188; 370; 371], fibrillin-1[204] and collagen[372]. Although several studies have addressed cell interactions with TE[205-207], it is still unknown if TE cell adhesions play a role in focal adhesion formation. The current study showed that FBLN4 and LTBP4 cell interactions upregulated pFAK, which promoted focal adhesion maturation by increasing the number and the length of focal adhesions. In a prior study, Burger *et al.* analyzed FBLN4 deficiency on cytoskeletal structure and dynamics. Newly formed actin fibers in mouse aortic SMC were visualized using fluorescence-labelled actin in transfected cells expressing a paxillin-EGFP fusion protein[347]. Paxillin is a part of focal adhesion complex[373-375]. Although Burger *et al.* did not perform quantifications of focal adhesions, it was clearly documented that FBLN4 is needed for actin stress fiber formation. These stress fibers were anchored in focal adhesions as elongated paxillin containing structures in wild type cells, versus small rounded podosome-like structures in FBLN4 deficient cells[347]. Of four SDC members, only SDC4-ECM interactions has been involved in focal adhesions[376; 377]. Treating cells with an anti-SDC4 antibody triggered focal adhesion formation in cell adhesion to FN[378].

Our data established the roles of FBLN4 and LTBP4 in cell contractility and migration. Interestingly, the majority of studies analyzing ECM proteins on cell contraction and migration focused on integrin-mediated cell-ECM adhesions[379-381]. Thus, the current study data contributed a new perspective about cell interactions with important elastic fiber proteins mediated by SDCs. Generally, SDCs are not well studied in cell contraction and migration upon ECM-cell adhesions, particularly SDC3 that received little attention in the ECM field. However, it has been shown that integrin α5β1 requires SDC4 engagement in order to promote focal adhesion formation and cell migration on a FN matrix[382]. In addition, SDC4 and integrins cooperatively interacting with FN induced focal adhesions and actin stress fibers in a Rho-dependent manner[188; 378].

As this study showed a significant elevation in total ERK1/2 and activation of RhoA upon interaction with FBLN4 and LTBP4, it suggests that ERK1/2 and RhoA are regulators for focal adhesion, cell contraction and migration induced by FBLN4 and LTBP4 interactions with SDCs.

However, to further prove that this is indeed the case, it would require a validation using specific inhibition of ERK1/2 and RhoA in cells interacting with FBLN4 and LTBP4.

Elastogenesis has been linked to cell proliferation[383-385], although the exact relationship is ill defined. It is known that contractility and proliferation of fibroblasts and SMC play pivotal roles in elastic tissues, including wound healing and aortic homeostasis [386; 387]. Proliferative smooth cells in the aorta of *Eln*$^{-/-}$ mice were associated with changes in the balance of matrix deposition, which resulted in thickening of the tunica media causing aortic stenosis[168]. Contrary, defective elastogenesis, caused by FBLN4 deficiency, resulted in aortic aneurysm in *Fbln4*$^{-/-}$ mice[115]. *Fbln4*$^{-/-}$ mice were shown to have increased proliferation of SMC in the aortic wall[176]. This was explained by the down-regulation of SMC contractile genes due to FBLN4 deficiency, which affected SMC differentiation from the proliferative to the contractile phenotype, contributing in aortic dilation[388]. Our data showed that FBLN4 cell interactions stimulated cell proliferation, suggesting the contribution of FBLN4 cell interactions in tissue matrix remodeling. This might be especially relevant for elastogenesis where the majority occurs during embryo-fetal as well as postnatal development when cells proliferate and differentiate into specific tissues.

In the proposed working model (Fig. 19B), cell interactions with FBLN4 and LTBP4 lead to an enhancement of focal adhesion and stress fiber formation regulated by ERK1/2 and RhoA^{GTP} upon signal transduction via SDC2 and SDC3, thus cell interaction events produce fibril structures of elastic fiber proteins including FBLN4, LTBP4 and TE. A similar mechanism has been demonstrated for FN fibril formation, as shown by preventing integrin-cell binding by antibody blockade with either anti-integrin or anti-FN antibodies[389]. However, integrins are not required for FBLN4 and LTBP4 cell interactions, instead SDC2 and SDC3 are the key cell receptors in these cell adhesions. Validation of this working model will provide new concepts of heparan sulfate proteoglycans function in elastogenesis.

5.1.5 Do FBLN4 and LTBP4 cell interactions collaterally function for elastogenesis?

Elastogenesis consists of multiple stages each of which involves sophisticated protein-protein interactions. Knockout mouse models elucidated the functional link between FBLN4 and LTBP4 in elastogenesis[19; 185]. Bultmann-Mellin *et al.* found that LTBP4 is required for fibrillar matrix deposition of FBLN4, and both LTBP4 isoforms interact with FBLN4[19]. We showed that FBLN4 induces an extended conformation of LTBP4 which promotes TE deposition[20]. Here, we

uncovered a novel cell interaction site on LTBP4 likely located at the 4-Cys domain region which matches the same N-terminal region mapped for FBLN4 and FBLN5 interactions[19; 21]. The stable conformational change on LTBP4 induced by a transient interaction with FBLN4 might leave the LTBP4 N-terminal region exposed to allow interactions with its cell receptor, SDC3. This in turn may facilitate TE deposition assisted by FBLN4 and FBLN5. This mechanism would result in anchoring elastic fibers to the cell surface at sites of focal adhesion formation, possibly promoting the formation of extended elastic fibers. Extended elastic fibers would create an optimal orientation for elastin crosslinking by LOX family members toward elastic fibers maturation.

The common cell receptor that binds to both, FBLN4 and LTBP4, is SDC3. As pointed out above, we assume that FBLN4 interacts with a heterodimer of SDC2 and SDC3 whereas LTBP4 interacts with a homodimer of SDC3. However, FBLN4 and LTBP4 interact with each other and may interact with the cells in a complex containing SDC2 and SDC3 in which LTBP4 interacts only with SDC3 whereas FBLN4 interacts with both. These assumptions of course require experimental validation. A considerable challenge remains the identification of specific mechanisms in which such complexes are involved in cell adhesion, signaling, and force generation that combine to establish the proper spatio-temporal control of elastic protein fibrillar deposition.

5.2 Future Directions

The detailed mechanistic aspects taking place downstream of the FBLN4 and LTBP4 cell interactions are not complete in term of affected signaling pathways that control focal adhesion, cell contraction, migration and proliferation. An extended project to analyze the signal transduction mechanisms underlying cell interactions with FBLN4 and LTBP4 is needed.

Several studies employed animal models of SDC[255; 256; 390]. Surprisingly, a *Sdc2* knockout mouse model has never been established up to the date of this thesis. In addition, the generated mouse models for SDC1, 3 and 4 have not been analyzed for elastogenesis in elastic tissues[255; 256; 390]. The deletion mouse model of SDC3 was utilized only to investigate the function of SDC3 in brain development[256]. In addition, SDC4 mouse models have been used to analyze the role of SDC4 in cartilage and bone formation[255; 390], but not in elastogenesis. A concise study analyzed *Sdc4*$^{-/-}$ knockout mice for wound healing showed delayed wound healing and impaired angiogenesis in *Sdc4*$^{-/-}$[254]. To fill the gap in the ECM research regarding the important function of

syndecans, in particular in elastogenesis, intensive investigations are required on both levels *in vivo* and *in vitro*. Characterizing elastogenesis in elastic tissues of knockout mouse models for SDC2 and SDC3 are needed at different developmental stages from embryogenesis to adult age to provide a complete understanding how these SDCs are involved in elastogenesis. A double SDC2/3 knockout mouse model may reveal the interplay among these SDCs in elastogenesis, which are predicted based on the current study to present with a phenotype similar to mouse models deficient in FBLN4 or LTBP4.

Wound healing is a highly complex process producing only partially functional scar tissue[391; 392]. This tissue lacks the integrity of organized elastic fibers as well as of collagen fibers, which contributes to the stiffness of scar tissue[392]. Elastin and elastic fiber proteins have been poorly analyzed during wound healing[393] and the expression profile of elastic fiber proteins in the progress of wound repair is not well characterized. FBLN4 and LTBP4 cell interactions intrinsically contributed in elastic fiber formation, and they enhanced skin fibroblast migration and proliferation which are required in wound healing. FBLN4 also plays a significant role in collagen fiber assembly[394]. It is unknown if LTBP4 functions in collagen fiber formation, however, new unpublished work performed in the Reinhardt lab showed LTBP4 colocalized with collagen fibers in human skin tissues. All these data together suggest that FBLN4 and LTBP4 play critical roles during wound healing in tissue remodeling and scar repair. To identify the roles of FBLN4 and LTBP4 in regulating wound healing and scarring, an *in vivo* study is required using wound healing models in mice. For this, it is first required to collect data about the expression patterns of FBLN4, LTBP4 and TE in wound tissue during healing in wild type animals and to determine how elastogenesis is affected during the wound healing process. Later, it is important to determine whether restoration of FBLN4 and LTBP4 expression to normal levels in wounded tissues would assist a proper wound healing and inhibit scar formation.

5.3 Conclusions

The main analyzed topics in this project are FBLN4 and LTBP4 cell interactions contributing novel insights into their roles in mediating the relationship between intracellular events and elastogenesis. As the objectives of the presented study were met, several fundamental findings were disclosed. There have been challenges along the road to achieve the main goals of this research which are explained in the results and the discussion sections. The novel data reflects

a better understanding for the influence of cell interactions with elastic fiber proteins on elastogenesis. In long term, these findings are expected to help design *in vitro* approaches for the generation of elastic fiber-rich biomaterials in which elasticity is wanted such as tissue-engineered blood vessels and tissue-engineered skin engraftments.

5. APPENDIX

The amino acid sequences of all the recombinant proteins used in this study are described below. Note that underlined sequences indicate the signal peptide for each recombinant, underlined sequences in italic font are for His-tag, shaded sequences are for V5-tag and sequences in shaded and italic font are for FLAG-tag.

5.1 FBLN4 recombinants

5.1.1 FBLN4 full length (F4_FL)

MRAWIFFLLCLAGRALAAPLAQDSEEPDSYTECTDGYEWDPDSQHCRDVNECLTIPEACKGEMKCINHYG
GYLCLPRSAAVINDLHGEGPPPPVPPAQHPNPCPPGYEPDDQDSCVDVDECAQALHDCRPSQDCHNLPGSY
QCTCPDGYRKIGPECVDIDECRYRYCQHRCVNLPGSFRCQCEPGFQLGPNNRSCVDVNECDMGAPCEQRC
FNSYGTFLCRCHQGYELHRDGFSCSDIDECSYSSYLCQYRCVNEPGRFSCHCPQGYQLLATRLCQDIDECES
GAHQCSEAQTCVNFHGGYRCVDTNRCVEPYIQVSENRCLCPASNPLCREQPSSIVHRYMTITSERRVPADV
FQIQATSVYPGAYNAFQIRAGNSQGDFYIRQINNVSAMLVLARPVTGPREYVLDLEMVTMNSLMSYRASS
VLRLTVFVGAYTF*HHHHHH*

5.1.2 F4_N1

MRAWIFFLLCLAGRALAAPLAQDSEEPDSYTECTDGYEWDPDSQHCRDVNECLTIPEACKGEMKCINHYG
GYLCLPRSAAVINDLHGEGPPPPVPPAQHPNPCPPGYEPDDQDSCV*HHHHHHHH*

5.1.3 F4_N1-3

MRAWIFFLLCLAGRALAAPLAQDSEEPDSYTECTDGYEWDPDSQHCRDVNECLTIPEACKGEMKCINHYG
GYLCLPRSAAVINDLHGEGPPPPVPPAQHPNPCPPGYEPDDQDSCVDVDECAQALHDCRPSQDCHNLPGSY
QCTCPDGYRKIGPECVDIDECRYRYCQHRCVNLPGSFRCQCEPGFQLGPNNRSCVENLYFQGGKPIPNPLLG
LDSTRTG*HHHHHHHH*

5.1.4 F4_N1-5

MRAWIFFLLCLAGRALAAPLAQDSEEPDSYTECTDGYEWDPDSQHCRDVNECLTIPEACKGEMKCINHYG
GYLCLPRSAAVINDLHGEGPPPPVPPAQHPNPCPPGYEPDDQDSCVDVDECAQALHDCRPSQDCHNLPGSY
QCTCPDGYRKIGPECVDIDECRYRYCQHRCVNLPGSFRCQCEPGFQLGPNNRSCVDVNECDMGAPCEQRC
FNSYGTFLCRCHQGYELHRDGFSCSDIDECSYSSYLCQYRCVNEPGRFSCHCPQGYQLLATRLCQENLYFQ
GGKPIPNPLLGLDSTRTG*HHHHHHHH*

5.1.5 F4_2-5

MRAWIFFLLCLAGRALAAPLADVDECAQALHDCRPSQDCHNLPGSYQCTCPDGYRKIGPECVDIDECRYR
YCQHRCVNLPGSFRCQCEPGFQLGPNNRSCVDVNECDMGAPCEQRCFNSYGTFLCRCHQGYELHRDGFSC
SDIDECSYSSYLCQYRCVNEPGRFSCHCPQGYQLLATRLCQ*HHHHHHHH*

5.1.6 F4_6C

MRAWIFFLLCLAGRALAAPLADIDECESGAHQCSEAQTCVNFHGGYRCVDTNRCVEPYIQVSENRCLCPAS
NPLCREQPSSIVHRYMTITSERRVPADVFQIQATSVYPGAYNAFQIRAGNSQGDFYIRQINNVSAMLVLARP
VTGPREYVLDLEMVTMNSLMSYRASSVLRLTVFVGAYTF*HHHHHHHH*

5.1.7 F4_N1,C

MRAWIFFLLCLAGRALAAPLAQDSEEPDSYTECTDGYEWDPDSQHCRDVNECLTIPEACKGEMKCINHYG
GYLCLPRSAAVINDLHGEGPPPPVPPAQHPNPCPPGYEPDDQDSCVCPASNPLCREQPSSIVHRYMTITSERR
VPADVFQIQATSVYPGAYNAFQIRAGNSQGDFYIRQINNVSAMLVLARPVTGPREYVLDLEMVTMNSLMS
YRASSVLRLTVFVGAYTFENLYFQGGKPIPNPLLGLDSTRTG*HHHHHHHH*

5.1.8 F4_N1,6C

MRAWIFFLLCLAGRALAAPLAQDSEEPDSYTECTDGYEWDPDSQHCRDVNECLTIPEACKGEMKCINHYG
GYLCLPRSAAVINDLHGEGPPPPVPPAQHPNPCPPGYEPDDQDSCVDIDECESGAHQCSEAQTCVNFHGGY
RCVDTNRCVEPYIQVSENRCLCPASNPLCREQPSSIVHRYMTITSERRVPADVFQIQATSVYPGAYNAFQIRA
GNSQGDFYIRQINNVSAMLVLARPVTGPREYVLDLEMVTMNSLMSYRASSVLRLTVFVGAYTFENLYFQG
GKPIPNPLLGLDSTRTG*HHHHHHHH*

5.1.9 F4_N1,4-6C

MRAWIFFLLCLAGRALAAPLAQDSEEPDSYTECTDGYEWDPDSQHCRDVNECLTIPEACKGEMKCINHYG
GYLCLPRSAAVINDLHGEGPPPPVPPAQHPNPCPPGYEPDDQDSCVDVNECDMGAPCEQRCFNSYGTFLCR
CHQGYELHRDGFSCSDIDECSYSSYLCQYRCVNEPGRFSCHCPQGYQLLATRLCQDIDECESGAHQCSEAQ
TCVNFHGGYRCVDTNRCVEPYIQVSENRCLCPASNPLCREQPSSIVHRYMTITSERRVPADVFQIQATSVYP
GAYNAFQIRAGNSQGDFYIRQINNVSAMLVLARPVTGPREYVLDLEMVTMNSLMSYRASSVLRLTVFVGA
YTFENLYFQGGKPIPNPLLGLDSTRTG*HHHHHHHH*

5.1.10 F4_4-6

MRAWIFFLLCLAGRALAAPLADVNECDMGAPCEQRCFNSYGTFLCRCHQGYELHRDGFSCSDIDECSYSS
YLCQYRCVNEPGRFSCHCPQGYQLLATRLCQDIDECESGAHQCSEAQTCVNFHGGYRCVDTNRCVEPYIQ
VSENRCLENLYFQGGKPIPNPLLGLDSTRTG*HHHHHHHH*

5.2 LTBP4 recombinants

5.2.1 LTBP4L full length (L4-L)

MPRPGTSGRRPLLLVLLLPLFAAATSAASPSPSPSQVVEVPGVPSRPASVAVCRCCPGQTSRRSRCIRAFCRV
RSCQPKKCAGPQRCLNPVPAVPSPSPSVRKRQVSLNWQPLTLQEARALLKRRRPRGPGGRGLLRRRPPQRA
PAGKAPVLCPLICHNGGVCVKPDRCLCPPDFAGKFCQLHSSGARPPAPAVPGLTRSVYTMPLANHRDDEH
GVASMVSVHVEHPQEASVVVHQVERVSGPWEEADAEAVARAEAAARAEAAAPYTVLAQSAPREDGYSD
ASGFGYCFRELRGGECASPLPGLRTQEVCCRGAGLAWGVHDCQLCSERLGNSERVSAPDGPCPTGFERVN
GSCEDVDECATGGRCQHGECANTRGGYTCVCPDGFLLDSSRSSCISQHVISEAKGPCFRVLRDGGCSLPILR
NITKQICCCSRVGKAWGRGCQLCPPFGSEGFREICPAGPGYHYSASDLRYNTRPLGQEPPRVSLSQPRTLPA
TSRPSAGFLPTHRLEPRPEPRPDPRPGPELPLPSIPAWTGPEIPESGPSSGMCQRNPQVCGPGRCISRPSGYTCA
CDSGFRLSPQGTRCIDVDECRRVPPPCAPGRCENSPGSFRCVCGPGFRAGPRAAECLDVDECHRVPPPCDLG
RCENTPGSFLCVCPAGYQAAPHGASCQDVDECTQSPGLCGRGACKNLPGSFRCVCPAGFRGSACEEDVDE
CAQEPPPCGPGRCDNTAGSFHCACPAGFRSRGPGAPCQDVDECARSPPPCTYGRCENTEGSFQCVCPMGFQ
PNTAGSECEDVDECENHLACPGQECVNSPGSFQCRTCPSGHHLHRGRCTDVDECSSGAPPCGPHGHCTNTE
GSFRCSCAPGYRAPSGRPGPCADVNECLEGDFCFPHGECLNTDGSFACTCAPGYRPGPRGASCLDVDECSE
EDLCQSGICTNTDGSFECICPPGHRAGPDLASCLDVDECRERGPALCGSQRCENSPGSYRCVRDCDPGYHA
GPEGTCDDVDECQEYGPEICGAQRCENTPGSYRCTPACDPGYQPTPGGGCQDVDECRNRSFCGAHAVCQN
LPGSFQCLCDQGYEGARDGRHCVDVNECETLQGVCGAALCENVEGSFLCVCPNSPEEFDPMTGRCVPPRT
SAGTFPGSQPQAPASPVLPARPPPPPLPRRPSTPRQGPVGSGRRECYFDTAAPDACDNILARNVTWQECCCT
VGEGWGSGCRIQQCPGTETAEYQSLCPHGRGYLAPSGDLSLRRDVDECQLFRDQVCKSGVCVNTAPGYSC

YCSNGYYYHTQRLECIDNDECADEEPACEGGRCVNTVGSYHCTCEPPLVLDGSQRRCVSNESQSLDDNLG
VCWQEVGADLVCSHPRLDRQATYTECCCLYGEAWGMDCALCPAQDSDDFEALCNVLRPPAYSPPRPGGF
GLPYEYGPDLGPPYQGLPYGPELYPPPALPYDPYPPPPGPFARREAPYGAPRFDMPDFEDDGGPYGESEAPA
PPGPGTRWPYRSRDTRRSFPEPEEPPEGGSYAGSLAEPYEELEAEECGILDGCTNGRCVRVPEGFTCRCFDG
YRLDMTRMACVDINECDEAEAASPLCVNARCLNTDGSFRCICRPGFAPTHQPHHCAPARPRAGKPIPNPLL
GLDSTRTG*HHHHHHHH*

5.2.2 LTBP4S full length (L4-S)

MAGGVRLLWVSLLVLLAQLGPQPGLGRLGERLRVRFTPVVCGLRCVHGPTGSRCTPTCAPRNATSVDSGA
PGGAAPGGPGFRAFLCPLICHNGGVCVKPDRCLCPPDFAGKFCQLHSSGARPPAPAIPGLTRSVYTMPLANH
RDDEHGVASMVSVHVEHPQEASVVVHQVERVSGPWEEADAEAVARAEAAARAEAAAPYTVLAQSAPRE
DGYSDASGFGYCFRELRGGECASPLPGLRTQEVCCRGAGLAWGVHDCQLCSERLGNSERVSAPDGPCPTG
FERVNGSCEDVDECATGGRCQHGECANTRGGYTCVCPDGFLLDSSRSSCISQHVISEAKGPCFRVLRDGGC
SLPILRNITKQICCCSRVGKAWGRGCQLCPPFGSEGFREICPAGPGYHYSASDLRYNTRPLGQEPPRVSLSQP
RTLPATSRPSAGFLPTHRLEPRPEPRPDPRPGPELPLPSIPAWTGPEIPESGPSSGMCQRNPQVCGPGRCISRPS
GYTCACDSGFRLSPQGTRCIDVDECRRVPPPCAPGRCENSPGSFRCVCGPGFRAGPRAAECLDVDECHRVP
PPCDLGRCENTPGSFLCVCPAGYQAAPHGASCQDVDECTQSPGLCGRGACKNLPGSFRCVCPAGFRGSACE
EDVDECAQEPPPCGPGRCDNTAGSFHCACPAGFRSRGPGAPCQDVDECARSPPPCTYGRCENTEGSFQCVC
PMGFQPNTAGSECEDVDECENHLACPGQECVNSPGSFQCRTCPSGHHLHRGRCTDVDECSSGAPPCGPHG
HCTNTEGSFRCSCAPGYRAPSGRPGPCADVNECLEGDFCFPHGECLNTDGSFACTCAPGYRPGPRGASCLD
VDECSEEDLCQSGICTNTDGSFECICPPGHRAGPDLASCLDVDECRERGPALCGSQRCENSPGSYRCVRDCD
PGYHAGPEGTCDDVDECQEYGPEICGAQRCENTPGSYRCTPACDPGYQPTPGGGCQDVDECRNRSFCGAH
AVCQNLPGSFQCLCDQGYEGARDGRHCVDVNECETLQGVCGAALCENVEGSFLCVCPNSPEEFDPMTGRC
VPPRTSAGTFPGSQPQAPASPVLPARPPPPPLPRRPSTPRQGPVGSGRRECYFDTAAPDACDNILARNVTWQ
ECCCTVGEGWGSGCRIQQCPGTETAEYQSLCPHGRGYLAPSGDLSLRRDVDECQLFRDQVCKSGVCVNTA
PGYSCYCSNGYYYHTQRLECIDNDECADEEPACEGGRCVNTVGSYHCTCEPPLVLDGSQRRCVSNESQSLD
DNLGVCWQEVGADLVCSHPRLDRQATYTECCCLYGEAWGMDCALCPAQDSDDFEALCNVLRPPAYSPPR
PGGFGLPYEYGPDLGPPYQGLPYGPELYPPPALPYDPYPPPPGPFARREAPYGAPRFDMPDFEDDGGPYGES
EAPAPPGPGTRWPYRSRDTRRSFPEPEEPPEGGSYAGSLAEPYEELEAEECGILDGCTNGRCVRVPEGFTCR
CFDGYRLDMTRMACVDINECDEAEAASPLCVNARCLNTDGSFRCICRPGFAPTHQPHHCAPARPRAGKPIP
NPLLGLDSTRTG*HHHHHHHH*

5.2.3 L4_LN

MPRPGTSGRRPLLLVLLLPLFAAATSAASPSPSPSQVVEVPGVPSRPASVAVCRCCPGQTSRRSRCIRAFCRV
RSCQPKKCAGPQRCLNPVPAVPSPSPSVRKRQVSLNWQPLTLQEARALLKRRRPRGPGGRGLLRRRPPQRA
PAGKAPVLCPLICHNGGVCVKPDRCLCPPDFAGKFCQLHSSGARPPAPAVPGLTRSVYTMPLANHRDDEH
GVASMVSVHVEHPQEASVVVHQVERVSGPWEEADAEAVARAEAAARAEAAAPYTVLAQSAPREDGYSD
ASGFGYCFRELRGGECASPLPGLRTQEVCCRGAGLAWGVHDCQLCSERLGNSERVSAPDGPCPTGFERVN
GSCEDVDECATGGRCQHGECANTRGGYTCVCPDGFLLDSSRSSCISQHVISEAKGPCFRVLRDGGCSLPILR
NITKQICCCSRVGKAWGRGCQLCPPFGSEGFREICPAGPGYHYSASDLRYNTRPLGQEPPRVSLSQPRTLPA
TSRPSAGFLPTHRLEPRPEPRPDPRPGPELPLPSIPAWTGPEIPESGPSSGMCQRNPQVCGPGRCISRPSGYTCA
CDSGFRLSPQGTRCIDVDECRRVPPPCAPGRCENSPGSFRCVCGPGFRAGPRAAECLDVDECHRVPPPCDLG
RCENTPGSFLCVCPAGYQAAPHGASCQDVDECTQSPGLCGRGACKNLPGSFRCVCPAGFRGSACEEDVDE
CAQEPPPCGPGRCDNTAGSFHCACPAGFRSRGPGAPCQDVDECARSPPPCTYGRCENTEGSFQCVCPMGFQ
PNTAGSECEDVDECENHLACPGQECVNSPGSFQCRTCPSGHHLHRGRCTGKPIPNPLLGLDSTRTG*HHHHH
HHH*

5.2.4 L4_SN

MAGGVRLLWVSLLVLLAQLGPQPGLGRLGERLRVRFTPVVCGLRCVHGPTGSRCTPTCAPRNATSVDSGA
PGGAAPGGPGFRAFLCPLICHNGGVCVKPDRCLCPPDFAGKFCQLHSSGARPPAPAIPGLTRSVYTMPLANH

RDDEHGVASMVSVHVEHPQEASVVVHQVERVSGPWEEADAEAVARAEAAARAEAAAPYTVLAQSAPRE
DGYSDASGFGYCFRELRGGECASPLPGLRTQEVCCRGAGLAWGVHDCQLCSERLGNSERVSAPDGPCPTG
FERVNGSCEDVDECATGGRCQHGECANTRGGYTCVCPDGFLLDSSRSSCISQHVISEAKGPCFRVLRDGGC
SLPILRNITKQICCCSRVGKAWGRGCQLCPPFGSEGFREICPAGPGYHYSASDLRYNTRPLGQEPPRVSLSQP
RTLPATSRPSAGFLPTHRLEPRPEPRPDPRPGPELPLPSIPAWTGPEIPESGPSSGMCQRNPQVCGPGRCISRPS
GYTCACDSGFRLSPQGTRCIDVDECRRVPPPCAPGRCENSPGSFRCVCGPGFRAGPRAAECLDVDECHRVP
PPCDLGRCENTPGSFLCVCPAGYQAAPHGASCQDVDECTQSPGLCGRGACKNLPGSFRCVCPAGFRGSACE
EDVDECAQEPPPCGPGRCDNTAGSFHCACPAGFRSRGPGAPCQDVDECARSPPPCTYGRCENTEGSFQCVC
PMGFQPNTAGSECEDVDECENHLACPGQECVNSPGSFQCRTCPSGHHLHRGRCTGKPIPNPLLGLDSTRTG
HHHHHHHH

5.2.5 L4_C

MRAWIFFLLCLAGRALAAPLADVDECSSGAPPCGPHGHCTNTEGSFRCSCAPGYRAPSGRPGPCADVNECL
EGDFCFPHGECLNTDGSFACTCAPGYRPGPRGASCLDVDECSEEDLCQSGICTNTDGSFECICPPGHRAGPD
LASCLDVDECRERGPALCGSQRCENSPGSYRCVRDCDPGYHAGPEGTCDDVDECQEYGPEICGAQRCENT
PGSYRCTPACDPGYQPTPGGGCQDVDECRNRSFCGAHAVCQNLPGSFQCLCDQGYEGARDGRHCVDVNE
CETLQGVCGAALCENVEGSFLCVCPNSPEEFDPMTGRCVPPRTSAGTFPGSQPQAPASPVLPARPPPPPLPRR
PSTPRQGPVGSGRRECYFDTAAPDACDNILARNVTWQECCCTVGEGWGSGCRIQQCPGTETAEYQSLCPH
GRGYLAPSGDLSLRRDVDECQLFRDQVCKSGVCVNTAPGYSCYCSNGYYYHTQRLECIDNDECADEEPAC
EGGRCVNTVGSYHCTCEPPLVLDGSQRRCVSNESQSLDDNLGVCWQEVGADLVCSHPRLDRQATYTECC
CLYGEAWGMDCALCPAQDSDDFEALCNVLRPPAYSPPRPGGFGLPYEYGPDLGPPYQGLPYGPELYPPPAL
PYDPYPPPPGPFARREAPYGAPRFDMPDFEDDGGPYGESEAPAPPGPGTRWPYRSRDTRRSFPEPEEPPEGG
SYAGSLAEPYEELEAEECGILDGCTNGRCVRVPEGFTCRCFDGYRLDMTRMACVDINECDEAEAASPLCVN
ARCLNTDGSFRCICRPGFAPTHQPHHCAPARPRAGKPIPNPLLGLDSTRTG*HHHHHHHH*

5.3 SDC recombinants

5.3.1 SDC2-ED

MRAWIFFLLCLAGRALAAPLA*MGSSHHHHHHSSGLVPRGSHM*ESRAELTSDKDMYLDNSSIEEASGVYPID
DDDYASASGSGADEDVESPELTTSRPLPKILLTSAAPKVETTTLNIQNKIPAQTKSPEETDKEKVHLSDSERK
MDPAEEDTNVYTEKHSDSLFKRTE*DYKDDDDK*

5.3.2 SDC3-ED

MRAWIFFLLCLAGRALAAPLA*MGSSHHHHHHSSGLVPRGSHM*AQRWRSENFERPVDLEGSGDDDSFPDDE
LDDLYSGSGSGYFEQESGIETAMRFSPDVALAVSTTPAVLPTTNIQPVGTPFEELPSERPTLEPATSPLVVTEV
PEEPSQRATTVSTTMATTAATSTGDPTVATVPATVATATPSTPAAPPFTATTAVIRTTGVRRLLPLPLTTVAT
ARATTPEAPSPPTTAAVLDTEAPTPRLVSTATSRPRALPRPATTQEPDIPERSTLPLGTTAPGPTEVAQTPTPE
TFLTTIRDEPAGPTEVAQTPTPETFLTTIRDEPEVPVSGGPSGDFELPEEETTQPDTANEVVAVGGAAAKASS
PPGTLPKGARPGPGLLDNAIDSGSSAAQLPQKSILERKEVLV*DYKDDDDK*

5.3.3 SDC4-ED

MRAWIFFLLCLAGRALAAPLA*MGSSHHHHHHSSGLVPRGSHM*ESIRETEVIDPQDLLEGRYFSGALPDDEDV
VGPGQESDDFELSGSGDLDDLEDSMIGPEVVHPLVPLDNHIPERAGSGSQVPTEPKKLEENEVIPKRISPVEE
SEDVSNKVSMSSTVQGSNIFERTEVLAGCPEH*DYKDDDDK*

REFERENCES

1. Kielty, C.M., Sherratt, M.J., and Shuttleworth, C.A. (2002). Elastic fibres. J Cell Sci 115, 2817-2828.
2. Kielty, C.M. (2006). Elastic fibres in health and disease. Expert Rev Mol Med 8, 1-23.
3. Urban, Z., and Davis, E.C. (2014). Cutis laxa: Intersection of elastic fiber biogenesis, TGFbeta signaling, the secretory pathway and metabolism. Matrix Biol 33, 16-22.
4. Kozel, B.A., Rongish, B.J., Czirok, A., Zach, J., Little, C.D., Davis, E.C., Knutsen, R.H., Wagenseil, J.E., Levy, M.A., and Mecham, R.P. (2006). Elastic fiber formation: a dynamic view of extracellular matrix assembly using timer reporters. J Cell Physiol 207, 87-96.
5. Halm, M., Schenke-Layland, K., Jaspers, S., Wenck, H., and Fischer, F. (2016). Visualizing tropoelastin in a long-term human elastic fibre cell culture model. Sci Rep 6, 20378.
6. Mecham, R.P. (2018). Elastin in lung development and disease pathogenesis. Matrix Biol in press.
7. Papke, C.L., and Yanagisawa, H. (2014). Fibulin-4 and fibulin-5 in elastogenesis and beyond: Insights from mouse and human studies. Matrix Biol 37, 142-149.
8. Pilecki, B., Holm, A.T., Schlosser, A., Moeller, J.B., Wohl, A.P., Zuk, A.V., Heumuller, S.E., Wallis, R., Moestrup, S.K., Sengle, G., et al. (2016). Characterization of Microfibrillar-associated Protein 4 (MFAP4) as a Tropoelastin- and Fibrillin-binding Protein Involved in Elastic Fiber Formation. J Biol Chem 291, 1103-1114.
9. Sato, F., Seino-Sudo, R., Okada, M., Sakai, H., Yumoto, T., and Wachi, H. (2017). Lysyl oxidase enhances the deposition of tropoelastin through the catalysis of tropoelastin molecules on the cell surface. Biol Pharm Bull 40, 1646-1653.
10. Zanetti, M., Braghetta, P., Sabatelli, P., Mura, I., Doliana, R., Colombatti, A., Volpin, D., Bonaldo, P., and Bressan, G.M. (2004). EMILIN-1 deficiency induces elastogenesis and vascular cell defects. Mol Cell Biol 24, 638-650.
11. Wagenseil, J.E., and Mecham, R.P. (2007). New insights into elastic fiber assembly. Birth Defects Res C Embryo Today 81, 229-240.
12. Hucthagowder, V., Sausgruber, N., Kim, K.H., Angle, B., Marmorstein, L.Y., and Urban, Z. (2006). Fibulin-4: a novel gene for an autosomal recessive cutis laxa syndrome. Am J Hum Genet 78, 1075-1080.

13. Dasouki, M., Markova, D., Garola, R., Sasaki, T., Charbonneau, N.L., Sakai, L.Y., and Chu, M.L. (2007). Compound heterozygous mutations in fibulin-4 causing neonatal lethal pulmonary artery occlusion, aortic aneurysm, arachnodactyly, and mild cutis laxa. Am J Med Genet A 143A, 2635-2641.

14. Renard, M., Holm, T., Veith, R., Callewaert, B.L., Ades, L.C., Baspinar, O., Pickart, A., Dasouki, M., Hoyer, J., Rauch, A., et al. (2010). Altered TGFbeta signaling and cardiovascular manifestations in patients with autosomal recessive cutis laxa type I caused by fibulin-4 deficiency. Eur J Hum Genet 18, 895-901.

15. Hebson, C., Coleman, K., Clabby, M., Sallee, D., Shankar, S., Loeys, B., Van Laer, L., and Kogon, B. (2014). Severe aortopathy due to fibulin-4 deficiency: molecular insights, surgical strategy, and a review of the literature. Eur J Pediatr 173, 671-675.

16. Callewaert, B.L., and Urban, Z. (1993). LTBP4-Related Cutis Laxa. In GeneReviews((R)), M.P. Adam, H.H. Ardinger, R.A. Pagon, S.E. Wallace, L.J.H. Bean, K. Stephens, andA. Amemiya, eds. (Seattle (WA).

17. Horiguchi, M., Inoue, T., Ohbayashi, T., Hirai, M., Noda, K., Marmorstein, L.Y., Yabe, D., Takagi, K., Akama, T.O., Kita, T., et al. (2009). Fibulin-4 conducts proper elastogenesis via interaction with cross-linking enzyme lysyl oxidase. Proc Natl Acad Sci USA 106, 19029-19034.

18. Djokic, J., Fagotto-Kaufmann, C., Bartels, R., Nelea, V., and Reinhardt, D.P. (2013). Fibulin-3, -4, and -5 are highly susceptible to proteolysis, interact with cells and heparin, and form multimers. J Biol Chem 288, 22821-22835.

19. Bultmann-Mellin, I., Conradi, A., Maul, A.C., Dinger, K., Wempe, F., Wohl, A.P., Imhof, T., Wunderlich, F.T., Bunck, A.C., Nakamura, T., et al. (2015). Modeling autosomal recessive cutis laxa type 1C in mice reveals distinct functions for Ltbp-4 isoforms. Dis Model Mech 8, 403-415.

20. Kumra, H., Nelea, V., Hakami, H., Pagliuzza, A., Djokic, J., Xu, J., Yanagisawa, H., and Reinhardt, D.P. (2019). Fibulin-4 exerts a dual role in LTBP-4L-mediated matrix assembly and function. Proc Natl Acad Sci USA 116, 20428-20437.

21. Noda, K., Dabovic, B., Takagi, K., Inoue, T., Horiguchi, M., Hirai, M., Fujikawa, Y., Akama, T.O., Kusumoto, K., Zilberberg, L., et al. (2013). Latent TGF-beta binding protein 4

promotes elastic fiber assembly by interacting with fibulin-5. Proc Natl Acad Sci USA 110, 2852-2857.

22. Kantola, A.K., Keski-Oja, J., and Koli, K. (2008). Fibronectin and heparin binding domains of latent TGF-beta binding protein (LTBP)-4 mediate matrix targeting and cell adhesion. Exp Cell Res 314, 2488-2500.
23. Frantz, C., Stewart, K.M., and Weaver, V.M. (2010). The extracellular matrix at a glance. J Cell Sci 123, 4195-4200.
24. Hynes, R.O., and Naba, A. (2012). Overview of the matrisome--an inventory of extracellular matrix constituents and functions. Cold Spring Harb Perspect Biol 4, a004903.
25. Naba, A., Clauser, K.R., Hoersch, S., Liu, H., Carr, S.A., and Hynes, R.O. (2012). The matrisome: in silico definition and in vivo characterization by proteomics of normal and tumor extracellular matrices. Mol Cell Proteomics 11, M111 014647.
26. Lu, P., Takai, K., Weaver, V.M., and Werb, Z. (2011). Extracellular matrix degradation and remodeling in development and disease. Cold Spring Harb Perspect Biol 3.
27. Hynes, R.O. (2012). Evolution: The evolution of metazoan extracellular matrix. J Cell Biol 196, 671-679.
28. Pankov, R., and Yamada, K.M. (2002). Fibronectin at a glance. J Cell Sci 115, 3861-3863.
29. Fass, D. (2012). Disulfide bonding in protein biophysics. Annu Rev Biophys 41, 63-79.
30. Reily, C., Stewart, T.J., Renfrow, M.B., and Novak, J. (2019). Glycosylation in health and disease. Nat Rev Nephrol 15, 346-366.
31. Lynch, M., Barallobre-Barreiro, J., Jahangiri, M., and Mayr, M. (2016). Vascular proteomics in metabolic and cardiovascular diseases. J Intern Med 280, 325-338.
32. Rojas, A., Anazco, C., Gonzalez, I., and Araya, P. (2018). Extracellular matrix glycation and receptor for advanced glycation end-products activation: a missing piece in the puzzle of the association between diabetes and cancer. Carcinogenesis 39, 515-521.
33. Feizi, A., Gatto, F., Uhlen, M., and Nielsen, J. (2017). Human protein secretory pathway genes are expressed in a tissue-specific pattern to match processing demands of the secretome. NPJ Syst Biol Appl 3, 22.
34. Unlu, G., Levic, D.S., Melville, D.B., and Knapik, E.W. (2014). Trafficking mechanisms of extracellular matrix macromolecules: insights from vertebrate development and human diseases. Int J Biochem Cell Biol 47, 57-67.

35. Mouw, J.K., Ou, G., and Weaver, V.M. (2014). Extracellular matrix assembly: a multiscale deconstruction. Nat Rev Mol Cell Biol 15, 771-785.

36. Shoulders, M.D., and Raines, R.T. (2009). Collagen structure and stability. Annu Rev Biochem 78, 929-958.

37. Ribeiro, J.F., dos Anjos, E.H., Mello, M.L., and de Campos Vidal, B. (2013). Skin collagen fiber molecular order: a pattern of distributional fiber orientation as assessed by optical anisotropy and image analysis. PLoS One 8, e54724.

38. van Zuijlen, P.P., Ruurda, J.J., van Veen, H.A., van Marle, J., van Trier, A.J., Groenevelt, F., Kreis, R.W., and Middelkoop, E. (2003). Collagen morphology in human skin and scar tissue: no adaptations in response to mechanical loading at joints. Burns 29, 423-431.

39. Mecham, R.P. (2001). Overview of extracellular matrix. Curr Protoc Cell Biol Chapter 10, Unit 10 11.

40. Rozario, T., and DeSimone, D.W. (2010). The extracellular matrix in development and morphogenesis: a dynamic view. Dev Biol 341, 126-140.

41. Bonnans, C., Chou, J., and Werb, Z. (2014). Remodelling the extracellular matrix in development and disease. Nat Rev Mol Cell Biol 15, 786-801.

42. Kai, F., Laklai, H., and Weaver, V.M. (2016). Force Matters: Biomechanical Regulation of Cell Invasion and Migration in Disease. Trends Cell Biol 26, 486-497.

43. Gjorevski, N., and Nelson, C.M. (2009). Bidirectional extracellular matrix signaling during tissue morphogenesis. Cytokine Growth Factor Rev 20, 459-465.

44. Bateman, J.F., Boot-Handford, R.P., and Lamande, S.R. (2009). Genetic diseases of connective tissues: cellular and extracellular effects of ECM mutations. Nat Rev Genet 10, 173-183.

45. Iozzo, R.V., and Gubbiotti, M.A. (2018). Extracellular matrix: The driving force of mammalian diseases. Matrix Biol 71-72, 1-9.

46. Socovich, A.M., and Naba, A. (2019). The cancer matrisome: From comprehensive characterization to biomarker discovery. Semin Cell Dev Biol 89, 157-166.

47. Yanagisawa, H., and Wagenseil, J. (2020). Elastic fibers and biomechanics of the aorta: Insights from mouse studies. Matrix Biol 85-86, 160-172.

48. Kozel, B.A., and Mecham, R.P. (2019). Elastic fiber ultrastructure and assembly. Matrix Biol 84, 31-40.

49. Rosenbloom, J., Abrams, W.R., and Mecham, R. (1993). Extracellular matrix 4: the elastic fiber. FASEB J 7, 1208-1218.

50. Ross, R., and Bornstein, P. (1969). The elastic fiber: the separation and partial characterization of its macromolecular components. J Cell Biol 40, 366-381.

51. Baldwin, A.K., Simpson, A., Steer, R., Cain, S.A., and Kielty, C.M. (2013). Elastic fibres in health and disease. Expert Rev Mol Med 15, e8.

52. Votteler, M., Berrio, D.A., Horke, A., Sabatier, L., Reinhardt, D.P., Nsair, A., Aikawa, E., and Schenke-Layland, K. (2013). Elastogenesis at the onset of human cardiac valve development. Development 140, 2345-2353.

53. Judge, D.P., and Dietz, H.C. (2005). Marfan's syndrome. Lancet 366, 1965-1976.

54. Hinton, R.B., Adelman-Brown, J., Witt, S., Krishnamurthy, V.K., Osinska, H., Sakthivel, B., James, J.F., Li, D.Y., Narmoneva, D.A., Mecham, R.P., et al. (2010). Elastin haploinsufficiency results in progressive aortic valve malformation and latent valve disease in a mouse model. Circ Res 107, 549-557.

55. Urban, Z., Zhang, J., Davis, E.C., Maeda, G.K., Kumar, A., Stalker, H., Belmont, J.W., Boyd, C.D., and Wallace, M.R. (2001). Supravalvular aortic stenosis: genetic and molecular dissection of a complex mutation in the elastin gene. Hum Genet 109, 512-520.

56. Uitto, J., Li, Q., and Urban, Z. (2013). The complexity of elastic fibre biogenesis in the skin--a perspective to the clinical heterogeneity of cutis laxa. Exp Dermatol 22, 88-92.

57. White, T.L., Lewis, P., Hayes, S., Fergusson, J., Bell, J., Farinha, L., White, N.S., Pereira, L.V., and Meek, K.M. (2017). The Structural Role of Elastic Fibers in the Cornea Investigated Using a Mouse Model for Marfan Syndrome. Invest Ophthalmol Vis Sci 58, 2106-2116.

58. Cain, S.A., McGovern, A., Baldwin, A.K., Baldock, C., and Kielty, C.M. (2012). Fibrillin-1 mutations causing Weill-Marchesani syndrome and acromicric and geleophysic dysplasias disrupt heparan sulfate interactions. PLoS One 7, e48634.

59. Hu, Q., Reymond, J.L., Pinel, N., Zabot, M.T., and Urban, Z. (2006). Inflammatory destruction of elastic fibers in acquired cutis laxa is associated with missense alleles in the elastin and fibulin-5 genes. J Invest Dermatol 126, 283-290.

60. Shapiro, S.D., Endicott, S.K., Province, M.A., Pierce, J.A., and Campbell, E.J. (1991). Marked longevity of human lung parenchymal elastic fibers deduced from prevalence of D-aspartate and nuclear weapons-related radiocarbon. J Clin Invest 87, 1828-1834.

61. Kielty, C.M., Woolley, D.E., Whittaker, S.P., and Shuttleworth, C.A. (1994). Catabolism of intact fibrillin microfibrils by neutrophil elastase, chymotrypsin and trypsin. FEBS Lett 351, 85-89.

62. Sugimoto, K., Nakamura, T., Tokunaga, T., Uehara, Y., Okada, T., Taniwaki, T., Fujimoto, T., and Mizuta, H. (2018). Matrix metalloproteinase promotes elastic fiber degradation in ligamentum flavum degeneration. PLoS One 13, e0200872.

63. Curci, J.A., Liao, S., Huffman, M.D., Shapiro, S.D., and Thompson, R.W. (1998). Expression and localization of macrophage elastase (matrix metalloproteinase-12) in abdominal aortic aneurysms. J Clin Invest 102, 1900-1910.

64. Bunton, T.E., Biery, N.J., Myers, L., Gayraud, B., Ramirez, F., and Dietz, H.C. (2001). Phenotypic alteration of vascular smooth muscle cells precedes elastolysis in a mouse model of Marfan syndrome. Circ Res 88, 37-43.

65. Shapiro, S.D., Campbell, E.J., Welgus, H.G., and Senior, R.M. (1991). Elastin degradation by mononuclear phagocytes. Ann N Y Acad Sci 624, 69-80.

66. Hornebeck, W., and Emonard, H. (2011). The cell-elastin-elastase(s) interacting triade directs elastolysis. Front Biosci (Landmark Ed) 16, 707-722.

67. Kadoya, K., Sasaki, T., Kostka, G., Timpl, R., Matsuzaki, K., Kumagai, N., Sakai, L.Y., Nishiyama, T., and Amano, S. (2005). Fibulin-5 deposition in human skin: decrease with ageing and ultraviolet B exposure and increase in solar elastosis. Br J Dermatol 153, 607-612.

68. Wagenseil, J.E., and Mecham, R.P. (2012). Elastin in large artery stiffness and hypertension. J Cardiovasc Transl Res 5, 264-273.

69. Keski-Oja, J., Mosher, D.F., and Vaheri, A. (1977). Dimeric character of fibronectin, a major cell surface-associated glycoprotein. Biochem Biophys Res Commun 74, 699-706.

70. McDonald, J.A., Quade, B.J., Broekelmann, T.J., LaChance, R., Forsman, K., Hasegawa, E., and Akiyama, S. (1987). Fibronectin's cell-adhesive domain and an amino-terminal matrix assembly domain participate in its assembly into fibroblast pericellular matrix. J Biol Chem 262, 2957-2967.

71. Sottile, J., and Wiley, S. (1994). Assembly of amino-terminal fibronectin dimers into the extracellular matrix. J Biol Chem 269, 17192-17198.

72. Singh, P., Carraher, C., and Schwarzbauer, J.E. (2010). Assembly of fibronectin extracellular matrix. Annu Rev Cell Dev Biol 26, 397-419.

73. Früh, S.M., Schoen, I., Ries, J., and Vogel, V. (2015). Molecular architecture of native fibronectin fibrils. Nat Commun 6, 7275.

74. Johansson, S., Svineng, G., Wennerberg, K., Armulik, A., and Lohikangas, L. (1997). Fibronectin-integrin interactions. Front Biosci 2, d126-146.

75. Wierzbicka-Patynowski, I., and Schwarzbauer, J.E. (2003). The ins and outs of fibronectin matrix assembly. J Cell Sci 116, 3269-3276.

76. Bloom, L., Ingham, K.C., and Hynes, R.O. (1999). Fibronectin regulates assembly of actin filaments and focal contacts in cultured cells via the heparin-binding site in repeat III13. Mol Biol Cell 10, 1521-1536.

77. Schwinn, M.K., Gonzalez, J.M., Jr., Gabelt, B.T., Sheibani, N., Kaufman, P.L., and Peters, D.M. (2010). Heparin II domain of fibronectin mediates contractility through an alpha4beta1 co-signaling pathway. Exp Cell Res 316, 1500-1512.

78. Huveneers, S., Truong, H., Fassler, R., Sonnenberg, A., and Danen, E.H. (2008). Binding of soluble fibronectin to integrin alpha5 beta1 - link to focal adhesion redistribution and contractile shape. J Cell Sci 121, 2452-2462.

79. Kumra, H., Sabatier, L., Hassan, A., Sakai, T., Mosher, D.F., Brinckmann, J., and Reinhardt, D.P. (2018). Roles of fibronectin isoforms in neonatal vascular development and matrix integrity. PLoS Biol 16, e2004812.

80. Mecham, R.P., and Davis, E. (1994). Elastic fiber structure and assembly. In Extracellular Matrix Assembly and Structure, P.D. Yurchenco, D.E. Birk, andR.P. Mecham, eds. (New York, Academic Press), pp 281-314.

81. Kielty, C.M., Sherratt, M.J., Marson, A., and Baldock, C. (2005). Fibrillin microfibrils. Adv Protein Chem 70, 405-436.

82. Thomson, J., Singh, M., Eckersley, A., Cain, S.A., Sherratt, M.J., and Baldock, C. (2019). Fibrillin microfibrils and elastic fibre proteins: Functional interactions and extracellular regulation of growth factors. Semin Cell Dev Biol 89, 109-117.

83. Kinsey, R., Williamson, M.R., Chaudhry, S., Mellody, K.T., McGovern, A., Takahashi, S., Shuttleworth, C.A., and Kielty, C.M. (2008). Fibrillin-1 microfibril deposition is dependent on fibronectin assembly. J Cell Sci 121, 2696-2704.

84. Sabatier, L., Chen, D., Fagotto-Kaufmann, C., Hubmacher, D., McKee, M.D., Annis, D.S., Mosher, D.F., and Reinhardt, D.P. (2009). Fibrillin assembly requires fibronectin. Mol Biol Cell 20, 846-858.

85. Kobayashi, N., Kostka, G., Garbe, J.H., Keene, D.R., Bachinger, H.P., Hanisch, F.G., Markova, D., Tsuda, T., Timpl, R., Chu, M.L., et al. (2007). A comparative analysis of the fibulin protein family. Biochemical characterization, binding interactions, and tissue localization. J Biol Chem 282, 11805-11816.

86. Schiavinato, A., Keene, D.R., Wohl, A.P., Corallo, D., Colombatti, A., Wagener, R., Paulsson, M., Bonaldo, P., and Sengle, G. (2016). Targeting of EMILIN-1 and EMILIN-2 to Fibrillin Microfibrils Facilitates their Incorporation into the Extracellular Matrix. J Invest Dermatol 136, 1150-1160.

87. Wallace, R.N., Streeten, B.W., and Hanna, R.B. (1991). Rotary shadowing of elastic system microfibrils in the ocular zonule, vitreous, and ligament nuchae. Curr Eye Res 10, 99-109.

88. Keene, D.R., Maddox, B.K., Kuo, H.J., Sakai, L.Y., and Glanville, R.W. (1991). Extraction of extendable beaded structures and their identification as fibrillin-containing extracellular matrix microfibrils. J Histochem Cytochem 39, 441-449.

89. Kielty, C.M., Cummings, C., Whittaker, S.P., Shuttleworth, C.A., and Grant, M.E. (1991). Isolation and ultrastructural analysis of microfibrillar structures from foetal bovine elastic tissues. J Cell Sci 99, 797-807.

90. Milewicz, D.M., Grossfield, J., Cao, S.N., Kielty, C., Covitz, W., and Jewett, T. (1995). A mutation in FBN1 disrupts profibrillin processing and results in isolated skeletal features of the Marfan syndrome. J Clin Invest 95, 2373-2378.

91. Ritty, T.M., Broekelmann, T., Tisdale, C., Milewicz, D.M., and Mecham, R.P. (1999). Processing of the fibrillin-1 carboxyl-terminal domain. J Biol Chem 274, 8933-8940.

92. Wallis, D.D., Putnam, E.A., Cretoiu, J.S., Carmical, S.G., Cao, S.N., Thomas, G., and Milewicz, D.M. (2003). Profibrillin-1 maturation by human dermal fibroblasts: proteolytic processing and molecular chaperones. J Cell Biochem 90, 641-652.

93. Hubmacher, D., El-Hallous, E., Nelea, V., Kaartinen, M.T., Lee, E.R., and Reinhardt, D.P. (2008). Biogenesis of extracellular microfibrils: Multimerization of the fibrillin-1 C-terminus into bead-like structures enables self-assembly. Proc Natl Acad Sci USA 105, 6548-6553.

94. Sakai, L.Y., Keene, D.R., Glanville, R.W., and Bächinger, H.P. (1991). Purification and partial characterization of fibrillin, a cysteine-rich structural component of connective tissue microfibrils. J Biol Chem 266, 14763-14770.

95. Reinhardt, D.P., Keene, D.R., Corson, G.M., Pöschl, E., Bächinger, H.P., Gambee, J.E., and Sakai, L.Y. (1996). Fibrillin 1: Organization in microfibrils and structural properties. J Mol Biol 258, 104-116.

96. Baldock, C., Koster, A.J., Ziese, U., Rock, M.J., Sherratt, M.J., Kadler, K.E., Shuttleworth, C.A., and Kielty, C.M. (2001). The supramolecular organization of fibrillin-rich microfibrils. J Cell Biol 152, 1045-1056.

97. Marson, A., Rock, M.J., Cain, S.A., Freeman, L.J., Morgan, A., Mellody, K., Shuttleworth, C.A., Baldock, C., and Kielty, C.M. (2005). Homotypic fibrillin-1 interactions in microfibril assembly. J Biol Chem 280, 5013-5021.

98. Lin, G., Tiedemann, K., Vollbrandt, T., Peters, H., Bätge, B., Brinckmann, J., and Reinhardt, D.P. (2002). Homo- and heterotypic fibrillin-1 and -2 interactions constitute the basis for the assembly of microfibrils. J Biol Chem 277, 50795-50804.

99. Glanville, R.W., Qian, R.Q., McClure, D.W., and Maslen, C.L. (1994). Calcium binding, hydroxylation, and glycosylation of the precursor epidermal growth factor-like domains of fibrillin-1, the Marfan gene protein. J Biol Chem 269, 26630-26634.

100. Raghunath, M., Hopfner, B., Aeschlimann, D., Luthi, U., Meuli, M., Altermatt, S., Gobet, R., Bruckner-Tuderman, L., and Steinmann, B. (1996). Cross-linking of the dermo-epidermal junction of skin regenerating from keratinocyte autografts. Anchoring fibrils are a target for tissue transglutaminase. J Clin Invest 98, 1174-1184.

101. Qian, R.Q., and Glanville, R.W. (1997). Alignment of fibrillin molecules in elastic microfibrils is defined by transglutaminase-derived cross-links. Biochemistry 36, 15841-15847.

102. Rock, M.J., Cain, S.A., Freeman, L.J., Morgan, A., Mellody, K., Marson, A., Shuttleworth, C.A., Weiss, A.S., and Kielty, C.M. (2004). Molecular basis of elastic fiber formation.

Critical interactions and a tropoelastin-fibrillin-1 cross-link. J Biol Chem 279, 23748-23758.

103. Zeyer, K.A., and Reinhardt, D.P. (2015). Fibrillin-containing microfibrils are key signal relay stations for cell function. J Cell Commun Signal 9, 309-325.

104. Abraham, P.A., Perejda, A.J., Carnes, W.H., and Uitto, J. (1982). Marfan syndrome. Demonstration of abnormal elastin in aorta. J Clin Invest 70, 1245-1252.

105. Judge, D.P., Biery, N.J., Keene, D.R., Geubtner, J., Myers, L., Huso, D.L., Sakai, L.Y., and Dietz, H.C. (2004). Evidence for a critical contribution of haploinsufficiency in the complex pathogenesis of Marfan syndrome. J Clin Invest 114, 172-181.

106. Pereira, L., Andrikopoulos, K., Tian, J., Lee, S.Y., Keene, D.R., Ono, R.N., Reinhardt, D.P., Sakai, L.Y., Jensen-Biery, N., Bunton, T., et al. (1997). Targeting of fibrillin-1 recapitulates the vascular phenotype of Marfan syndrome in the mouse. Nat Genet 17, 218-222.

107. Pereira, L., Lee, S.Y., Gayraud, B., Andrikopoulos, K., Shapiro, S.D., Bunton, T., Biery, N.J., Dietz, H.C., Sakai, L.Y., and Ramirez, F. (1999). Pathogenetic sequence for aneurysm revealed in mice underexpressing fibrillin-1. Proc Natl Acad Sci USA 96, 3819-3823.

108. Carta, L., Pereira, L., Arteaga-Solis, E., Lee-Arteaga, S.Y., Lenart, B., Starcher, B., Merkel, C.A., Sukoyan, M., Kerkis, A., Hazeki, N., et al. (2006). Fibrillins 1 and 2 perform partially overlapping functions during aortic development. J Biol Chem 281, 8016-8023.

109. Tamburro, A.M., Bochicchio, B., and Pepe, A. (2003). Dissection of human tropoelastin: exon-by-exon chemical synthesis and related conformational studies. Biochemistry 42, 13347-13362.

110. Rauscher, S., Baud, S., Miao, M., Keeley, F.W., and Pomes, R. (2006). Proline and glycine control protein self-organization into elastomeric or amyloid fibrils. Structure 14, 1667-1676.

111. Schrader, C.U., Heinz, A., Majovsky, P., Karaman Mayack, B., Brinckmann, J., Sippl, W., and Schmelzer, C.E.H. (2018). Elastin is heterogeneously cross-linked. J Biol Chem 293, 15107-15119.

112. Eyre, D.R., Paz, M.A., and Gallop, P.M. (1984). Cross-linking in collagen and elastin. Annu Rev Biochem 53, 717-748.

113. Robertson, I.B., Horiguchi, M., Zilberberg, L., Dabovic, B., Hadjiolova, K., and Rifkin, D.B. (2015). Latent TGF-beta-binding proteins. Matrix Biol 47, 44-53.

114. Yanagisawa, H., Davis, E.C., Starcher, B.C., Ouchi, T., Yanagisawa, M., Richardson, J.A., and Olson, E.N. (2002). Fibulin-5 is an elastin-binding protein essential for elastic fibre development in vivo. Nature 415, 168-171.

115. McLaughlin, P.J., Chen, Q., Horiguchi, M., Starcher, B.C., Stanton, J.B., Broekelmann, T.J., Marmorstein, A.D., McKay, B., Mecham, R., Nakamura, T., et al. (2006). Targeted disruption of fibulin-4 abolishes elastogenesis and causes perinatal lethality in mice. Mol Cell Biol 26, 1700-1709.

116. El-Hallous, E., Sasaki, T., Hubmacher, D., Getie, M., Tiedemann, K., Brinckmann, J., Bätge, B., Davis, E.C., and Reinhardt, D.P. (2007). Fibrillin-1 interactions with fibulins depend on the first hybrid domain and provide an adapter function to tropoelastin. J Biol Chem 282, 8935-8946.

117. Nakamura, T., Lozano, P.R., Ikeda, Y., Iwanaga, Y., Hinek, A., Minamisawa, S., Cheng, C.F., Kobuke, K., Dalton, N., Takada, Y., et al. (2002). Fibulin-5/DANCE is essential for elastogenesis in vivo. Nature 415, 171-175.

118. Lucero, H.A., and Kagan, H.M. (2006). Lysyl oxidase: an oxidative enzyme and effector of cell function. Cell Mol Life Sci 63, 2304-2316.

119. Cai, L., Xiong, X., Kong, X., and Xie, J. (2017). The Role of the Lysyl Oxidases in Tissue Repair and Remodeling: A Concise Review. Tissue Eng Regen Med 14, 15-30.

120. Liu, X., Zhao, Y., Gao, J., Pawlyk, B., Starcher, B., Spencer, J.A., Yanagisawa, H., Zuo, J., and Li, T. (2004). Elastic fiber homeostasis requires lysyl oxidase-like 1 protein. Nat Genet 36, 178-182.

121. Maki, J.M., Rasanen, J., Tikkanen, H., Sormunen, R., Makikallio, K., Kivirikko, K.I., and Soininen, R. (2002). Inactivation of the lysyl oxidase gene Lox leads to aortic aneurysms, cardiovascular dysfunction, and perinatal death in mice. Circulation 106, 2503-2509.

122. Hornstra, I.K., Birge, S., Starcher, B., Bailey, A.J., Mecham, R.P., and Shapiro, S.D. (2003). Lysyl oxidase is required for vascular and diaphragmatic development in mice. J Biol Chem 278, 14387-14393.

123. Lee, U.J., Gustilo-Ashby, A.M., Daneshgari, F., Kuang, M., Vurbic, D., Lin, D.L., Flask, C.A., Li, T., and Damaser, M.S. (2008). Lower urogenital tract anatomical and functional

phenotype in lysyl oxidase like-1 knockout mice resembles female pelvic floor dysfunction in humans. Am J Physiol Renal Physiol 295, F545-555.

124. Bressan, G.M., Daga-Gordini, D., Colombatti, A., Castellani, I., Marigo, V., and Volpin, D. (1993). Emilin, a component of elastic fibers preferentially located at the elastin-microfibril interface. J Cell Biol 121, 201-212.

125. Doliana, R., Mongiat, M., Bucciotti, F., Giacomello, E., Deutzmann, R., Volpin, D., Bressan, G.M., and Colombatti, A. (1999). EMILIN, a component of the elastic fiber and a new member of the C1q/tumor necrosis factor superfamily of proteins. J Biol Chem 274, 16773-16781.

126. Schiavinato, A., Keene, D.R., Imhof, T., Doliana, R., Sasaki, T., and Sengle, G. (2017). Fibulin-4 deposition requires EMILIN-1 in the extracellular matrix of osteoblasts. Sci Rep 7, 5526.

127. Mecham, R.P., and Gibson, M.A. (2015). The microfibril-associated glycoproteins (MAGPs) and the microfibrillar niche. Matrix Biol 47, 13-33.

128. Gibson, M.A., Kumaratilake, J.S., and Cleary, E.G. (1989). The protein components of the 12- nanometer microfibrils of elastic and nonelastic tissues. J Biol Chem 264, 4590-4598.

129. Cain, S.A., Morgan, A., Sherratt, M.J., Ball, S.G., Shuttleworth, C.A., and Kielty, C.M. (2006). Proteomic analysis of fibrillin-rich microfibrils. Proteomics 6, 111-122.

130. Gibson, M.A., Finnis, M.L., Kumaratilake, J.S., and Cleary, E.G. (1998). Microfibril-associated glycoprotein-2 (MAGP-2) is specifically associated with fibrillin-containing microfibrils but exhibits more restricted patterns of tissue localization and developmental expression than its structural relative MAGP-1. J Histochem Cytochem 46, 871-886.

131. Weinbaum, J.S., Broekelmann, T.J., Pierce, R.A., Werneck, C.C., Segade, F., Craft, C.S., Knutsen, R.H., and Mecham, R.P. (2008). Deficiency in microfibril-associated glycoprotein-1 leads to complex phenotypes in multiple organ systems. J Biol Chem 283, 25533-25543.

132. Craft, C.S., Zou, W., Watkins, M., Grimston, S., Brodt, M.D., Broekelmann, T.J., Weinbaum, J.S., Teitelbaum, S.L., Pierce, R.A., Civitelli, R., et al. (2010). Microfibril-associated glycoprotein-1, an extracellular matrix regulator of bone remodeling. J Biol Chem 285, 23858-23867.

133. Combs, M.D., Knutsen, R.H., Broekelmann, T.J., Toennies, H.M., Brett, T.J., Miller, C.A., Kober, D.L., Craft, C.S., Atkinson, J.J., Shipley, J.M., et al. (2013). Microfibril-associated glycoprotein 2 (MAGP2) loss of function has pleiotropic effects in vivo. J Biol Chem 288, 28869-28880.

134. Holm, A.T., Wulf-Johansson, H., Hvidsten, S., Jorgensen, P.T., Schlosser, A., Pilecki, B., Ormhoj, M., Moeller, J.B., Johannsen, C., Baun, C., et al. (2015). Characterization of spontaneous air space enlargement in mice lacking microfibrillar-associated protein 4. Am J Physiol Lung Cell Mol Physiol 308, L1114-1124.

135. Milicevic, N.M., Schmidt, F., Kunz, N., Kalies, K., Milicevic, Z., Schlosser, A., Holmskov, U., Sorensen, G.L., and Westermann, J. (2016). The role of microfibrillar-associated protein 4 (MFAP4) in the formation and function of splenic compartments during embryonic and adult life. Cell Tissue Res 365, 135-145.

136. Schlosser, A., Pilecki, B., Hemstra, L.E., Kejling, K., Kristmannsdottir, G.B., Wulf-Johansson, H., Moeller, J.B., Fuchtbauer, E.M., Nielsen, O., Kirketerp-Moller, K., et al. (2016). MFAP4 Promotes Vascular Smooth Muscle Migration, Proliferation and Accelerates Neointima Formation. Arterioscler Thromb Vasc Biol 36, 122-133.

137. Yanagisawa, H., and Davis, E.C. (2010). Unraveling the mechanism of elastic fiber assembly: The roles of short fibulins. Int J Biochem Cell Biol 42, 1084-1093.

138. Jensen, S.A., Reinhardt, D.P., Gibson, M.A., and Weiss, A.S. (2001). Protein interaction studies of MAGP-1 with tropoelastin and fibrillin-1. J Biol Chem 276, 39661-39666.

139. Lemaire, R., Bayle, J., Mecham, R.P., and Lafyatis, R. (2007). Microfibril-associated MAGP-2 stimulates elastic fiber assembly. J Biol Chem 282, 800-808.

140. Toyoshima, T., Nishi, N., Kusama, H., Kobayashi, R., and Itano, T. (2005). 36-kDa microfibril-associated glycoprotein (MAGP-36) is an elastin-binding protein increased in chick aortae during development and growth. Exp Cell Res 307, 224-230.

141. Bhushan, R., Altinbas, L., Jager, M., Zaradzki, M., Lehmann, D., Timmermann, B., Clayton, N.P., Zhu, Y., Kallenbach, K., Kararigas, G., et al. (2019). An integrative systems approach identifies novel candidates in Marfan syndrome-related pathophysiology. J Cell Mol Med 23, 2526-2535.

142. Davis, E.C., and Mecham, R.P. (1998). Intracellular trafficking of tropoelastin. Matrix Biol 17, 245-254.

143. Bashir, M.M., Indik, Z., Yeh, H., Ornstein-Goldstein, N., Rosenbloom, J.C., Abrams, W., Fazio, M., Uitto, J., and Rosenbloom, J. (1989). Characterization of the complete human elastin gene. Delineation of unusual features in the 5'-flanking region. J Biol Chem 264, 8887-8891.

144. Indik, Z., Yeh, H., Ornstein-Goldstein, N., Kucich, U., Abrams, W., Rosenbloom, J.C., and Rosenbloom, J. (1989). Structure of the elastin gene and alternative splicing of elastin mRNA: implications for human disease. Am J Med Genet 34, 81-90.

145. Indik, Z., Yoon, K., Morrow, S.D., Cicila, G., Rosenbloom, J., Rosenbloom, J., and Ornstein-Goldstein, N. (1987). Structure of the 3' region of the human elastin gene: great abundance of Alu repetitive sequences and few coding sequences. Connect Tissue Res 16, 197-211.

146. Vrhovski, B., and Weiss, A.S. (1998). Biochemistry of tropoelastin. Eur J Biochem 258, 1-18.

147. Baldock, C., Oberhauser, A.F., Ma, L., Lammie, D., Siegler, V., Mithieux, S.M., Tu, Y., Chow, J.Y., Suleman, F., Malfois, M., et al. (2011). Shape of tropoelastin, the highly extensible protein that controls human tissue elasticity. Proc Natl Acad Sci U S A 108, 4322-4327.

148. Tarakanova, A., Yeo, G.C., Baldock, C., Weiss, A.S., and Buehler, M.J. (2018). Molecular model of human tropoelastin and implications of associated mutations. Proc Natl Acad Sci U S A 115, 7338-7343.

149. Parks, W.C., and Deak, S.B. (1990). Tropoelastin heterogeneity: implications for protein function and disease. Am J Respir Cell Mol Biol 2, 399-406.

150. Muiznieks, L.D., Weiss, A.S., and Keeley, F.W. (2010). Structural disorder and dynamics of elastin. Biochem Cell Biol 88, 239-250.

151. Rauscher, S., and Pomes, R. (2012). Structural disorder and protein elasticity. Adv Exp Med Biol 725, 159-183.

152. Vrhovski, B., Jensen, S., and Weiss, A.S. (1997). Coacervation characteristics of recombinant human tropoelastin. Eur J Biochem 250, 92-98.

153. Dyksterhuis, L.B., Baldock, C., Lammie, D., Wess, T.J., and Weiss, A.S. (2007). Domains 17-27 of tropoelastin contain key regions of contact for coacervation and contain an unusual turn-containing crosslinking domain. Matrix Biol 26, 125-135.

154. Wise, S.G., Mithieux, S.M., Raftery, M.J., and Weiss, A.S. (2005). Specificity in the coacervation of tropoelastin: solvent exposed lysines. J Struct Biol 149, 273-281.

155. Jensen, S.A., Vrhovski, B., and Weiss, A.S. (2000). Domain 26 of tropoelastin plays a dominant role in association by coacervation. J Biol Chem 275, 28449-28454.

156. Merla, G., Brunetti-Pierri, N., Piccolo, P., Micale, L., and Loviglio, M.N. (2012). Supravalvular aortic stenosis: elastin arteriopathy. Circ Cardiovasc Genet 5, 692-696.

157. He, D., Miao, M., Sitarz, E.E., Muiznieks, L.D., Reichheld, S., Stahl, R.J., Keeley, F.W., and Parkinson, J. (2012). Polymorphisms in the human tropoelastin gene modify in vitro self-assembly and mechanical properties of elastin-like polypeptides. PLoS One 7, e46130.

158. Metcalfe, K., Rucka, A.K., Smoot, L., Hofstadler, G., Tuzler, G., McKeown, P., Siu, V., Rauch, A., Dean, J., Dennis, N., et al. (2000). Elastin: mutational spectrum in supravalvular aortic stenosis. Eur J Hum Genet 8, 955-963.

159. Pober, B.R. (2010). Williams-Beuren syndrome. N Engl J Med 362, 239-252.

160. Collins, R.T., 2nd. (2013). Cardiovascular disease in Williams syndrome. Circulation 127, 2125-2134.

161. Collins, R.T., 2nd. (2018). Cardiovascular disease in Williams syndrome. Curr Opin Pediatr 30, 609-615.

162. Tassabehji, M., Metcalfe, K., Hurst, J., Ashcroft, G.S., Kielty, C., Wilmot, C., Donnai, D., Read, A.P., and Jones, C.J. (1998). An elastin gene mutation producing abnormal tropoelastin and abnormal elastic fibres in a patient with autosomal dominant cutis laxa. Hum Mol Genet 7, 1021-1028.

163. Urban, Z., Gao, J., Pope, F.M., and Davis, E.C. (2005). Autosomal dominant cutis laxa with severe lung disease: synthesis and matrix deposition of mutant tropoelastin. J Invest Dermatol 124, 1193-1199.

164. Rodriguez-Revenga, L., Iranzo, P., Badenas, C., Puig, S., Carrio, A., and Mila, M. (2004). A novel elastin gene mutation resulting in an autosomal dominant form of cutis laxa. Arch Dermatol 140, 1135-1139.

165. Megarbane, H., Florence, J., Sass, J.O., Schwonbeck, S., Foglio, M., de Cid, R., Cure, S., Saker, S., Megarbane, A., and Fischer, J. (2009). An autosomal-recessive form of cutis laxa is due to homozygous elastin mutations, and the phenotype may be modified by a heterozygous fibulin 5 polymorphism. J Invest Dermatol 129, 1650-1655.

166. Olsen, D.R., Fazio, M.J., Shamban, A.T., Rosenbloom, J., and Uitto, J. (1988). Cutis laxa: reduced elastin gene expression in skin fibroblast cultures as determined by hybridizations with a homologous cDNA and an exon 1-specific oligonucleotide. J Biol Chem 263, 6465-6467.

167. Sephel, G.C., Byers, P.H., Holbrook, K.A., and Davidson, J.M. (1989). Heterogeneity of elastin expression in cutis laxa fibroblast strains. J Invest Dermatol 93, 147-153.

168. Li, D.Y., Brooke, B., Davis, E.C., Mecham, R.P., Sorensen, L.K., Boak, B.B., Eichwald, E., and Keating, M.T. (1998). Elastin is an essential determinant of arterial morphogenesis. Nature 393, 276-280.

169. Wendel, D.P., Taylor, D.G., Albertine, K.H., Keating, M.T., and Li, D.Y. (2000). Impaired distal airway development in mice lacking elastin. Am J Respir Cell Mol Biol 23, 320-326.

170. Hirano, E., Knutsen, R.H., Sugitani, H., Ciliberto, C.H., and Mecham, R.P. (2007). Functional rescue of elastin insufficiency in mice by the human elastin gene: implications for mouse models of human disease. Circ Res 101, 523-531.

171. Timpl, R., Sasaki, T., Kostka, G., and Chu, M.L. (2003). Fibulins: a versatile family of extracellular matrix proteins. Nat Rev Mol Cell Biol 4, 479-489.

172. de Vega, S., Iwamoto, T., and Yamada, Y. (2009). Fibulins: multiple roles in matrix structures and tissue functions. Cell Mol Life Sci 66, 1890-1902.

173. Giltay, R., Timpl, R., and Kostka, G. (1999). Sequence, recombinant expression and tissue localization of two novel extracellular matrix proteins, fibulin-3 and fibulin-4. Matrix Biol 18, 469-480.

174. Choudhury, R., McGovern, A., Ridley, C., Cain, S.A., Baldwin, A., Wang, M.C., Guo, C., Mironov, A.J., Drymoussi, Z., Trump, D., et al. (2009). Differential regulation of elastic fiber formation by fibulins -4 and -5. J Biol Chem 284, 24553-24567.

175. Massam-Wu, T., Chiu, M., Choudhury, R., Chaudhry, S.S., Baldwin, A.K., McGovern, A., Baldock, C., Shuttleworth, C.A., and Kielty, C.M. (2010). Assembly of fibrillin microfibrils governs extracellular deposition of latent TGF beta. J Cell Sci 123, 3006-3018.

176. Hanada, K., Vermeij, M., Garinis, G.A., de Waard, M.C., Kunen, M.G., Myers, L., Maas, A., Duncker, D.J., Meijers, C., Dietz, H.C., et al. (2007). Perturbations of vascular homeostasis and aortic valve abnormalities in fibulin-4 deficient mice 1. Circ Res 100, 738-746.

177. Giltay, R., Kostka, G., and Timpl, R. (1997). Sequence and expression of a novel member (LTBP-4) of the family of latent transforming growth factor-beta binding proteins. FEBS Lett 411, 164-168.

178. Saharinen, J., Taipale, J., Monni, O., and Keski-Oja, J. (1998). Identification and characterization of a new latent transforming growth factor-beta-binding protein, LTBP-4. J Biol Chem 273, 18459-18469.

179. Koli, K., Hyytiäinen, M., Ryynanen, M.J., and Keski-Oja, J. (2005). Sequential deposition of latent TGF-beta binding proteins (LTBPs) during formation of the extracellular matrix in human lung fibroblasts. Exp Cell Res 310, 370-382.

180. Dabovic, B., Chen, Y., Choi, J., Vassallo, M., Dietz, H.C., Ramirez, F., von, M.H., Davis, E.C., and Rifkin, D.B. (2009). Dual functions for LTBP in lung development: LTBP-4 independently modulates elastogenesis and TGF-beta activity. J Cell Physiol 219, 14-22.

181. Isogai, Z., Ono, R.N., Ushiro, S., Keene, D.R., Chen, Y., Mazzieri, R., Charbonneau, N.L., Reinhardt, D.P., Rifkin, D.B., and Sakai, L.Y. (2003). Latent transforming growth factor beta-binding protein 1 interacts with fibrillin and is a microfibril-associated protein. J Biol Chem 278, 2750-2757.

182. Urban, Z., Hucthagowder, V., Schurmann, N., Todorovic, V., Zilberberg, L., Choi, J., Sens, C., Brown, C.W., Clark, R.D., Holland, K.E., et al. (2009). Mutations in LTBP4 cause a syndrome of impaired pulmonary, gastrointestinal, genitourinary, musculoskeletal, and dermal development. Am J Hum Genet 85, 593-605.

183. Callewaert, B., Su, C.T., Van Damme, T., Vlummens, P., Malfait, F., Vanakker, O., Schulz, B., Mac Neal, M., Davis, E.C., Lee, J.G., et al. (2013). Comprehensive clinical and molecular analysis of 12 families with type 1 recessive cutis laxa. Hum Mutat 34, 111-121.

184. Dabovic, B., Robertson, I.B., Zilberberg, L., Vassallo, M., Davis, E.C., and Rifkin, D.B. (2015). Function of latent TGFbeta binding protein 4 and fibulin 5 in elastogenesis and lung development. J Cell Physiol 230, 226-236.

185. Bultmann-Mellin, I., Essers, J., van Heijingen, P.M., von Melchner, H., Sengle, G., and Sterner-Kock, A. (2016). Function of Ltbp-4L and fibulin-4 in survival and elastogenesis in mice. Dis Model Mech 9, 1367-1374.

186. Davis, E.C., and Mecham, R.P. (1996). Selective degradation of accumulated secretory proteins in the endoplasmic reticulum - A possible clearance pathway for abnormal tropoelastin. J Biol Chem 271, 3787-3794.

187. Jaques, A., and Serafini-Fracassini, A. (1985). Morphogenesis of the elastic fiber: an immunoelectronmicroscopy investigation. J Ultrastruct Res 92, 201-210.

188. Zhong, C., Chrzanowska-Wodnicka, M., Brown, J., Shaub, A., Belkin, A.M., and Burridge, K. (1998). Rho-mediated contractility exposes a cryptic site in fibronectin and induces fibronectin matrix assembly. J Cell Biol 141, 539-551.

189. Sternlicht, M.D., and Werb, Z. (2001). How matrix metalloproteinases regulate cell behavior. Annu Rev Cell Dev Biol 17, 463-516.

190. Stevens, M.M., and George, J.H. (2005). Exploring and engineering the cell surface interface. Science 310, 1135-1138.

191. Kim, S.H., Turnbull, J., and Guimond, S. (2011). Extracellular matrix and cell signalling: the dynamic cooperation of integrin, proteoglycan and growth factor receptor. J Endocrinol 209, 139-151.

192. Brennan, J.R., and Hocking, D.C. (2016). Cooperative effects of fibronectin matrix assembly and initial cell-substrate adhesion strength in cellular self-assembly. Acta Biomater 32, 198-209.

193. Saldin, L.T., Cramer, M.C., Velankar, S.S., White, L.J., and Badylak, S.F. (2017). Extracellular matrix hydrogels from decellularized tissues: Structure and function. Acta Biomater 49, 1-15.

194. Caliari, S.R., and Burdick, J.A. (2016). A practical guide to hydrogels for cell culture. Nat Methods 13, 405-414.

195. Lutolf, M.P., Lauer-Fields, J.L., Schmoekel, H.G., Metters, A.T., Weber, F.E., Fields, G.B., and Hubbell, J.A. (2003). Synthetic matrix metalloproteinase-sensitive hydrogels for the conduction of tissue regeneration: engineering cell-invasion characteristics. Proc Natl Acad Sci U S A 100, 5413-5418.

196. Wang, P., Hu, Z., Cao, X., Huang, S., Dong, Y., Cheng, P., Xu, H., Shu, B., Xie, J., Wu, J., et al. (2019). Fibronectin precoating wound bed enhances the therapeutic effects of autologous epidermal basal cell suspension for full-thickness wounds by improving epidermal stem cells' utilization. Stem Cell Res Ther 10, 154.

197. Danen, E.H., Sonneveld, P., Brakebusch, C., Fassler, R., and Sonnenberg, A. (2002). The fibronectin-binding integrins alpha5beta1 and alphavbeta3 differentially modulate RhoA-GTP loading, organization of cell matrix adhesions, and fibronectin fibrillogenesis. J Cell Biol 159, 1071-1086.

198. Woods, A., Longley, R.L., Tumova, S., and Couchman, J.R. (2000). Syndecan-4 binding to the high affinity heparin-binding domain of fibronectin drives focal adhesion formation in fibroblasts. Arch Biochem Biophys 374, 66-72.

199. Pfaff, M., Reinhardt, D.P., Sakai, L.Y., and Timpl, R. (1996). Cell adhesion and integrin binding to recombinant human fibrillin-1. FEBS Lett 384, 247-250.

200. Sakamoto, H., Broekelmann, T., Cheresh, D.A., Ramirez, F., Rosenbloom, J., and Mecham, R.P. (1996). Cell-type specific recognition of RGD- and non-RGD-containing cell binding domains in fibrillin-1. J Biol Chem 271, 4916-4922.

201. Bax, D.V., Bernard, S.E., Lomas, A., Morgan, A., Humphries, J., Shuttleworth, A., Humphries, M.J., and Kielty, C.M. (2003). Cell adhesion to fibrillin-1 molecules and microfibrils is mediated by alpha5 beta1 and alphav beta3 integrins. J Biol Chem 278, 34605-34616.

202. Jovanovic, J., Takagi, J., Choulier, L., Abrescia, N.G., Stuart, D.I., van der Merwe, P.A., Mardon, H.J., and Handford, P.A. (2007). αVß6 is a novel receptor for human fibrillin-1: Comparative studies of molecular determinants underlying integrin-RGD affinity and specificity. J Biol Chem 282, 6743-6751.

203. Tiedemann, K., Bätge, B., Müller, P.K., and Reinhardt, D.P. (2001). Interactions of fibrillin-1 with heparin/heparan sulfate: Implications for microfibrillar assembly. J Biol Chem 276, 36035-36042.

204. Bax, D.V., Mahalingam, Y., Cain, S., Mellody, K., Freeman, L., Younger, K., Shuttleworth, C.A., Humphries, M.J., Couchman, J.R., and Kielty, C.M. (2007). Cell adhesion to fibrillin-1: Identification of an Arg-Gly-Asp-dependent synergy region and a heparin-binding site that regulates focal adhesion formation. J Cell Sci 120, 1383-1392.

205. Bax, D.V., Rodgers, U.R., Bilek, M.M., and Weiss, A.S. (2009). Cell adhesion to tropoelastin is mediated via the C-terminal GRKRK motif and integrin alphaVbeta3. J Biol Chem 284, 28616-28623.

206. Lee, P., Bax, D.V., Bilek, M.M., and Weiss, A.S. (2014). A novel cell adhesion region in tropoelastin mediates attachment to integrin alphaVbeta5. The Journal of biological chemistry 289, 1467-1477.

207. Broekelmann, T.J., Kozel, B.A., Ishibashi, H., Werneck, C.C., Keeley, F.W., Zhang, L., and Mecham, R.P. (2005). Tropoelastin interacts with cell-surface glycosaminoglycans via its COOH-terminal domain. J Biol Chem 280, 40939-40947.

208. Mecham, R.P., Hinek, A., Entwistle, R., Wrenn, D.S., Griffin, G.L., and Senior, R.M. (1989). Elastin binds to a multifunctional 67-kilodalton peripheral membrane protein. Biochemistry 28, 3716-3722.

209. Hinek, A., Pshezhetsky, A.V., von Itzstein, M., and Starcher, B. (2006). Lysosomal sialidase (neuraminidase-1) is targeted to the cell surface in a multiprotein complex that facilitates elastic fiber assembly. J Biol Chem 281, 3698-3710.

210. Tatano, Y., Takeuchi, N., Kuwahara, J., Sakuraba, H., Takahashi, T., Takada, G., and Itoh, K. (2006). Elastogenesis in cultured dermal fibroblasts from patients with lysosomal beta-galactosidase, protective protein/cathepsin A and neuraminidase-1 deficiencies. J Med Invest 53, 103-112.

211. Wahart, A., Hocine, T., Albrecht, C., Henry, A., Sarazin, T., Martiny, L., El Btaouri, H., Maurice, P., Bennasroune, A., Romier-Crouzet, B., et al. (2019). Role of elastin peptides and elastin receptor complex in metabolic and cardiovascular diseases. FEBS J 286, 2980-2993.

212. Tang, J.C., Liu, J.H., Liu, X.L., Liang, X., and Cai, X.J. (2015). Effect of fibulin-5 on adhesion, migration and invasion of hepatocellular carcinoma cells via an integrin-dependent mechanism. World J Gastroenterol 21, 11127-11140.

213. Yang, Z., Mu, Z., Dabovic, B., Jurukovski, V., Yu, D., Sung, J., Xiong, X., and Munger, J.S. (2007). Absence of integrin-mediated TGFbeta1 activation in vivo recapitulates the phenotype of TGFbeta1-null mice. J Cell Biol 176, 787-793.

214. Sarrazin, S., Lamanna, W.C., and Esko, J.D. (2011). Heparan sulfate proteoglycans. Cold Spring Harb Perspect Biol 3.

215. Danielson, K.G., Martinez-Hernandez, A., Hassell, J.R., and Iozzo, R.V. (1992). Establishment of a cell line from the EHS tumor: biosynthesis of basement membrane

constituents and characterization of a hybrid proteoglycan containing heparan and chondroitin sulfate chains. Matrix 12, 22-35.

216. Shriver, Z., Capila, I., Venkataraman, G., and Sasisekharan, R. (2012). Heparin and heparan sulfate: analyzing structure and microheterogeneity. Handb Exp Pharmacol, 159-176.

217. Esko, J.D., and Lindahl, U. (2001). Molecular diversity of heparan sulfate. J Clin Invest 108, 169-173.

218. Carlsson, P., Presto, J., Spillmann, D., Lindahl, U., and Kjellen, L. (2008). Heparin/heparan sulfate biosynthesis: processive formation of N-sulfated domains. J Biol Chem 283, 20008-20014.

219. Sheng, J., Liu, R., Xu, Y., and Liu, J. (2011). The dominating role of N-deacetylase/N-sulfotransferase 1 in forming domain structures in heparan sulfate. J Biol Chem 286, 19768-19776.

220. Ai, X., Do, A.T., Lozynska, O., Kusche-Gullberg, M., Lindahl, U., and Emerson, C.P., Jr. (2003). QSulf1 remodels the 6-O sulfation states of cell surface heparan sulfate proteoglycans to promote Wnt signaling. J Cell Biol 162, 341-351.

221. Ai, X., Do, A.T., Kusche-Gullberg, M., Lindahl, U., Lu, K., and Emerson, C.P., Jr. (2006). Substrate specificity and domain functions of extracellular heparan sulfate 6-O-endosulfatases, QSulf1 and QSulf2. J Biol Chem 281, 4969-4976.

222. Hammond, E., Khurana, A., Shridhar, V., and Dredge, K. (2014). The Role of Heparanase and Sulfatases in the Modification of Heparan Sulfate Proteoglycans within the Tumor Microenvironment and Opportunities for Novel Cancer Therapeutics. Front Oncol 4, 195.

223. Manon-Jensen, T., Itoh, Y., and Couchman, J.R. (2010). Proteoglycans in health and disease: the multiple roles of syndecan shedding. FEBS J 277, 3876-3889.

224. Fitzgerald, M.L., Wang, Z., Park, P.W., Murphy, G., and Bernfield, M. (2000). Shedding of syndecan-1 and -4 ectodomains is regulated by multiple signaling pathways and mediated by a TIMP-3-sensitive metalloproteinase. J Cell Biol 148, 811-824.

225. Kreuger, J., Perez, L., Giraldez, A.J., and Cohen, S.M. (2004). Opposing activities of Dally-like glypican at high and low levels of Wingless morphogen activity. Dev Cell 7, 503-512.

226. De Rossi, G., Evans, A.R., Kay, E., Woodfin, A., McKay, T.R., Nourshargh, S., and Whiteford, J.R. (2014). Shed syndecan-2 inhibits angiogenesis. J Cell Sci 127, 4788-4799.

227. Tantravahi, R.V., Stevens, R.L., Austen, K.F., and Weis, J.H. (1986). A single gene in mast cells encodes the core peptides of heparin and chondroitin sulfate proteoglycans. Proc Natl Acad Sci U S A 83, 9207-9210.

228. Elenius, K., and Jalkanen, M. (1994). Function of the syndecans--a family of cell surface proteoglycans. J Cell Sci 107 (Pt 11), 2975-2982.

229. Lindahl, U., Backstrom, G., Hook, M., Thunberg, L., Fransson, L.A., and Linker, A. (1979). Structure of the antithrombin-binding site in heparin. Proc Natl Acad Sci U S A 76, 3198-3202.

230. Abedini, A., Tracz, S.M., Cho, J.H., and Raleigh, D.P. (2006). Characterization of the heparin binding site in the N-terminus of human pro-islet amyloid polypeptide: implications for amyloid formation. Biochemistry 45, 9228-9237.

231. Kreuger, J., and Kjellen, L. (2012). Heparan sulfate biosynthesis: regulation and variability. J Histochem Cytochem 60, 898-907.

232. Gallagher, J.T., Turnbull, J.E., and Lyon, M. (1992). Patterns of sulphation in heparan sulphate: polymorphism based on a common structural theme. Int J Biochem 24, 553-560.

233. Sasisekharan, R., and Venkataraman, G. (2000). Heparin and heparan sulfate: biosynthesis, structure and function. Curr Opin Chem Biol 4, 626-631.

234. Bernfield, M., Gotte, M., Park, P.W., Reizes, O., Fitzgerald, M.L., Lincecum, J., and Zako, M. (1999). Functions of cell surface heparan sulfate proteoglycans. Annu Rev Biochem 68, 729-777.

235. Woods, A. (2001). Syndecans: transmembrane modulators of adhesion and matrix assembly. J Clin Invest 107, 935-941.

236. Iozzo, R.V., Zoeller, J.J., and Nystrom, A. (2009). Basement membrane proteoglycans: modulators Par Excellence of cancer growth and angiogenesis. Mol Cells 27, 503-513.

237. Couchman, J.R., Gopal, S., Lim, H.C., Norgaard, S., and Multhaupt, H.A. (2015). Fell-Muir Lecture: Syndecans: from peripheral coreceptors to mainstream regulators of cell behaviour. Int J Exp Pathol 96, 1-10.

238. Gopal, S., Couchman, J., and Pocock, R. (2016). Redefining the role of syndecans in C. elegans biology. Worm 5, e1142042.

239. Kim, C.W., Goldberger, O.A., Gallo, R.L., and Bernfield, M. (1994). Members of the syndecan family of heparan sulfate proteoglycans are expressed in distinct cell-, tissue-, and development-specific patterns. Mol Biol Cell 5, 797-805.

240. Dews, I.C., and Mackenzie, K.R. (2007). Transmembrane domains of the syndecan family of growth factor coreceptors display a hierarchy of homotypic and heterotypic interactions. Proc Natl Acad Sci USA 104, 20782-20787.

241. Choi, Y., Kwon, M.J., Lim, Y., Yun, J.H., Lee, W., and Oh, E.S. (2015). Trans-regulation of Syndecan Functions by Hetero-oligomerization. J Biol Chem 290, 16943-16953.

242. Roper, J.A., Williamson, R.C., and Bass, M.D. (2012). Syndecan and integrin interactomes: large complexes in small spaces. Curr Opin Struct Biol 22, 583-590.

243. Deepa, S.S., Yamada, S., Zako, M., Goldberger, O., and Sugahara, K. (2004). Chondroitin sulfate chains on syndecan-1 and syndecan-4 from normal murine mammary gland epithelial cells are structurally and functionally distinct and cooperate with heparan sulfate chains to bind growth factors. A novel function to control binding of midkine, pleiotrophin, and basic fibroblast growth factor. J Biol Chem 279, 37368-37376.

244. Elfenbein, A., and Simons, M. (2013). Syndecan-4 signaling at a glance. J Cell Sci 126, 3799-3804.

245. Multhaupt, H.A., Yoneda, A., Whiteford, J.R., Oh, E.S., Lee, W., and Couchman, J.R. (2009). Syndecan signaling: when, where and why? Journal of physiology and pharmacology : an official journal of the Polish Physiological Society 60 Suppl 4, 31-38.

246. Lunde, I.G., Herum, K.M., Carlson, C.C., and Christensen, G. (2016). Syndecans in heart fibrosis. Cell Tissue Res 365, 539-552.

247. O'Connell, M.P., Billings, P.C., Fiori, J.L., Deirmengian, G., Roach, H.I., Shore, E.M., and Kaplan, F.S. (2007). HSPG modulation of BMP signaling in fibrodysplasia ossificans progressiva cells. J Cell Biochem 102, 1493-1503.

248. Cornelison, D.D., Wilcox-Adelman, S.A., Goetinck, P.F., Rauvala, H., Rapraeger, A.C., and Olwin, B.B. (2004). Essential and separable roles for Syndecan-3 and Syndecan-4 in skeletal muscle development and regeneration. Genes Dev 18, 2231-2236.

249. Yoshizawa, K., Inaba, K., Mannen, H., Kikuchi, T., Mizutani, M., and Tsuji, S. (2003). Analyses of beta-1 syntrophin, syndecan 2 and gem GTPase as candidates for chicken muscular dystrophy. Exp Anim 52, 391-396.

250. Al-Salam, S., and Al-Ashari, M. (2009). Expression of Galectin-3, CD138, p16INK4a, and TTF-1 in mucinous bronchioloalveolar adenocarcinoma after Hodgkin lymphoma. Appl Immunohistochem Mol Morphol 17, 351-356.

251. Alexander, C.M., Reichsman, F., Hinkes, M.T., Lincecum, J., Becker, K.A., Cumberledge, S., and Bernfield, M. (2000). Syndecan-1 is required for Wnt-1-induced mammary tumorigenesis in mice. Nat Genet 25, 329-332.

252. Stepp, M.A., Gibson, H.E., Gala, P.H., Iglesia, D.D., Pajoohesh-Ganji, A., Pal-Ghosh, S., Brown, M., Aquino, C., Schwartz, A.M., Goldberger, O., et al. (2002). Defects in keratinocyte activation during wound healing in the syndecan-1-deficient mouse. J Cell Sci 115, 4517-4531.

253. Rops, A.L., Gotte, M., Baselmans, M.H., van den Hoven, M.J., Steenbergen, E.J., Lensen, J.F., Wijnhoven, T.J., Cevikbas, F., van den Heuvel, L.P., van Kuppevelt, T.H., et al. (2007). Syndecan-1 deficiency aggravates anti-glomerular basement membrane nephritis. Kidney Int 72, 1204-1215.

254. Echtermeyer, F., Streit, M., Wilcox-Adelman, S., Saoncella, S., Denhez, F., Detmar, M., and Goetinck, P. (2001). Delayed wound repair and impaired angiogenesis in mice lacking syndecan-4. J Clin Invest 107, R9-R14.

255. Echtermeyer, F., Bertrand, J., Dreier, R., Meinecke, I., Neugebauer, K., Fuerst, M., Lee, Y.J., Song, Y.W., Herzog, C., Theilmeier, G., et al. (2009). Syndecan-4 regulates ADAMTS-5 activation and cartilage breakdown in osteoarthritis. Nat Med 15, 1072-1076.

256. Hienola, A., Tumova, S., Kulesskiy, E., and Rauvala, H. (2006). N-syndecan deficiency impairs neural migration in brain. The Journal of cell biology 174, 569-580.

257. Rhiner, C., Gysi, S., Frohli, E., Hengartner, M.O., and Hajnal, A. (2005). Syndecan regulates cell migration and axon guidance in C. elegans. Development 132, 4621-4633.

258. Steigemann, P., Molitor, A., Fellert, S., Jackle, H., and Vorbruggen, G. (2004). Heparan sulfate proteoglycan syndecan promotes axonal and myotube guidance by slit/robo signaling. Curr Biol 14, 225-230.

259. Kirkpatrick, C.A., and Selleck, S.B. (2007). Heparan sulfate proteoglycans at a glance. J Cell Sci 120, 1829-1832.

260. De Cat, B., and David, G. (2001). Developmental roles of the glypicans. Seminars in cell & developmental biology 12, 117-125.

261. Veugelers, M., De Cat, B., Ceulemans, H., Bruystens, A.M., Coomans, C., Durr, J., Vermeesch, J., Marynen, P., and David, G. (1999). Glypican-6, a new member of the glypican family of cell surface heparan sulfate proteoglycans. The Journal of biological chemistry 274, 26968-26977.

262. Nakato, H., Futch, T.A., and Selleck, S.B. (1995). The division abnormally delayed (dally) gene: a putative integral membrane proteoglycan required for cell division patterning during postembryonic development of the nervous system in Drosophila. Development (Cambridge, England) 121, 3687-3702.

263. Baeg, G.H., Lin, X., Khare, N., Baumgartner, S., and Perrimon, N. (2001). Heparan sulfate proteoglycans are critical for the organization of the extracellular distribution of Wingless. Development (Cambridge, England) 128, 87-94.

264. Taneja-Bageshwar, S., and Gumienny, T.L. (2012). Two functional domains in C. elegans glypican LON-2 can independently inhibit BMP-like signaling. Dev Biol 371, 66-76.

265. Gumienny, T.L., MacNeil, L.T., Wang, H., de Bono, M., Wrana, J.L., and Padgett, R.W. (2007). Glypican LON-2 is a conserved negative regulator of BMP-like signaling in Caenorhabditis elegans. Current biology : CB 17, 159-164.

266. Filmus, J., and Selleck, S.B. (2001). Glypicans: proteoglycans with a surprise. The Journal of clinical investigation 108, 497-501.

267. Williams, E.H., Pappano, W.N., Saunders, A.M., Kim, M.S., Leahy, D.J., and Beachy, P.A. (2010). Dally-like core protein and its mammalian homologues mediate stimulatory and inhibitory effects on Hedgehog signal response. Proc Natl Acad Sci USA 107, 5869-5874.

268. De Cat, B., Muyldermans, S.Y., Coomans, C., Degeest, G., Vanderschueren, B., Creemers, J., Biemar, F., Peers, B., and David, G. (2003). Processing by proprotein convertases is required for glypican-3 modulation of cell survival, Wnt signaling, and gastrulation movements. The Journal of cell biology 163, 625-635.

269. Rothblum, K., Stahl, R.C., and Carey, D.J. (2004). Constitutive release of alpha4 type V collagen N-terminal domain by Schwann cells and binding to cell surface and extracellular matrix heparan sulfate proteoglycans. The Journal of biological chemistry 279, 51282-51288.

270. Kim, M.S., Saunders, A.M., Hamaoka, B.Y., Beachy, P.A., and Leahy, D.J. (2011). Structure of the protein core of the glypican Dally-like and localization of a region important for hedgehog signaling. Proc Natl Acad Sci USA 108, 13112-13117.

271. Dwivedi, P.P., Grose, R.H., Filmus, J., Hii, C.S., Xian, C.J., Anderson, P.J., and Powell, B.C. (2013). Regulation of bone morphogenetic protein signalling and cranial osteogenesis by Gpc1 and Gpc3. Bone 55, 367-376.

272. Miao, H.L., Pan, Z.J., Lei, C.J., Wen, J.Y., Li, M.Y., Liu, Z.K., Qiu, Z.D., Lin, M.Z., Chen, N.P., and Chen, M. (2013). Knockdown of GPC3 inhibits the proliferation of Huh7 hepatocellular carcinoma cells through down-regulation of YAP. J Cell Biochem 114, 625-631.

273. Filmus, J., and Capurro, M. (2014). The role of glypicans in Hedgehog signaling. Matrix biology : journal of the International Society for Matrix Biology 35, 248-252.

274. Veugelers, M., Cat, B.D., Muyldermans, S.Y., Reekmans, G., Delande, N., Frints, S., Legius, E., Fryns, J.P., Schrander-Stumpel, C., Weidle, B., et al. (2000). Mutational analysis of the GPC3/GPC4 glypican gene cluster on Xq26 in patients with Simpson-Golabi-Behmel syndrome: identification of loss-of-function mutations in the GPC3 gene. Hum Mol Genet 9, 1321-1328.

275. Campos-Xavier, A.B., Martinet, D., Bateman, J., Belluoccio, D., Rowley, L., Tan, T.Y., Baxova, A., Gustavson, K.H., Borochowitz, Z.U., Innes, A.M., et al. (2009). Mutations in the heparan-sulfate proteoglycan glypican 6 (GPC6) impair endochondral ossification and cause recessive omodysplasia. Am J Hum Genet 84, 760-770.

276. DeBaun, M.R., Ess, J., and Saunders, S. (2001). Simpson Golabi Behmel syndrome: progress toward understanding the molecular basis for overgrowth, malformation, and cancer predisposition. Mol Genet Metab 72, 279-286.

277. Pilia, G., Hughes-Benzie, R.M., MacKenzie, A., Baybayan, P., Chen, E.Y., Huber, R., Neri, G., Cao, A., Forabosco, A., and Schlessinger, D. (1996). Mutations in GPC3, a glypican gene, cause the Simpson-Golabi-Behmel overgrowth syndrome. Nat Genet 12, 241-247.

278. Veugelers, M., Vermeesch, J., Watanabe, K., Yamaguchi, Y., Marynen, P., and David, G. (1998). GPC4, the gene for human K-glypican, flanks GPC3 on xq26: deletion of the GPC3-GPC4 gene cluster in one family with Simpson-Golabi-Behmel syndrome. Genomics 53, 1-11.

279. White, G.R., Kelsey, A.M., Varley, J.M., and Birch, J.M. (2002). Somatic glypican 3 (GPC3) mutations in Wilms' tumour. Br J Cancer 86, 1920-1922.

280. Jen, Y.H., Musacchio, M., and Lander, A.D. (2009). Glypican-1 controls brain size through regulation of fibroblast growth factor signaling in early neurogenesis. Neural development 4, 33.

281. Forsberg, E., and Kjellén, L. (2001). Heparan sulfate: lessons from knockout mice. J Clin Invest 108, 175-180.

282. Allen, N.J., Bennett, M.L., Foo, L.C., Wang, G.X., Chakraborty, C., Smith, S.J., and Barres, B.A. (2012). Astrocyte glypicans 4 and 6 promote formation of excitatory synapses via GluA1 AMPA receptors. Nature 486, 410-414.

283. Cano-Gauci, D.F., Song, H.H., Yang, H., McKerlie, C., Choo, B., Shi, W., Pullano, R., Piscione, T.D., Grisaru, S., Soon, S., et al. (1999). Glypican-3-deficient mice exhibit developmental overgrowth and some of the abnormalities typical of Simpson-Golabi-Behmel syndrome. J Cell Biol 146, 255-264.

284. Tang, T., Li, L., Tang, J., Li, Y., Lin, W.Y., Martin, F., Grant, D., Solloway, M., Parker, L., Ye, W., et al. (2010). A mouse knockout library for secreted and transmembrane proteins. Nat Biotechnol 28, 749-755.

285. Capurro, M., Izumikawa, T., Suarez, P., Shi, W., Cydzik, M., Kaneiwa, T., Gariepy, J., Bonafe, L., and Filmus, J. (2017). Glypican-6 promotes the growth of developing long bones by stimulating Hedgehog signaling. The Journal of cell biology 216, 2911-2926.

286. Grisaru, S., Cano-Gauci, D., Tee, J., Filmus, J., and Rosenblum, N.D. (2001). Glypican-3 modulates BMP- and FGF-mediated effects during renal branching morphogenesis. Dev Biol 231, 31-46.

287. Paine-Saunders, S., Viviano, B.L., Zupicich, J., Skarnes, W.C., and Saunders, S. (2000). glypican-3 controls cellular responses to Bmp4 in limb patterning and skeletal development. Dev Biol 225, 179-187.

288. Song, H.H., Shi, W., Xiang, Y.Y., and Filmus, J. (2005). The loss of glypican-3 induces alterations in Wnt signaling. The Journal of biological chemistry 280, 2116-2125.

289. Dowling, C., and Allen, N.J. (2018). Mice Lacking Glypican 4 Display Juvenile Hyperactivity and Adult Social Interaction Deficits. Brain plasticity (Amsterdam, Netherlands) 4, 197-209.

290. Farhy-Tselnicker, I., van Casteren, A.C.M., Lee, A., Chang, V.T., Aricescu, A.R., and Allen, N.J. (2017). Astrocyte-Secreted Glypican 4 Regulates Release of Neuronal Pentraxin 1 from Axons to Induce Functional Synapse Formation. Neuron 96, 428-445 e413.

291. Okamoto, K., Tokunaga, K., Doi, K., Fujita, T., Suzuki, H., Katoh, T., Watanabe, T., Nishida, N., Mabuchi, A., Takahashi, A., et al. (2011). Common variation in GPC5 is associated with acquired nephrotic syndrome. Nat Genet 43, 459-463.

292. Okamoto, K., Honda, K., Doi, K., Ishizu, T., Katagiri, D., Wada, T., Tomita, K., Ohtake, T., Kaneko, T., Kobayashi, S., et al. (2015). Glypican-5 Increases Susceptibility to Nephrotic Damage in Diabetic Kidney. The American journal of pathology 185, 1889-1898.

293. Hynes, R.O. (2002). Integrins: bidirectional, allosteric signaling machines. Cell 110, 673-687.

294. Takada, Y., Ye, X., and Simon, S. (2007). The integrins. Genome Biol 8, 215.

295. Harburger, D.S., and Calderwood, D.A. (2009). Integrin signalling at a glance. J Cell Sci 122, 159-163.

296. Campbell, I.D., and Humphries, M.J. (2011). Integrin structure, activation, and interactions. Cold Spring Harb Perspect Biol 3.

297. Larson, R.S., Corbi, A.L., Berman, L., and Springer, T. (1989). Primary structure of the leukocyte function-associated molecule-1 alpha subunit: an integrin with an embedded domain defining a protein superfamily. The Journal of cell biology 108, 703-712.

298. Luo, B.H., Carman, C.V., and Springer, T.A. (2007). Structural basis of integrin regulation and signaling. Annu Rev Immunol 25, 619-647.

299. Nieuwenhuizen, W., and Gravesen, M. (1981). Anticoagulant and calcium-binding properties of high molecular weight derivatives of human fibrinogen, produced by plasmin (fragments X). Biochim Biophys Acta 668, 81-88.

300. Xiong, J.P., Stehle, T., Goodman, S.L., and Arnaout, M.A. (2003). Integrins, cations and ligands: making the connection. Journal of thrombosis and haemostasis : JTH 1, 1642-1654.

301. Larsen, M., Artym, V.V., Green, J.A., and Yamada, K.M. (2006). The matrix reorganized: extracellular matrix remodeling and integrin signaling. Curr Opin Cell Biol 18, 463-471.

302. Ruoslahti, E. (1996). RGD and other recognition sequences for integrins. Annu Rev Cell Biol 12, 697-715.

303. Barczyk, M., Carracedo, S., and Gullberg, D. (2010). Integrins. Cell Tissue Res 339, 269-280.

304. Moser, M., Legate, K.R., Zent, R., and Fassler, R. (2009). The tail of integrins, talin, and kindlins. Science (New York, NY) 324, 895-899.

305. Laukaitis, C.M., Webb, D.J., Donais, K., and Horwitz, A.F. (2001). Differential dynamics of alpha 5 integrin, paxillin, and alpha-actinin during formation and disassembly of adhesions in migrating cells. The Journal of cell biology 153, 1427-1440.

306. Ramirez, F., Caescu, C., Wondimu, E., and Galatioto, J. (2018). Marfan syndrome; A connective tissue disease at the crossroads of mechanotransduction, TGFbeta signaling and cell stemness. Matrix biology : journal of the International Society for Matrix Biology 71-72, 82-89.

307. Kubota, A., Juanola-Falgarona, M., Emmanuele, V., Sanchez-Quintero, M.J., Kariya, S., Sera, F., Homma, S., Tanji, K., Quinzii, C.M., and Hirano, M. (2019). Cardiomyopathy and altered integrin-actin signaling in Fhl1 mutant female mice. Hum Mol Genet 28, 209-219.

308. Coudert, A.E., Del Fattore, A., Baulard, C., Olaso, R., Schiltz, C., Collet, C., Teti, A., and de Vernejoul, M.C. (2014). Differentially expressed genes in autosomal dominant osteopetrosis type II osteoclasts reveal known and novel pathways for osteoclast biology. Laboratory investigation; a journal of technical methods and pathology 94, 275-285.

309. Desgrosellier, J.S., and Cheresh, D.A. (2010). Integrins in cancer: biological implications and therapeutic opportunities. Nat Rev Cancer 10, 9-22.

310. Has, C., Sparta, G., Kiritsi, D., Weibel, L., Moeller, A., Vega-Warner, V., Waters, A., He, Y., Anikster, Y., Esser, P., et al. (2012). Integrin alpha3 mutations with kidney, lung, and skin disease. The New England journal of medicine 366, 1508-1514.

311. Shukrun, R., Vivante, A., Pleniceanu, O., Vax, E., Anikster, Y., Dekel, B., and Lotan, D. (2014). A human integrin-alpha3 mutation confers major renal developmental defects. PLoS One 9, e90879.

312. Allegra, M., Gagnoux-Palacios, L., Gache, Y., Roques, S., Lestringant, G., Ortonne, J.P., and Meneguzzi, G. (2003). Rapid decay of alpha6 integrin caused by a mis-sense mutation in the propeller domain results in severe junctional epidermolysis bullosa with pyloric atresia. The Journal of investigative dermatology 121, 1336-1343.

313. Bunting, M., Harris, E.S., McIntyre, T.M., Prescott, S.M., and Zimmerman, G.A. (2002). Leukocyte adhesion deficiency syndromes: adhesion and tethering defects involving beta 2 integrins and selectin ligands. Curr Opin Hematol 9, 30-35.

314. Nurden, A.T., Pillois, X., Fiore, M., Alessi, M.C., Bonduel, M., Dreyfus, M., Goudemand, J., Gruel, Y., Benabdallah-Guerida, S., Latger-Cannard, V., et al. (2015). Expanding the Mutation Spectrum Affecting alphaIIbbeta3 Integrin in Glanzmann Thrombasthenia: Screening of the ITGA2B and ITGB3 Genes in a Large International Cohort. Hum Mutat 36, 548-561.

315. Bouvard, D., Brakebusch, C., Gustafsson, E., Aszodi, A., Bengtsson, T., Berna, A., and Fassler, R. (2001). Functional consequences of integrin gene mutations in mice. Circ Res 89, 211-223.

316. Ruoslahti, E. (1996). Integrin signaling and matrix assembly. Tumour Biol 17, 117-124.

317. Ginsberg, M.H. (1995). Integrins: Dynamic regulation of ligand binding. Biochem Soc Trans 23, 439-446.

318. Huang, X., Griffiths, M., Wu, J., Farese, R.V., Jr., and Sheppard, D. (2000). Normal development, wound healing, and adenovirus susceptibility in beta5-deficient mice. Mol Cell Biol 20, 755-759.

319. Lane, N.E., Yao, W., Nakamura, M.C., Humphrey, M.B., Kimmel, D., Huang, X., Sheppard, D., Ross, F.P., and Teitelbaum, S.L. (2005). Mice lacking the integrin beta5 subunit have accelerated osteoclast maturation and increased activity in the estrogen-deficient state. Journal of bone and mineral research : the official journal of the American Society for Bone and Mineral Research 20, 58-66.

320. Robb, B.W., Wachi, H., Schaub, T., Mecham, R.P., and Davis, E.C. (1999). Characterization of an in vitro model of elastic fiber assembly. Mol Biol Cell 10, 3595-3605.

321. Lidholt, K., Weinke, J.L., Kiser, C.S., Lugemwa, F.N., Bame, K.J., Cheifetz, S., Massague, J., Lindahl, U., and Esko, J.D. (1992). A single mutation affects both N-acetylglucosaminyltransferase and glucuronosyltransferase activities in a Chinese hamster ovary cell mutant defective in heparan sulfate biosynthesis. Proc Natl Acad Sci U S A 89, 2267-2271.

322. Cooper, A.R., Patel, S., Senadheera, S., Plath, K., Kohn, D.B., and Hollis, R.P. (2011). Highly efficient large-scale lentiviral vector concentration by tandem tangential flow filtration. J Virol Methods 177, 1-9.

323. Kohfeldt, E., Maurer, P., Vannahme, C., and Timpl, R. (1997). Properties of the extracellular calcium binding module of the proteoglycan testican. FEBS Lett 414, 557-561.

324. Engvall, E., and Ruoslahti, E. (1977). Binding of soluble form of fibroblast surface protein, fibronectin, to collagen. Int J Cancer 20, 1-5.

325. Jilek, F., and Hormann, H. (1978). Cold-insoluble globulin (fibronectin), IV[1-35 affinity to soluble collagen of various types. Hoppe-Seyler's Zeitschrift fur physiologische Chemie 359, 247-250.

326. Horzum, U., Ozdil, B., and Pesen-Okvur, D. (2014). Step-by-step quantitative analysis of focal adhesions. MethodsX 1, 56-59.

327. Zeyer, K.A., Zhang, R.M., Kumra, H., Hassan, A., and Reinhardt, D.P. (2019). The fibrillin-1 RGD integrin binding site regulates gene expression and cell function through microRNAs. J Mol Biol 431, 401-421.

328. Zhang, M., Dang, L., Guo, F., Wang, X., Zhao, W., and Zhao, R. (2012). Coenzyme Q(10) enhances dermal elastin expression, inhibits IL-1alpha production and melanin synthesis in vitro. Int J Cosmet Sci 34, 273-279.

329. Koli, K., Wempe, F., Sterner-Kock, A., Kantola, A., Komor, M., Hofmann, W.K., von Melchner, H., and Keski-Oja, J. (2004). Disruption of LTBP-4 function reduces TGF-beta activation and enhances BMP-4 signaling in the lung. The Journal of cell biology 167, 123-133.

330. Tumova, S., Woods, A., and Couchman, J.R. (2000). Heparan sulfate chains from glypican and syndecans bind the Hep II domain of fibronectin similarly despite minor structural differences. The Journal of biological chemistry 275, 9410-9417.

331. Selander-Sunnerhagen, M., Ullner, M., Persson, E., Teleman, O., Stenflo, J., and Drakenberg, T. (1992). How an epidermal growth factor (EGF)-like domain binds calcium. J Biol Chem 267, 19642-19649.

332. Klass, C.M., Couchman, J.R., and Woods, A. (2000). Control of extracellular matrix assembly by syndecan-2 proteoglycan. J Cell Sci 113, 493-506.

333. Gondelaud, F., and Ricard-Blum, S. (2019). Structures and interactions of syndecans. The FEBS journal 286, 2994-3007.

334. David, G. (1993). Integral membrane heparan sulfate proteoglycans. FASEB journal : official publication of the Federation of American Societies for Experimental Biology 7, 1023-1030.

335. Lyon, M., Rushton, G., Askari, J.A., Humphries, M.J., and Gallagher, J.T. (2000). Elucidation of the structural features of heparan sulfate important for interaction with the Hep-2 domain of fibronectin. The Journal of biological chemistry 275, 4599-4606.

336. Tapon, N., and Hall, A. (1997). Rho, Rac and Cdc42 GTPases regulate the organization of the actin cytoskeleton. Curr Opin Cell Biol 9, 86-92.

337. Raftopoulou, M., and Hall, A. (2004). Cell migration: Rho GTPases lead the way. Dev Biol 265, 23-32.

338. Ridley, A.J., and Hall, A. (1992). The small GTP-binding protein rho regulates the assembly of focal adhesions and actin stress fibers in response to growth factors. Cell 70, 389-399.

339. Ridley, A.J., Paterson, H.F., Johnston, C.L., Diekmann, D., and Hall, A. (1992). The small GTP-binding protein rac regulates growth factor-induced membrane ruffling. Cell 70, 401-410.

340. Nobes, C.D., and Hall, A. (1995). Rho, rac, and cdc42 GTPases regulate the assembly of multimolecular focal complexes associated with actin stress fibers, lamellipodia, and filopodia. Cell 81, 53-62.

341. Machesky, L.M., and Hall, A. (1997). Role of actin polymerization and adhesion to extracellular matrix in Rac- and Rho-induced cytoskeletal reorganization. The Journal of cell biology 138, 913-926.

342. Ilic, D., Kovacic, B., Johkura, K., Schlaepfer, D.D., Tomasevic, N., Han, Q., Kim, J.B., Howerton, K., Baumbusch, C., Ogiwara, N., et al. (2004). FAK promotes organization of fibronectin matrix and fibrillar adhesions. J Cell Sci 117, 177-187.

343. Oeckler, R.A., Kaminski, P.M., and Wolin, M.S. (2003). Stretch enhances contraction of bovine coronary arteries via an NAD(P)H oxidase-mediated activation of the extracellular signal-regulated kinase mitogen-activated protein kinase cascade. Circ Res 92, 23-31.

344. Dessy, C., Kim, I., Sougnez, C.L., Laporte, R., and Morgan, K.G. (1998). A role for MAP kinase in differentiated smooth muscle contraction evoked by alpha-adrenoceptor stimulation. The American journal of physiology 275, C1081-1086.

345. Roberts, R.E. (2001). Role of the extracellular signal-regulated kinase (Erk) signal transduction cascade in alpha(2) adrenoceptor-mediated vasoconstriction in porcine palmar lateral vein. Br J Pharmacol 133, 859-866.

346. Tong, J., Li, L., Ballermann, B., and Wang, Z. (2016). Phosphorylation and Activation of RhoA by ERK in Response to Epidermal Growth Factor Stimulation. PLoS One 11, e0147103.

347. Burger, J., van Vliet, N., van Heijningen, P., Kumra, H., Kremers, G.J., Alves, M., van Cappellen, G., Yanagisawa, H., Reinhardt, D.P., Kanaar, R., et al. (2019). Fibulin-4 deficiency differentially affects cytoskeleton structure and dynamics as well as TGFbeta signaling. Cell Signal 58, 65-78.

348. Garcia, A.J., Vega, M.D., and Boettiger, D. (1999). Modulation of cell proliferation and differentiation through substrate-dependent changes in fibronectin conformation. Mol Biol Cell 10, 785-798.

349. Swindle, C.S., Tran, K.T., Johnson, T.D., Banerjee, P., Mayes, A.M., Griffith, L., and Wells, A. (2001). Epidermal growth factor (EGF)-like repeats of human tenascin-C as ligands for EGF receptor. The Journal of cell biology 154, 459-468.

350. Silberstein, G.B., Flanders, K.C., Roberts, A.B., and Daniel, C.W. (1992). Regulation of mammary morphogenesis: evidence for extracellular matrix-mediated inhibition of ductal budding by transforming growth factor-beta 1. Dev Biol 152, 354-362.

351. Klinowska, T.C., Soriano, J.V., Edwards, G.M., Oliver, J.M., Valentijn, A.J., Montesano, R., and Streuli, C.H. (1999). Laminin and beta1 integrins are crucial for normal mammary gland development in the mouse. Dev Biol 215, 13-32.

352. Jones, S., and Thornton, J.M. (1995). Protein-protein interactions: a review of protein dimer structures. Prog Biophys Mol Biol 63, 31-65.

353. Koike, R., Kidera, A., and Ota, M. (2009). Alteration of oligomeric state and domain architecture is essential for functional transformation between transferase and hydrolase with the same scaffold. Protein science : a publication of the Protein Society 18, 2060-2066.

354. Dayhoff, J.E., Shoemaker, B.A., Bryant, S.H., and Panchenko, A.R. (2010). Evolution of protein binding modes in homooligomers. J Mol Biol 395, 860-870.

355. Sterner-Kock, A., Thorey, I.S., Koli, K., Wempe, F., Otte, J., Bangsow, T., Kuhlmeier, K., Kirchner, T., Jin, S., Keski-Oja, J., et al. (2002). Disruption of the gene encoding the latent transforming growth factor-beta binding protein 4 (LTBP-4) causes abnormal lung development, cardiomyopathy, and colorectal cancer. Genes Dev 16, 2264-2273.

356. Takagi, K., and Kawase, O. (1967). An electron microscopic study of elastogenesis in embryonic chick aorta. J Electron Microsc (Tokyo) 16, 330-339.

357. Fukuda, Y., Ferrans, V.J., and Crystal, R.G. (1984). Development of elastic fibers of nuchal ligament, aorta, and lung of fetal and postnatal sheep: an ultrastructural and electron microscopic immunohistochemical study. The American journal of anatomy 170, 597-629.

358. Rifkin, D.B. (2005). Latent transforming growth factor-beta (TGF-beta) binding proteins: orchestrators of TGF-beta availability. J Biol Chem 280, 7409-7412.

359. Hamaia, S.W., Pugh, N., Raynal, N., Nemoz, B., Stone, R., Gullberg, D., Bihan, D., and Farndale, R.W. (2012). Mapping of potent and specific binding motifs, GLOGEN and GVOGEA, for integrin alpha1beta1 using collagen toolkits II and III. The Journal of biological chemistry 287, 26019-26028.

360. Meneghetti, M.C., Hughes, A.J., Rudd, T.R., Nader, H.B., Powell, A.K., Yates, E.A., and Lima, M.A. (2015). Heparan sulfate and heparin interactions with proteins. Journal of the Royal Society, Interface 12, 0589.

361. Carey, D.J. (1997). Syndecans: multifunctional cell-surface co-receptors. The Biochemical journal 327 (Pt 1), 1-16.

362. Geiger, B., Bershadsky, A., Pankov, R., and Yamada, K.M. (2001). Transmembrane crosstalk between the extracellular matrix--cytoskeleton crosstalk. Nat Rev Mol Cell Biol 2, 793-805.

363. Morgan, M.R., Humphries, M.J., and Bass, M.D. (2007). Synergistic control of cell adhesion by integrins and syndecans. Nature reviews Molecular cell biology 8, 957-969.

364. Ashcroft, G.S., Kielty, C.M., Horan, M.A., and Ferguson, M.W.J. (1997). Age-related changes in the temporal and spatial distributions of fibrillin and elastin mRNAs and proteins in acute cutaneous wounds of healthy humans. J Pathol 183, 80-89.

365. Dalton, B.A., McFarland, C.D., Underwood, P.A., and Steele, J.G. (1995). Role of the heparin binding domain of fibronectin in attachment and spreading of human bone-derived cells. J Cell Sci 108 (Pt 5), 2083-2092.

366. Kramer, K.L., and Yost, H.J. (2002). Ectodermal syndecan-2 mediates left-right axis formation in migrating mesoderm as a cell-nonautonomous Vg1 cofactor. Dev Cell 2, 115-124.

367. Baldwin, A.K., Cain, S.A., Lennon, R., Godwin, A., Merry, C.L., and Kielty, C.M. (2014). Epithelial-mesenchymal status influences how cells deposit fibrillin microfibrils. J Cell Sci 127, 158-171.

368. Budatha, M., Roshanravan, S., Zheng, Q., Weislander, C., Chapman, S.L., Davis, E.C., Starcher, B., Word, R.A., and Yanagisawa, H. (2011). Extracellular matrix proteases contribute to progression of pelvic organ prolapse in mice and humans. J Clin Invest 121, 2048-2059.

369. Lambaerts, K., Wilcox-Adelman, S.A., and Zimmermann, P. (2009). The signaling mechanisms of syndecan heparan sulfate proteoglycans. Curr Opin Cell Biol 21, 662-669.

370. Hocking, D.C., Smith, R.K., and McKeown-Longo, P.J. (1996). A novel role for the integrin-binding III-10 module in fibronectin matrix assembly. J Cell Biol 133, 431-444.

371. Dzamba, B.J., Bultmann, H., Akiyama, S.K., and Peters, D.M. (1994). Substrate-specific binding of the amino terminus of fibronectin to an integrin complex in focal adhesions. The Journal of biological chemistry 269, 19646-19652.

372. Petroll, W.M., Ma, L., and Jester, J.V. (2003). Direct correlation of collagen matrix deformation with focal adhesion dynamics in living corneal fibroblasts. J Cell Sci 116, 1481-1491.

373. Parsons, J.T. (2003). Focal adhesion kinase: the first ten years. J Cell Sci 116, 1409-1416.

374. Schlaepfer, D.D., and Mitra, S.K. (2004). Multiple connections link FAK to cell motility and invasion. Current opinion in genetics & development 14, 92-101.

375. Hu, Y.L., Lu, S., Szeto, K.W., Sun, J., Wang, Y., Lasheras, J.C., and Chien, S. (2014). FAK and paxillin dynamics at focal adhesions in the protrusions of migrating cells. Sci Rep 4, 6024.

376. Woods, A., and Couchman, J.R. (1994). Syndecan 4 heparan sulfate proteoglycan is a selectively enriched and widespread focal adhesion component. Mol Biol Cell 5, 183-192.

377. Baciu, P.C., and Goetinck, P.F. (1995). Protein kinase C regulates the recruitment of syndecan-4 into focal contacts. Mol Biol Cell 6, 1503-1513.

378. Saoncella, S., Echtermeyer, F., Denhez, F., Nowlen, J.K., Mosher, D.F., Robinson, S.D., Hynes, R.O., and Goetinck, P.F. (1999). Syndecan-4 signals cooperatively with integrins in a Rho-dependent manner in the assembly of focal adhesions and actin stress fibers. Proc Natl Acad Sci USA 96, 2805-2810.

379. Moore, S.W., Roca-Cusachs, P., and Sheetz, M.P. (2010). Stretchy proteins on stretchy substrates: the important elements of integrin-mediated rigidity sensing. Dev Cell 19, 194-206.

380. Parsons, J.T., Horwitz, A.R., and Schwartz, M.A. (2010). Cell adhesion: integrating cytoskeletal dynamics and cellular tension. Nature reviews Molecular cell biology 11, 633-643.

381. Huttenlocher, A., and Horwitz, A.R. (2011). Integrins in cell migration. Cold Spring Harb Perspect Biol 3, a005074.

382. Mostafavi-Pour, Z., Askari, J.A., Parkinson, S.J., Parker, P.J., Ng, T.T., and Humphries, M.J. (2003). Integrin-specific signaling pathways controlling focal adhesion formation and cell migration. The Journal of cell biology 161, 155-167.

383. Urban, Z., Riazi, S., Seidl, T.L., Katahira, J., Smoot, L.B., Chitayat, D., Boyd, C.D., and Hinek, A. (2002). Connection between elastin haploinsufficiency and increased cell proliferation in patients with supravalvular aortic stenosis and Williams-Beuren syndrome. Am J Hum Genet 71, 30-44.

384. Robert, L. (2005). Cell-elastin interaction and signaling. Pathologie-biologie 53, 399-404.

385. Sen, S., Bunda, S., Shi, J., Wang, A., Mitts, T.F., and Hinek, A. (2011). Retinoblastoma protein modulates the inverse relationship between cellular proliferation and elastogenesis. The Journal of biological chemistry 286, 36580-36591.

386. Karnik, S.K., Brooke, B.S., Bayes-Genis, A., Sorensen, L., Wythe, J.D., Schwartz, R.S., Keating, M.T., and Li, D.Y. (2003). A critical role for elastin signaling in vascular morphogenesis and disease. Development (Cambridge, England) 130, 411-423.

387. Wong, T., McGrath, J.A., and Navsaria, H. (2007). The role of fibroblasts in tissue engineering and regeneration. The British journal of dermatology 156, 1149-1155.

388. Huang, J., Davis, E.C., Chapman, S.L., Budatha, M., Marmorstein, L.Y., Word, R.A., and Yanagisawa, H. (2010). Fibulin-4 deficiency results in ascending aortic aneurysms: a potential link between abnormal smooth muscle cell phenotype and aneurysm progression. Circ Res 106, 583-592.

389. Fogerty, F.J., Akiyama, S.K., Yamada, K.M., and Mosher, D.F. (1990). Inhibition of binding of fibronectin to matrix assembly sites by anti-integrin (alpha 5 beta 1) antibodies. J Cell Biol 111, 699-708.

390. Bertrand, J., Stange, R., Hidding, H., Echtermeyer, F., Nalesso, G., Godmann, L., Timmen, M., Bruckner, P., Dell'Accio, F., Raschke, M.J., et al. (2013). Syndecan 4 supports bone fracture repair, but not fetal skeletal development, in mice. Arthritis Rheum 65, 743-752.

391. Han, G., and Ceilley, R. (2017). Chronic Wound Healing: A Review of Current Management and Treatments. Adv Ther 34, 599-610.

392. Pugliese, E., Coentro, J.Q., Raghunath, M., and Zeugolis, D.I. (2018). Wound healing and scar wars. Adv Drug Deliv Rev 129, 1-3.

393. Rnjak, J., Wise, S.G., Mithieux, S.M., and Weiss, A.S. (2011). Severe burn injuries and the role of elastin in the design of dermal substitutes. Tissue engineering Part B, Reviews 17, 81-91.

394. Papke, C.L., Tsunezumi, J., Ringuette, L.J., Nagaoka, H., Terajima, M., Yamashiro, Y., Urquhart, G., Yamauchi, M., Davis, E.C., and Yanagisawa, H. (2015). Loss of fibulin-4 disrupts collagen synthesis and maturation: implications for pathology resulting from EFEMP2 mutations. Hum Mol Genet 24, 5867-5879.